Third-Order NLO Properties and Optical Limiting Behavior of Pure and Decorated Graphene Complex Systems

A thesis submitted to Bharathidasan University, Tiruchirappalli in partial fulfilment of the requirements for the award of the

Degree of

DOCTOR OF PHILOSOPHY IN PHYSICS

By

Mrs. G.Muruganandi

(Ref. No.47229/Ph.D.K2/Physics/Part-Time/dt. 30.01.2015)

Under the guidance of **Dr. M.B. Jessie Raj**



PG and Research Department of Physics Bishop Heber College (Autonomous)

Accredited at 'A' Grade by NAAC, College with Excellence by UGC, STAR College Status by DBT

Tiruchirappalli - 620 017, India

April 2022

Dr. M.B. Jessie Raj

Assistant Professor PG and Research Department of Physics Bishop Heber College (Autonomous) Tiruchirappalli-620 017 India.



CERTIFICATE

I hereby certify that the thesis entitled "Third-Order NLO Properties and Optical Limiting Behavior of Pure and Decorated Graphene Complex Systems" submitted to Bharathidasan University, Tiruchirappalli for the award of the degree of Doctor of Philosophy in Physics is a record of original work independently carried out by Mrs. G. Muruganandi under my guidance and supervision in the PG and Research Department of Physics, Bishop Heber College (Autonomous), Tiruchirappalli-620 017.

I further certify that no part of the thesis has been submitted anywhere else for any other degree, diploma, associateship, fellowship or any other similar titles.

(M.B. Jessie Raj)

Research Supervisor

Mrs. G. Muruganandi

Research Scholar

PG and Research Department of Physics

Bishop Heber College (Autonomous)

Tiruchirappalli-620 017

India.



DECLARATION

I hereby declare that the thesis entitled "Third-Order NLO Properties and Optical Limiting Behavior of Pure and Decorated Graphene Complex Systems" is a record of original work independently carried out by me in the PG and Research Department of Physics, Bishop Heber College (Autonomous), Tiruchirappalli under the guidance and supervision of Dr. M.B. Jessie Raj, Assistant Professor, PG and Research Department of Physics, Bishop Heber College (Autonomous), Tiruchirappalli during the period 2015 – 2020.

I further declare that this thesis does not form part of any other thesis or dissertation on the basis of which a degree or diploma was conferred earlier.

(G. Muruganandi)

Acknowledgment

First of all, I wish and thank the **Almighty** for giving me the strength to complete my ambition of doing research to get the Ph.D. degree.

It is with my deep sense of gratitude that I acknowledge my research supervisor Dr. M.B. Jessie Raj, Assistant Professor, P.G. and Research Department of Physics, Bishop Heber College (Autonomous), Tiruchirappalli for the continuous support, dedicated help, advice, inspiration, and encouragement throughout my Ph.D., study and related research. Her constant guidance, cooperation, motivation, and support have always kept me going ahead. During our course of interaction during the last five years, I have learned extensively from her, including how to raise new possibilities, how to regard an old question from a new perspective, how to approach a problem by systematic thinking, data-driven decision making and exploiting serendipity.

I would like to express my earnest thanks to **Dr. D. Paul Dhayabaran**, The Principal, Bishop Heber College (Autonomous), Tiruchirappalli who permitted me to do research work in this prestigious institution.

I record my sincere gratitude to **Dr. C. Ravidhas**, Assistant Professor and Head, P.G. and Research Department of Physics, Bishop Heber College (Autonomous), Tiruchirappalli for his support, encouragements and kind gestures during the tenure of my research.

My special words of thanks to **Dr. T.C. Sabari Girisun**, Assistant Professor, School of Physics, Bharathidasan University, Tiruchirappalli for being the member of the Doctoral Committee and introducing me to the wonderful world of nonlinear optics. I place a sincere word of thanks to him for providing research and laser facilities in the Nanophotonics Laboratory, School of Physics, Bharathidasan University, Tiruchirappalli.

I also owe a debt of thanks to **Dr. S. Gowri**, Assistant Professor, Department of Physics, Cauvery College for Women (Autonomous), Trichirappalli for being the member of the Doctoral Committee, and providing continuous support, guidance, cooperation, encouragement and for facilitating all the requirements, going out of her way.

I am grateful to my research colloborator **Dr. S. Vinitha**, Assistant Professor (Senior), Vellore Institute of Technology (VIT), Chennai for extending her research facilities.

I place on record my hearty thanks to all the **Faculty**Members and Supporting Staff of Department of Physics along with the Librarian, Bishop Heber College (Autonomous), Tiruchirappalli for their kind co-operation, encouragements and help in many aspects throughout.

I place my respectable gratitude to the **Management**, the **Principal**, the **Head and Colleagues** of Department of Physics of Aadhavan College of Arts and Science, Alathur, Manapparai for their co-operation to complete my research successfully.

I thank my friends **Dr. M. Saravanan and Dr. N. Priyadarshani** in the Nanophotonics Laboratory, School of Physics, Bharathidasan University, Tiruchirappalli for their team spirit, timely help and research discussions.

I would like to express my deepest gratitude to **my Parents**, **Husband**, **Son**, **Family Members** and **Friends**. This dissertation would not have been possible without their warm love, continued patience, and endless support.

- G. Muruganandi

Preface

Considering the factors of a sudden hike in the utilization of high intense short-wavelength (green) lasers and eye of human has maximum sensitivity (88 %) to green color, the need for laser safety devices have increased tremendously. Particularly with extensive use of continuous wave (CW) lasers at power levels ranging from µW to kW in various applications, the need for protecting the human eye and sensors used in handling the CW output has become increasingly important. Laser damages can be avoided by NLO phenomena like optical-limiting effect (OL) wherein a medium exhibits high transmittance at low-intensity light and attenuate an intense optical beam, limiting the output fluence at a certain range. Many known NLO materials such as carbon-based suspensions, fullerenes, phthalocyanines, nanoparticles, metal nanowires, carbon nanotube, organic chromophores, and porphyrins could serve as candidates for practical optical limiters. In this line of search, the versatile chemistry of carbon materials, functionalizing as a building block of many fascinating new stable and structurally improved carbon nanomaterials, has resulted in special attention in studying carbonaceous matter at the nanoscale. Among them, graphene (G) and its derivatives like graphene oxide (GO), reduced graphene oxide (rGO) have attracted great attention due to its promising properties like high flexibility and thermal stability. However, the basic requirement of high linear transmittance limits the possible usage as a power limiter.

Improvement of linear transmittance along with enhanced NLO action can be achieved through nanocomposite formation that possesses rGO as host-matrix and known NLO material as a decorative element. In the choice of inorganic materials, barium borate (BBO) nanostructures will be an interesting candidate, as it possesses large second harmonic generation (SHG) and has unique characteristics like wide transparency and high optical damage threshold. Thus decorating BBO nanorods upon rGO can yield BBO:rGO nanocomposite with interesting NLO properties. Compared to inorganic NLO materials, the inclusion of semiorganic NLO materials in rGO can yield high NLO coefficient nanocomposites. In particular, the derivatives of 2-amino 5-nitropyridine and 4-dimethyl aminopyridine with the interaction of orthophosphoric acid (2A5NPDP, DMAPDP) and boric acid (2A5NPFB), are efficient NLO materials as it can attach inorganic elements to its herringbone pattern. Inclusion of these semiorganic NLO materials like 2A5NPFB, 2A5NPDP, and DMAPDP as decorative elements in rGO can yield interesting nanocomposites that possess stronger nonlinear refraction, which is beneficial for power limiting applications.

Thus this thesis aims to investigate the following pure and decorated rGO nanocomposite for optical limiting applications

- 1. Graphene oxide (GO) and Reduced Graphene Oxide (rGO)
- 2. BBO Nanorods decorated Reduced Graphene Oxide (rGO:BBO)
- 3. 2A5NPFB decorated Graphene Oxide (GO: 2A5NPFB)
- 4. 2A5NPDP decorated Graphene Oxide (GO: 2A5NPDP)
- 5. DMAPDP decorated Graphene Oxide (GO: DMAPDP)

The prepared nanohybrid exhibited superior NLO properties and optical limiting action compared to their individual compounds, making them potential candidates for optical limiting applications. Thus the present investigation to tune and modify the optical properties of these pure and decorated reduced graphene oxide will open up the possibility to identify suitable optical limiters that can be used for safety devices against the mostly utilized continuous-wave green lasers.

Chapter I begins with a *general introduction* followed by a brief description of the fundamentals of nonlinear optics. The origin of NLO effects, various third-order NLO phenomena, the concept of optical limiting is discussed. The materials selection and scope of the research are briefly described.

Chapter II describes the preparation of graphene oxide and reduced graphene oxide. Reduced graphene oxide (rGO) was prepared by a reduction method using hydrazine, sodium borohydride, and ascorbic acid as a reductant. Z-scan results show that the materials possess a self-defocusing nature. rGO reduced by hydrazine monohydrate (rGO-H) has a better optical limiting action.

Chapter III deals with the preparation and characterization of **barium borate decorated reduced graphene oxide**. By the simple hydrothermal method, nanorods of barium borate were successfully loaded on reduced graphene oxide sheets. The nonlinear refractive index of nanocomposite was found to be almost four times higher than GO which resulted in superior optical power limiting action.

Chapter IV presents the synthesis and characterization of **2-amino 5-nitropyridinium tetrafluoroborate decorated graphene oxide**. 2A5NPFB crystal and 2A5NPFB decorated GO exhibit saturable absorption, self-defocusing, and optical limiting action. Here 2A5NPFB decorated GO nanocomposite exhibits superior optical limiting action than 2A5NPFB crystals.

Chapter V deals with the synthesis and characterization of **2-amino 5-nitiropyridinium dihydrogen phosphate decorated Graphene Oxide**. The NLO response of thermo-optic origin was studied using the Z-scan technique. Interaction of 2A5NPDP with GO sheets enhanced the third-order NLO properties and thus 2A5NPDP decorated GO exhibit superior OL action.

Chapter VI describes the preparation and characterization of 4-dimethyl aminopyridinium dihydrogen phosphate decorated graphene oxide. SEM image portrays the formation of nanoparticles with grain size in the range of 45-170 nm. Here DMAPDP nanoparticles decorated GO are found to be superior than pure DMAPDP for the protection of photosensitive components.

Chapter VII presents the **summary and future directions** in detail. Superior nanohybrids suitable for optical limiting applications against continuous-wave green (532 nm, 50 mW) lasers are identified and presented in detail.

Papers Published in International Journals

- 1. Effect of reducing agents in tuning the third-order optical nonlinearity and optical limiting behavior of reduced graphene oxide
 - **G. Muruganandi**, M. Saravanan, G. Vinitha, M.B. Jessie Raj, T.C. Sabari Girisun

Chemical Physics 488-489 (2017) 55-61.

- 2. Nonlinear Optical Behavior of Nanostructured 4-Dimethyl Aminopyridinium Dihydrogen Phosphate
 - **G. Muruganandi**, M. B. Jessie Raj, T.C. Sabari Girisun International Journal of Nanoscience 4 (2017) 1760036-1760041.
- 3. Barium borate nanorod decorated reduced graphene oxide for optical power limiting applications
 - **G. Muruganandi**, M. Saravanan, G. Vinitha, M. B. Jessie Raj, T.C. Sabari Girisun

Optical Materials 75 (2018) 612-618.

- 4. Second and third-order NLO response of 2-amino 5-nitropyridinium tetrafluoroborate
 - G. Muruganandi, M.B. Jessie Raj

Optik, 182 (2019) 755-760.

Papers Presented in International Conferences

- "Nonlinear Optical Behaviour of Nanostructured 4-Dimethyl- Aminopyridinium Dihydrogen Phosphate", International Conference on Frontiers in Nanoscience and Nanotechnology, 26-28 February 2016, SASTRA University, Thanjavur.
- Characterization 2. "Preparation and of 4-Dimethyl Aminopyridinium Dihydrogen Chloride", International Engineering, Conference on Advances in Science Technology, 3-4 March 2016, SBM College of Engineering and Technology, Dindigul.
- 3. "Optical Limiting Behavior of Reduced Graphene Oxide prepared using Hydrazine Monohydrate Under CW Laser Excitation", National Conference on Nanophotonics (NCNP- 2016) on 18-19 March, 2016 at Bharathidasan University, Tiruchirappalli.
- 4. "Second and third-order NLO response of 2-amino-5-nitropyridinium tetrafluoroborate", International Conference on Advances in Materials (AiM-2017) on 07 April 2017 at M. Kumarasamy College of Engineering, Karur.
- 5. "2A5NPFB for SHG and OL applications", International Conference on Material Physics (ICOMP-2018) on 29 January 2018 at Bishop Heber College, Tiruchirappalli.
- "Optical studies on 2A5NP Decorated Graphene Oxide Composites", International Conference on Sustainable Energy Technologies (i-SET 2018) on June 27-28, 2018 at Bharathidasan University, Tiruchirappalli.

Content

Chapter	Title	Page
I	Introduction to Nonlinear Optics and	01
	Materials	
II	Graphene Oxide and Reduced Graphene Oxide	48
	Nanostructures	
III	Barium Borate Nanorod Decorated Reduced	67
	Graphene Oxide	
IV	2-amino 5-nitropyridinium Tetrafluoroborate	89
	Decorated Graphene Oxide	
V	2-amino 5-nitropyridinium Tetrafluoroborate	111
	Decorated Graphene Oxide	
VI	4-Dimethyl Aminopyridinium Dihydrogen	134
	Phosphate Decorated Graphene Oxide	
VII	Summary and Future Directions	157
	Annexure: Copy of the Reprints	

Chapter - I

Introduction to Nonlinear Optics and Materials

CHAPTER I

Introduction to Nonlinear Optics and Materials

LASER is one of the greatest inventions in the history of Science. Over the last nearly six-decade, its arrival created many enrapturing new fields, among which nonlinear optics (NLO) undoubtedly has the broadest scope and now it ranges from paramount studies in interaction of light with matter to exhilarating applications such as frequency conversion and optical limiting. Modern thriving efforts in molecular engineering propose that organic NLO materials acquire comparably better NLO properties than inorganic. Due to the stronger NLO response, graphene oxide (GO) stand high among the layer structured carbonaceous materials in this domain. However, the basic requirement of high linear transmittance limits the possible usage of NLO devices. Improvement of linear transmittance along with enhanced NLO action can be achieved through nanocomposite formation. Inclusion of NLO materials like barium borate, 2-amino 5-nitropyridnium fluoroborate, 2-amino 5-nitropyridnium dihydrogen phosphate, 4-dimethul aminopyridnium dihydrogen phosphate (BBO, 2A5NPFB, 2A5NPDP, and DMAPDP) as decorative elements in GO can yield interesting nanocomposites that possess stronger nonlinearity, which is beneficial for power limiting applications. Thus this thesis aims to investigate the several GO complex system for NLO applications.

1.1 Introduction

LASER (Light Amplification by Stimulated Emission of Radiation) is one of the revolutionary inventions to mankind. LASER is a source that emits a kind of light of unrivaled purity and intensity which is incomparable to already known sources of electromagnetic radiation. Its arrival a six decades ago, created many fascinating new fields, among which nonlinear optics (NLO) undoubtedly has the broadest scope and most influential proponents. The field of nonlinear optics is almost sixty years old and the interest in the field has grown now it from continuously and ranges fundamental (formulating basic theories) in the interaction of light with matter to exciting applications such as frequency conversion and optical limiting [1]. The impact of NLO on science and technology has been twofold. First, it has enhanced the understanding of fundamental light-matter interactions. Second, it has been a driving force in rejuvenating optical technology in several areas of science and engineering. The second and the third-order phenomena and devices are now at understanding and development [2], stage.

Under normal conditions, the response of a medium to light is linear and as a consequence, most optical phenomena can be described with a linear refractive index. At sufficient high-intensity light, the response of the material depends on the intensity which results in an entirely new field of nonlinear optics. Nonlinear optics describes the behavior of light in a medium in which the dielectric polarization responds nonlinearly to the electric field (values of the electric field comparable to interatomic electric fields, typically 10^8 V/m) of the light. This nonlinearity is only observed at very high light intensities that are provided by lasers [3]. The field of nonlinear optics begins with the observation of second-harmonic generation by

Franken and coworkers in 1961, shortly after the demonstration of the first working laser by Maiman in 1960 [4, 5].

The design, synthesis, characterization, and understanding of new molecular assemblies with suitable optical nonlinearities carry out an active field of research at the interface of Physics, Chemistry and Materials Science. Demand in this area of materials exemplifies an important theme in the contemporary subject: to know the exact influence of a molecule in deciding the required properties of the material for various device applications. This leads to the academic curiosity which motivated the early forays by synthetic chemists into the NLO arena. The integrative chain of developments from a new molecule with interesting properties to a functioning NLO device is necessarily long and perplexing; the majority of studies totted in this field have fixated on chromophore design and elucidation of molecular structure-activity correlations. In this search, the versatile chemistry of carbon materials, functionalizing as a building block of many stable fascinating new and structurally improved carbon nanomaterials, has resulted in a strong interest in studying the carbonaceous matter for NLO applications. Among them, graphene with two dimensional one-atom-thick sp² bonded carbon networks has attracted great attention due to its promising properties like high flexibility and thermal stability. Attracted by the fascinating behavior of graphene, this thesis focuses on the structural and characterization of pure and composites of graphene oxide for various NLO applications like frequency conversion and optical limiting.

This chapter throws light on the origin of NLO, various NLO phenomena, the concept of frequency conversion and optical limiting, with its theory. Also, the selection of materials for investigation is elaborated.

1.2 Origin and Nature of Nonlinear Optics

The invention of laser has unlocked a new perspective in science and technology and particularly the study of optics at high intensities. The interaction of the electromagnetic field of light (normally highintensity laser light) with an NLO material results in the generation of new electromagnetic fields. The electric field interacts with inherent charges in the material causing the original beam to be altered in phase, frequency, amplitude or polarization when light passes through a species. Such interactions expound the field of "Nonlinear Optics" and describes the deviation from the linear behavior as defined by the laws of classical optics [6]. The optical parameters of the medium were independent of the intensity of light propagating in the medium before the arrival of lasers. The reason is that the electric field strength generated by the conventional light sources (non-laser light) is of the order of 10³ V/cm. Since the interatomic field strength is in the range 10⁷ to 10¹⁰ V/cm, the field due to the light does not affect the atoms and so the material behaves linearly. Alternately intense laser radiation, which generates a field of strength 10⁸ to 10⁹ V/cm, passes through the material, this high field influences the atoms which eventuate the induced dipoles oscillating with higher amplitudes. When the amplitude of the oscillation is small, the linear effect is observed, flipside when it is large higher harmonic terms are found. At such high fields, the optical properties depend on intensity. Thus new electromagnetic fields can be generated that are altered in phase, frequency, amplitude, etc. [7].

The interaction of the electromagnetic field with matter induces polarization in that matter. In linear optics, there is an instantaneous displacement (polarization) of the electron density of the atom by the electric field **E** of the light wave. The displacement of the electron

density away from the nucleus results in a charge separation (an induced dipole), with the electric dipole moment **P**. With the small fields, the strength of the applied field is proportional to the displacement of charges from the equilibrium position and leads to the relation,

Polarization (**P**) =
$$\alpha$$
 . **E** (1.1)

where α is the linear polarizability of the medium (**P** and **E** are vectors). If the field oscillates with a frequency, then the induced polarization will have the same frequency and phase, responded is instantaneous. Most applications of experiments with NLO are carried out on bulk or macroscopic materials and in this case, the linear polarization is given in the following equation,

$$\mathbf{P} = \varepsilon_0 \,\chi^{(1)}. \,\mathbf{E} \tag{1.2}$$

where ε_0 is the permittivity in free space (8.85 × 10⁻¹² C²N⁻¹m⁻²), $\chi^{(1)}$ is the linear susceptibility of a collection of molecules (on which the parameters of the dielectric constant and refractive index have a bearing). The electric field inside the material is lowered by the polarization that opposes the electric field. The reduction in the field intensity in the volume element containing the molecule of interest is by a factor (1+ ε), where ε is the dielectric constant of the medium. The proportionality constant is related to the dielectric constant by

$$\varepsilon = 1 + 4 \pi \chi^{(1)} \tag{1.3}$$

and is related to the refractive index of the medium 'n' by

$$\chi^{(1)} = n^2 - 1 \tag{1.4}$$

The susceptibility $\chi^{(1)}$ is a second rank tensor because it relates all the components of the polarization vector to all the components of the electric field vector. It contains all the information about the medium

needed to relate the polarization in a particular direction to various Cartesian components of the electric field vector in an arbitrary direction [7-9]. However, when the material is subjected to an intense electric field (i.e. a laser), the polarization is no longer a linear function of the applied field. Then the nonlinear polarization is expressed by,

$$\mathbf{P} = \varepsilon_0 \left(\mathbf{P_o} + \chi^{(1)} \cdot \mathbf{E} + \chi^{(2)} \cdot \mathbf{E} \cdot \mathbf{E} + \chi^{(3)} \cdot \mathbf{E} \cdot \mathbf{E} \cdot \mathbf{E} + \ldots \right)$$
 (1.5)

where $\mathbf{P_o}$ is the static dipole moment per unit volume of the sample, $\chi^{(2)}$ and $\chi^{(3)}$ are the second and third-order susceptibilities respectively (parameters that determine the magnitude of the second and third-order nonlinear optical responses)

The relations are tensor but, we have used them in scalar form. In nonlinear terms, the product of two or more oscillating fields gives oscillation at a combination of frequencies and therefore the above equation can be expressed in terms of frequency as:

$$P(-\omega_0) = \varepsilon_0 \begin{cases} \chi^{(1)}(-\omega_0; \omega_1) \cdot E(\omega_0) + \chi^{(2)}(-\omega_0; \omega_1, \omega_2) \cdot E(\omega_1 \cdot \omega_2) + \\ \chi^{(3)}(-\omega_0; \omega_1, \omega_2, \omega_3) \cdot E(\omega_1 \cdot \omega_2 \cdot \omega_3) \dots \end{cases}$$
(1.6)

where $x^{(2)}$, $x^{(3)}$ are the nonlinear susceptibilities of the medium.

- $\mathbf{x}^{(1)}$ Linear term responsible for material's linear optical properties like refractive index, dispersion, birefringence, and absorption.
- $x^{(2)}$ Quadratic term which describes second-harmonic generation in noncentrosymmetric materials.
- x⁽³⁾ Cubic term responsible for third-harmonic generation, stimulated Raman scattering, phase conjugation, and optical bi-stability. Hence the induced polarization is capable of multiplying the fundamental frequency to second, third and even higher harmonics.

Microscopically, when a molecule is subjected to laser light, the polarizability of the molecule can be driven beyond the linear regime. Therefore, the nonlinear molecular polarization **P** (which is a function of the applied field and leads to nonlinear effects) can now be expressed as,

$$\mathbf{P} = \varepsilon_0 \left[\alpha_{ij} \mathbf{E} + \beta_{ijk} \mathbf{E} \cdot \mathbf{E} + \gamma_{ijkl} \mathbf{E} \cdot \mathbf{E} \cdot \mathbf{E} + \dots \right]$$
 (1.7)

where α_{ij} is Polarizability, β_{ijk} is First order hyperpolarizability (second-order effects), γ_{ijkl} is Second-order hyperpolarizability (third-order effects) and i, j, k, l correspond to the molecular coordinates with increasing field strength. The nonlinear effects become more important due to the high powers of the field \mathbf{E} (Eqn. 1.6). Since α is much greater than β and γ , nonlinear optical effects are not commonly observed before the advent of laser and its associated large electric fields. An important point to note is that for β (or $\chi^{(2)}$) to be non-zero, the molecules (or material) need to be non-centrosymmetric and γ is the first non-zero nonlinear term for centrosymmetric media [9, 10]. For a centrosymmetric material, the nonlinear susceptibility $\mathbf{x}^{(2)}$ vanishes. Since 11 of 32 crystal classes possess inversion symmetry, this rule is very powerful. To understand the above-mentioned case, an isotropic crystal with inversion symmetry ($\mathbf{x} \rightarrow -\mathbf{x}$, $\mathbf{y} \rightarrow -\mathbf{y}$, $\mathbf{z} \rightarrow -\mathbf{z}$) is considered. Then

$$-P_i^{(2)} = \varepsilon_0 \sum_{j,k} \chi_{ijk}^{(2)} \left(-E_j \right) \left(-E_k \right)$$
 (1.8)

Thus $P_i^{(2)} = 0$ and hence $x^{(2)} = 0$. This result can be understood intuitively by considering the motion of an electron in a non-parabolic potential well. Because of the nonlinearity of the associated restoring force, the atomic response will show significant harmonic distortion (Fig. 1.1). Part (a) shows the waveform of the incident monochromatic electromagnetic wave of frequency ω . Under linear response (Part (b)),

there is no distortion with the polarization of the medium. Part (c) shows the induced polarization for the case of a nonlinear medium with inversion symmetry. Although significant waveform distortion is evident, only odd harmonics of the fundamental frequency are present. In a nonlinear medium with the noncentrosymmetric arrangement, both odd and even harmonics are present (Part (d)) in the waveform associated with the atomic response.

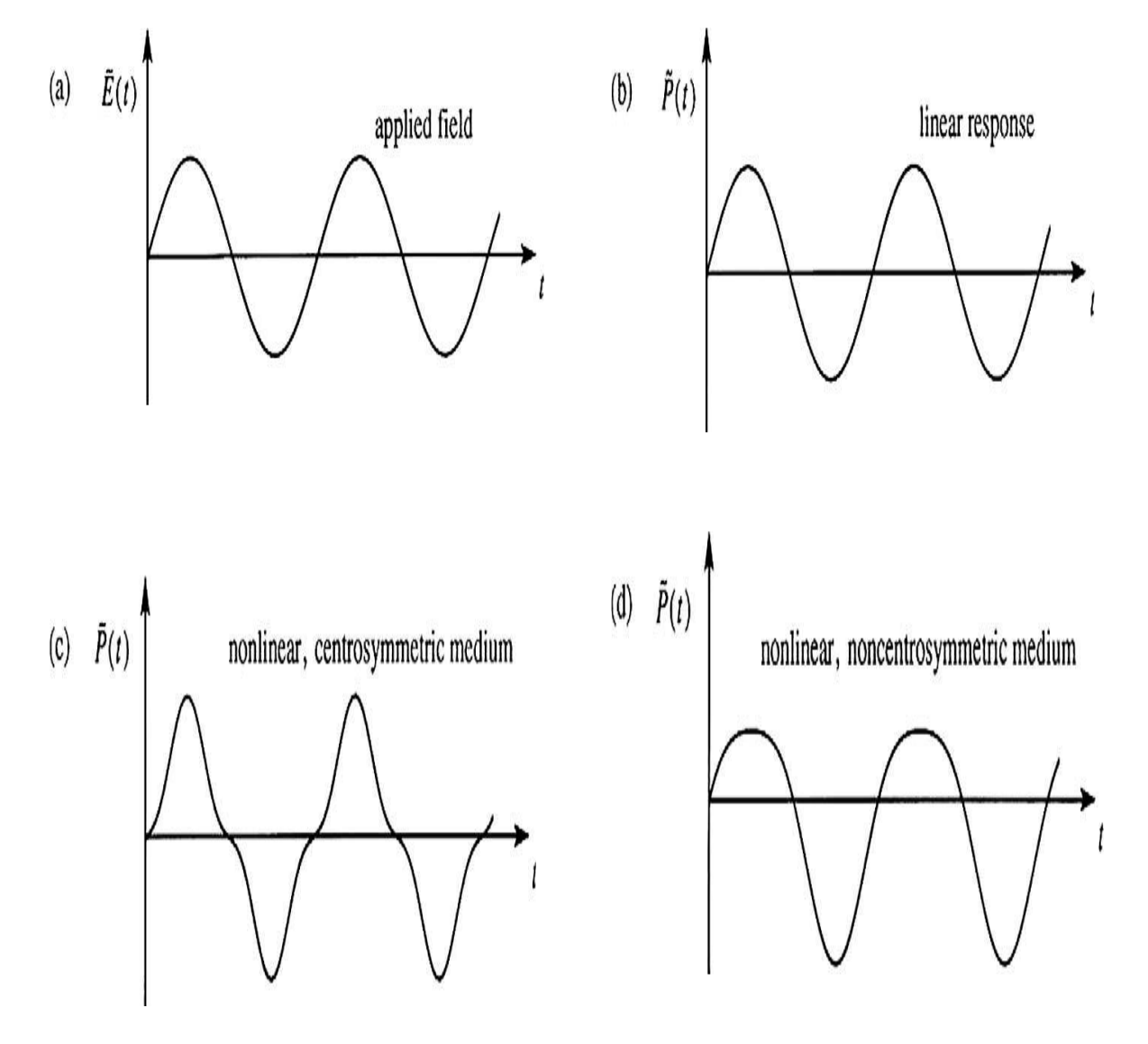


Figure 1.1 Waveforms Associated with the Atomic Response

The medium for which the polarization is described by a nonlinear relation of the type Eqn. 1.5 is called as "**Nonlinear Optical Medium**".

1.3 Nonlinear Absorption and Nonlinear Refraction

The achromatic changes in the optical properties of a material can be convinced due to the intense monochromatic radiation. Nonlinear absorption (NLA) refers to the change in transmittance of a material as a function of intensity or fluence. The probability of a material absorbing more than one photon before relaxing to the ground state can be greatly enhanced when it is passed through sufficient high intensities. As early as 1931, with the aid of secondorder quantum perturbation theory, Goppert - Mayer derived the probability for two-photon transition [11]. Since the invention of the laser, not only this phenomenon of simultaneous absorption of two photons has been observed in a wide variety of materials and the multiphoton (n>2) absorption has also been widely studied. Also, population redistribution induced by intense laser field leads to interesting counter plays of stimulated emission and absorption, complicated energy transitions in complex molecular systems and the generation of free carriers in solids. These signified phenomena are demonstrated optically in a reduced (saturable) or increased (reverse Several effects saturable) absorption. produced by nonlinear absorption in the frequency-dependent transmittance of material have led to varieties of applications in science and technology such as nonlinear spectroscopy and optical limiting. Several mechanisms are proposed to understand the intensity dependence of nonlinear absorption.

When the incident intensity is well above the saturation intensity, then the excited state can become significantly populated. In a system such as polyatomic molecules, there is a high density of states near the state involved in the excitation. The excited electron can rapidly make transitions to one of these states before it eventually

transits back to the ground state. Such a process of absorbing one more photon by the electron before relaxing to the ground-state is called an **excited state absorption**. **Saturable absorption** (SA) is termed as when the absorption cross-section of the excited state is smaller than that of the ground state, the transmission of the system is increased when the system is highly excited. When the absorption cross-section of the excited state is larger than that of the ground state, then the system will be less transmissive when excited. This is called **reverse saturable absorption** (RSA). The absorption of a photon with energy greater than the bandgap will enhance an electron to the conduction band, where it turns as a free carrier in semiconductors. If it absorbs another photon, before recombination with holes in the valence band, it is called as **free carrier absorption**. In the weak absorption regime, the attenuation (dI/dZ) may be described as

$$\frac{dI}{dz} = -\alpha_0 I - \alpha_c N_c(I)I \tag{1.9}$$

where α_0 is ground state absorption cross-section, $N_c(I)$ is the intensity-dependent carrier density and α_c is the free-carrier cross-section [12].

Two-photon absorption (2PA) involves a transition from the ground state of a system to the high-lying state by the simultaneous absorption of two photons from an incident radiation field as shown in Fig. 1.2. This process involves different selection rules than those of single-photon absorption. Hence 2PA spectroscopy compliments linear absorption spectroscopy in studying the excited states of systems. Either two photons from the same optical field oscillating at frequency ω are absorbed to make a transition at 2ω or two optical fields at frequencies ω_e (pump) and ω_p (probe) are absorbed to have a transition

at $\omega_e + \omega_p$. In both cases, the intermediate states are not real (virtual) and hence two photons are absorbed simultaneously. For a single beam, the 2PA is obtained by the relation,

$$\frac{dI}{dz} = -\alpha I - \beta I^2 \tag{1.10}$$

where dI/dz is an optical loss, α is the linear absorption coefficient and β is the 2PA coefficient, which is a macroscopic property characterizing the material.

Three photon absorption (3PA) involves the transition to excited state by simultaneous absorption of three photons from incident radiation as displayed in Fig. 1.2. These cases are shown involving one, two and three fields. For 3PA, the attenuation of a beam is given by

$$\frac{dI}{dz} = -\alpha I - \gamma I^3 \tag{1.11}$$

where γ is the 3PA coefficient. 3PA is a fifth-order nonlinear process and is related to fifth-order susceptibility. Similarly, nonlinear absorption can be extended to an arbitrary number of absorbed photons. **Multiphoton absorption** (NPA) refers to the simultaneous absorption of 'n' photons from a laser beam. The optical loss associated with this mechanism is

$$\frac{dI}{dz} = -\left(\alpha + \gamma^{(n+1)}I^n\right)I\tag{1.12}$$

where $\gamma^{(n+1)}$ is the (n+1) photon absorption coefficient and has unit m^{2n-1}/W^n .

The normalized transmittance for 2PA is given by [2]

CW Gaussian beam,
$$T = \frac{(1-R)^2 \exp(-\alpha L)}{q_0}$$
 (1.13)

Pulsed Gaussian beam,
$$T = \frac{\left(1 - R\right)^2 \exp\left(-\alpha L\right)}{\sqrt{\pi}q_0} \int_{-\infty}^{\infty} \ln\left[1 + q_0 \exp\left(-x^2\right)\right] dx \quad (1.14)$$

where,
$$q_0 = \frac{\beta(1-R)I_0(1-\exp(-\alpha L))}{\alpha}$$
 (1.18)

The normalized transmittance for 3PA is given by [2]

CW Gaussian beam,
$$T = \frac{(1-R)^2 \exp(-\alpha L)}{p_0} \ln(\sqrt{1+p_0^2} + p_0)$$
 (1.19)

Pulsed Gaussian beam,

$$T = \frac{(1 - R)^{2} \exp(-\alpha L)}{\sqrt{\pi} p_{0}} \int_{-\infty}^{\infty} \ln\left[\sqrt{1 + p_{0} \exp(-2x^{2})} + p_{0} \exp(-x^{2})\right] dx$$
 (1.20)

where,
$$p_0 = \sqrt{2\gamma (1-R)^2 I_0^2 L_{eff}}$$
 (1.21)

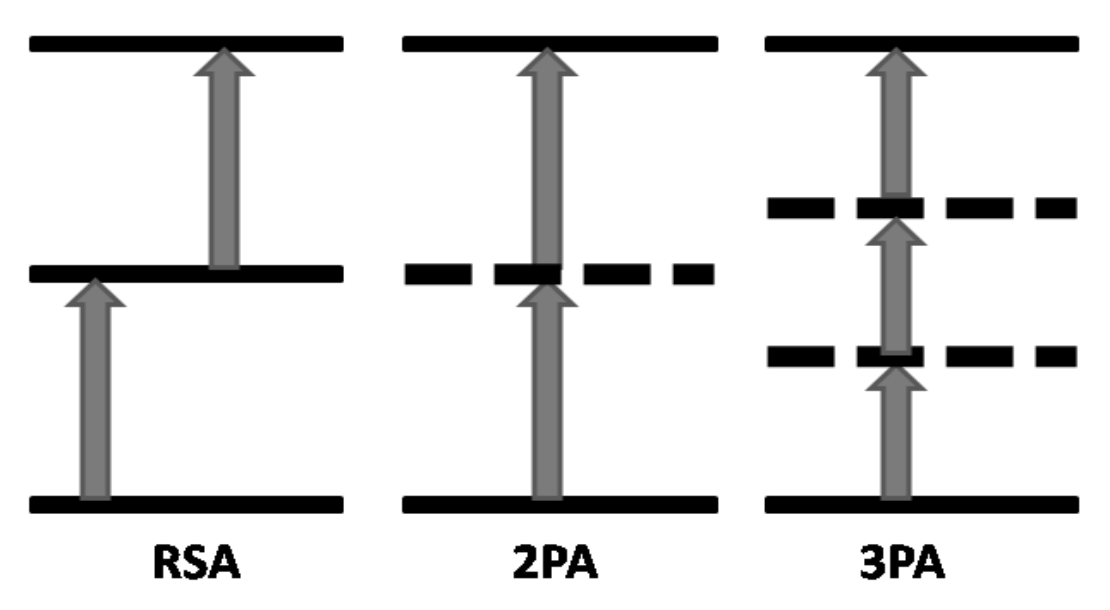


Figure 1.2 Nonlinear Absorption – (a) RSA, (b) 2PA and (c) 3PA

The nonlinear refractive index is referred to be change in the refractive index or spatial distribution of the refractive index of a medium due to the presence of optical waves. Nonlinear refraction has led to a variety of riveting applications and also paramount to many fundamental investigations. Distinct physical phenomena associated with this nonlinear refraction are listed in Table 1.1. In laser domain,

thus refractive index can be given as

$$n = n_0 + \Delta n = n_0 + n_2 I \tag{1.22}$$

where n is the total refractive index, n_0 is the linear refractive index, n_2 is the nonlinear refractive index and I is the intensity of the light.

Table 1.1 Typical Values of Nonlinear Refractive Index

Mechanism	$n_2 (cm^2 / W)$	x ⁽³⁾ (esu)	Response Time (s)
Electronic polarization	10-16	10-14	10-15
Molecular orientation	10-14	10-12	10-12
Electrostriction	10-14	10-12	10-9
Saturated absorption	10-10	10-8	10-8
Thermal effects	10-6	10-4	10-3
Photorefractive effect	Large	Large	Intensity-dependent

The time-averaged intensity of the optical field Eqn. 1.22 is given by

$$I = \frac{n_0 C}{2\pi} |E(\omega)|^2 \tag{1.23}$$

where $E(\omega)$ is the amplitude of the incident light. The nonlinear refractive index is related to the third-order nonlinear optical susceptibility by the relation

$$n_2 = \frac{12\pi^2}{n_0^2 c} \chi^{(3)} \tag{1.24}$$

Even a small change in the refractive index in the order of 10-8 can lead to the dramatic nonlinear optical effect. The origin of thermal nonlinear optical effect is termed as some fraction of the incident laser

power is absorbed while passing through an optical material. The change in the refractive index is due to the increase in the temperature of the illuminated portion of the material. Thermal effects can be expressed by the power/intensity in a continuous wave (CW) laser and by the pulse energy (fluence) in a pulsed laser. In the case of a CW laser beam, thermal effects are usually more dominant. The maximum temperature at the center of the laser beam with radius R is

$$T_1^{max} = \frac{\alpha I^{max} R^2}{K} \tag{1.25}$$

where α is the linear absorption coefficient, I^{max} is the laser intensity at the center of the laser and k is the thermal conductivity.

Nonlinear refraction due to thermal contributions is the change in the index due to a temperature rise ΔT that can be expressed by

$$\Delta n = \frac{dn}{dT} \Delta T \tag{1.26}$$

where $\frac{dn}{dT}$ is called the thermo-optic coefficient. In most liquids and solids, it is due to a density change (i.e., expansion) with temperature. Since the density decreases in expansion and the refractive index are proportional to density, this contribution $\frac{dn}{dT}$ is generally negative [1]. In some semiconductors, the absorption band edges are red-shifted with temperature (Franz–Keldish effect). This produces a positive thermo-optic coefficient. When a laser beam with a Gaussian intensity distribution is incident upon a medium, a refractive index gradient is induced in the medium as the index follows the shape of the beam. Hence, the medium acts as a positive or negative lens to focus or defocus the laser beam. Self-focusing occurs when a light beam of non-uniform intensity falls on a medium with a nonlinear index of refraction. As illustrated in Fig. 1.3(a), since the nonlinear index follows the shape of the beam (for local effects without

saturation), an index gradient is induced in the medium. For a positive nonlinearity, with greater index, larger phase retardation is induced at the on-axis than in the wings of the beam. This has the effect of creating a positive lens that tends to focus the beam [1]. For thick media with negative nonlinearities, the beam diverges rather than collapses due to the negative lens effect. For most cases, when the temperature increases the nonlinear refractive index decreases. Thus in a medium, that absorbs part of a Gaussian beam, the index at the on-axis is smaller than that in the wings, and the beam thus diverges (Fig. 1.3(b)). This is called a self-defocusing. Negative nonlinearities can also occur in resonant systems.

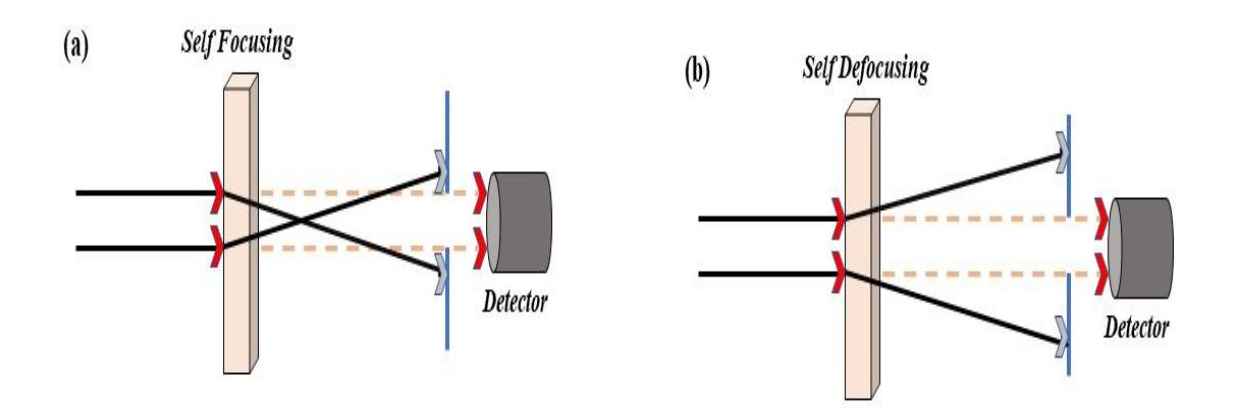


Figure 1.3 Schematic Illustrations of (a) self-focusing $(n_2 > 0)$ and (b) Self- defocusing $(n_2 < 0)$

1.4 Frequency Doubling: Second Harmonic Generation

In the history of nonlinear optics, the discovery of optical harmonic generation marked the birth of the field [4]. The effect has since found wide applications as a means to extend the coherent light sources to shorter wavelengths. Probably the simplest second-order process is the second harmonic generation. In this process, an intense laser beam of angular frequency $\omega_1 = 2\pi v_1$ is passed through a crystal having a nonzero value of $\chi^{(2)}$ such that the beam emerging

from the crystal contains the angular frequencies ω_1 of the input beam and also $\omega_2 = 2\omega_1$, twice the frequency of the input beam. This can be shown to occur by considering the field incident on a medium has the form

$$\mathbf{E} = \mathbf{E}_0 \cos \omega \mathbf{t} \tag{1.27}$$

Substituting this in Eqn. 1.5,

$$\mathbf{P} = \varepsilon_0 (\mathbf{P}_0 + \chi^{(1)}.E_0 \cos \omega t + \chi^{(2)}.E_0^2 \cos^2 \omega t + \chi^{(3)}.E_0^3 \cos^3 \omega t + \dots)$$
 (1.28)

using the following relations

$$\cos^2 \omega = \frac{1 + \cos 2\omega}{2}$$
 ; $\cos^3 \omega = \frac{\cos 3\omega + 3\cos \omega}{4}$

Now rewriting Eqn. 1.28 can be written as

$$\mathbf{P} = \varepsilon_0 [\mathbf{P}_0 + (\frac{1}{2}\chi^{(2)}.E_0^2 + \chi^{(1)} + \frac{3}{4}\chi^{(3)}.E_0^2)E_0 \cos \omega t + \frac{1}{2}\chi^{(2)}.E_0^2 \cos 2\omega t + \frac{1}{4}\chi^{(3)}.E_0^3 \cos 3\omega t + \dots]$$
(1.29)

The first term is a constant term. It gives rise to a dc field across the medium, the effect of which is of comparatively little practical importance. The second follows the external polarization and is called the first or fundamental harmonic of polarization; the third oscillates at a frequency 2ω and is called the second harmonic of polarization, the fourth is called the third harmonic of polarization and so on. The polarization oscillating at a frequency 2ω radiates an electromagnetic wave of the same frequency, which propagates with the same velocity as that of the incident wave. The wave, thus, produced, has the same characteristics of directionality and monochromatic as the incident wave and is emitted in the same direction. This phenomenon is known as the *Second Harmonic Generation* (SHG).

The goal when attempting to generate useful second-harmonic radiation is to maximize its intensity. Under certain conditions, it is **16** | P a g e

possible to convert nearly all of the fundamental frequency of the beam to the second harmonic frequency. It is described as a simple picture of SHG from a wave standpoint in Eqn. 1.9. However, it can also be considered from the photon standpoint. Consider the energylevel diagram of Fig. 1.2(b). It shows two photons of the fundamental frequency,ω, each with energy ħω, combining to produce an energy of The energy levels $\hbar\omega$ and $2\hbar\omega$ are shown as dashed lines because they are not Eigen states of the material in which the second harmonic radiation is generated but are instead levels of the combined material-photon beam system. In that sense, they are known as virtual levels, since they are not levels that accrue population. Instead, two photons of frequency ω are destroyed and one photon of frequency 2ω is simultaneously created as indicated in Fig. 1.2(b). Similarly the other second-order effects such as sum and difference frequency generation, optical parametric oscillation can be explained [7].

In general, crystals that show second harmonic generation are doubly refracting. It is possible to cut the crystal so that the velocity of the ordinary beam of one harmonic is equal to the velocity of the extraordinary beam of the other harmonic. The first and second harmonics can then travel at the same velocity and maintain the constant phase relation through the crystal. This arrangement is known as phase matching. Phase matching plays a very important role in determining what nonlinear processes will predominate in any given experimental arrangement. Perfect phase matching is possible in noncubic crystals if one uses a combination of ordinary and extraordinary rays at different frequencies. It has been observed that the efficiency of the harmonic generation depends not only on the

intensity of the exciting radiation but also on its direction of propagation in crystal.

Suppose a plane wave at a frequency ω and its second harmonic at 2ω , are propagating in the Z-direction, through a nonlinear material of length L, then the Second Harmonic Generation efficiency, $\mathrm{Eff}_{(SHG)}$ in terms of the fundamental wave vector and second harmonic wave vector is given by

$$Eff_{(SHG)} \propto \frac{\sin[(\frac{1}{2})(2k_1 - k_2)L]}{(\frac{1}{2})(2k_1 - k_2)}$$
 (1.30)

where k_1 and k_2 are the propagation wavenumbers at frequencies ω and 2ω respectively, ($k = 2\pi n/\lambda$), n being the refractive index of the medium which characterizes the spatial variation or the phase of the fundamental and harmonic radiations respectively. This will be maximum when

$$\frac{[(2k_1 - k_2)L]}{2} = \frac{\pi}{2}, \text{ (i.e) } L = \pi/(2k_1 - k_2) = \lambda/[4(n_\omega - n_{2\omega})]$$
 (1.31)

where n_{ω} and $n_{2\omega}$ are the refractive indices at ω and 2ω respectively.

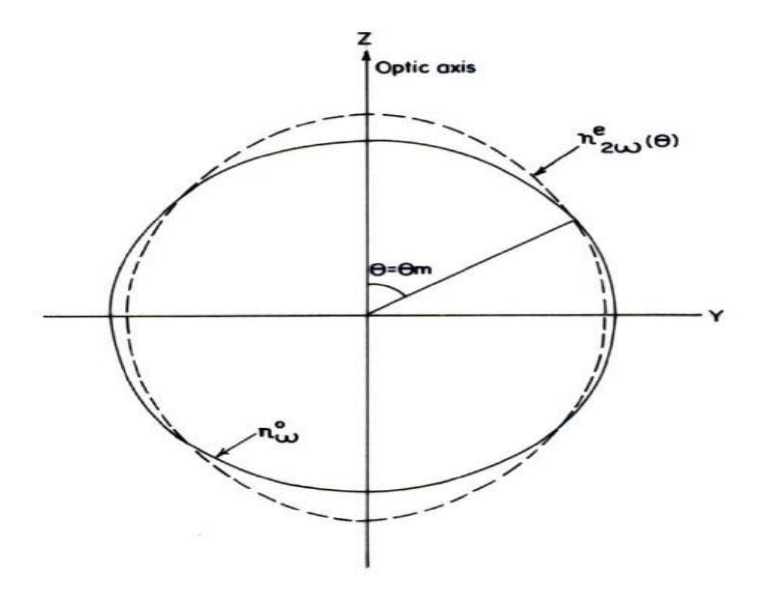


Figure 1.4 Phase Matching – Second Harmonic Generation.

The magnitude of L given by the above equation is called the coherence length for the second harmonic radiation. The expression for intensity is given by

$$I \qquad \propto \qquad \frac{\sin^2[(\frac{1}{2})(2k_1 - k_2)L]}{[(\frac{1}{2})(2k_1 - k_2)]^2} \tag{1.32}$$

for I to be maximum $(2k_1-k_2)L = 0$ (i.e) $k_2 = 2k_1$. For efficient frequency doubling, this relation must be satisfied (Fig. 1.4). This requirement is called the phase-matching criterion which follows that $n_{2\omega} = n_{\omega}$. Thus phase-matching condition becomes refractive index criterion and is one of the key component for device fabrication [7].

1.5 Optical Limiting

An optical limiting (OL) is an effect in which the power, irradiance, energy, or fluence transmitted by an optical system is kept below the maximum value, regardless of the magnitude of the input, while maintaining high transmittance at low input powers. The amplified applications of such an effect are the protection of sensitive optical sensors and components from laser damage. There are countless viable applications for such effects, including laser power regulation or stabilization, or restoration of signal levels in optical data transmission or logic systems. An ideal optical limiter exhibits a linear transmission below the threshold, but above this limit, its output intensity is constant. Optical limiters have been exploited in a variety of footing where a decreasing transmission with increasing excitation is enticing. Range of NLO phenomena used to design an optical limiter includes absorptive processes such as reverse saturable absorption, two-photon absorption, and free-carrier absorption, refractive processes such as self-focusing, self-defocusing, photorefraction, and optically induced scattering [13-15].

Although there is a great variety of OL effect, most of them can be classified into two categories: one is the energy spreading, and the other is the energy-absorbing. The nonlinear refraction based OL effect can be induced by the self-focusing, self-defocusing, scattering, refraction, and aberration in nonlinear optical media. In this condition, the key requirement is to place an aperture in front of a detector and the limiting is due to the change in the spatial energy distribution of the transmitted laser beam. When the input laser intensity increases, there will be more portions of the incident laser energy spreading, as a result, the portion passing through a small aperture will decrease accordingly. Consequently, all devices based on these mechanisms can be called energy spreading optical limiters. The nonlinear absorption-based optical limiting does not require any aperture or pinhole and the OL relies on the fact that the transmissivity for some nonlinearly absorbing media decreases when the input laser intensity increases. The major nonlinear optical absorption mechanisms employed for OL are reverse saturable absorption and two-photon absorption. They are generally called as the energy-absorbing optical limiters [16].

In a nonlinear absorbing medium, the transmitted laser intensity I can be generally expressed as

$$I(Z) = T(I_0)I_0 (1.34)$$

where I_0 is the input intensity, $T(I_0)$ is the transmissivity of the medium and it is a decreasing function of I_0 . The RSA is a two-step and sequential one-photon absorption process and is displayed in Fig. 1.2. In this case, a certain number of molecules are excited to an excited state 2. For a properly chosen medium, the excited molecules may make a further transition from the excited state 2 to a higher excited state 3 via another N_2 in state 2 and the incident intensity I.

On the other hand, N_2 is proportional to I and N_1 , *i.e.*, $N_2 = s_{12} / N_1$, where σ_{12} is the cross-section of the transition from the ground state 1 to the state 2. As intensity increases, the molecule number N_2 continuously grows and the sequential one-photon absorption due to the transition from state 2 to state 3 become more significant, provided that the cross-section,

$$\frac{dI(Z)}{dZ} = \sigma_{12} \left(N_1 - N_2 \right) I(Z) - \sigma_{23} N_2 I(Z) \tag{1.35}$$

In the simplest case, it can be assumed that $N_1 >> N_2$, $N_3 > 0$, where N_0 is the density of the absorbing molecules. Then

$$\frac{dI(Z)}{dZ} = \sigma_{12}N_0I(Z) - b\sigma_{12}\sigma_{23}N_0I^2(Z) = \alpha_0I(Z) - \beta I^2(Z)$$
(1.36)

where $b = bs_{12}s_{23}N_0$ and $a_0 = s_{12}N_0$ is the nonlinear and linear absorption coefficient respectively. The solution of Eqn. 1.39 is

$$I(Z) = \frac{I_0 e^{-\alpha_0 Z}}{1 + (1 - e^{-\alpha_0 Z}) \frac{\beta}{\alpha_0} I_0}$$
(1.37)

If the linear absorption coefficient is assumed to be small, then

$$T(I_0) = \frac{I(Z)}{I_0} = \frac{T_0}{1 + \beta Z I_0}$$
 (1.38)

Here, T_0 is the linear transmissivity of the sample medium for a weak input light signal and $T(I_0)$ is the intensity-dependent dynamic transmissivity of the same medium for a high-intensity laser beam. From Eqn. 1.38 it can be seen that the dynamic transmissivity decreases when the input intensity increases. This is the simplest quantitative description of RSA [17].

In the 2PA process, the molecular transition from the ground state 1 to an excited state 2 is accomplished via an intermediate state that is represented by a virtual energy level as shown in Fig. 1.2. Here 2PA based devices are suitable not only for optical limiting but also for other applicable purposes such as optical power stabilization, optical pulse reshaping, optical spatial field reshaping as it exhibits the advantage of (i) negligible linear absorption loss for weak signal, (ii) extremely fast temporal response and (iii) retaining high beam quality of the transmitted signal [18].

All materials exhibiting nonlinear absorption must also exhibit nonlinear refraction. This can usually be expressed as

$$n_{eff} = n_0 + n_2 I + \sigma_r N_{ex} (1.39)$$

where n_2 describes instantaneous index changes proportional to incident irradiance and σ_r describes the change in the index due to the population of excited states. Third-order optical nonlinearities, n_2 is related to the 2PA coefficient by Kramers - Kronig relations [13]. As focused beam has a spatially varying irradiance, the induced refractive index change varies across the beam profile, causing the beam to be strongly distorted upon propagation. Near focus, the beam is usually brightest in the center, so for a negative index change, the nonlinear material will behave like a lens with negative focal length, and the beam is defocused. This process is referred to as self-defocusing. If the sign of the index change is positive, self-focusing results. An advantage of this method over nonlinear absorption devices is that there is no need to absorb a large amount of energy in the nonlinear material, which could cause thermal damage problems.

In case of nonlinear absorption, for low incident intensity or fluence, the device has linear transmittance. For 2PA, this transmittance may be nearly 100 % and the input-output curve has a slope of 45°. On the other hand, RSA materials require a certain amount of linear

absorption and thus input-output slope in the linear regime is less than 45 °. At critical intensity or threshold in an ideal limiter, the transmittance changes abruptly and exhibits an inverse intensity or fluence dependence. Thus the output is clamped at some value that can presumably be less than the amount required to damage the sensor. This clamped output is called optical limiting value. In real materials, this optical limiting threshold is defined as the input intensity or fluence for which the transmittance decreased by a factor of 2 from its value in a linear regime as shown in Fig. 1.5 [2].

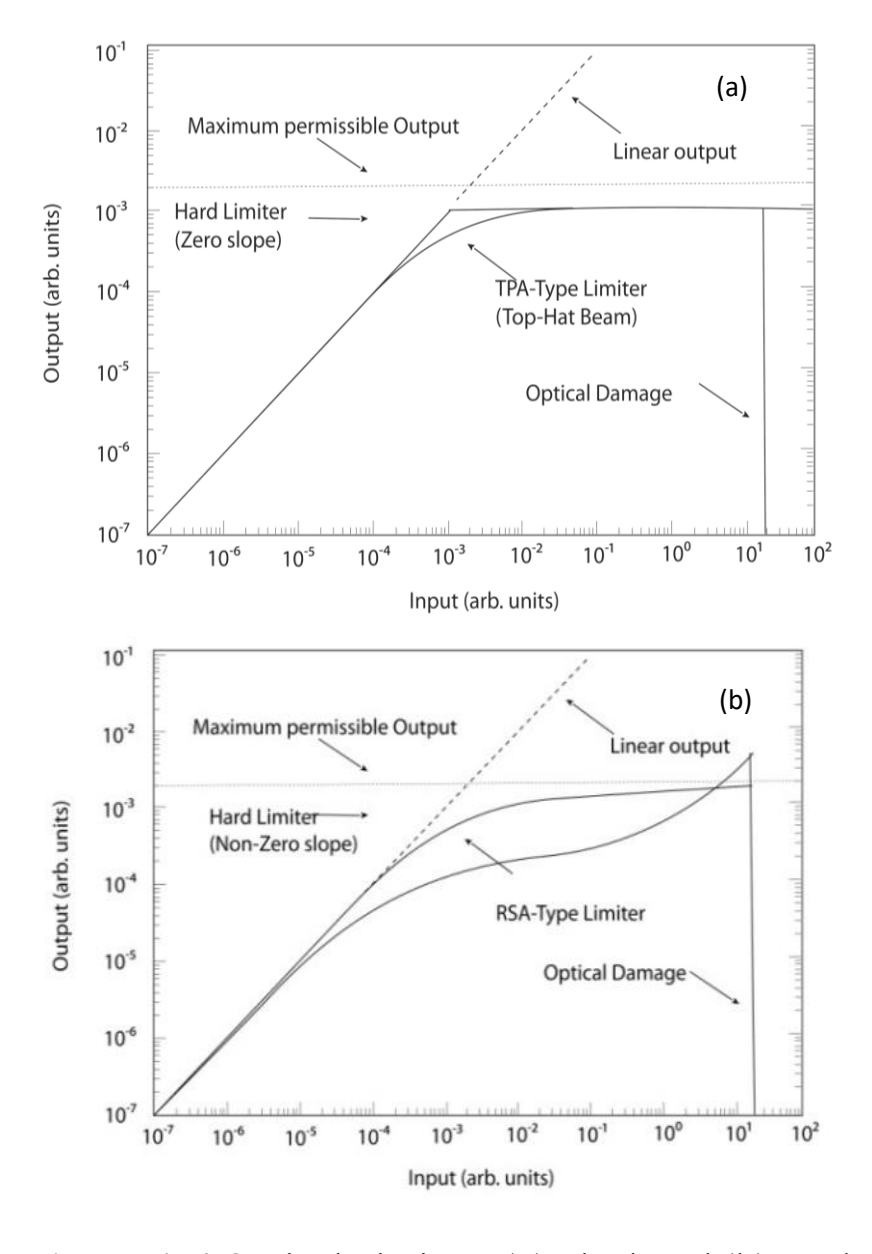


Figure 1.5 Optical Limiters (a) Ideal and (b) Real

An optical limiter must protect a wide range of incident intensity or fluence. Thus if the input-output slope is nonzero, at some point above the threshold, the device will fail to provide protection. In some cases, the material itself may be damaged if its damage threshold is below this point. Any of these situations will define a maximum input for which the device will provide effective limiting. The ratio of this input value to the threshold is called the dynamic range of the limiter.

Most of the laser safety devices available in market are limited in their applications. Traditional fixed-line filters works on selective absorption or reflection of unwanted wavelengths that can be effective against both dazzling and damages. But it is limited in application as advanced knowledge of the threat wavelengths is required. Tunable filters fix the threat wavelength and fine-tune a filter to remove the unwanted radiation. These devices are limited due to their slow response time and ineffective against laser damages sources. Optical limiters (OL) provides decreasing of transmittance as a function of intensity so that the high intensity radiation is effectively suppressed. Limits of optical limiters are although minimal to be ignored, one major concern is that it works on the principle of NLO and thus sensitive to experimental conditions. Detailed investigation on the influence of laser wavelength, peak intensities, pulse duration in altering the optical limiting threshold should be known precisely.

1.6 Definition of the Problem and Materials Selection

Nonlinear optical (NLO) materials play a major role in nonlinear optics and in general, they have made a greater impact on information technology and industrial applications, in particular. In 1989, a new group of nonlinear materials called semiorganic was introduced. These metal complexes satisfy very different demands of second-order NLO materials such as switchable, tunable and multidimensional

properties depending on the suitable interplay of structure-property relationships. It offers a wide range of metals with different oxidation states and ligands, which can give rise to tunable electronic properties. Semiorganic NLO crystals are expected to possess the advantages of both inorganic and organic materials. The metal-organic coordination complexes can provide an enhancement physicochemical stability, breaking up of the centrosymmetry of the ligand in the crystal and an increase in NLO intensity via the metalligand bridging interactions. The central metal ion not only offers a certain anisotropic field to keep the NLO-active chromophore ligands in a favorable acentric arrangement but is also involved in the NLO process. The hyperpolarizability value can drastically vary with the electronic configuration of metal ions.

Nonlinear organic materials have proved to be interesting candidates for several applications like second harmonic generation, electro-optic modulation, frequency mixing, optical parametric oscillation, etc. The superiority of organic NLO materials results from their versatility and the possibility of tailoring them for a particular end use [19]. The optical nonlinearity of organic molecules can be enhanced by adding strong electron-donating and withdrawing entities as well as optimizing the distance between donor and acceptor. This generates a highly polarizable charge transfer compound with an asymmetric electron distribution. Studies show that conjugated organic molecules with large delocalized π-electron systems exhibit measurable nonlinear optical and electro-optical effects. The ideal material that can have potential applications in nonlinear optical devices should possess a combination of properties as high laser damage threshold, fast optical response, flexible for molecular design, optical transparency, mechanical stability, thermal stability and ease of fabrication [20]. Compared with inorganic NLO materials, organic materials may fulfill many of these requirements, but there are also some drawbacks to organic NLO materials, such as environmental stability, mechanical strength, and performance at low and high temperatures. Since organic materials offer a very wide range of chemical modification, some of these problems can be overcome [21]. Recent growing efforts in molecular engineering suggest that organic NLO materials possess comparably better NLO properties than inorganic and hence, their tremendous practical potentials have been anticipated.

As second-order nonlinearity is the most commonly occurring nonlinear optical phenomenon, it is necessary to know some of the basic requirements of materials to exhibit second-order nonlinear (SONLO) effects [15]. As a general rule, the basic requirements apart from the noncentrosymmetric of the crystal structure are,

- i) The material should be polarizable (the electrons need to be greatly perturbed from their equilibrium positions)
- ii) Asymmetric charge distribution (incorporation of a donor-acceptor molecule)
- iii) A pathway of π -conjugated electrons
- iv) Relatively large d_{ijk} coefficient $(d_{ijk} = \chi_{ijk}/2)$
- v) Moderate birefringence
- vi) Wide transparency range for operating wavelengths
- vii) High laser-induced damage threshold
- viii) Ease of growth
- ix) Low materials cost
- x) Good mechanical, thermal and chemical stability

An optical limiter must protect a wider range of incident intensity or fluence. Thus if the input-output slope is non-zero, at some point above the threshold, the device will fail to provide protection. In some cases, the material itself may be damaged if its damage threshold is below this point. Any of these situations will define a maximum input for which the device will provide effective limiting. The ratio of this input value to the threshold is called the dynamic range of the limiter. In consolidation, the desirable attributes that are essential for an optical limiter are [15],

- i) Low threshold
- ii) Wide dynamic range
- iii) Fast optical response
- iv) Broadband response
- v) Low insertion loss / high linear transmittance
- vi) Optical clarity / low optical scattering
- vii) Color neutrality
- viii) Robustness

The main interest in this work is focused on the identification of novel materials for NLO applications. The major concerns of the electro-optical sensors that are widely used in laser applications are susceptible to overexposure leading to permanent optical damage. Laser protection measures are typically realized using conventional effects. optical filters based on absorption or interference Unfortunately, these filters work only for predefined wavelength, but not beyond. A laser beam of high intensity can damage the retina and optical components, for this reason, significant research effort has been invested into optical power limiting materials to achieve some measure of protection from such high-intensity laser beams. An ideal

optical limiting material must possess high linear transmittance, color neutrality, robustness, broadband limiting response, low limiting threshold and high damage threshold for practical applications. However, single materials that meet all the characteristics are currently unavailable in the pre-realm of graphene. This is because graphene is an interesting layered carbonaceous material that has two-dimensional one-atom-thick sp²-bonded carbon networks, which has attracted great attention due to its unique electronic, mechanical, optical and thermal properties. Oxygen-containing groups, such as hydroxyl, epoxy, carbonyl, and carboxylic on GO sheets not only promote the dispersion of GO but also can be used to decorate the GO surface with various functional groups. The most attractive property of GO is that it can be (partly) reduced to graphene-like sheets by removing the oxygen-containing groups with the recovery of a conjugated structure. The reduced GO (rGO) sheets are usually considered as one kind of chemically derived graphene. Layer structured carbonaceous materials like GO and rGO stand high in this domain due to their stronger nonlinear optical response. However, the basic requirement of high linear transmittance limits the possible usage as a power limiter [22-24].

Improvement of linear transmittance along with enhanced NLO action can be achieved through nanocomposite formation that possesses rGO as host-matrix and known NLO material as a decorative element. The availability of several types of oxygen-containing functional groups on the basal plane and the sheet edge allows GO to interact with a wide range of inorganic and organic materials so that functional hybrids and composites with unusual properties can be readily synthesized. In the process of nanocomposite formation, optimization of rGO that resembles the behavior of

graphene is very important and different reduction processes result in different properties that in turn affect the final performance of materials or devices composed of rGO. Though the final target to achieve perfect graphene is hard to reach, research efforts have continuously made it closer. The reduction of graphene was mainly aimed at eliminating epoxy and hydroxyl groups on the plane, while others, e.g. carboxyl, carbonyl, and ester groups, will present at the edges or defective areas of rGO sheet. These functional groups will act as nucleation centers to allow decoration of many organic/inorganic NLO materials and thus optimization of desired content of these oxygen-containing functional groups is very important. In the choice of inorganic materials, barium borate (BBO) nanostructures will be an interesting candidate, as it possesses large second harmonic unique characteristics generation (SHG) and has like transparency, large birefringence, high optical threshold and excellent mechanical properties [14]. Especially 1D nanostructures are an ideal system not only for understanding the functional phenomena in low dimensional systems but also for developing new generation nanodevices with high performance. Recent reports show that barium borate nanorods possess superior third-order NLO properties than benchmark OL materials like C60 [25-28]. Thus decorating BBO nanorods upon rGO can yield BBO-rGO nanocomposite.

Compared to inorganic NLO materials, the inclusion of semiorganic NLO materials in rGO can yield high NLO coefficient nanocomposites. This is because the carbon atom has the great ability to form a stable hybridized bonds like a two-electron covalent bond σ Csp³- Csp³ and a four-electron bond σ + π Csp²- Csp² which provides diverse properties of organic compounds. The presence of π -electrons in an organic molecule differentiate organic NLO materials from

inorganic systems. Among the available chromophore, a polarizable organic molecule 4-dimethyl aminopyridine (DMAP), can be selected as a guest and anchored onto inorganic host orthophosphoric acid. The hydrogen bond networks formed will provide new crystalline material, 4-dimethylaminopyridinium semiorganic dihvdrogen phosphate (DMAPDP) with improved stabilities [29, 30]. Also, 2-amino 5-nitropyridine (2A5NP) can induce a high NLO character with a strong donor (NH₂) and acceptor (NO₂) group through a push-pull mechanism. In particular, the derivatives of 2-amino 5-nitropyridine with the interaction of orthophosphoric acid (2A5NP dihydrogen phosphate (2A5NPDP)) and boric acid (2A5NP fluoroborate (2A5NPFB)), are efficient NLO materials as it can attach inorganic elements to its herringbone pattern [31-35]. Manivannan et. al., reported that the crystal structure of host-guest hydrogen-bonded semiorganic NLO material 2-amino 5-nitropyrinium fluoroborate (2A5NPFB) belongs to noncentric space group Fdd2. Spectral analysis and the second harmonic generation capability of 2A5NPFB was discussed [36]. Rajkumar et. al., have grown bulk single crystals of 2-amino 5nitropyrinium dihydrogen phosphate (2A5NPDP) by Sankaranarayanan-Ramasamy method [37].Earlier Pricilla Jeyakumari et. al., have reported the synthesis, growth, and characterization of 2A5NPDP single crystals. Their SHG efficiency and phase matching capability were determined [38]. Y. Morel et. al., reported the three-photon absorption behavior of 2A5NPDP under nano pulse excitation. Their absorbance properties and polarization dependence for different crystal orientations were discussed [39]. Single crystals of 4-dimethyl aminopyridinium dihydrogen phosphate (DMAPDP) were grown by slow evaporation by Dhanuskodi et.al., Their thermal stability and thermo coefficients were determined by an improved photopyroelectric effect [40]. Earlier the laser damage **30 |** Page

studies along with crystal and molecular structure of DMAPDP were reported [41]. Inclusion of these semiorganic NLO materials as decorative elements in GO can yield interesting nanocomposites suitable for power limiting applications.

Table 1.2 NLO Coefficients of Prominent NLO Materials

Compound	Notable NLO coefficients	Prominent NLO Phenomenon
β-BBO [14]	η_{SHG} = 6 times KDP, LDT = 5 GW/cm ²	SHG
2A5NPFB [36]	η_{SHG} = 40 times KDP, LDT = 7.48 GW/cm ²	SHG
2A5NPDP [37]	η_{SHG} = 4.17 times KDP, LDT = 2.76 GW/cm ²	SHG
DMAPDP [40]	$LDT = 4.8 \text{ GW/cm}^2$	THG
BBO NR [25]	$\beta = 0.17 \times 10^{-10} \mathrm{m/W}$	OL
GO [22]	$\beta = 6.19 \times 10^{-11} \mathrm{m/W}$	OL
GO/Au [23]	$\beta = 1.1 \times 10^{-11} \mathrm{m/W}$	OL
GO-Ag [23]	$\beta = 30 \times 10^{-11} \mathrm{m/W}$	OL
rGO-PbS [24]	$\beta = 7.9 \times 10^{-10} \mathrm{m/W}$	OL

 η_{SHG} = SHG efficiency; LDT = Laser Damage Threshold; β = Nonlinear absorption coefficient; SHG = Second Harmonic Generation; THG = Third Harmonic Generation; OL = Optical Limiting

Table 1.2 summarizes the notable materials chosen for investigation along with their prominent NLO phenomena and its NLO

Coefficients. It is to be noted that barium borate, 2A5NPFB, 2A5NPDP and DMAPDP are identified as well-known NLO crystals useful for harmonic generation applications. At the same time, after the discovery of Graphene notable work on NLO behaviour Graphene Oxide is also made and it revealed the possible utilization of the material in optical limiting applications. As the literature portrays the possibility of improving NLO coefficients of Graphene systems through functionalization, several works on Graphene derivatives are made all over the world. Based on this facts, attempts are made to incorporate known inorganic (BBO) and semiorganic (2A5NPFB, 2A5NPDP and DMAPDP) NLO upon Graphene Oxide and study their NLO response. Thus this thesis aims to investigate the following pure and decorated GO nanocomposite for frequency doubling and optical limiting applications

- 1. Graphene oxide (GO) and Reduced Graphene Oxide (rGO)
- 2. Barium borate nanorods decorated Reduced Graphene Oxide (rGO: BBO)
- 3. 2-amino 5-nitiropyridinium fluoroborate decorated Graphene Oxide (GO: 2A5NPFB)
- 4. 2-amino 5-nitiropyridinium dihydrogen phosphate decorated Graphene Oxide (GO: 2A5NPDP)
- 5. 4-Dimethyl- aminopyridinium Dihydrogen Phosphate decorated Graphene Oxide (GO: DMAPDP)

1.7 Experimental Techniques

1.7.1 Crystal Growth: Solvent Evaporation Method

A solid which consists of atoms or molecules arranged periodically is called crystal. In the 20th century, contributions of crystal growth in fabricating electronic and optical devices have 32 | Page

thrown more light on the importance of crystals. Crystal growth is a controlled phase of transformation, either from solid or liquid or from gaseous phase to solid phase. Fundamental aspects of crystal growth had been derived from early crystallization experiments in the 18^{th} and 19^{th} centuries. Crystal growth is a highly complex phase change phenomenon that deals with the technology of controlling phase transition that leads to solids. The crystal growth methods are broadly classified into four main categories depending on the phase transition involved in the process as Solid-state growth (Solid \rightarrow Solid), Melt growth (Liquid \rightarrow Solid), Vapor growth (Vapor \rightarrow Solid) and Solution growth (Liquid \rightarrow Solid) [42-46].

Among these methods, low-temperature solution growth (LTSG method) is the easiest and most effective way for growing a variety of crystals at the ambient condition or even at room temperature. Materials having low to high solubility in the temperature range ambient to 70 °C and at atmospheric pressure can be grown by using a low-temperature solution growth method. In this method, a saturated solution of the material is prepared in a suitable solvent and crystallization is initiated by slow cooling of the solution or by the slow evaporation of the solvent. In the Slow evaporation method, the temperature is fixed constant and provision is made for evaporation. With non-toxic solvents like water, it is permissible to allow evaporation into the atmosphere. Typical growth conditions involve temperature stabilization to about ± 0.01 °C and rates of evaporation of a few mm³/hr. This method is the only one that can be used with materials having a very small temperature coefficient of solubility [47-54].

The advantages of crystal growth from low-temperature solution nearer the ambient temperature result in simple and straight forward equipment design which gives a good degree of control accuracy at ± 0.02 °C. Due to the precise temperature control, the supersaturation can be very accurately controlled. Also, an efficient stirring of solution reduces fluctuations to a minimum. The low-temperature solution growth technique is well suited to those materials which suffer from decomposition in the melt or the solid at higher temperatures and the materials which undergo structural transformations while cooling from the melting point and numerous organic and inorganic materials which fall in this category can be crystallized by using this technique. The low-temperature solution growth technique also allows a variety of different morphologies and the polymorphic forms of the same substance can be grown by varying the growth conditions of a solvent [55]. The proximity to ambient temperature reduces the possibility of major thermal shock to the crystal both during growth and removal from the apparatus.

1.7.2 Nanomaterial Preparation: Hydrothermal Synthesis

Since the size and shape of nanostructures, size distribution and surface chemistry have a great impact on features and behaviors of the nanocomposite, preparation methods play a key role in practical aspects. Also, the preparation method determines the degree of structural defects and impurities present in the particles as well as the distribution of such defects thereby manipulation of behaviors of nanocomposite can be achieved. Although nanocomposite can be synthesized in different ways, here hydrothermal method is adopted. Some parameters like temperature, pressure, reaction time, type and concentration of precursors can be changed to obtain the desired shape and/or size of products. The hydrothermal process is environmentally friendly since it does not involve any organic solvents or post-treatments. Therefore, the hydrothermal technique has been

widely used to synthesis hybrid complexes as powders, nanoparticles and single crystals using closed-system physical and chemical processes flowing in aqueous solutions at temperatures above 100 °C and pressures above 1 atm. The advantages of the hydrothermal synthesis method include the ability to synthesize crystals of substances which are unstable near the melting point, and the ability to synthesize large crystals of high quality [56, 57].

The main parameters of hydrothermal synthesis, which define both the processes kinetics and the properties of resulting products, are the initial pH of the medium, the duration and temperature of synthesis, and the pressure in the system. The synthesis is carried out in autoclaves which are sealed steel cylinders that can withstand high temperatures and pressure for a long time. Nanopowders are normally produced using either high-temperature hydrolysis reactions of various compounds directly in the autoclave or hydrothermal treatment of reaction products at room temperature; the latter case is based on the sharp increase in the rate of crystallization of many amorphous phases in hydrothermal conditions. In the first case, the autoclave is loaded with an aqueous solution of precursor salts, in the second case - with a suspension of products derived from solution reactions flowing under normal conditions. There is normally no need to use special equipment and maintain a temperature gradient [58, 59].

In the preparation of borate and pyridine derivative decorated graphene oxide composites by hydrothermal method, the autoclave was loaded with an aqueous solution of precursor salts. Care was taken to choose the appropriate temperature for a hydrothermal reaction so that the synthesized molecules do not dissociate themselves during composite formation. At chosen high temperature

and pressure, oxygen-containing functional groups in graphene oxide can undergo reduction along with dehydration by water. The elevated temperatures enhance dehydration rates and cause the high diffusivity of reactants in such situations. High supersaturation obtained in this procedure leads to the nucleation of decorative elements upon graphene oxide. The positively charged decorative complexes can then be intimately mixed with aqueous dispersions of negatively charged GO through electrostatic attraction. Further, the π - π interactions between the GO sheets support the self-assembly process. In fact, as an advantage, a hydrothermal reaction not only results in an easy one-pot reaction for the synthesis of the composite but also efficiently reduces the GO sheets incorporated in the composite. Thus by adopting the hydrothermal method, graphene oxide composites were prepared and used for various characterization.

1.8 Characterization Techniques

In the present study, preliminary identification and crystalline arrangement were analyzed using single-crystal X-ray diffraction was carried out by using $Bruker\ Kappa\ Apex\ II$ diffractometer, with MoKa radiation (λ = 0.71073 Å) in STIC, Cochin. Powder X-ray diffraction of the grown crystals was performed in a $PANalytical\ Xpertpro\ diffractometer$ (Netherlands) using CuKa radiation (λ = 1.5418 Å) in the Department of Physics of Alagappa University, Karaikudi. FTIR spectra were recorded by using $Thermo\ Nicolet\ 370\ FTIR\ spectrophotometer$ (USA) and by applying the KBr pellet technique in STIC, Cochin. Laser Raman studies were carried out using InVia, Renishaw, UK $High\ Resolution\ Raman\ spectrometer$ at the Department of Physics of Bharathidasan University, Tiruchirappalli. The thermal property of the samples was studied by TG-DTA and differential scanning calorimetry (DSC) analyses by using a Perkin Elmer, Diamond TG/DTA and

Mettler Toledo DSC 822e available at STIC, Cochin. The optical properties of the grown crystals were determined from UV-Vis-NIR absorption spectra recorded with a Varian, Cary 5000 spectrophotometer in STIC, Cochin. Nonlinear optical properties of the grown crystals were analyzed by Kurtz Perry powder second harmonic generation (SHG) test using Nd: YAG laser ($\lambda = 1064$ nm) at the Nanophotonics Laboratory, Department of Physics of Bharathidasan University, Tiruchirappalli. The Z-scan studies were performed by using long-lasting diode-pumped Nd: YAG (532 nm, 50 mW) in the Department of Physics, Madras University, Chennai. To realize the practical applications of the materials selected for investigations, it is essential to predict the second and third-order NLO properties. Hence to find suitable materials for frequency conversion and optical limiting applications, the following experiments were performed.

1.8.1 Powder SHG Test

To find suitable materials with desired NLO properties in crystal engineering, one can utilize the theories and the experiments to predict the magnitude of the NLO coefficients of the newly synthesized substances. It is a difficult, time consuming and expensive endeavor to develop single crystal growth methods for new materials. However, for effective analysis, the NLO coefficients of the crystals must be somehow estimated beforehand to optimize the conditions for single crystal growth towards the practical applications. Therefore a relatively rapid and simple method of screening new candidates for frequency conversion applications before crystal growth is needed.

In this context, Kurtz and Perry powder technique represents the first real means of screening the materials for second-order NLO applications. The advantage of this method is that it not only provides a nonlinear coefficient (d_{ij}) values but also determines whether the

material is phase matchable or not. Kurtz and Perry developed a semiquantitative approach to the theory of SHG from powders. Boyd et. al., [2] have shown that the SHG intensity by a single particle can be related by assuming no absorption and low dispersion,

$$I_{2\omega}\alpha \left[d^2L_c^2 \sin^2\left(\frac{\pi r}{2L_c}\right) \right] \tag{1.39}$$

where d is NLO coefficient, r is particle size and L_c is coherence length.

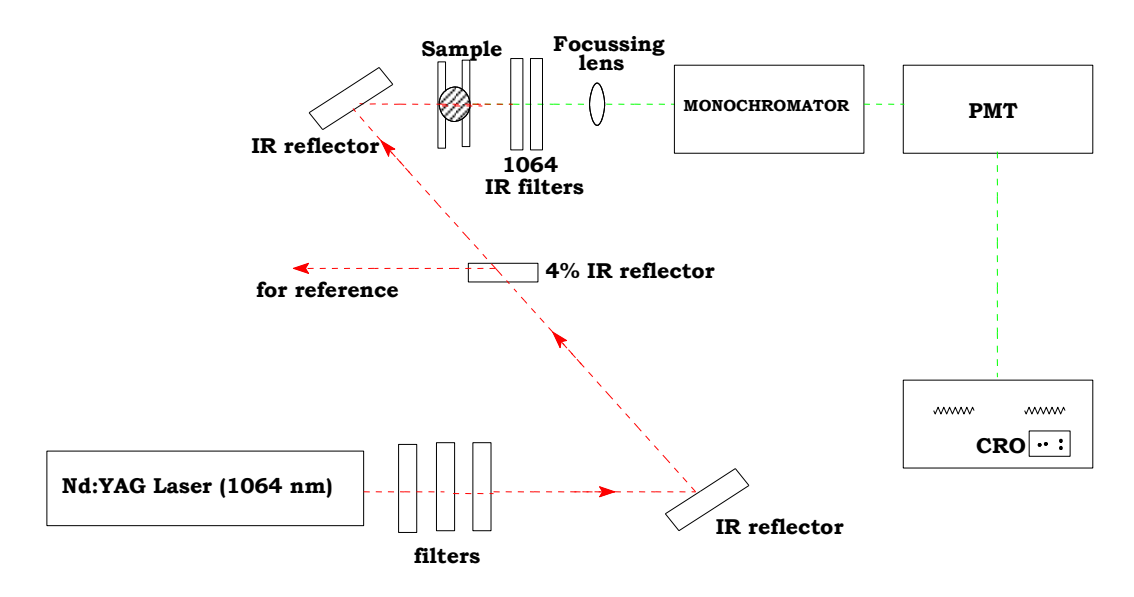


Figure 1.6 Experimental Setup for Powder SHG Measurement

The powder SHG measurements were performed by applying a modified Kurtz-Perry method. The experimental setup for the Kurtz-Perry powder technique used in the present investigation is shown in Fig. 1.6. In this, the particles were initially ground and sieved to obtain a desired particle size range. Then the powder sample was packed tightly in a capillary tube and illuminated by using a Q-switched Nd: YAG laser (1064 nm, 8 ns, 10Hz). The low energy (~ 9mJ) beam is used for excitation. A photodiode was used as a reference to monitor pulse-to-pulse fluctuations in the input beam. The fundamental transmitted wave, IR (1064 nm) was blocked by using RG850.

1.8.2 Z-Scan Study

The intense monochromatic radiation from a laser can induce profound changes in the optical properties of a material. Nonlinear absorption refers to the change in transmittance of a material as a function of input intensity or fluence. For the effective performance of all-optical switches and limiting devices, strong nonlinear absorption is an essential criterion. Nonlinear absorption has also been employed to enhance the optical spectroscopic study of materials. The nonlinear index of refraction or the third-order NLO susceptibility is an important parameter in the optical limiting applications. Measurement techniques include degenerate four-wave mixing, Z-scan, optical Kerr effect and ellipse rotation interferometric methods, two-beam coupling, beam self-bending and third-harmonic generation [18]. Z-scan is a popular technique that is particularly useful for the simultaneous measurement of both the nonlinear refractive index and nonlinear coefficient. The Z-scan absorption method has gained rapid acceptance as a standard technique due to its simplicity in technique and interpretation through the nonlinear optics community. However, it must always be recognized that this method is sensitive to all nonlinear mechanisms that give rise to a change in the refractive index and/or nonlinear absorption coefficient. Various Z-scan methods for data analysis include single beam Z scan, eclipsing Z scan, two-color Z-scan, time-resolved excite probe Z-scan and top hat beam Z-scan [61].

The study of nonlinearity by using the single-beam Z-scan method is based on the intensity dependence of the thin sample along a laser beam. A Gaussian beam is focused by a spherical lens onto the sample and the variation in the beam profile is observed at the far-field as the sample is taken through the focus of the lens. The beam

propagation direction is taken as the Z direction and the sample is moved along that direction, and hence this technique is known as the Z-scan technique. By properly monitoring the transmittance change through a small aperture placed at the far-field position (closed aperture), one can determine the amplitude of the phase shift. By moving the sample through the focus and without placing an aperture at the detector, (open aperture), one can measure the intensity-dependent absorption as the change of the transmittance through the sample. When both methods (closed and open ones) are used for the measurements, the ratio of the signals determines the nonlinear refraction in the sample [18].

Sheik- Bahae et al. [61] and David J. Hagan et al. [60] developed a sensitive self-focusing measurement technique that involves focusing a laser beam through a thin sample and detecting the light transmitted by a small aperture in the far-field. If E is the peak electric field of a Gaussian beam traveling in the +Z direction, then

$$E(z,r,t) = E_0(t) \frac{\omega_0}{\omega(z)} \exp\left(-\frac{r^2}{\omega^2(z)} - \frac{ikr^2}{2R(z)}\right) e^{-i\phi(z,t)}$$
(1.40)

where $\omega^2(z) = \omega_0^2 \left(1 + \frac{z^2}{z_0^2}\right)$ is the beam radius with beam waist as ω_0 and

$$R(z) = z \left(1 + \frac{z^2}{z_0^2}\right)$$
 is the radius of curvature of the wavefront at Z , Z_0

 $(=k\omega_0^2/2)$ is the diffraction length of the beam, $(k=2\pi/\lambda)$ is the wave vector and λ is the wavelength of the laser.

It is important to note that, if the sample length is smaller enough to change the beam diameter within the sample either due to diffraction or nonlinear refraction that can be neglected, the medium is regarded as *thin media*, in which case the self-refraction process is

referred as *external self-action*. For linear diffraction, this implies that L<< Z_0 , while for nonlinear refraction, L<< Z_0 / $\Delta \phi_0$. In most cases, $\Delta \phi_0$ is small and eventually L<< Z_0 is an essential criterion to be achieved. A diode-pumped Nd: YAG laser (532 nm) was used as the excitation source for the *Z*-scan technique. The Gaussian profile laser beam was focused on a 1 mm cuvette containing the 1 mM concentration solution by a lens of focal length 3.5 cm to produce a beam of the waist (ω_0) 15.35 µm. The condition for diffraction length ($Z_0 = \pi \omega_0^2/\lambda > L$) was satisfied so that the sample is considered as a thin medium. The transmission of the beam through an aperture placed in the far-field was measured using a photo detector fed to the digital power meter. For the open aperture *Z*-scan, a lens was used to collect the entire laser beam transmitted through the sample that replaced the aperture.

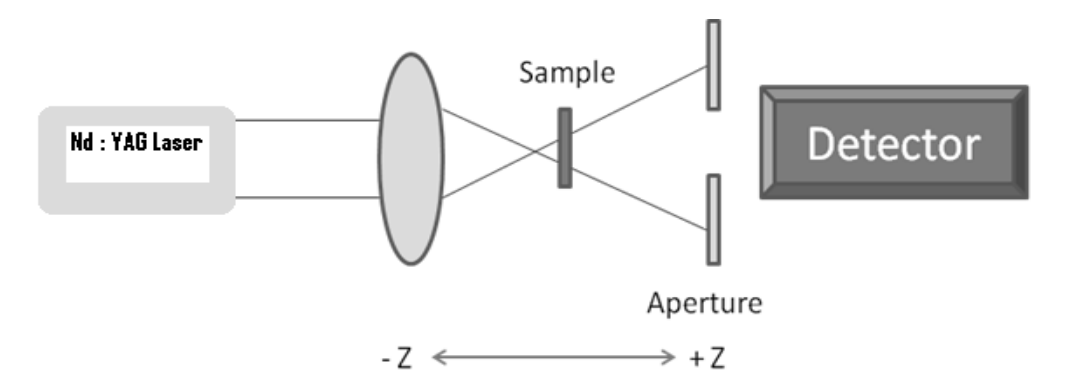


Figure 1.7 Experimental Setup for Z-Scan Measurement

The nonlinear parameters under CW laser illumination were determined by the well-known closed Z-scan set up formulated by Sheik-Bahae et al. [61] and David J. Hagan et al. [60]. The difference between the normalized peak and valley transmission (ΔT_{p-v}) in closed aperture pattern is written in terms of the on-axis phase shift $\Delta \Phi$ at the focus as,

$$\Delta T_{p-\nu} = 0.406(1-S)^{0.25} \left| \Delta \phi \right| \tag{1.41}$$

$$S = 1 - \exp(-2 r_a^2 / \omega_a^2)$$
 (1.42)

where S is the aperture linear transmittance, r_a is the aperture and ω_a is the beam radius at the aperture.

The nonlinear refractive index is given as,

$$n_2 = \frac{\Delta \phi}{K I_0 L_{eff}} \tag{1.43}$$

where $K = 2\pi / \lambda$ (λ is the wavelength of laser), I_0 is the intensity of the laser beam at the focus (Z=0), L_{eff} is the effective thickness of the sample ($L_{eff} = [1-exp(-\alpha L)]/\alpha$), α is the linear absorption coefficient and L is the thickness of the sample. From the open aperture Z-scan data, the nonlinear absorption coefficient β is estimated as,

$$\beta = \frac{2\sqrt{2}\Delta T}{I_0 L_{eff}} \tag{1.44}$$

where ΔT is the one valley value at the open aperture Z-scan curve. The value of β will be negative for saturable absorption and positive for reverse saturable absorption. The real and imaginary parts of the third-order nonlinear optical susceptibility $x^{(3)}$ are defined as

$$\operatorname{Re} \chi^{(3)} = \frac{10^{-4} \left(\varepsilon_0 C^2 n_0^2 n_2 \right)}{\pi} \left(\operatorname{cm}^2 / W \right)$$
 (1.45)

$$\operatorname{Im} \chi^{(3)} = \frac{10^{-2} \left(\varepsilon_0 C^2 n_0^2 \lambda \beta \right)}{4 \pi^2} \text{ (cm / W)}$$
 (1.46)

where ε_0 is the permittivity of vacuum, n_0 is the linear refractive index of the sample and c is the velocity of light in vacuum.

The third-order nonlinear optical susceptibility is thus

$$\chi^{(3)} = \sqrt{\left(\text{Re}(\chi^{(3)})\right)^2 + \left(\text{Im}(\chi^{(3)})\right)^2}$$
 (1.47)

Optical limiting is the nonlinear process in which beyond a

particular fluence (called as onset limiting threshold) the transmittance gets attenuated by a nonlinear process providing the possibility to avoid induced laser damage. The optical limiting curve can be directly drawn by performing the Z-scan experiment at a single position (preferably peak or valley position of closed aperture Z-scan mode). Here the input is varied and the corresponding output is measured.

1.9 Conclusion

The applications of NLO materials are many and hence the demand and search for materials seem to be never-ending. Especially with a need for compact, maintenance-free all-solid-state devices to produce short wavelength (Blue-Green) lasers along with urgent attention in producing safeguarded photosensitive components from an intense laser beam, the discussion presented in the upcoming chapters will be very essential for the research community.

1.10 References

- 1. Y.R. Shen, *The principles of nonlinear optics*, John Wiley, New York, 1984.
- 2. Richard L. Sutherland, *Handbook of nonlinear optics*, Marcel Decker Inc, New York, 2003.
- 3. R.W. Boyd, Nonlinear optics, Academic Press, Boston, 1992.
- 4. P.A. Franken, A.E. Hill, C.W. Peters, G. Weinreich, *Phys. Rev. Lett.* 7 (1961) 118.
- 5. R.W. Munn and C.N. Ironside, (1994), *Principles and applications of nonlinear optical materials*, CRC Press, Inc., USA.
- 6. N.J. Long, Angew. Chem. Int. Ed. Engl. 34 (1995) 21.
- 7. B.B. Laud, *Lasers and nonlinear optics*, New Age international Ltd., New Delhi, 2004.

- 8. P.N. Prasad, D.J. Williams, *Introduction to nonlinear optical effects in organic molecules and polymers*, Wiley, New York, 1991.
- 9. D.S. Chemla, J. Zyss, *Nonlinear optical properties of organic molecules and crystals*, Academic Press, Orlando, 1987.
- 10. D.J. Williams, Angew. Chem, Int. Ed., Engl 23 (1984) 690.
- 11. M. Goppert Meyer, Ann. Phys. 9 (1931) 273.
- 12. M. Rashidian, D. Dorranian, Rev. Adv. Mater. Sci. 40 (2015) 110.
- 13. V.G. Dmitriev, G.G. Gurzadyan, D.N. Nikogosyam, *Handbook of nonlinear optical crystals*, Springer-Verlag, New York, 1999.
- 14. P. Becker, Adv. Mater. 10 13 (1998) 979.
- 15. T.C. Sabari Girisun, *Investigations on Certain Thiourea Based NLO Materials for Frequency Conversion and Optical Limiting Applications*, Ph.D. Thesis, Bharathidasan University, India, 2010.
- 16. M. Bass, Handbook of nonlinear optics, Volume IV Optical properties of materials, nonlinear optics, quantum optics, McGraw Hill, New York, 2010.
- 17. G.S. He, S.H. Liu, *Physics of Nonlinear Optics*, World Scientific Publishing, Singapore, 1999.
- M.G. Kuzyk, W. Dirk, Characterization techniques and Tabulations for organic nonlinear optical materials, Marcel Dekker, New York, 1998.
- 19. H.S. Nalwa, S. Miyata, *Nonlinear optics of organic molecules and polymers*, CRC Press Inc., New York, 1996.
- C. Bosshard, K. Sutter, R. Schlesser, P. Gunter, J. Opt. Soc. Am. B., 10 (1993) 867.
- 21. S.R. Marder, J.W. Perry, W.P. Schaefer, Science, 245 (1989) 626.
- 22. G. Muruganandi, M. Saravanan, G. Vinitha, M.B. Jessie Raj, T.C. Sabari Girisun, *Chem. Phys.*, 488 (2017) 55.
- I. Fuks-Janczarek, J.M. Nunzi, B. Sahraoui, I.V. Kityk,
 J. Berdowski, A.M. Caminade, J. Roncali, Opt. Commun., 209

- (2002)461.
- 24. H. Zeng, J. Han, D. Qian, G. Yuzong, Optik, 125 (2014) 6558.
- 25. W.T. Silfvast, *Laser fundamentals*, Cambridge University Press, New Delhi, 1998.
- 26. C Babeela, T.C. Sabari Girisun, Opt. Mater., 49 (2015) 190.
- 27. T.C. Sabari Girisun, Madhura Somaiyaji, N. Priyadarshani, S. Venugopal Rao, *Mater. Res. Bull.*, 87 (2017) 102.
- 28. T.C. Sabari Girisun, M. Saravanan, G. Vinitha *Opt. Laser Technol.*, 89 (2017) 54.
- 29. J.F. Nicoud, C. Serbutoviez, Y. Barrans, D. Chasseau, I.G. Luneau, I. Ledoux, J. Zyss, *Nonlinear Optics* 9 (1995) 127.
- 30. M.S. Wong, J.F. Nicoud, C. Runser, A. Fort, M. Barzoukas, *Nonlinear Optics* 9 (1995) 181.
- 31. R. Masse, J. Zyss, Molecular Eng., 1 (1991) 413.
- 32. J. Pecaut. Y. L. Fur, R. Masse, Acta Cryst., B49 (1993) 535.
- 33. J. Pecaut. J.P. Levy, R. Masse, J. Mater. Chem., 3 (1993) 999.
- 34. Y.L. Fur, M. Bagieu-Beucher, R. Masse, J.F. Nicoud, J.P. Levy, *Chem. Mater.*, 8 (1995) 68.
- 35. J. Pecaut, R. Masse, J. Mater. Chem., 4 (1994) 1851.
- 36. S. Manivannan, S. Dhanuskodi, K. Kirschbaum, S. K. Tiwari, Cryst. Growth & Design, 5 4 (2005) 1463.
- 37. M.A. Rajkumar, S.S. John Xavier, S. Anbarasu, P.A. Devarajan, *Optik*, 127 4 (2016) 2187.
- 38. A. Pricilla Jeyakumari, S. Manivannan, S. Dhanuskodi, Spectrochimica Acta A- Mol. Biomol. Spect., 67 1 (2007) 83-86.
- 39. Y. Morel, J. Zaccaro, A. Ibanez, PL. Baldeck, *Opt. Comm.*, 201 (2002) 4.

- 40. S. Dhanuskodi, S. Manivannan, K. Kirschbaum, J. Philip, S. Selladurai, *J. Cryst. Growth*, 290 2 (2006) 548.
- 41. S. Manivannan, S. Dhanuskodi, *Cryst. Growth and Design*, 4 (2004) 845.
- 42. D. Elwell and H.J. Scheel, *Crystal growth from high temperature* solutions, Academic Press, London- New York, 1975.
- 43. H.J. Scheel, *Historical introduction*, Chapter 1 in *Handbook of crystal growth*, Elsevier, Amsterdam, 1993/1994.
- 44. J.W. Mullin, *Industrial crystallization* 78, Plenum Press, New York, 1976.
- 45. H.E. Buckley, *Crystal Growth*, John Wiley and Sons, Inc. New York, 1951.
- 46. R.A. Laudice, *The growth* of *single crystals*, Prentice Hall, Inc. New York, 1970.
- 47. B.R. Pamplin, Crystal growth, Pergamon Press, Oxford, 1980.
- 48. J.C. Brice, *Crystal growth process*, John Wiley and Sons, New York, 1986.
- 49. K.A. Jackson, *Mechanism of growth in liquids metals and solidification*, ASM, Cleveland, 1958.
- 50. J.B. Mullin, B.W. Straughan, W.S. Brickell, *J. Phy. Chem. Solids*, 26 (1965) 782.
- 51. R. Udea, J.U. Mullin, *Crystal growth and characterization*, Proc. ISSCG-2 spring school North Holland, Amsterdam, 1975.
- 52. H.K. Heinisch, Crystals *in gels and Liesegang rings*, Cambridge University Press, Cambridge, 1988.
- 53. A.A. Ballman and R.A. Laudise, *The art and science of growing crystals*, John Wiley and sons, New York, 1963.
- 54. J.A. James, R.C. Kell, *Crystal growth*, Pergman press, New York, 1975.

- 55. R.M. Hopper, R.S. Naranes, B.J. Hearole, J.N. Sherwood, *Crystal growth*, Pergamon press, New York, 1980.
- 56. K. Byrappa, M. Yoshimura, *Handbook of Hydrothermal Technology*, Noyes Publications, New Jersey, USA, 2001.
- 57. A. Rabenau, Angew. Chem. Int. Ed., 24 (1985) 1026.
- 58. A. N. Lobachev, *Crystallization processes under hydrothermal conditions*, Consultants Bureau, New York, 1973.
- 59. R. Roy, J. Solid State Chem., 111 (1994) 11.
- 60. D.J. Hagan, E.W. Van Stryland, M.J. Soileau, Y.Y. Wu, S. Guhu, *Opt. Lett.*, 13 (1988) 315.
- 61. M. Sheik-Bahae, A.A. Said, T.H. Wei, D.J. Hagan, E.W. Van Stryland, *IEEE J. Quant. Electron.* 26 (1990) 760.

Chapter - II

Graphene Oxide and Reduced Graphene Oxide Nanostructures

CHAPTER II

Graphene Oxide and Reduced Graphene Oxide Nanostructures

Reduced graphene oxide (rGO) was prepared by reduction method using hydrazine, sodium borohydride and ascorbic acid as reductant and its structure, morphology, emission, absorption and nonlinear optical properties were investigated. The third-order NLO properties of dispersed graphene oxide (GO) and reduced graphene oxide (rGO) was measured using an Nd: YAG green CW laser (532 nm, 50 mW) by employing the Z-scan technique. Results show that the materials possess negative nonlinearity and self-defocusing nature which is responsible for the optical limiting behavior in the regime of interest. It is interesting to note that reduced graphene oxide obtained with different reducing agents show tunable NLO coefficients which may arise due to change in the functional group's concentration and layers of graphene sheets. Hydrazine reduced rGO was found to possess an improved thermal and photostability, and excellent durability, which signifies the scope of utilizing them as smart materials for NLO applications like optical limiters.

2.1 Introduction

The optical limiting (OL) effect is a phenomenon wherein a medium will exhibit high transmittance at a low-intensity light and attenuate an intense optical beam, limiting the output fluence at a certain range. With the extensive use of continuous wave (CW) lasers at power levels ranging from µW to kW in various applications, the need for protecting the human eye and the sensors used in handling the CW output has become increasingly important. The human eye has its spectral sensitivity maximum at a green regime [1]. With widespread usage of low power CW lasers in green (532 nm) region, optical limiters are the most necessary thing to ascertain safety precautions. Nonlinear optical (NLO) materials suitable for passivemode optical limiting and switching applications are currently being explored with great interest. The versatile chemistry of carbon materials, functionalizing as a building block of many fascinating new stable and structurally improved carbon nanomaterials, has resulted a huge interest in studying carbonaceous matter at the nanoscale. Known materials that are found to exhibit a strong OL effect and explored as candidates for practical optical limiters, includes fullerenes [2], phthalocyanines [3], nanoparticles [4], metal nanowires [5], carbon nanotube [6] and organic chromophores [7]. Graphene (G), two-dimensional one-atom-thick sp2-bonded carbon networks, has attracted great attention due to its unique electronic, mechanical, optical and thermal properties [8]. Recently, various methods of preparing graphene have been developed for realizing their potential applications.

Graphene oxide (GO) provides an easy way to produce chemically derived graphene. Oxygen-containing groups, such as hydroxyl, epoxy, carbonyl, and carboxylic on GO sheets not only promote the

dispersion of GO but also can be used to decorate the GO surface with various functional groups. The most attractive property of GO is that it can be (partly) reduced to graphene-like sheets by removing the oxygen-containing groups with the recovery of a conjugated structure [9]. The reduced GO (rGO) sheets are usually considered as one kind of chemically derived graphene. Some other names have also been given to rGO, such as functionalized graphene, chemically modified graphene, chemically converted graphene, or reduced graphene. rGO is a key topic, and different reduction processes result in different properties that in turn affect the final performance of materials or devices composed of rGO. Though the final target to achieve perfect graphene is hard to reach, research efforts have continuously made it closer. The reduction of graphene was mainly aimed at eliminating epoxy and hydroxyl groups on the plane, while others, e.g. carboxyl, carbonyl, and ester groups, present at the edges or defective areas of rGO sheet. Li et. al., [10] reduced GO using hydrazine in a solvent, and the carboxyl groups attached to the GO are preserved after reduction. It exhibits many noteworthy properties, such as a high surface area, superior thermal conductivity, high carrier mobility, and remarkable optical properties. Zhang et. al., [11] reported Z-scan measurements of the nonlinear refraction of graphene due to large sp² hybridized carbon conjugated structure under pulsed excitations [12]. Although the investigation of rGO in the pulsed regime is available in the literature, the study of nonlinear response in the CW regime is still now not available. The main motivation of the present work is to make a systematic investigation of the nonlinear optical properties and their correlation with the structure of some finely dispersed GO and rGO sheets. To hut more light onto the underlying physical mechanisms of the nonlinear optical response, Z-scan experiments was conducted using Nd: YAG (532 nm, 50 mW) laser excitation.

2.2 Materials Preparation

2.2.1 Reduced GO by Using Hydrazine Monohydrate (rGO-H)

Graphene oxide was obtained by a modified method originally proposed by Hummers [13]. First, graphite oxide was synthesized by powerful oxidants (NaNO₃, H₂SO₄, and KMnO₄). The details of this procedure are described elsewhere [13]. Then, GO was obtained by sonication of graphene oxide in 100 ml distilled water for three hours. After that, 1 ml of hydrazine monohydrate (N₂H₂) which acts as a reducing agent was added into the suspension and it was placed in an oil bath at 80 °C for 30 minutes. The oil bath was removed and the solution was placed in a condenser for 24 hours, yielding a black precipitate. After cooling the solution to room temperature (30 °C) the solution was centrifuged and dried to achieve rGO powder.

2.2.2 Reduced GO by Using Sodium Borohydride (rGO-N)

GO (50 mg), was mixed with 50 ml of methanol and they were allowed to disperse for 1 hour. Sodium borohydride (NaBH₄) of 568 g which acts as a reducing agent was added into the solution. The solution was placed in a condenser along with the stirring process at 70 °C for 2 hours. The resulting solution was washed with methanol and double distilled water until the pH becomes neutral. The particles were settled down at the bottom. The clear solution was pipetted out and the sample was dried at 30 °C.

2.2.3 Reduced GO by Using Ascorbic Acid (rGO-A)

GO (0.1 g), was mixed with ascorbic acid (0.1 g). They were mixed with 100 ml of double-distilled water. The solution was allowed to disperse for 30 minutes at 60 °C. 30% of H_2O_2 was added to the solution and once again they were allowed to disperse for 30 minutes

at 60 °C. The resulting solution was washed with double distilled water. Followed by centrifugation, the sample was dried at 120 °C.

2.2.4 Characterization

XRD using a powder X-ray diffractometer with CuKa radiation employing a scanning rate of 0.02 s⁻¹ in the angle of 10 to 80 degrees was recorded. IR studies were carried out by FTIR spectrometer JASCO 460 PLUS from 400 cm⁻¹ to 4000 cm⁻¹ to assign the vibrations functional group of GO and rGO. Morphologies of these samples were investigated by Scanning Electron Microscope (SEM) analysis using Hitachi SEM 400. The optical absorption spectrum was collected for dispersed GO and rGO using UV-Vis-NIR Perkin Elmer Spectrophotometer. The room temperature (30 °C) emission studies were carried out using a Perkin Elmer LS 55 luminescence spectrometer.

2.3 XRD Analysis

The X-ray diffraction pattern (Fig. 2.1) for GO gives a sharp peak at 12° which corresponds to an interlayer spacing of 0.72 nm and it is indexed as (002) plane of GO. Larger interplanar distance arises due to of intercalated water molecules the presence and oxygen functionalities such as carboxyl, epoxy, carbonyl groups, and other The peak shows the crystalline nature of the functional groups. sample due to sp² hybridization. In XRD of rGO (Fig. 2.1), the main peak of GO disappeared completely. rGO has broad peaks located at 26°, 23°, and 24° with the interlayer spacing of 0.34 nm, 0.38 nm, and 0.75 nm for rGO-H, rGO-N, rGO-A respectively and are attributed to the spacing between the carbon layers depending on the reducing agents. The interplanar distance value of rGO-H and rGO-N are calculated to be d=0.34 nm and 0.38 nm respectively which is much smaller than that of GO (0.72 nm).

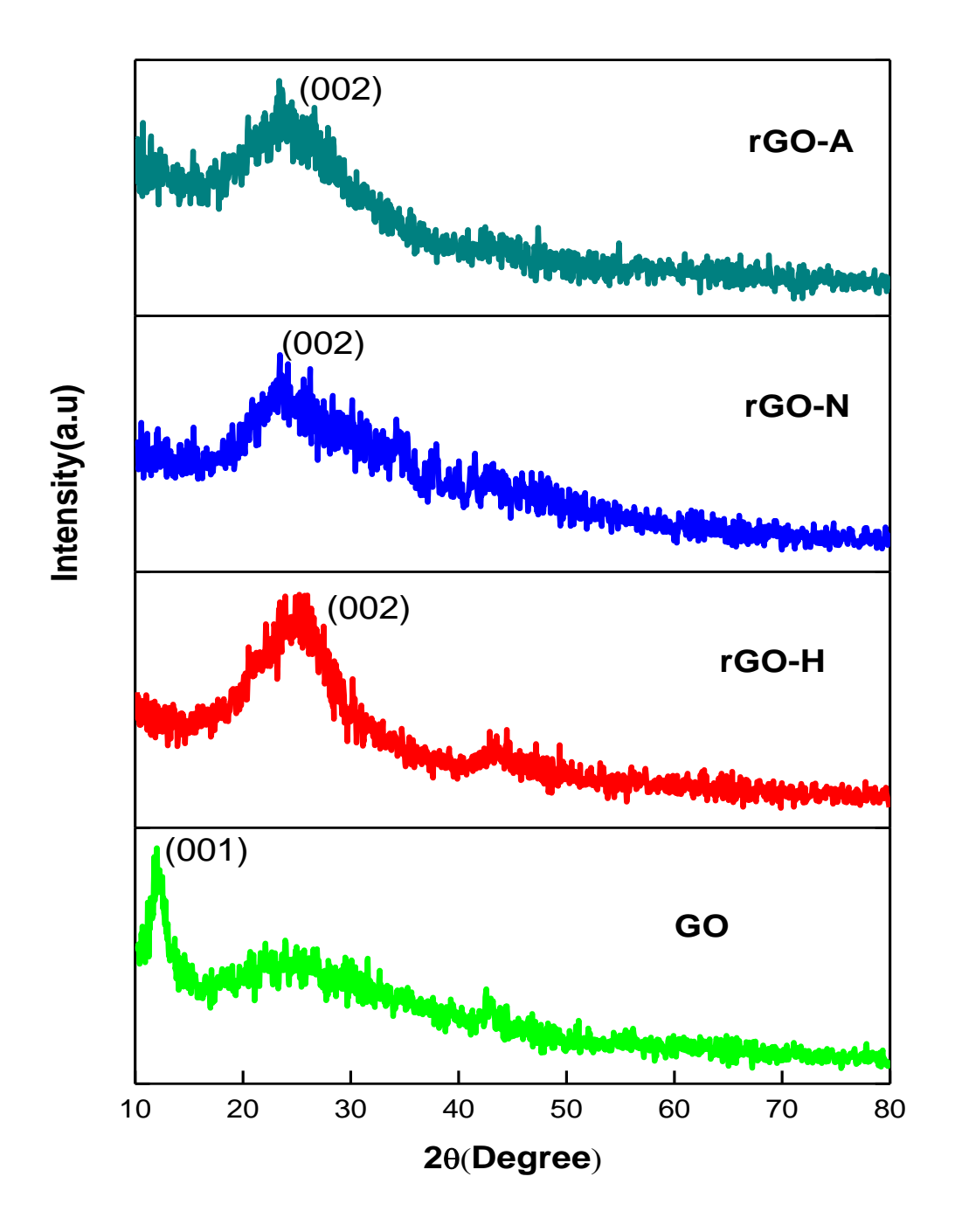


Figure 2.1 XRD Pattern of GO and rGO

This confirms the effective removal of the functional groups and the layers are brought quite close to each other. But in sodium borohydride, additional minor peaks were observed at 34°, 37°, 41° due to the irregular stacking of graphene layers which indicate that the functional groups are not completely removed. This can be

evidenced by the interplanar value of rGO-A (d= 0.75 nm) which is quite closer to the value of GO. Based on the interplanar distance it is confirmed that hydrazine monohydrate (N_2H_2) is the best reducing agent when compared to sodium borohydride (N_3H_4) and ascorbic acid ($C_6H_8O_6$) which points out that the functional groups are not removed completely in the later mentioned reducing agents.

2.4 FTIR Analysis

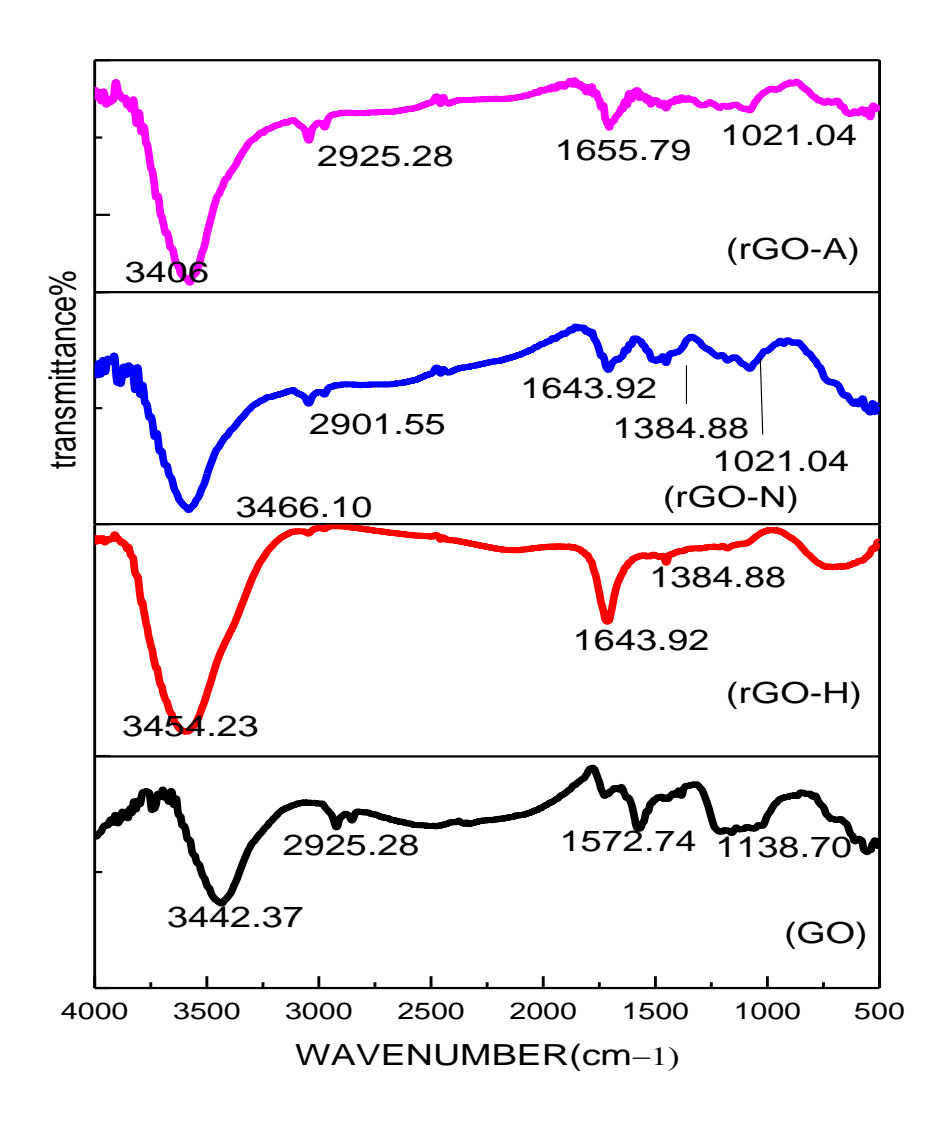


Figure 2.2 FTIR Pattern of GO and rGO

Fig. 2.2 shows the comparative FTIR spectra of GO and RGO. While no significant peak is found in graphite, the presence of different

types of oxygen functionality in graphite oxide was confirmed by the peaks at 3442 cm⁻¹ (O-H stretching vibrations), 2925 cm⁻¹ (C-H stretching vibration), 1572 cm⁻¹ and 1138 cm⁻¹ (C-C, C-O stretching vibration of carboxyl and carbonyl groups present at the edges of the graphene oxide sheets). rGO-H shows peaks at 1643 and 1158 cm⁻¹ (C=C stretching vibration of the graphene sheets) which confirms the presence of carbon in the sample. rGO-N shows a peak at 2901 cm⁻¹ (C-H stretching vibration), 1643 cm⁻¹ and 1384 cm⁻¹ (C=C stretching vibration) and 1021 cm⁻¹ (C-O stretching). rGO-A shows the peak at 2925 cm⁻¹ which corresponds to the C-H stretching vibration and also absorption peak at 1655 cm⁻¹ represents the C=C, C-O stretching vibration. Thus FTIR spectrum indicates that among the three reducing agents, hydrazine monohydrate is a strong reductant that has reduced C-H and C-O groups, effectively and sodium borohydride is a mild reducing agent and ascorbic acid partially reduces the functional groups.

2.5 SEM Analysis

In Fig. 2.3, SEM image of GO has a layered structure and ultrathin inhomogeneous graphene sheets. Moreover in the recorded picture, it is possible to distinguish the edges of the individual sheets. SEM images revealed that the reduced GO material consists of randomly aggregated, thin crumpled sheets closely associated with each other and forming disordered sheets. The thickness of rGO-H is more than the other two rGO's, this is because of strong van der Waal forces between the stacked layers. As most of the functional groups were removed in this rGO-H, there should be a strong van der Waal forces between the layers which make the rGO sheets thick than graphene oxide sheets. It can be concluded that rGO-H is an efficiently

reduced and Hydrazine monohydrate was found to be a better reductant.

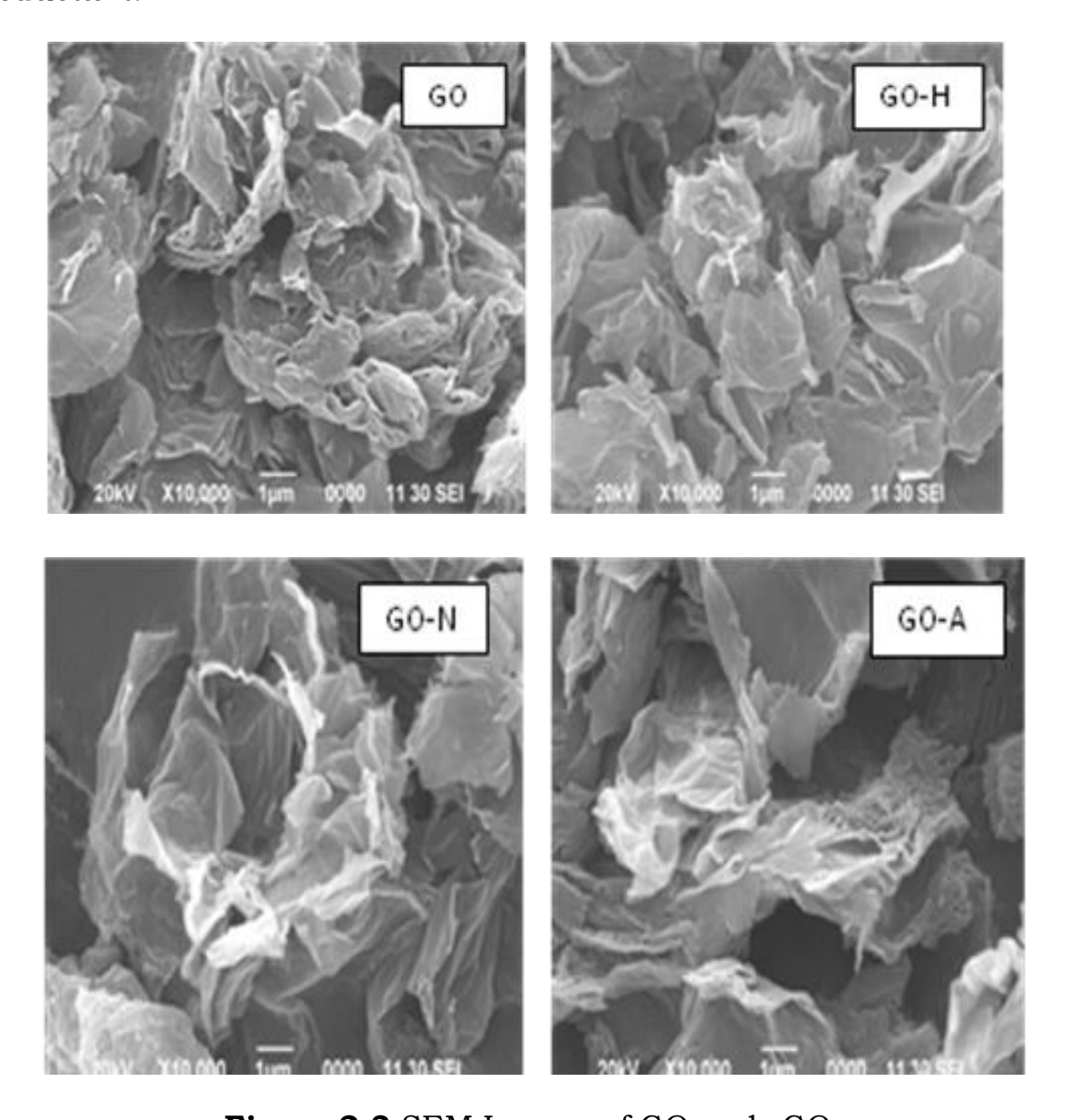


Figure 2.3 SEM Images of GO and rGO

2.6 Emission and Absorption Studies

Under the excitation of 325 nm lamp, GO exhibits an intensive blue luminescent emission at 360 nm (Fig. 2.4). It is believed that the blue PL emission is related to oxidation of graphite that causes the formation of graphite islands in GO which in turn produces a disruption of the π -network and thus opens up a bandgap in the electronic structure.

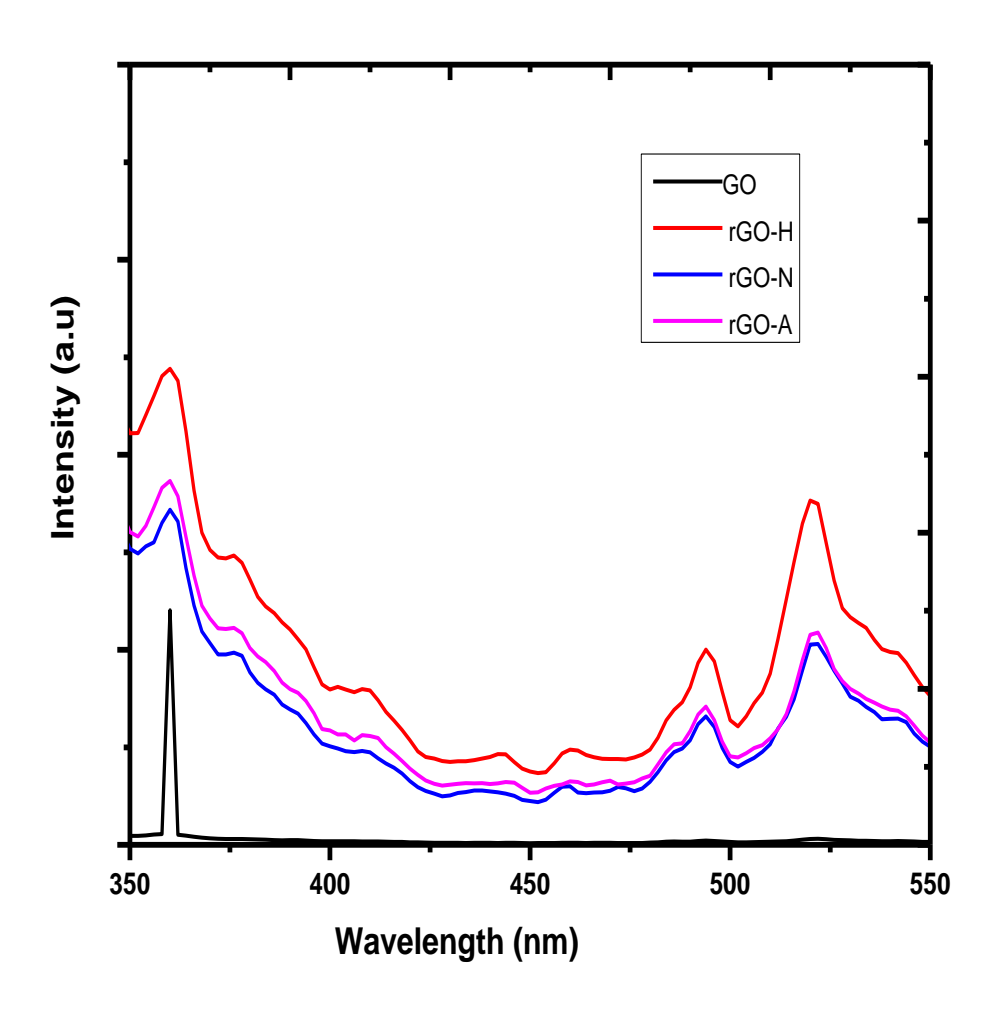


Figure 2.4 Emission Spectrum of GO and rGO

In general, GO shows very weak PL because of the isolated sp² domains generated by oxidation. These sp² domains have opened heterogeneous electronic band gaps which are intrinsically correlated to their sizes, shapes, and fractions. In principle, large sp² domains have narrower energy gaps than those smaller ones and emit longer wavelengths when excited at appropriated wavelengths. However, the epoxy groups on the basal plane and carboxylic groups at the edge of GO often induce non-radiative recombination of localization electronhole pairs, leading to a very low quantum yield. After reacting with reducing agents bright PL appeared in rGO-H, rGO-N, and rGO-A. The emission peaks at 493 nm and 521 nm are the defect peaks which

arise due to different reducing agents. The reduction of GO results in the formation of zero regions in the rGO sheets with some of the functional groups remaining still unreduced even after the reduction process. Moreover, the emission peak at 521 nm can be ascribed to the surface defects.

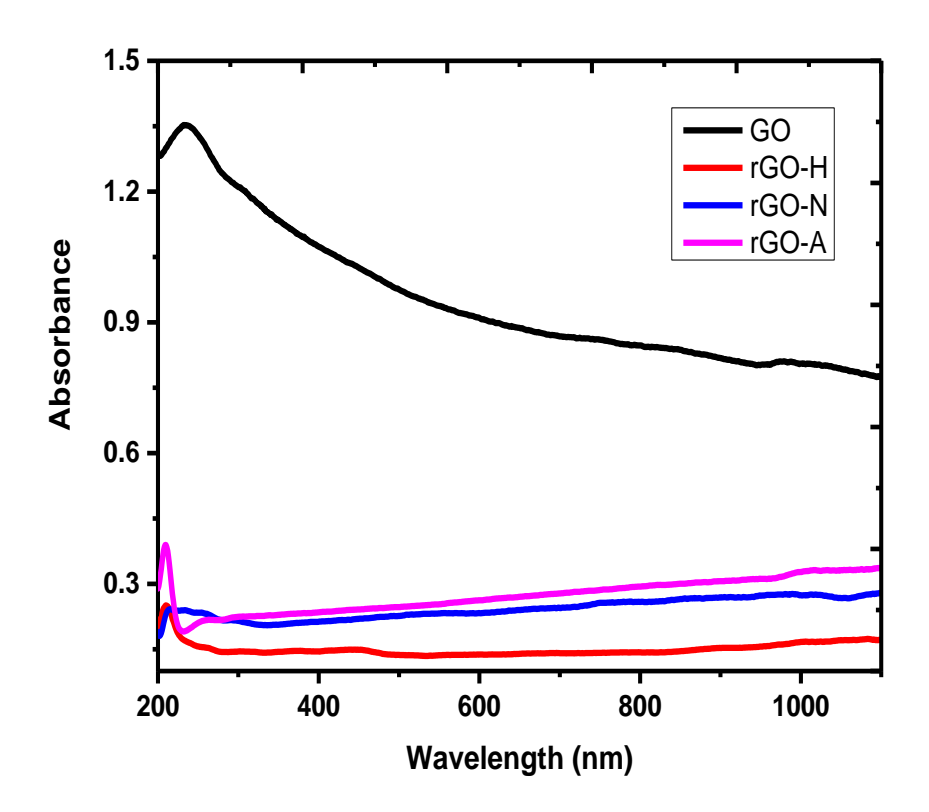


Figure 2.5 UV-Vis-NIR Absorbance Spectrum of GO and rGO

As shown in the absorbance spectrum (Fig. 2.5) GO exhibits a π^* absorption band at 234 nm. rGO-H, rGO-N and rGO-A exhibits an absorption peak at 210, 215 and 208 nm respectively, which indicates the blue-shifted absorption with respect to the parent graphene oxide. Interestingly, shifting in the absorption peak occurs due to the decrease in functional groups and an increase in aromatic rings, causes electrons to be easily excited at a lower energy level. From the blue-shifted peaks, it can be confirmed that the electronic conjugation within the sheets was restored after the reduction reaction. rGO shows

a blue shift which is due to the weak interlayer coupling between the layers. Among the absorbance patterns of the reduced GO, rGO-H shows less absorption due to the efficient reduction of all the functional groups. When comparing to rGO-H, the other two reduced samples rGO-N and rGO-A shows more absorption as they are mild reductants and less efficient in removing the functional groups.

2.7 Third-Order NLO Properties and Optical Limiting Analysis

A diode-pumped Nd: YAG laser (532 nm) was used as the excitation source for the Z-scan technique. The Gaussian profile laser beam was focused using convex lens of focal length 3.5 cm to produce a beam of the waist (ω_0) 15.35 µm. The recorded Z-scan pattern is shown in Fig. 2.6. OA Z-scan data shows (Fig. 2.6 (a)) maxima for normalized transmittance at the principal focus (Z = 0) and hence the observed nonlinear absorption is due to saturable absorption (SA) nature of the material. SA can arise when the first excited state has a lower absorption cross-section compared to the ground state. In CA Zscan (Fig. 2.6 (b)), the peak valley pattern of the normalized transmittance curve obtained under the closed aperture configuration shows the characteristic self-defocusing behavior of the propagation in the samples. The absorption saturation in the sample enhances the peak and decreases the valley in the closed aperture Z-scan and results in distortions in the symmetry of the Z-scan about Z=0. The recorded normalized closed aperture Z-scan curve exhibits a pre-focal transmittance maximum (peak) followed by a post-focal transmittance minimum (valley) signature for the samples. This peak-valley signature indicates the self-defocusing property and it is represented by negative nonlinear refractive index n2. The sign of the nonlinear index of refraction n₂ of a sample is thus immediately clear from the shape of the graph. Since closed aperture data obtained from Z-scan will

contain both nonlinear refraction and nonlinear absorption components, it is necessary to separate the nonlinear absorption components from the nonlinear refraction to extract pure nonlinear refraction [14].

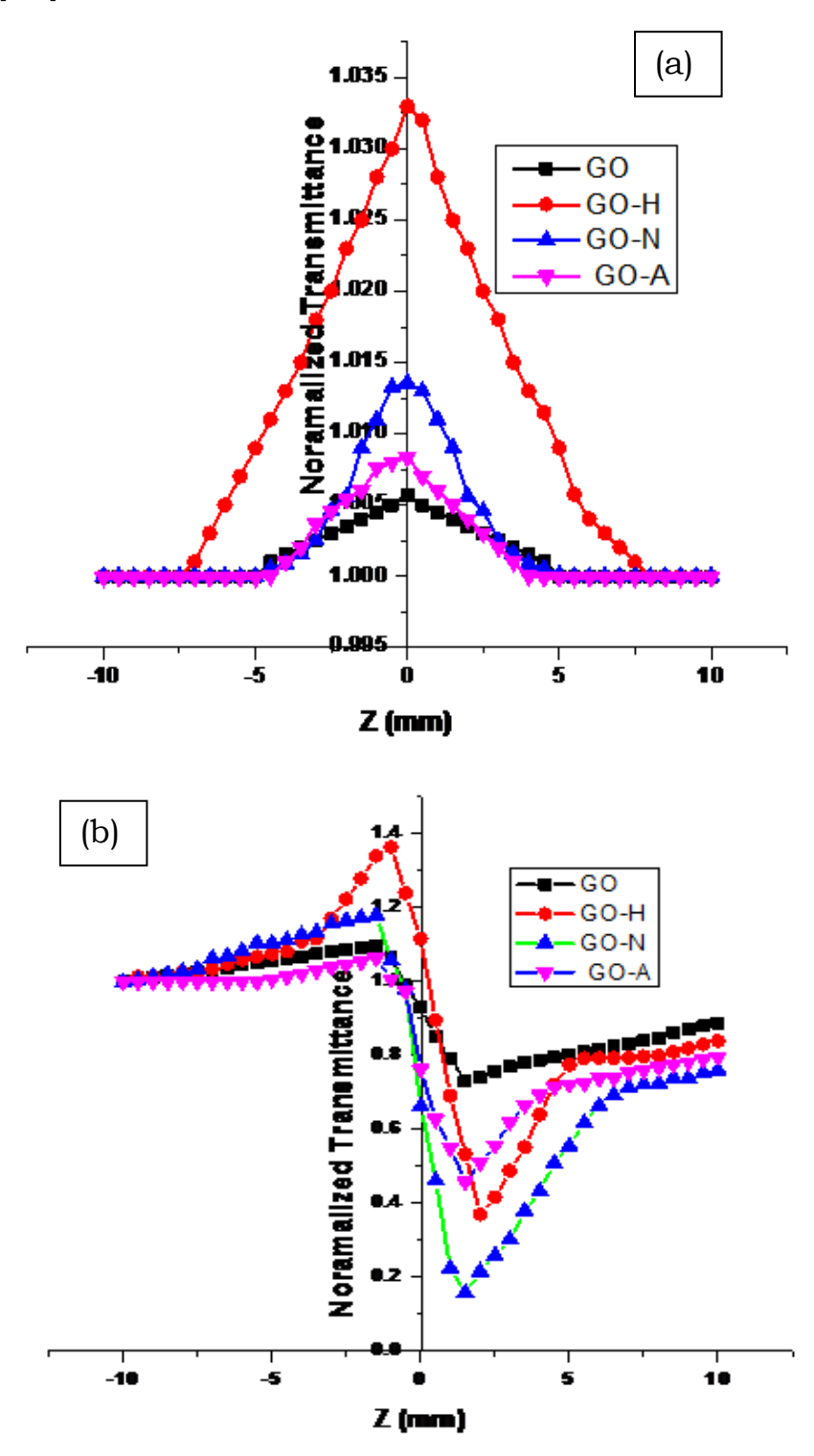


Figure 2.6 (a) OA and (b) CA Z-Scan Pattern of GO and rGO

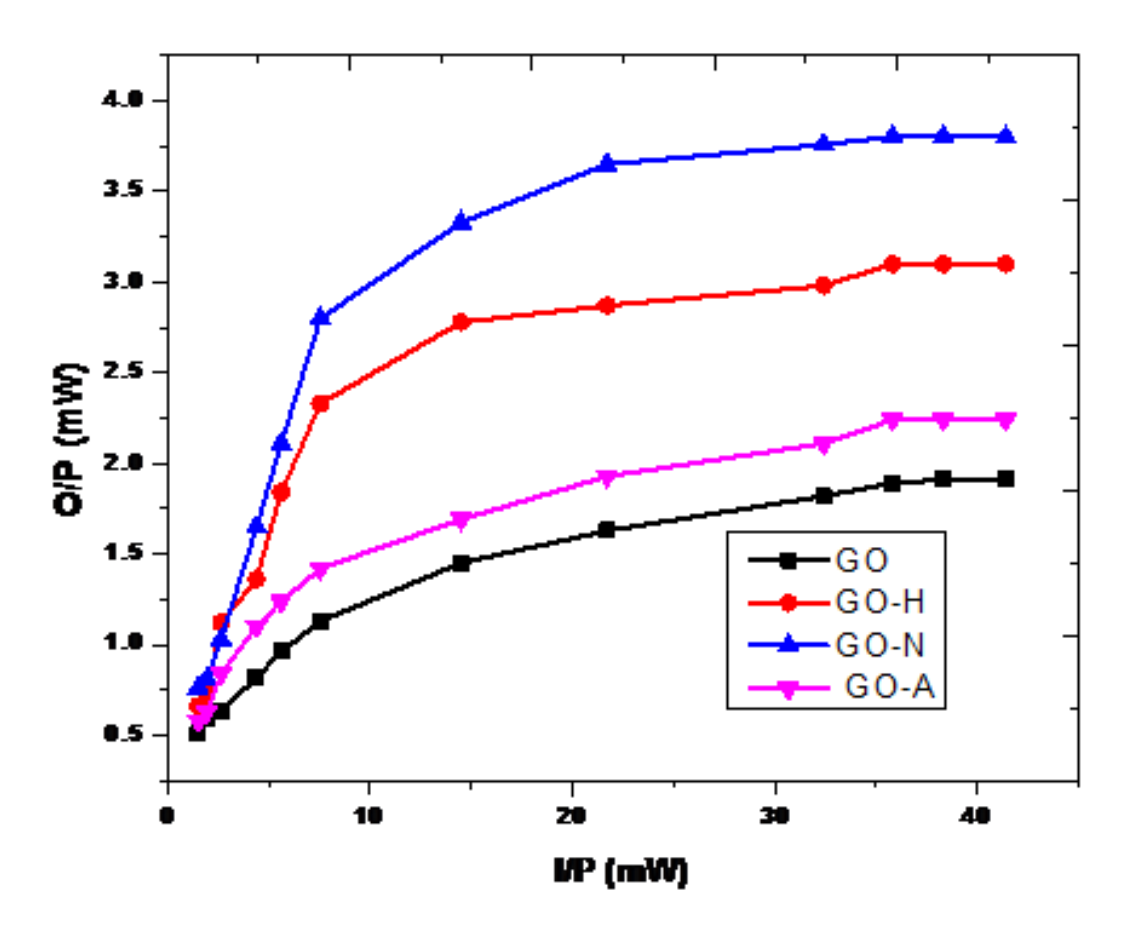


Figure 2.7 OL Pattern of GO and rGO

Under CW laser excitation, the nonlinear refraction behavior of the sample is equivalent to the formation of the induced positive or negative lens resulting in self-focusing or self-defocusing behavior [15]. The third-order NLO coefficients such as nonlinear refractive index, real part of nonlinear optical susceptibility, imaginary part of nonlinear optical susceptibility and third-order nonlinear optical susceptibility were calculated from the relation [16]

$$\Delta T_{p-\nu} = 0.406(1-S)^{0.25} |\Delta \phi| \tag{2.1}$$

where S is the aperture linear transmittance and is calculated using the relation

S= 1- exp
$$(-2 r_a^2 / \omega_a^2)$$
 (2.2)

where r_a is the aperture and ω is the beam radius at the aperture. The nonlinear refractive index is given by

$$n_2 = \frac{\Delta \phi}{KI_0 L_{eff}} \tag{2.3}$$

where, $K = 2\pi/\lambda$ (λ is the laser wavelength), I_0 is the intensity of the laser beam at the focus (Z=0), $L_{eff} = (1-exp(-\alpha L)/\alpha)$.

The real and imaginary parts of the third-order nonlinear optical susceptibility $\mathbf{x}^{(3)}$ are defined as

Re
$$\chi^{(3)} = \frac{10^{-4} \left(\varepsilon_0 C^2 n_0^2 n_2 \right)}{\pi} (cm^2 / W)$$
 (2.4)

$$\operatorname{Im} \chi^{(3)} = \frac{10^{-2} \left(\varepsilon_0 C^2 n_0^2 \lambda \beta \right)}{4\pi^2} \text{ (cm / W)}$$
 (2.5)

where ε_0 is the permittivity of vacuum, n_0 is the linear refractive index of the sample and c is the velocity of light in vacuum. The third-order nonlinear optical susceptibility is thus

$$\chi^{(3)} = \sqrt{\left(\text{Re}\left(\chi^{(3)}\right)\right)^2 + \left(\text{Im}\left(\chi^{(3)}\right)\right)^2}$$
(2.6)

When the medium is irradiated by laser, a small portion of its energy is absorbed by the particles and get thermally agitated. Hence the numbers of particles are thermally agitated due to the local heating of the absorbing medium and it results in temperature variation of the sample medium. Thus, the nonlinearity is temperature-dependent and the observed increase in third-order optical nonlinearity is attributed to thermal nonlinearity.

Estimated NLO coefficients are summarized in Table 2.1. It is interesting to note that obtained reduced graphene oxide with different reducing agents show tunable NLO coefficients which may arise due to

change in the functional group's concentration and layers of graphene sheets [17-22].

Table 2.1 Third-Order NLO Coefficients of GO and rGO

Parameters	GO	rGO-H	rGO-N	rGO-A
Nonlinear refractive index (n ₂) x 10 ⁻⁸ cm ² /W	1.58	4.18	4.39	2.60
Nonlinear absorption coefficient (β) x 10-3 cm/W	5.86	7.73	5.90	5.88
Real part of the third-order susceptibility [Re(x³)] x 10-6 esu	0.90	2.38	2.50	1.48
Imaginary part of the third-order susceptibility [Im(x ³)] x 10 ⁻⁶ esu	1.41	1.87	1.42	1.42
Third-order nonlinear optical susceptibility (x ³) x 10 ⁻⁶ esu	1.68	3.03	2.88	2.05
Limiting threshold (mW)	32.5	32.5	32.5	32.5
Clamping value (mW)	1.9	3	3.6	3.1

As it is known that, hydrazine is the strongest reducing agent that has effectively reduced graphene oxide (rGO-H) and it shows higher NLO coefficients among the prepared graphene oxide. The larger value of $x^{(3)}$ in the order of 10^{-6} esu was mainly due to the larger delocalization and thus materials are expected to be a suitable candidate for sensor protection in the CW low power regime. All the materials exhibit optical limiting and rGO reduced by hydrazine monohydrate (rGO-H) has a better optical limiting action [23].

Demonstrated optical limiters with clamping value of 1.9-3.1 mW are very essential, as even a 1-5 mW CW laser exposed to eyes directly for few seconds can damage them permanently.

2.8 Conclusion

Graphene oxide was successfully prepared by a modified Hummers method and rGO were prepared from the graphene oxide by reduction method using hydrazine, sodium borohydride, and ascorbic acid as reductant. The preliminary identification of the sample was carried out by the powder XRD pattern. The reduced GO material consists of randomly aggregated, thin crumpled sheets closely associated with each other and forming disordered sheets. The emission peak in the near UV region at 365 nm corresponds to the band emission of rGO. The nonlinear optical response of thermo-optic origin exhibited by the sample at low CW laser powers (532 nm, 50 mW) was studied and the optical limiting action based on nonlinear refraction was demonstrated. The defocusing nature and large nonlinear saturable absorption coefficient make the sample to behave as a good optical limiter in the low power regime. All the materials exhibit optical limiting and rGO reduced by hydrazine monohydrate (rGO-H) has a better optical limiting action. Higher NLO coefficients of rGO-H was mainly due to the larger delocalization that occurred in the graphene-like sheets. Thus hydrazine reduced rGO can be an excellent alternate for GO as low power optical limiters for CW green lasers.

2.9 References

- 1. S. Kaladevi, C. Vijayan, M.P. Kothiyal, *Opt. & Laser Technol.*, 38 (2006) 512.
- 2. LW. Tutt, A. Kost Nature 356 (1992) 225.
- 3. Chunying He, Wubiao Duan, Guang Shi, Yiqun Wu, Qiuyun Ouyang, Yinglin Song, *Appl. Surf. Sci.*, 255 (2009) 4696.

- 4. YP. Sun, JE. Riggs, HW. Rollins, R. Guduru, *J. Phys. Chem.*, B103 (1999) 77.
- 5. LW. Tutt, TF. Boggess, Prog. Quan. Elect., 17 (1993) 299.
- 6. QD. Zheng, SK. Gupta, GS. He, LS. Tan, PN. Prasad, *Adv. Func. Mater.*, 18 (2008) 2770.
- 7. Haijun Zeng, Junhe Han, Dongjin Qian, Yuzong Gu, *Optik* 125 (2014) 6558.
- 8. Panit Chantharasupawong, Reji Philip, Narayanan T. Narayanan, Parambath M. Sudeep, Akshay Mathkar, Pulickel M. Ajayan, Jayan Thomas, *J. Phys. Chem. C*, 116 (2012) 25955.
- 9. Hongtao Liu, Lei Zhang, Yunlong Guo, Cheng Cheng, Lianjiang Yang, Lang Jiang, Gui Yu, Wenping Hu, Yunqi Liu, Daoben Zhu, *J. Mater. Chem.*, C 1 (2013) 3104.
- 10. D. Li, M.B. Mueller, S. Gilje, R.B. Kaner, G.G. Wallace, *Nature Nanotechnol.* 3 (2008) 101.
- X.L. Zhang, Z.B. Liu, X.C. Li, Q. Ma, X.D. Chen, J.G. Tian, Y.S. Chen, Opt. Exp., 21 (2013) 7511.
- 12. L. Shahriary, A.A. Athawale, *IJREEE*, 2 (2014) 58.
- 13. W.S. Hummers Jr, R.E. Offeman, *J. Amer. Chem. Soc.*, 80 (1958) 1339.
- 14. M. Sheik-Bahae, A.A. Said, T.H. Wei, D.J. Hagan, E.W. Van Stryland, *IEEE J. Quant. Electron.*, 26 (1990) 760.
- 15. M. Saravanan, T.C. Sabari Girisun, G. Vinitha, J. Mater. Sci. 51 (2016) 3289.
- 16. T.C. Sabari Girisun, S. Dhanuskodi, *Chem. Phys. Lett.*, 491 (2010) 248.
- 17. F. Miao, H. Zhan, Y. Chen, Appl. Phys. Lett., 96 (2010) 033107.
- N. Liaros, P. Aloukos, A. Kolokithas-Ntoukas, A. Bakandritsos,
 T. Szabo, R. Zboril, S. Couris, J. Phys. Chem. C., 117 (2013)
 6842.

- 19. Z. Chan, W. Chen, Y. Huang, X. Xiao, X. Ye, RSC Adv., 4 (2014) 39697.
- Y. Chen, Y. Zhang, F. Pan, J. Liu, K. Wang, C. Zhang, S. Cheng,
 L. Lu, W. Zhang, Z. Zhang, X. Zhi, ACS Nano., 10 (2016) 8169.
- 21. S. Zhipei, A. Martinez, F. Wang, Nat. Phot., 10 (2016) 842.
- Q. Guo, Y. Yao, Z.C. Luo, Z. Qin, G. Xie, M. Liu, J. Kang,
 S. Zhang, G. Bi, X. Liu, J. Qiu, ACS Nano., 10 (2016) 9463.
- 23. G. Muruganandi, M. Saravanan, G. Vinitha, M.B. Jessie Raj, T.C. Sabari Girisun, *Chem. Phys.*, 488 (2017) 55.

Chapter - III

Barium Borate Nanorod Decorated Reduced Graphene Oxide

CHAPTER III

Barium Borate Nanorod Decorated Reduced Graphene Oxide

By simple hydrothermal method, nanorods of barium borate were successfully loaded on reduced graphene oxide sheets. Powder XRD confirms the incorporation of barium borate (20= 29°, (202)) along with the transition of graphene oxide ($2\theta = 12^{\circ}$, (001)) into reduced graphene oxide ($2\theta = 25^{\circ}$, (002)). In the FTIR spectra, the presence of characteristic absorption peaks of rGO (1572 and 2928 cm⁻¹) and barium borate (510, 760 and 856 cm⁻¹) further evidences the formation of BBO:rGO nanocomposite. FESEM images portray the existence of graphene sheets as thin layers and growth of barium borate as nanorods on the sheets of reduced graphene oxide. Ground-state absorption studies reveal the hypsochromic shift in the absorption maxima of the graphene layers due to the reduction of graphene oxide and hypochromic shift in the absorbance intensity due to the inclusion of highly transparent barium borate. The photoluminescence of BBO:rGO shows maximum emission in the UV region. Optical nonlinearity of BBO:rGO nanocomposite was studied by the Z-scan technique using CW diode-pumped Nd: YAG laser (532 nm, 50 mW). Both nanocomposite and individual counterparts possess saturable absorption and self-defocusing behavior. Third-order NLO coefficients of BBO:rGO nanocomposite is found to be higher than bare graphene oxide. Strong nonlinear refraction (self-defocusing) and lower onset limiting threshold make the BBO:rGO nanocomposite preferable candidate for laser safety devices.

3.1 Introduction

The major concerns of the electro-optical sensors that are widely used in laser applications are susceptible to overexposure leading to permanent optical damage. Since the invention of the laser in 1960, the protection of human eyes and sensors against intended or unintended damage by laser radiation has been an ongoing research Laser protection measures are typically realized using field. conventional optical filters based on linear absorption or interference Unfortunately, these filters work only for predefined wavelength, but not beyond [1]. So a laser beam of high intensity can easily damage the retina and hence significant research effort has been invested on optical power limiting (OL) materials to achieve some measure of protection from such high-intensity laser beams. efficient optical limiting material exhibits high transmittance for low-intensity ambient light, while strongly attenuating intense and potentially dangerous laser beams and thus can be utilized in applications like laser damage prevention and laser beam shaping [2]. Layer structured carbonaceous materials like graphene oxide (GO) stand high in this domain due to their stronger nonlinear optical response. However, the basic requirement of high linear transmittance limits possible usage as a power limiter. Improvement of linear transmittance along with enhanced nonlinear action can be achieved through nanocomposite formation. The availability of several types of oxygen-containing functional groups on the basal plane (epoxide groups) and the sheet edge (ketone groups) allows GO to interact with a wide range of inorganic materials so that functional hybrids and composites with unusual properties can be readily synthesized. In the choice of inorganic materials, barium borate (BBO) nanostructures will be an interesting candidate as it possesses high second harmonic

generation (SHG) efficiency and has unique characteristics like wide transparency, large birefringence, high laser damage threshold and excellent mechanical properties. In the wide variety of morphologies, 1D nanostructures provide an opportunity to understand both behaviors in ultralow dimension functional and to high-performance next-generation devices. Efficient transport of optical excitations due to two-dimensional confinements arising from makes intrinsic anisotropic nature also fabrication nanostructures promising route. Furthermore, it is generally accepted that 1D nanostructures provide a good system to investigate the relationship between properties and structures [3, 4]. The origin of large nonlinear optical susceptibility in BBO arises from the anionic structural units and as boron atoms have two kinds of co-ordination, a boron atom co-ordinates with three oxygen atom to form triangle [BO₃] unit and with four oxygen atom to form tetrahedral [BO₄] unit. The network of interconnected [BO₃] and [BO₄] forms infinite chains of [B₃O₆], [B₃O₃] anionic groups whose negative charge is compensated by the Ba²⁺ cations and hence resulting in a diversity of structures. Hence most of the research is focused on β-BBO nanostructures and reports show that nanorods, nanoplates, and network like structures of β-BBO exhibit higher SHG performance than bulk form. Also, γ-BBO (rich in BO₃ unit) nanostructure exhibited higher third-order nonlinearities in the continuous wave (CW) regime demonstrating maximum thermal stability against intense laser radiations among the known NLO materials and hence rendering them ideal for optical limiting applications [5]. Based on these facts, this chapter reports the optical limiting performance of y-BBO nanorod decorated rGO with CW laser pulses at a wavelength of 532 nm. It is found that BBO: rGO nanocomposite possesses stronger nonlinear refraction which is beneficial for power limiting applications.

3.2 Material Preparation

Hydrothermal method is an elegant technique to prepare and incorporate barium borate upon graphene sheets. Preparation of barium borate decorated reduced graphene oxide nanocomposite involves a three-step process. In the first step, graphene oxide (GO) was prepared from graphene flakes by Modified Hummer's method [6]. In the second step, the obtained GO was reduced to reduced graphene oxide (rGO) by using ascorbic acid as reducing agent [7]. In the third step of the employed experimental procedure, 10 mmol of BaCl₂.2H₂O, 15 mmol of H₃BO₃ and 20 mmol of NaOH were dissolved in 60 ml distilled water and used as starting precursor to obtain barium borate [5]. To the above-mentioned solution, 20 mg of rGO was added and continuously stirred for 8 hours to attain homogenous mixing. The solution was then transformed into a 100 ml autoclave setup and placed in an oven at 120 °C for 24 hours. The obtained slurry was washed with water and ethanol several times to remove the suspended impurities and other byproducts. Finally, the obtained powder was dried at 60 °C for 12 hours resulting in the formation of ash-colored powder. In each step, the obtained powders were taken out and indexed as GO, rGO, and BBO: rGO for further characterization.

3.3 Structural Confirmation

The prepared samples were subjected to powder X-ray diffraction using CuKa radiation (1.54 Å) in the angle of 10° -80°. Fig. 3.1 shows the recorded XRD patterns of GO, rGO, and BBO: rGO. The characteristic peak (001) observed at $2\theta = 12^{\circ}$ confirms the formation of graphene oxide in the modified Hummer's method. After the reduction process, no diffraction peaks of GO (001) were observed and the presence of diffraction peak at $2\theta = 12^{\circ}$ signatures the formation of

rGO and thus ascribes that GO was efficiently reduced by the reducing agent.

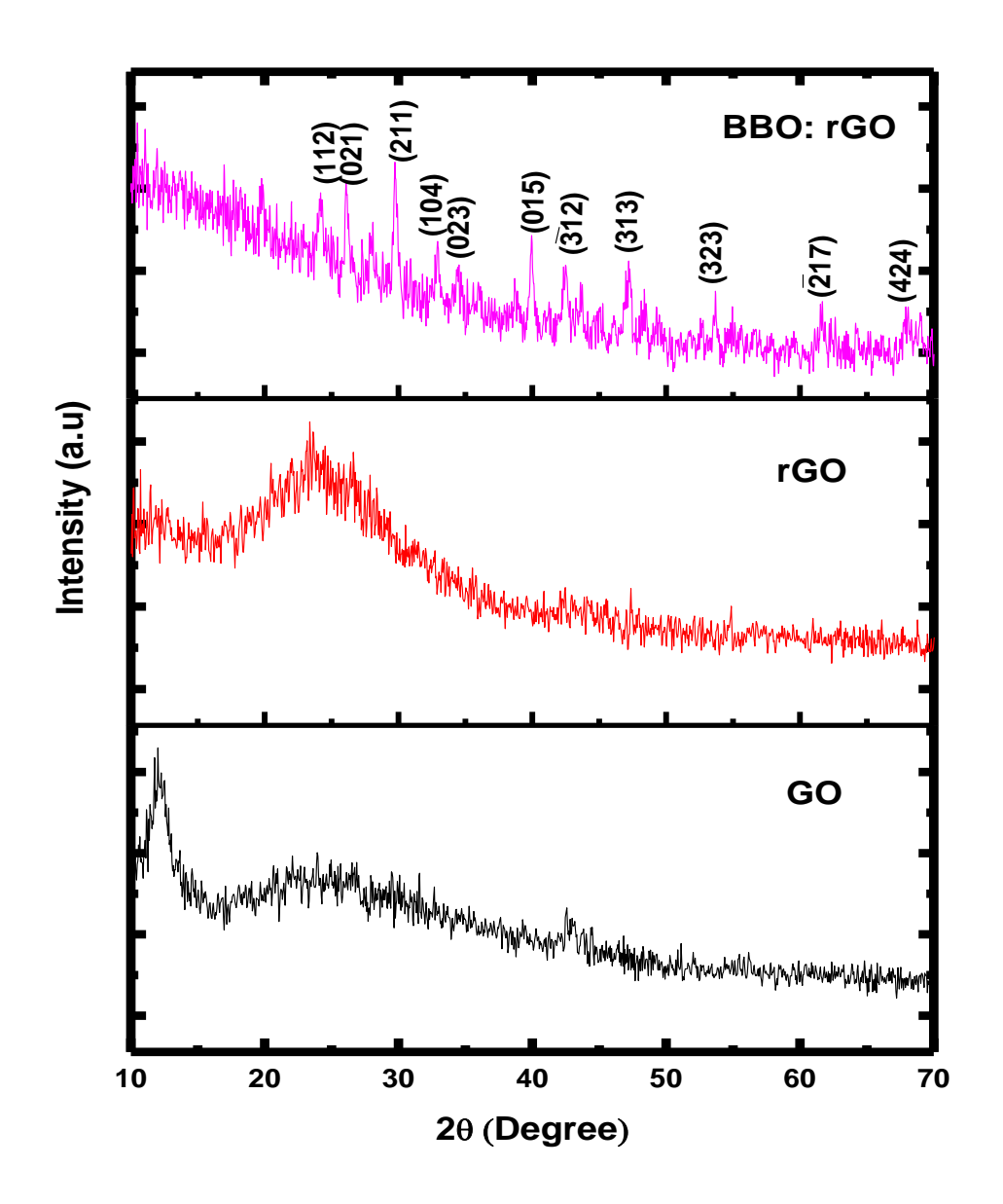


Figure 3.1 XRD Pattern of GO, rGO, and BBO: rGO

Recorded XRD pattern of BBO: rGO forecast the diffraction peaks of both rGO with BBO and thus confirms the formation of the nanocomposite. All the additional peaks were indexed and found to be consistent with the values in the standard card of γ -BBO [JCPDS: 01-071-2501]. As the samples were prepared at low temperature (120°C),

γ-BBO was obtained, which is expected to attain a higher third-order NLO coefficient [5]. The peak at $2\theta = 24^{\circ}$, 26° , 29° , 32° , 34° , 40° , 42° , 47° , 53° , 61° and 68° represents (1 1 2), (0 2 1), (2 1 1), (1 0 4), (0 2 3), (0 1 5), (3 1 2), (3 1 3), (3 2 3), (2 1 7) and (4 2 4) planes of barium borate and thus formation of BBO:rGO nanocomposite is confirmed. The widths of the reflection peaks are considerably broadened, indicating the crystalline particles fall in the nanoscale range [8]. The average grain size of BBO:rGO composite was deliberated to be 17 nm from the Debye–Scherrer equation [5]. No characteristic peaks that correspond to the possible byproducts and other impurities are noted ensuring the purity of sample.

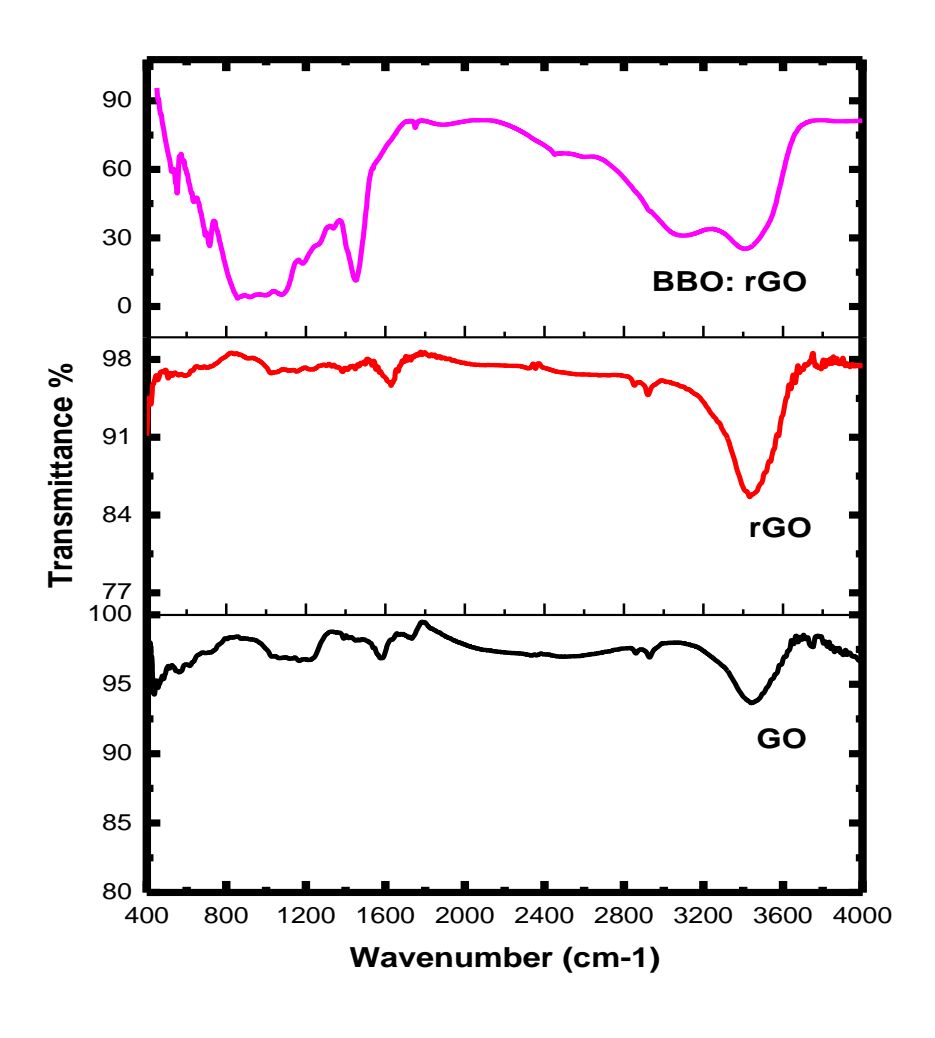


Figure 3.2 FTIR Pattern of GO, rGO, and BBO: rGO

IR spectra were recorded with JASCO 460 PLUS FTIR spectrometer in the range of 400 – 4000 cm⁻¹ to identify various functional groups and the available molecular vibration of the samples. The recorded FTIR spectra of the samples (Fig. 3.2) show strong absorption peaks which corresponds to the various vibrational modes of the prepared samples. The observed vibrational peaks and the corresponding modes of vibrations are assigned in Table 3.1.

Table 3.1 Vibrational Assignments of GO, rGO, and BBO: rGO

Peak Assignments	Peak Positions (cm ⁻¹)			
	GO	rGO	BBO:rGO	
C=C stretching (sp ² hybridized)	1572	1655	1572	
C-H stretching (aromatic hydrocarbons and C-OH stretching)	2925	2925	2928	
O-H stretching (hydroxyl groups)	3442	3406	3438	
C=O stretching (carboxyl groups)	2324	2325	-	
C=O stretching (carbonyl groups)	1738	-	-	
C-O stretching (epoxy groups)	1243	1381	-	
C-O stretching (alkoxy groups)	1207	1028	1207	
B-O-B bond	-	-	760, 510	
B-O bond in BO ₃ unit	-	-	856	

It is interesting to note that the in the modified Hummer's method, graphene sheets were successfully incorporated with various oxygen-containing functional groups such as aromatic hydrocarbons (2825 cm⁻¹), hydroxyl (3442 cm⁻¹), carboxyl (2324 cm⁻¹), carbonyl (1738 cm⁻¹), epoxy (1243 cm⁻¹) and alkoxy (1207 cm⁻¹) groups. Ascorbic acid is a mild reducing agent that removes carboxyl groups during reduction and leaves most of the functional groups in the graphene sheets. It is interesting to note that, during the incorporation of BBO upon graphene layers, some of the functional groups were effectively removed. Removal of epoxy groups from Graphene sheet is confirmed by the absence of peak at 1243 cm⁻¹ (GO) and 1381 cm⁻¹ (rGO). Similarly disappearance of FTIR peaks at 2324 cm⁻¹ and 1738 cm⁻¹ of GO exposes the removal of carboxyl and carbonyl groups in BBO-rGO respectively. Also in the FTIR spectrum of BBO: rGO, the additional absorption peaks at 510 and 760 cm⁻¹ corresponds to the bending vibrations of B-O-B bond [9] and peak at 856 cm⁻¹ is due to stretching vibration of B-O bond in BO₃ unit [5] of barium borate (y-BBO), by which the formation of BBO: rGO composite was confirmed.

Morphologies of the samples were investigated by Field Emission Scanning Electron Microscope (FEI-QUANTA-FEG 250). FESEM images (Fig. 3.3) show the panoramic morphology of the products. Fig. 3.3(a) shows the presence of graphene layers as thin crumpled sheets and here the observed folding was due to the harsh oxidation that took place during the employed Hummer's process. Compared to the GO image, rGO (Fig. 3.3(b)) shows less agglomeration and individual sheets are easily identifiable. This demonstrates the reduction of graphene oxide upon ascorbic acid interaction. From the FESEM image of BBO: rGO composite (Fig. 3.3(c)), BBO nanorods are grown randomly on the surface of rGO sheets. These nanorods

possess a uniform diameter of 22 nm and 3.0 μ m length. The possible growth mechanism can be explained as follows: During the third step of the hydrothermal process, Ba²⁺ sticks on the surface of graphene layers and forms as barium borate. These BBO acts as nucleation sites and grows as elongated nanorod upon the graphene layers. Similar formation of pure γ -BBO nanorods due to prolonged heating (120°C, 24 hours), was already reported [5]. As hydrothermal technique cannot control the content of loading, barium borate nanorods appear to be clustered. Thus the morphological analysis pictures that barium borate nanorods are randomly arranged on the layers of reduced graphene oxide.

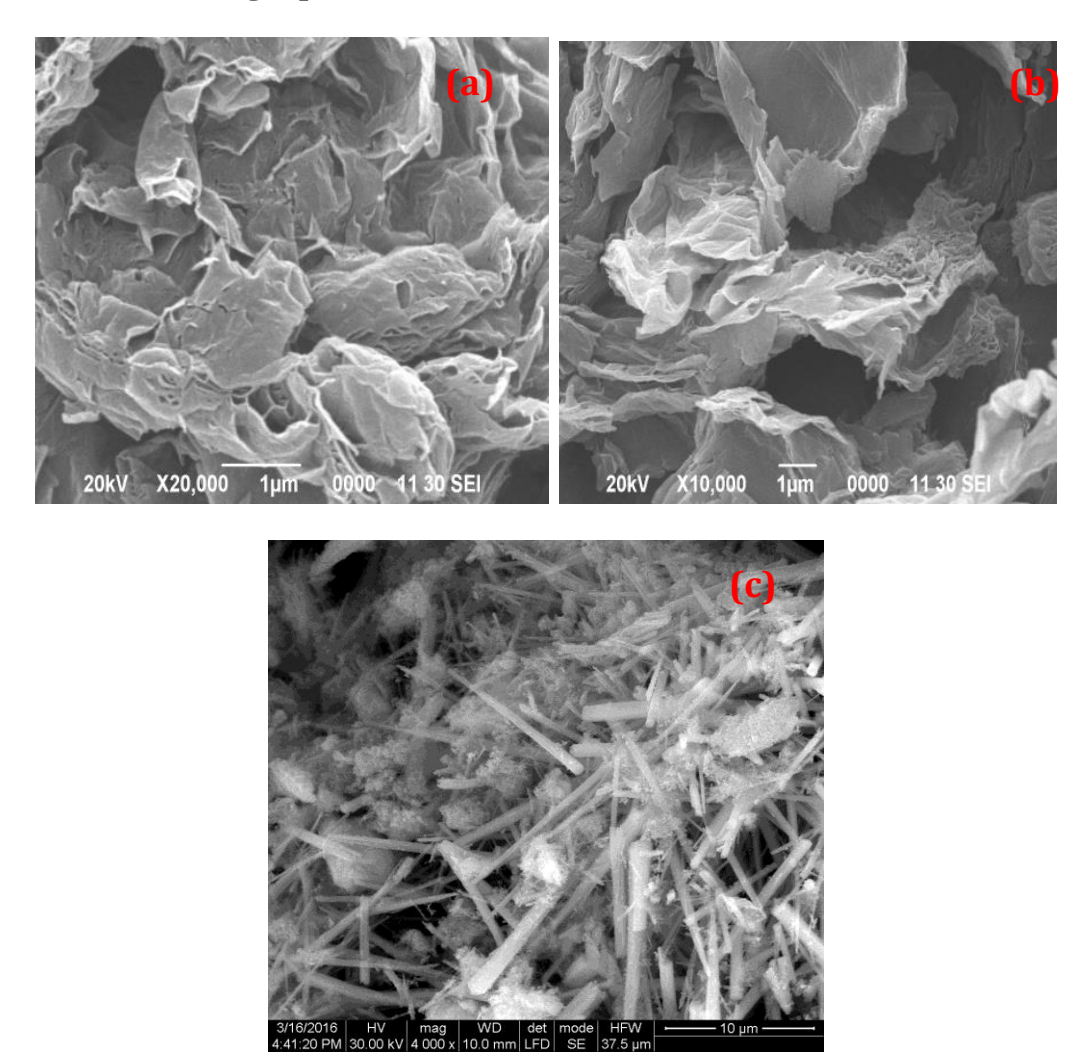


Figure 3.3 FESEM Images of (a) GO, (b) rGO and (c) BBO: rGO

3.4 Linear Absorption and Emission Properties

Linear optical properties of the samples were investigated by UV-Vis-NIR spectroscopy in the range 200–2500 nm (Fig. 3.4). The maximum absorption peak of GO, rGO, and BBO: rGO was observed at 236 nm, 210 nm, and 207 nm respectively. The maximum absorption peak corresponds to the π - π * transition of the aromatic C=C bond [10].

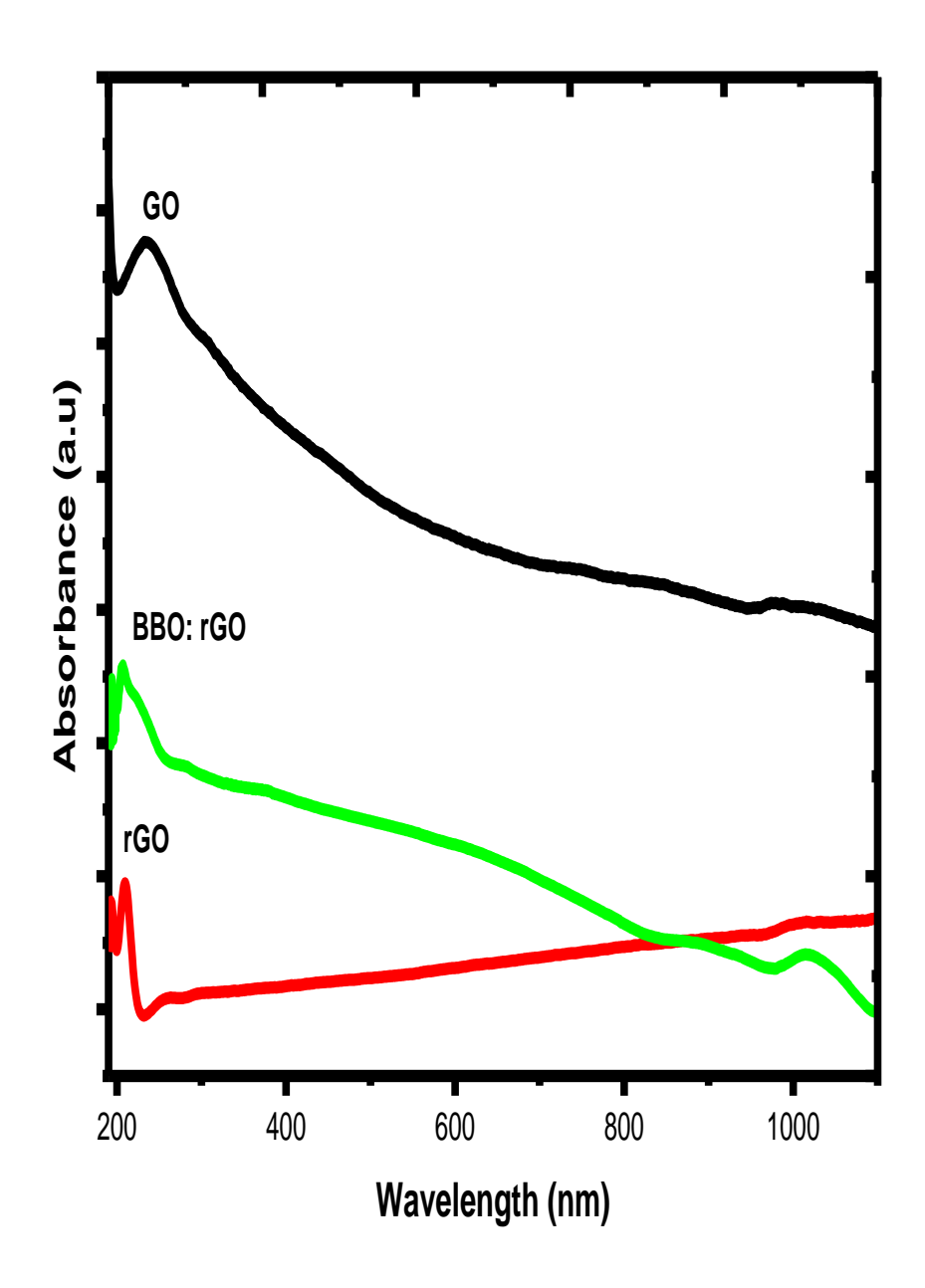


Figure 3.4 Absorption Spectrum of GO, rGO and BBO: rGO

Interestingly, shifting in the absorption peak of GO and rGO (263 nm to 210 nm) occurs due to the decrease in functional groups and weak interlayer coupling between the layers causes electrons to easily excite at lower energy. A similar blue shift in the absorption maxima (207 nm) of BBO: rGO arises from the restored electronic conjugation within the sheets due to the reduction and inclusion of barium borate. Among the inorganic NLO material, barium borate possesses low cutoff in the UV region (below 200 nm) and hence the observed maxima are the characteristic peak of graphene sheets. In BBO: rGO beyond 250 nm, the composite was observed to be highly transparent and the absorbance was almost insignificant due to the incorporation of highly transparent (Visible-NIR) barium borate [5, 11]. The hypochromic shift in the absorbance intensity of BBO: rGO clearly shows that the transparent properties of barium borate is found to be dominant in the composite and hence attain the essential criteria of optical limiter i.e., high linear transmittance.

Emission studies were carried out by Fluoromax 4 spectrophotometer under the excitation of 325 nm wavelength scanned over the domain 350 - 650 nm. Under the exposure of 325 nm light, GO exhibits a blue luminescence at 360 nm (Fig. 3.5) due to isolated sp² domains generated by the oxidation process. Here the epoxy groups on basal plane and carboxylic groups at GO edge often induce non-radiative recombination of localized electron-hole pairs, leading to very weak emission. Hence upon reduction of functional groups, rGO showed a bright blue emission at 360 nm. Also, the emission peak at 493 nm in the PL spectrum of rGO was ascribed to the surface defects formed during the reduction process. In the PL spectrum of BBO:rGO, the characteristic peak of graphene is slightly red-shifted to 370 nm (sp² domains of rGO) due to the

incorporation of barium borate. An additional peak at 350 nm arises due to the radiative annihilation of self-trapped exciton localized in the crystal defects of barium borate [5]. Thus incorporation of barium borate in rGO sheets and alteration in the electronic states due to these interactions is confirmed from the emission studies.

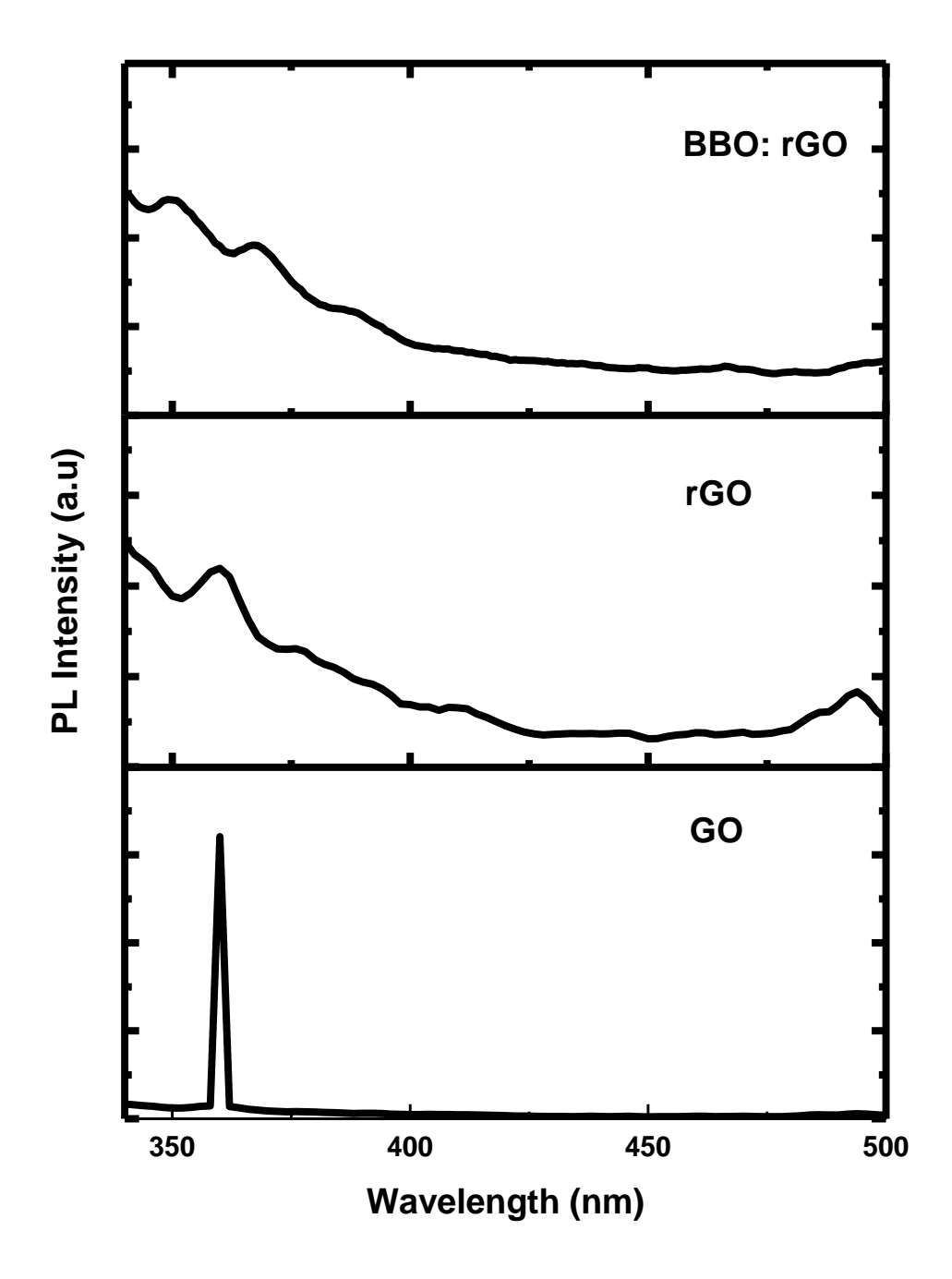


Figure 3.5 Emission Spectrum of GO, rGO and BBO: rGO

3.5 Third-order nonlinear optical refraction and absorption

The Z-scan technique is a single beam method for measuring the sign and magnitude of nonlinear absorption and refraction coefficients simultaneously. This technique uses a single laser beam in tight focus geometry. The transmittance of a nonlinear medium through a finite aperture is measured in the far-field as a function of the sample position 'Z' referenced with respect to the focal plane. Nonlinear absorption and nonlinear refraction can be measured all together when an aperture is placed in front of the detector (closed aperture). Nonlinear absorption is detected when the aperture is absent (open aperture). The third-order nonlinear optical properties of the samples, dispersed in ethylene glycol by ultrasonication were studied by closed and open Z-scan technique. The sample cell was moved using a translation system along the propagation direction (Z-axis) of a focused Gaussian beam from Nd:YAG (532 nm) laser through its focal plane. By moving the sample through the focus, the intensitydependent nonlinear refraction and absorption can be measured from the changes of the transmittance through the sample. Under similar Z-scan geometry, the optical limiting behavior of the samples was also investigated [12].

Fig. 3.6 shows the closed aperture pattern of GO, rGO, and BBO: rGO composite. In the obtained closed aperture curves, the peak precedes the valley indicating a negative variation of the nonlinear index (n₂) arising due to the self-defocusing mechanism. The observed nonlinearity is of thermal in origin, as the materials were excited with a continuous-wave laser. Here the laser heating induced thermal nonlinearity which arises from the absorption of a tightly focused beam. This produces a spatial distribution of temperature and refractive index creating a thermal lens resulting in severe phase

distortion of the propagating beam. Although all the samples exhibit self-defocusing behavior, the peak-valley difference and width of the pattern are not uniform. BBO:rGO possesses a broader peak-valley pattern with maximum peak-valley difference confirming the enhanced nonlinear refraction. Fig. 3.7 shows the open aperture pattern of GO, rGO, BBO: rGO composite. In the pattern, the maximum lies near the focus (Z=0) and hence exhibit nonlinear absorption. The peak pattern reveals the presence of saturable absorption property, where the absorption of light decreases with increasing light intensity. At sufficiently high incident light intensity, atoms in the ground state get excited to higher state at such a rate that there is insufficient time to decay back to the ground state before the ground state becomes depleted and hence absorption gets subsequently saturated. As in the case of nonlinear refraction, the strength of nonlinear absorption (peak position, ΔT) varies with sample and BBO: rGO possesses stronger nonlinear absorption.

Earlier the obtained experimental data was fitted with the theoretical normalized equation as proposed by Sheik Bahae [13,14]

$$T_{N} = 1 + \Delta \phi \frac{4x}{(1+x^{2})(9+x^{2})}$$
 (3.1)

$$T[Z, S=1] = \sum_{m=0}^{\infty} \left[\frac{\left(-q_0(z,0)\right)^m}{(m+1)^{\frac{3}{2}}} \right]$$
(3.2)

In Fig. 3.6 and Fig. 3.7, the solid line represents the theoretical fit and dotted symbols represent the experimental data. As seen the fit matches well with experimental data ensuring the reliability of measured normalized transmittance. From the peak-valley difference (ΔT_{p-v}) of closed aperture and peak value (ΔT_p) of open aperture, the nonlinear refractive index and nonlinear absorption coefficient of the material was estimated using the relations [15, 16]

$$n_2 = \frac{|\Delta \varphi|}{K I_0 L_{eff}} \tag{3.3}$$

$$\beta = \frac{2\sqrt{2\Delta T}}{I_0 L_{eff}} \tag{3.4}$$

where $k=2\pi/\lambda$ (λ is the wavelength of laser), I_0 is the intensity of the laser beam at the focus (z=0), $L_{\rm eff}=\frac{[1-\exp(-\alpha L)]}{\alpha}$ is the effective thickness of the sample, α is the linear absorption coefficient and L is the thickness of the sample, ΔT is the one peak value at the open aperture Z-scan curve and I_0 was calculated to be 4.38 KW/cm².

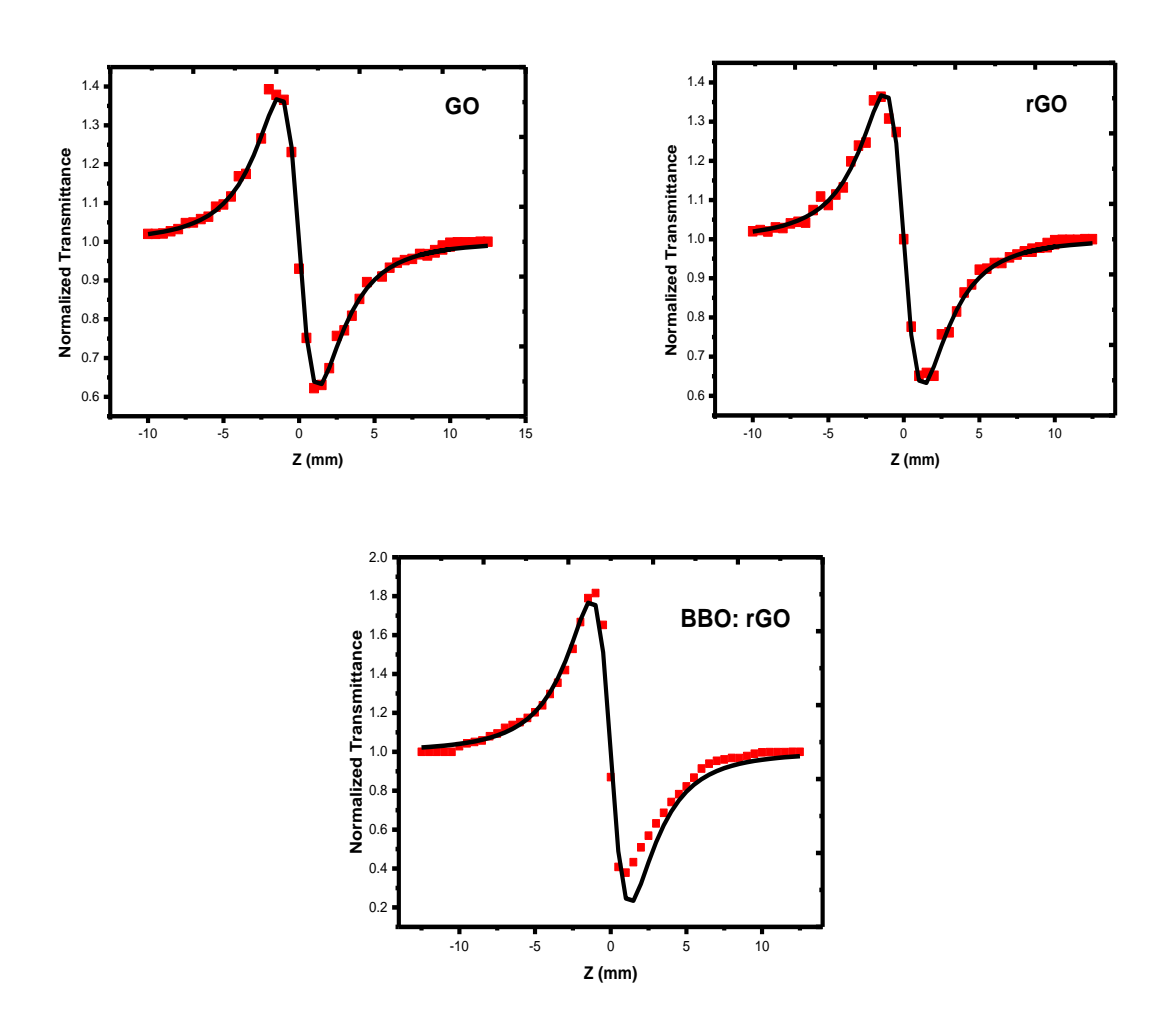


Figure 3.6 Closed Aperture Pattern of (a) GO (b) rGO and (c) BBO: rGO

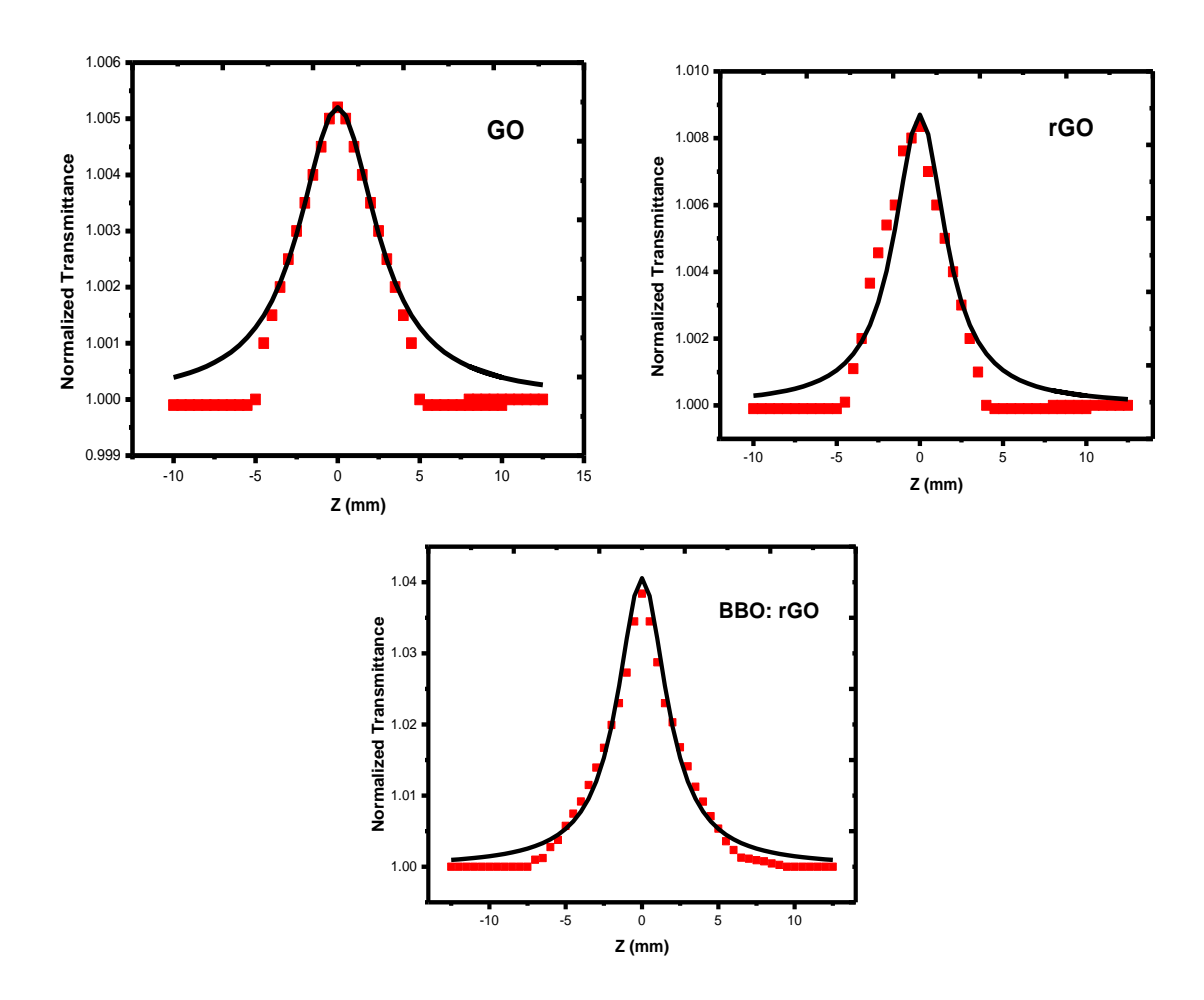


Figure 3.7 Open Aperture Pattern of (a) GO (b) rGO and (c) BBO: rGO

From the estimated nonlinear absorption coefficient and nonlinear refractive index, third-order NLO susceptibility was calculated as [17]

Re
$$x^{(3)} = \frac{10^{-4} C^2 n_0^2 n_2 \epsilon_0}{\pi}$$
 (esu) (3.5)

Im
$$x^{(3)} = \frac{10^{-2}C^2 n_0^2 \beta \lambda \epsilon_0}{4\pi^2}$$
 (esu) (3.6)

$$\chi^{3} = \sqrt{[Re \,\chi^{3}]^{2} + [Im \,\chi^{3}]^{2}} \quad \text{(esu)}$$

The estimated third-order NLO coefficient of the samples are summarized in Table 3.2. As photoexcitation is made under CW mode, thermal nonlinearity is found to be more dominant and the contribution due to electronic effects is negligibly small. It is 82 | Page

interesting to observe that, all samples exhibit strong nonlinear refraction than nonlinear absorption. This is evident from the fact that the imaginary part of third-order NLO susceptibility is greater than the real part of third-order NLO susceptibility. As the Kerr component contributes much to the observed nonlinearity, molecular and textural arrangements play a dominant role in deciding the strength of nonlinearity. Here the removal of functional groups upon reduction, incorporation of barium borate and morphology of inorganic species contributes to the observed Kerr nonlinearity. Especially nonlinear refraction drastically varies, as the nonlinear refractive index of created thermal lens strongly relies on its potential to create the spatial variation in temperature and density. As expected the combination of BBO and rGO has yielded a composite system that possesses the advantage of both elements leading to enhanced third-order nonlinearity.

3.6 Optical Limiting and Third-order NLO Coefficients

The optical limiting behavior of GO, rGO, and BBO: rGO is shown in Fig. 3.8. The optical limiting behavior is investigated by plotting the output power versus the input power. The transmitted output intensity obeys Beer's law and is found to vary linearly with the input intensities at very low input intensities. Beyond a critical value, the output starts deviating to become nonlinear and the transmitted intensity reaches a plateau and gets saturated. From the critical point, the input power at which the nonlinearity saturate is termed as onset limiting threshold and its corresponding output power is called as limiting amplitude. All the samples exhibit strong limiting action and are found to be varying with respect to their strength of nonlinearity. Here the observed nonlinearity mainly originates due to the self-defocusing nature of the samples. BBO:rGO with strong nonlinear

refraction possess strong optical limiting action with the lowest onset limiting threshold.

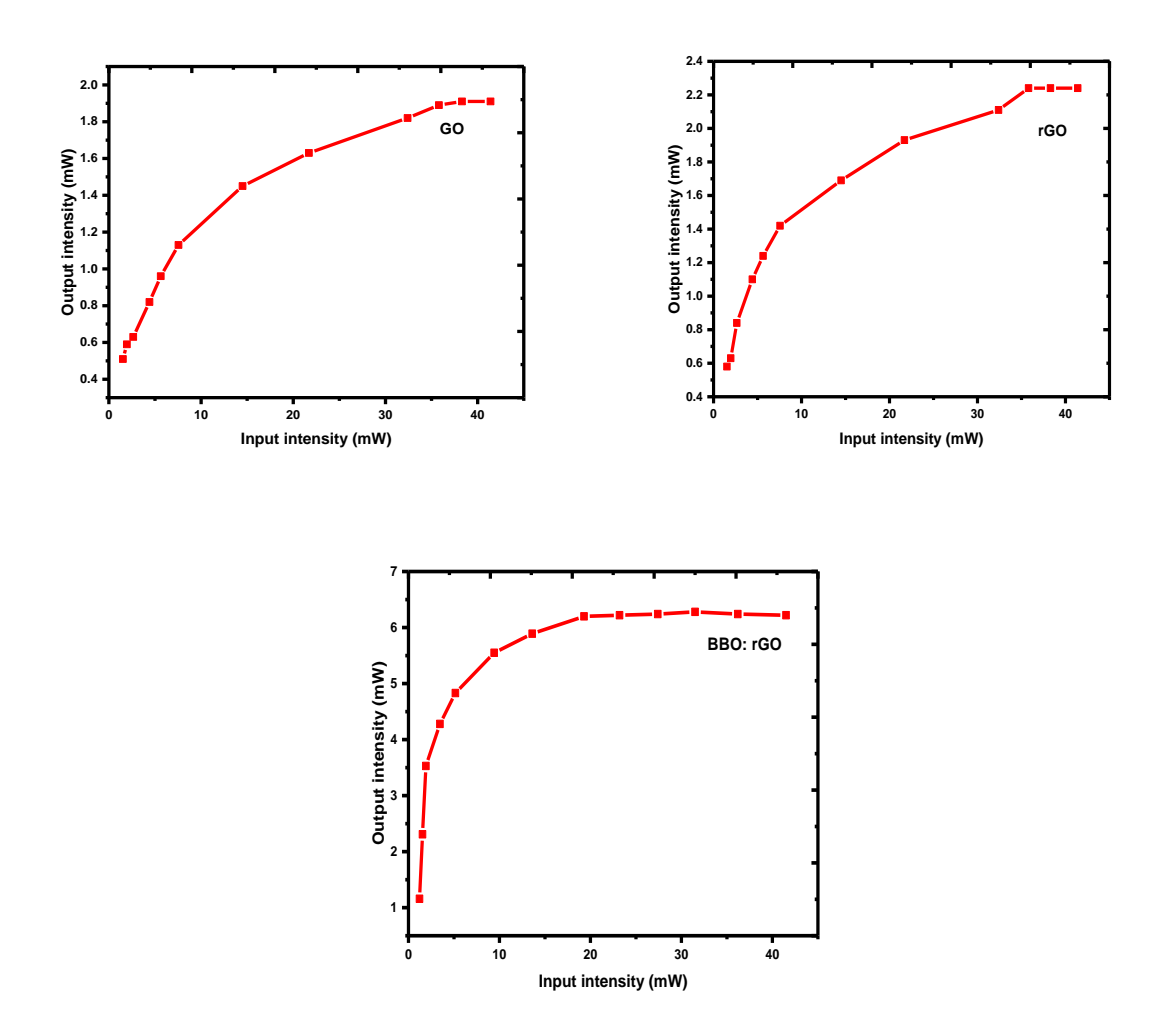


Figure 3.8 Optical Limiting Pattern of a) GO (b) rGO and (c) BBO: rGO

The estimated third-order NLO coefficient (Table 3.2) exposes the dominance of BBO: rGO composite over individual counterpart. Here upon reduction the nonlinear absorption coefficient and nonlinear refractive index of rGO was found to be increased. Appreciable changes in the third-order NLO coefficients of rGO shows the influence of functional groups and textural arrangements of graphene layers. Interestingly BBO:rGO composite possesses enhanced nonlinear refraction with almost four-fold increase in nonlinear refractive index than pure GO.

Table 3.2 Third-order NLO Coefficients of BBO: rGO Composite

Parameters	GO	rGO	γ-BBO [5]	BBO:rGO
Nonlinear refractive index (n ₂) x 10^{-8} cm ² /W	1.58	2.60	8.3	6.26
Nonlinear absorption coefficient (β) x 10 ⁻³ cm/W	5.86	5.88	8.8	6.05
Real part of the third- order susceptibility [Re(x³)] x 10-6 esu	0.90	1.48	-	4.48
Imaginary part of the third-order susceptibility [Im(x³)] x 10-6 esu	1.41	1.42	-	1.83
Third-order nonlinear optical susceptibility (x³) x 10-6 esu	1.68	2.05	4.34	4.84
Limiting threshold (mW)	32.5	32.5	32.6	9.51
Clamping value (mW)	1.9	3.1	0.85	6.23

The reason for such enhanced nonlinear refraction is due to the contribution of graphene sheets and barium borate, which possess high thermal conducting properties. Upon CW laser excitation, both rGO and BBO involve themselves in the photoexcitation resulting in enhanced thermal nonlinearity. Also, the 1D morphology of BBO contributes to channelized optical expiation. Similarly, nonlinear

absorption is also slightly increased which arises due to change in the electronic band structure of composite. The nonlinear absorption coefficient of BBO: rGO composite is higher than GO and rGO, which is due to the additional involvement of BBO. This enhancement has resulted in the higher third-order NLO susceptibility of BBO: rGO composite and thus suggesting in the superiority of composite over its counterparts [18]. As the excitation being CW and the samples possess saturable absorption, the observed nonlinear limiting behavior mainly originates from the self-defocusing nature. As BBO: rGO composite possesses enhanced nonlinear refraction, it has a low onset-limiting threshold (19.4 mW) arising from the strong thermal lens behavior. Thus the BBO nanorods decorated rGO are identified to superior in its third-order NLO behavior and can be considered a preferable candidate for optical limiting applications than pure graphene systems.

3.7 Conclusion

Barium borate – reduced graphene oxide nanocomposite was prepared by the hydrothermal method. XRD and FTIR analysis confirmed the presence of barium borate in the composite. FESEM shows the nanorods of barium borate on the sheets of reduced graphene oxide. From absorption spectrum, the transparent nature of barium borate in the UV and visible regions was proved. The photoluminescence of BBO:rGO showed the maximum emission in the UV region which is due to direct transitions involving the valence band and conduction band in the bandgap region. The nonlinear optical properties were studied using the Z-scan method with Nd: YAG (532 nm, 50 mW) laser. The peak followed by a valley normalized transmittance obtained from the closed aperture curves indicated that the sign of nonlinear refractive index is negative and self-defocusing

optical nonlinearity. In the open aperture pattern, the peak- like pattern shows the saturable nature of the material. Third-order NLO susceptability of BBO:rGO composite is greater than its parent material. It is noteworthy that the nanocomposite has a good nonlinear response and it can be a preferable optical limiter than its individual counter parts.

3.8 References

- 1. Ritt Gunnar, Bernd Eberle, Sensors 15 (2015) 792.
- 2. Jinhui Zhu, Yongxi Li, Yu Chen, Jun Wang, Bin Zhang, Jinjuan Zhang, Werner J.Blau, *Carbon* 49 (2011) 1900.
- 3. Qingrui Zhao, Xi Zhu, Xue Bai, Haihua Fan, Yi Xie, Eur. J. Inorg. Chem., 13 (2007) 1829.
- 4. Zhengshan Tian, Chunxiang Xu, Jitao Li, Gangyi Zhu, Jing Wu, Zengliang Shi, Yueyue Wang, *New. J. Chem.* 39 (2015) 6907.
- 5. C. Babeela, T.C. Sabari Girisun, Opt. Mater., 49 (2015) 190.
- 6. Leila Shahriary, Anjali A. Athawale, *Int. J. Ren. Energ. Envi. Eng.*, 02 (2014) 58.
- 7. G. Muruganandi, M. Saravanan, G. Vinitha, M.B. Jessie Raj, T.C. Sabari Girisun, *Chem. Phys.*, 488 (2017) 55.
- 8. You-Fu Zhou, Mao-Chun Hong, Yan-Qing Xu, Bai-Quan Chen, Chang-Zhang Chen, Yuan-Sheng Wang, *J. Crys. Grow.* 276 (2005) 478.
- 9. P. Muralimanohar, R. Parasuraman, J. Rajeev Gandhi, M.Rathnakumari, P. Sureshkumar, *Optik*, 127 (2016) 8956.
- 10. Vahib Babaahmadi, Majid Montazer, Coll. Surf. A: Physiochem. Eng. Asp., 506 (2016) 507.

- 11. C. Babeela, T. C. Sabari Girisun, G. Vinitha, *J. Phys. D: Appl. Phys.*, 48 (2015) 065102.
- 12. M. Saravanan, T.C. Sabari Girisun, G. Vinitha, *J. Mater. Sci.*, 51 (2016) 3289.
- 13. FLS. Cuppo, AM. Figueiredo Neto, SL. Go'mez, P. Palffy-Muhoray, J. Opt. Soc. Am. B 19 (2002) 1342.
- 14. T.C. Sabari Girisun, S. Dhanuskodi, *Chem. Phys. Lett.*, 491 (2010) 248.
- 15. M. Sheik-Bahae, AA. Said, T. Wei, DJ. Hagan, Van Stryland EW *IEEE J Quant. Electron*, 26 (1990) 760.
- 16. RL. Sutherland, *Handbook of nonlinear optics*, Marcel Dekker, NewYork (2003).
- 17. T.C. Sabari Girisun, S. Dhanuskodi, G. Vinitha, *Mater. Chem. Phys.*, 129 (2011) 9.
- 18. G. Muruganandi, M. Saravanan, G. Vinitha, M.B. Jessie Raj, T.C. Sabari Girisun, Opt. Mater., 75 (2018) 612.

Chapter - IV

2-amino 5-nitropyridinium Tetrafluoroborate Decorated Graphene Oxide

CHAPTER IV

2-amino 5-nitropyridinium Tetrafluoroborate Decorated Graphene Oxide

Based on host-quest chemistry, a semiorganic NLO material 2-amino 5-nitropyridinium tetrafluoroborate [2A5NPFB] was synthesized and grown as single crystals. Further, GO:2A5NPFB composite was prepared by the hydrothermal method. SXRD of 2A5NPFB reveals its crystal structural parameters as orthorhombic crystal system, Fdd2 space group, a=22.474 (1) Å, b=30.127 (9) Å, c=4.9584 (1) Å and $a=\beta=y=90^{\circ}$. Protonation site, charge transfer interaction and molecular structure were studied by FTIR analysis. The carbonaceous layered structure appears as a thin layer upon which 2A5NPFB appears as bright spots in the SEM image. 2A5NPFB possesses strong absorption (λ_{max} =350 nm) in the ultraviolet region and has a broad transparency window (420-1100 nm). While the inclusion of GO has induced absorption in the visible region. Kurtz and Z-scan technique explores the second and third-order NLO response of 2A5NPFB and GO: 2A5NPFB. Compared to KDP crystal, 2A5NPFB single-crystal possesses 35 times higher SHG efficiency. 2A5NPFB and its graphene composite exhibit saturable absorption, self-defocusing and optical limiting action under continuous-wave Nd: YAG green laser. Higher NLO coefficients and nonlinear refraction induced stronger optical limiting action was observed in GO: 2A5NPFB composite.

4.1 Introduction

Considering the factors of a sudden hike in the utilization of high intense short-wavelength (green) lasers and eye of humans has maximum sensitivity (88 %) to green color, the need for a second harmonic generation (SHG) and optical limiting (OL) material have increased tremendously [1]. Thus frequency doublers made second-order nonlinear optical (SONLO) materials capable of converting longer wavelength (IR) to visible (green) wavelength radiation are of considerable interest. Also, optical limiters made of third-order nonlinear optical (TONLO) materials that can protect the optical components from intense laser radiation are under limelight [2, 3]. Thus the investigation of materials has reached a point of balance between second and third-order nonlinearity, which ultimately requires a material with high NLO coefficients. In this line of search, 2-amino 5-nitropyridine (2A5NP) can induce a high NLO character with a strong donor (NH₂) and acceptor (NO₂) group through the push-pull mechanism [4-6]. In particular, the derivatives of 2-amino 5-nitropyridine are efficient NLO materials as they can attach inorganic elements to their herringbone pattern [7-9]. Some of the important compounds belonging to this class include: 2A5NP dihydrogen dihydrogen phosphate, 2A5NP arsenate, 2A5NP acetophosphate, 2A5NP fluoroborate, 2A5NP chloride, 2A5NP bromide and 2A5NP L-monohydrogen tartrate [9-11]. In particular, 2-amino 5-nitropyridinium fluoroborate [2A5NPFB] was identified to be an excellent frequency doubler with high SHG efficiency of 40 times KDP [12].

Although this compound was already investigated as a harmonic generator and their powder SHG efficiency was available in the literature, their bulk second and third-order NLO response remains unexplored. Especially the possible utilization of these compounds as a decorative element in carbonaceous layered material has a potential interest in the field of nonlinear optics. Among the carbonaceous layered structures, graphene oxide (GO) has recently emerged as a new carbon-based nanoscale material that provides an alternative path to graphene. It is known that structurally, the GO is similar to a graphene sheet with its base having oxygen-containing groups. Since these groups have a high affinity to water molecules, it is hydrophilic and can be easily dissolved in water and other solvents which allows it to be uniformly deposited in the form of thin films and also can act as host matrix. The basal planes and edges of the GO are functionalizing with exogenous groups, such as hydroxyl, epoxy and carbonyl groups which are attached at the edges. Then oxygen-containing functional groups disrupt the aromatic regions in the basal plane so that the layer of GO consists of both aromatic regions and oxidized aliphatic six-membered rings, which leads to distorted sp³- hybridized geometry and results in the insulating property of GO. Thus GO can act as an interesting platform to load/ functionalize desired materials to form potential hybrids or composites. Also, the report shows the graphene layer can enhance the properties of the functionalized unit. Specifically, as linear transmittance is poor for GO, it is combined with certain semiorganic NLO material like 2A5NPFB to attain composites with better optical properties.

Based on these facts, this chapter aims to investigate the second and third-order NLO response of 2A5NPFB single crystal grown by slow evaporation method and its graphene composite. The SHG capability (Kurtz technique) and optical limiting (Z-scan technique) behavior of pure and graphene composite of 2A5NPFB are presented in detail.

4.2 Material Preparation

By acid-base reaction, a semiorganic NLO material 2-amino 5-nitropyridinium fluoroborate [2A5NPFB] was synthesized [12]. Here the reaction involves a proton transfer between the nitrogen atom (basic acceptor) of 2-amino 5-nitropyridinium molecule and the hydrogen atom (acidic donor) of tetrafluoroboric acid. This induces the formation of semiorganic material, 2A5NPFB through the hydrogen bond formed by the electrostatic interaction between the 2A5NP+ cation and BF₄- anion. In a typical experimental procedure, 1 mole of 2A5NP was treated with 2 mole of HBF₄ acid in an aqueous medium (20 mole of H₂O). The solution was thoroughly mixed with a magnetic stirrer and maintained at 60 °C using a water bath. As 2A5NPFB possesses positive solubility temperature gradient in water, the controlled solvent evaporation method was employed to grow single crystals at ambient temperature. Single crystals with an average dimension of 9 x 7 x 5 mm³ (Fig. 4.1) were grown in 25 days.



Figure 4.1 Single Crystals of 2A5NPFB

2A5NPFB derivative-based GO composite was prepared by a simple hydrothermal method. Here the prepared GO (as described in Chapter II) and 2A5NPFB were used as starting precursors. In the employed synthesis procedure, 20 mg of GO dissolved in 100 ml water was mixed with the above-mentioned reaction mechanism. The obtained solution was stirred for 4 hours under the heating condition of 60 °C to obtain the GO:2A5NPFB composite in powder form.

4.3 Structural Confirmation

Initially, the obtained crystals were subjected to single-crystal XRD (SXRD) to confirm the formation of hybrid material through the estimation of the lattice parameter and space group. SXRD shows that 2A5NPFB possess orthorhombic crystal system with acentric spacegroup Fdd2 having lattice parameter a=22.474 (1) Å, b=30.127 (9) Å, c=4.9584 (1) Å and $\alpha=\beta=\gamma=90^{\circ}$. As the estimated lattice constants were found to be different from the cell constants of the parent molecule (2A5NP, HBF₄) and consistent with the already reported values of 2A5NPFB [12], the formation of semiorganic system was confirmed. In the recorded XRD pattern of 2A5NPFB powder depicted in Fig. 4.2, the prominent peaks confirm the perfect crystalline nature of the material. All the reflections were indexed for the orthorhombic system and the corresponding lattice parameters were estimated using the AUTOX program. As shown in Table 4.1, the lattice parameters of 2A5NPFB agree very well in both the modes of XRD. Upon decoration in GO, the crystalline nature of the semiorganic is slightly reduced and the pattern exactly resembles the XRD pattern of 2A5NPFB with a in peak position. As 2A5NPFB belongs noncentrosymmetric space group, it can be used for the generation of short-wavelength lasers through the frequency doubling phenomenon [7].

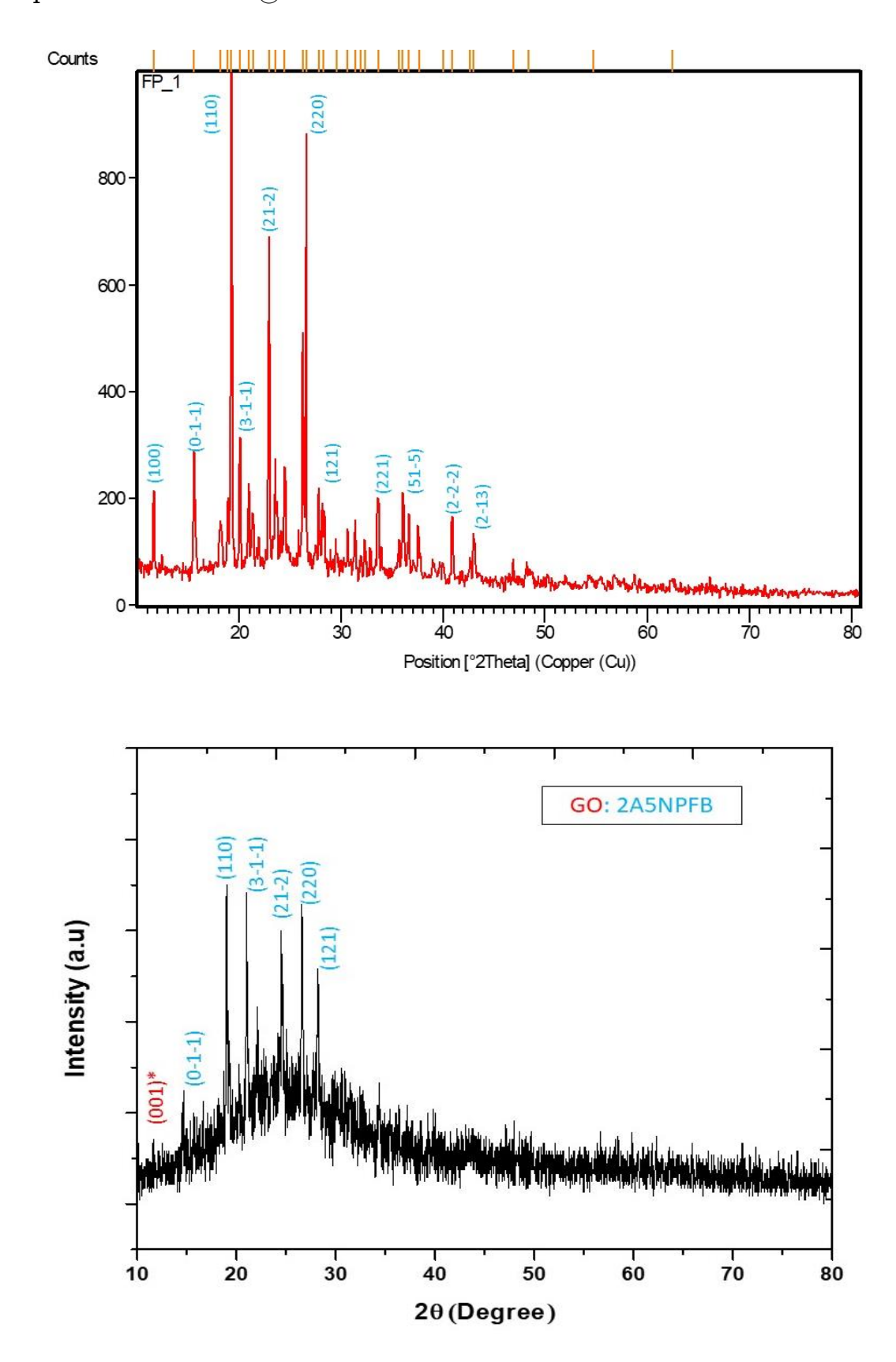
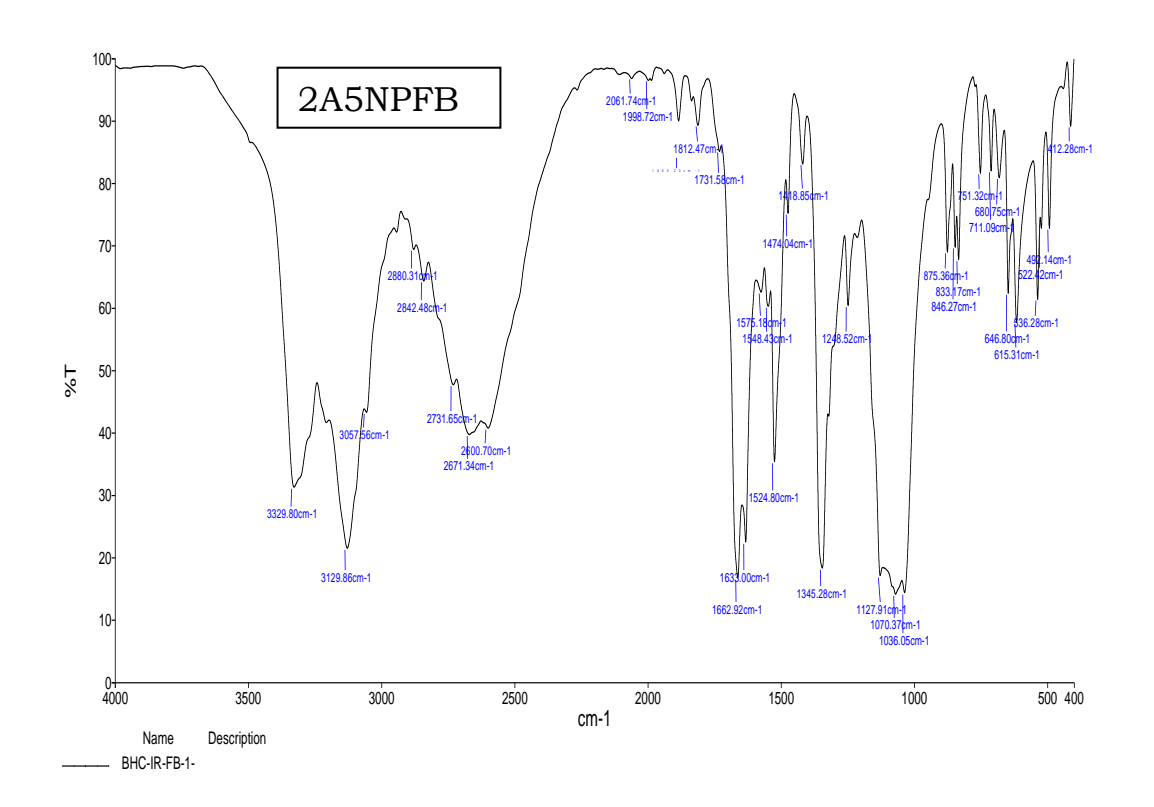


Figure 4.2 Powder XRD of 2A5NPFB and GO: 2A5NPFB

Table 4.1 Structural Parameters of 2A5NPFB Crystal

Lattice	Experimental		Reported	
parameters	SXRD	PXRD	Value [12]	
a (Å)	22.474 (1)	22.47	22.474 (4)	
b (Å)	30.127 (9)	30.12	30.128 (5)	
c (Å)	4.9584 (1)	4.95	4.9583 (8)	
a (°)	90	90	90	
β (°)	90	90	90	
γ (°)	90	90	90	
System	Orthorhombic	Orthorhombic	Orthorhombic	

The molecular arrangement of 2A5NPFB was analyzed and its protonation site was identified by FTIR analysis [13]. The recorded FTIR spectrum is shown in Fig. 4.3. The charge transfer interaction between tetrafluoroboric acid (donor) and 2-amino 5-nitropyridinium (acceptor) was ascertained through the peaks in the range of 3100-3500 cm⁻¹ [14]. The presence of peaks at 3329, 3129 cm⁻¹ corresponds to the N-H...F hydrogen bond which confirms the presence of intramolecular hydrogen bonding between the nitrogen of 2A5NP+ cation and the fluorine atom of the BF₄- anion. The asymmetric stretching vibration of aromatic C=N was shifted to 1662 cm⁻¹ than its parental 2A5NP+ at 1648 cm⁻¹. Also due to protonation, the peak which corresponds to N-H bending (1633 cm⁻¹) of 2A5NPFB deviated from the parental arrangement and this has resulted in the increased hyperpolarizability of the molecule.



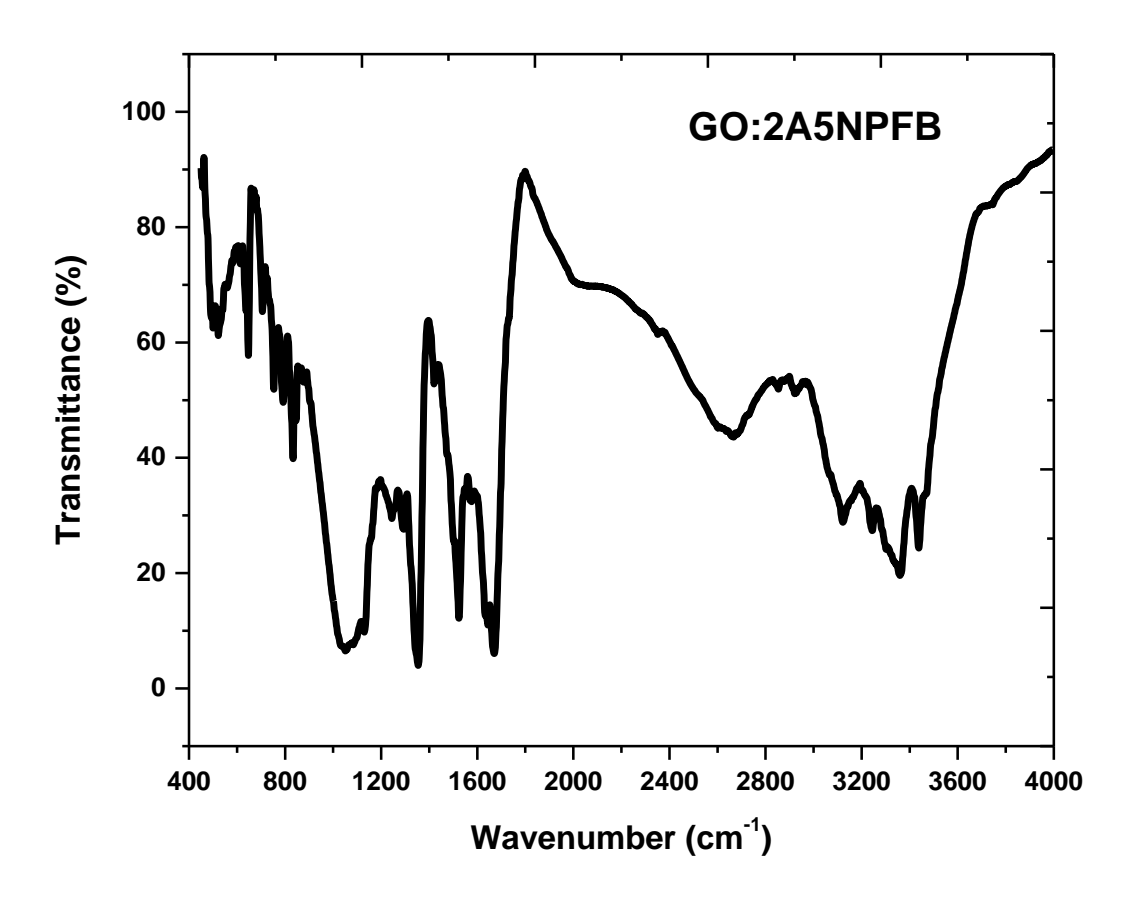


Figure 4.3 FTIR Pattern of 2A5NPFB and GO: 2A5NPFB

Chapter IV: 2A5NPFB @ GO

Table 4.2 FTIR Peak Assignment of 2A5NPFB and GO: 2A5NPFB

Wavenumber (cm ⁻¹)					
2A5NP	2A5NPFB	GO	GO: 2A5NPFB	Assignment	
		3442	3437	O-H stretching of hydroxyl groups	
-	3329		3207	ν (N-HF)	
-	3129			ν (N=HF)	
		2925	2921	C-H stretching	
		2324		C=O stretching of carboxy groups	
		1729		C=O stretching of carbonyl groups	
1648	1662		1644	ν (C=N)	
1632	1633			δ (N-H)	
		1572	1436	C=C stretching	
1332	1345		1331	ν (N-O)	
		1228	1051	C=O stretching of epoxy groups	
-	751, 711, 680		750	ν (BF ₄)-	
	v - stretching	vibrations	and δ - bend	ing vibrations	

 ν - stretching vibrations and δ - bending vibrations

The presence of peaks at 1474, 1418, 1345 cm⁻¹ represents the symmetric stretching vibrations of N-O. The vibrations in the lower wavenumber domain 500-800 cm⁻¹ confirm the presence of inorganic elements. In particular, the peaks at 751, 711, 680, 536 cm⁻¹ corresponds to symmetric stretching and asymmetric bending of BF₄-[12].Prepared anions respectively composites possess the characteristic peak of both GO and 2A5NP which ascertains the formation of hybrid materials. Slight shifts in the peak positions are due to the interaction of graphene layers and 2A5NP molecules. It can be seen that the aromatic asymmetric stretching vibration of 2A5NP+ at 1633 cm⁻¹ is shifted to a higher wavenumber for GO:2A5NPFB (1644 cm⁻¹). The incorporation of inorganic species is confirmed by the presence of new peaks at 750 cm⁻¹ (BF⁴⁻ anion) in 2A5NPFB. The observed FTIR peaks were confirmed with the parent molecule 2A5NP and the assignments are given in Table 4.2.

The textural arrangement of composites was examined by SEM studies using Hitachi SEM 400. The recorded SEM image of GO and GO: 2A5NPFB derivatives composite is as shown in Fig. 4.4. The carbonaceous layered structure appears as a thin layer in SEM and is a clear indication of the presence of graphene layers. In Fig. 4.4(a) wrinkled paper-like ultrathin sheets with stacking was observed for GO due to the harsh oxidation process during the synthesis. Fig. 4.4(b) shows the dense aggregates regions observed in samples confirmed that thin, continuous, and twisted like structures randomly oriented and many thin layers entangled with each other with overlapped oxidized edges. It is also noticed that certain bright spots additionally appear which depict the successful attachment of 2A5NPFB on the surface of GO. Here the possible growth mechanism can be explained as follows: 2A5NP+ cations interact with inorganic

anions (BF⁴⁻) to form them as 2A5NPFB. This molecule interacts with graphene layers via the attached oxygen-containing functional groups and creates a nucleation site. This nucleation grows as clusters due to the agglomeration of 2A5NP molecules. As the preparation was employed in a simple hydrothermal setup, agglomeration of 2A5NP derivative molecules takes place and thus forms irregular structures. It is also to be observed that the loading and agglomeration vary with respect to the nature of inorganic species. Thus incorporation of 2A5NPFB upon GO sheets was confirmed from SEM analysis.

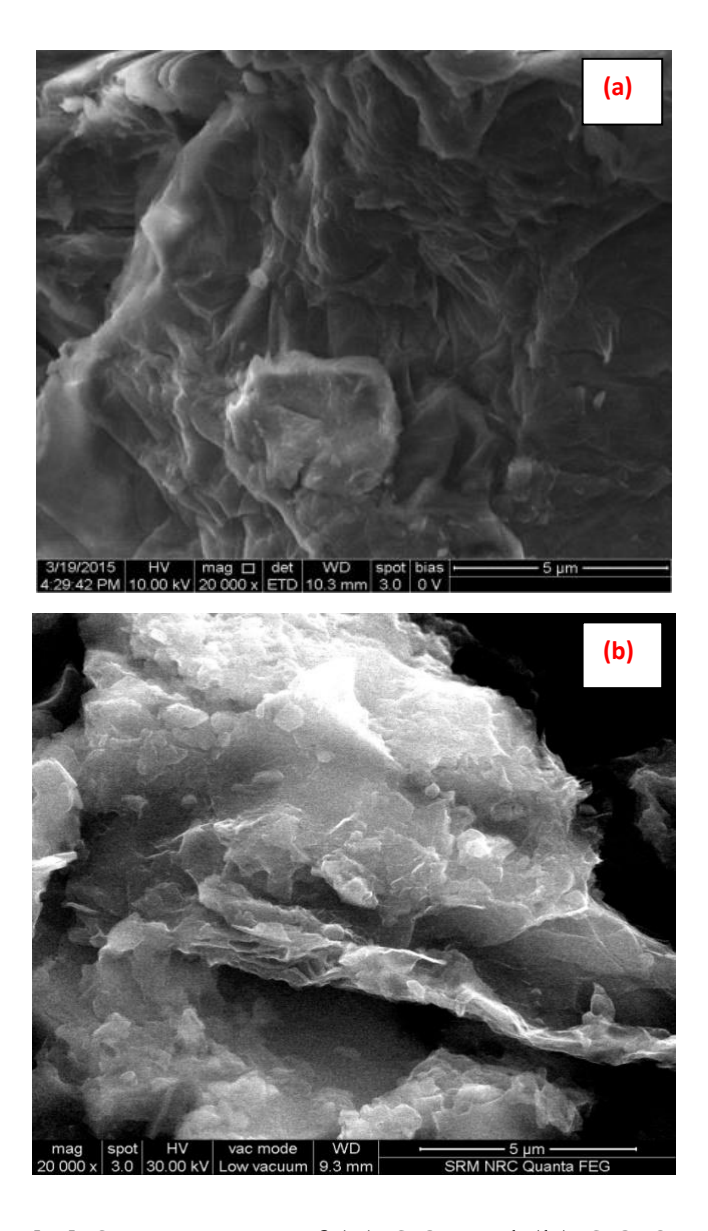


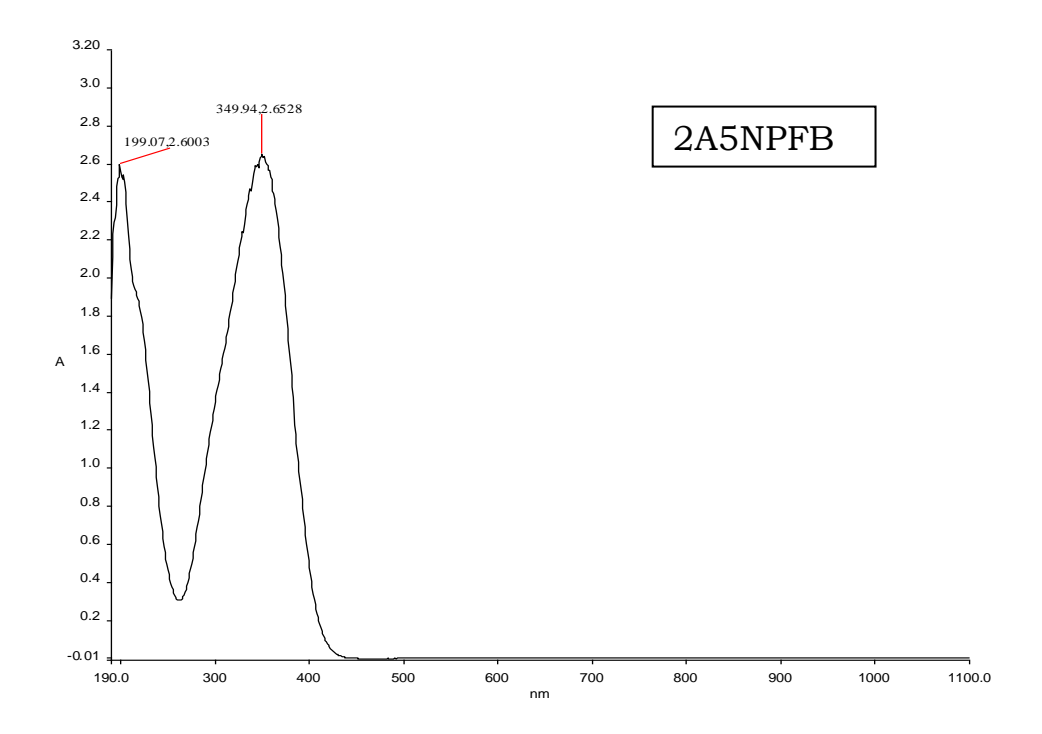
Figure 4.4 SEM Image of (a) GO and (b) GO:2A5NPFB

4.4. Linear Optical Properties

The optical properties of prepared samples were examined by the UV-Visible absorption spectrum using the Bio-drop Duo spectrometer. Initially, the samples were dissolved in water at a concentration of 3 mg/ml before recording the absorption spectrum. The graph was drawn between absorbance and wavelength and is shown in Fig. 4.5. UV-VIS absorption pattern of 2A5NPFB (Fig. 4.5(a)) exposes the significant absorption in the ultraviolet region with absorption maxima at λ_{max} = 199 nm, 350 nm. Hence the cutoff wavelength of 2A5NPFB was estimated to be 350 nm. Also, the material has a wide optical window of 420-1100 nm, with almost negligible absorption in the visible and NIR region. Here it is to be noted that alteration in intramolecular charge transfer takes place due to the formation of 2-amino 5-nitropyridine cation which lengthens C-NO₂ and shortens C- NH₂, C=C, C=N bond lengths [12]. This complex formation redshift the transparency of parental 2-amino 5-nitropyridine by 40 nm [11]. Thus lower cutoff along with a wide range of transparency in UV and visible region enables good transmission which makes 2A5NPFB to be an entrant material for NLO applications in both second-order (second-harmonic generation) and third-order (optical limiting) NLO applications [15, 16].

In the recorded UV-vis absorbance spectrum (Fig. 4.5(b)) of GO:2A5NPFB, it can be observed that GO possesses strong absorption in the UV and visible region. The absorption maxima of GO is at 235 nm and it corresponds to the electronic transition involving π - π * states. For pure 2A5NP maximum absorption occurs at 590 nm. The absorbance of GO is higher in the visible region while 2A5NP possess lower absorbance. This interesting combination of absorbing GO with

transparent 2A5NP has resulted in the alterations of electronic states associated with graphene and 2A5NP.



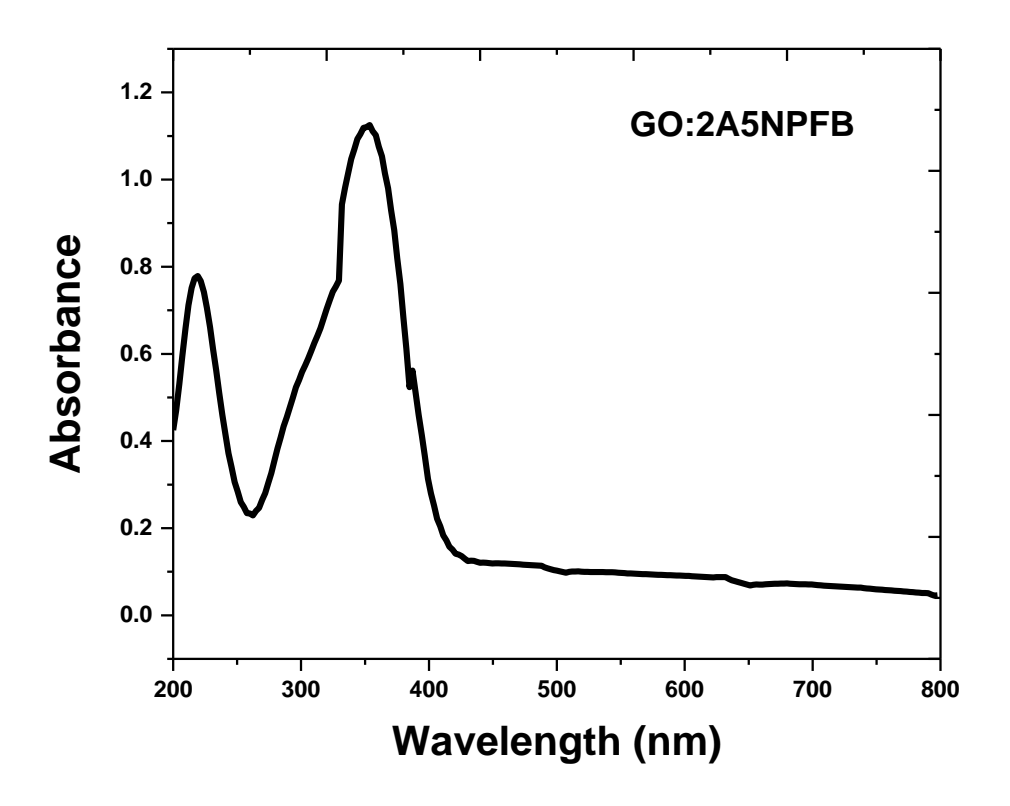


Figure 4.5 Absorbance Spectrum of 2A5NPFB and GO: 2A5NPFB

In the UV-Vis absorption pattern of composite (Fig. 4.5(b)), the characteristic peak of both GO and 2A5NP was observed and thus it confirms the formation of composite materials. The absorption maximum, cut-off wavelength and optical transmittance window of composites are 219 nm, 352 nm, 405 nm, and 405-1100 nm respectively. Due to the incorporation of inorganic species, the absorption maxima of 2A5NP suffered a bathochromic shift in the crystal transparency due to the less polarizable nature of 2A5NP cation compared to the molecular equivalent. The linear transmittance suffered a strong shift in the characteristic peak of 2A5NP suggesting the dominance of 2A5NP derivatives in the composite. As expected the linear transmittance of the composite is higher than GO, which is an essential criterion for the optical limiting applications.

4.5 Second and Third Order NLO Properties

4.5.1 Second Harmonic Generation Test

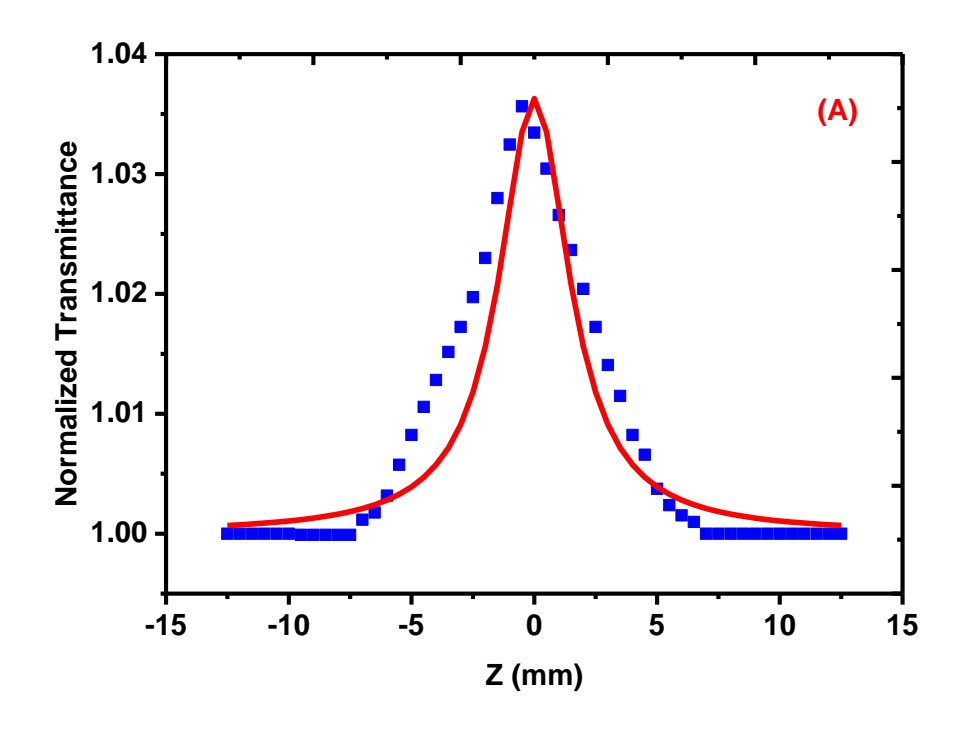
The second harmonic generation test on the bulk crystal of 2A5NPFB was made by the Kurtz method [17]. A defect-free 2A5NPFB crystal of dimension 7 × 5 × 3 mm³ was cut and polished from the grown crystals for the SHG test. Here the crystal was illuminated using an Nd: YAG laser (1064 nm, 10 Hz, 5 ns, 20 mJ). The input laser with a spot radius of 1 mm was directed on the crystal. The transmitted light was filtered through the IR filter and was measured using a photodetector. When a laser of 1064 nm was radiated directly on the crystal, a green light beam of double frequency 532 nm was observed which indicates that 2A5NPFB possesses SHG behavior. The second harmonic generation efficiency of the 2A5NPFB sample was estimated by taking the KDP crystal (3 x 3 x 3 mm³) as a reference system. The test shows a green signal output of 2722 mV and 80 mV for 2A5NPFB and KDP respectively. Thus frequency doubling efficiency

of 2A5NPFB single crystal was found almost 35 times higher than KDP crystal. The observed higher second harmonic generation efficiency arises mainly from the highest density of the chromophores. Although 2A5NPFB possesses a very high second-order NLO coefficient than other materials, its major concern is the non-phase matchable property of the material [12]. Also, the composite of GO:2A5NPFB did not show any SHG signal which may arise due to the dominance of graphene layers. Thus the materials were further subjected to its third-order NLO studies.

4.5.2 Z-Scan Studies

The third-order NLO properties of 2A5NPFB and GO: 2A5NPFB composite were studied by the Z-scan experiment. The nonlinear refractive index and the nonlinear absorption coefficient of 2A5NPFB and GO:2A5NPFB were determined by the Sheik-Bahae formalism [3, 18], where a Gaussian beam from a Nd:YAG laser (532 nm, 50 mW) was used as the excitation source. Fig. 4.6 and Fig. 4.7 gives the nonlinear open aperture (OA) and closed aperture (CA) pattern of 2A5NPFB and GO:2A5NPFB respectively. Although 2A5NPFB shows a negligible linear absorption at the excitation domain, it has strong nonlinear absorption which is seen from the peak pattern in open aperture Z-scan mode [8]. At the same time, the inclusion of GO in the composite has greatly increased the linear absorption in the visible region, which in turn enhances the saturable absorption of the composite. Thus 2A5NPFB and GO:2A5NPFB exhibit minimum absorbance at the focus exposing the presence of saturable absorption with negative nonlinear absorption coefficient (Fig. 4.6(A) and Fig. 4.7(A)). The closed aperture Z-scan curve in Fig. 4.6(B) and Fig. 4.7(B) has a peak-valley pattern which indicates the presence of self-defocusing behavior with the negative nonlinear refractive index.

The ratio of closed-aperture to open-aperture transmittance is taken to estimate the pure nonlinear refractive index of the samples.



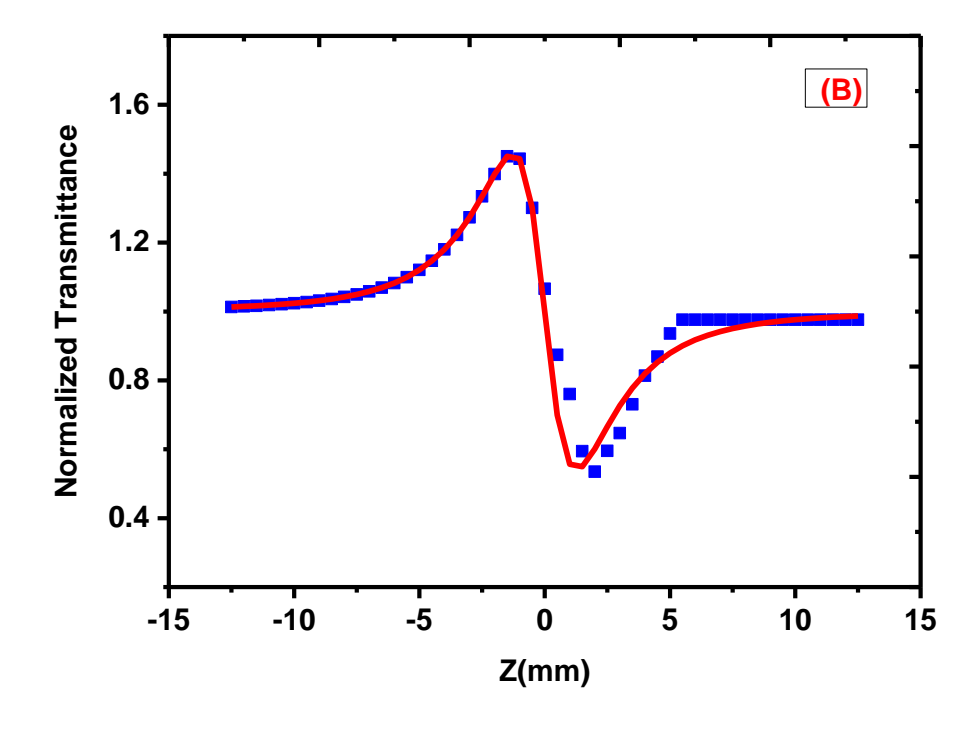
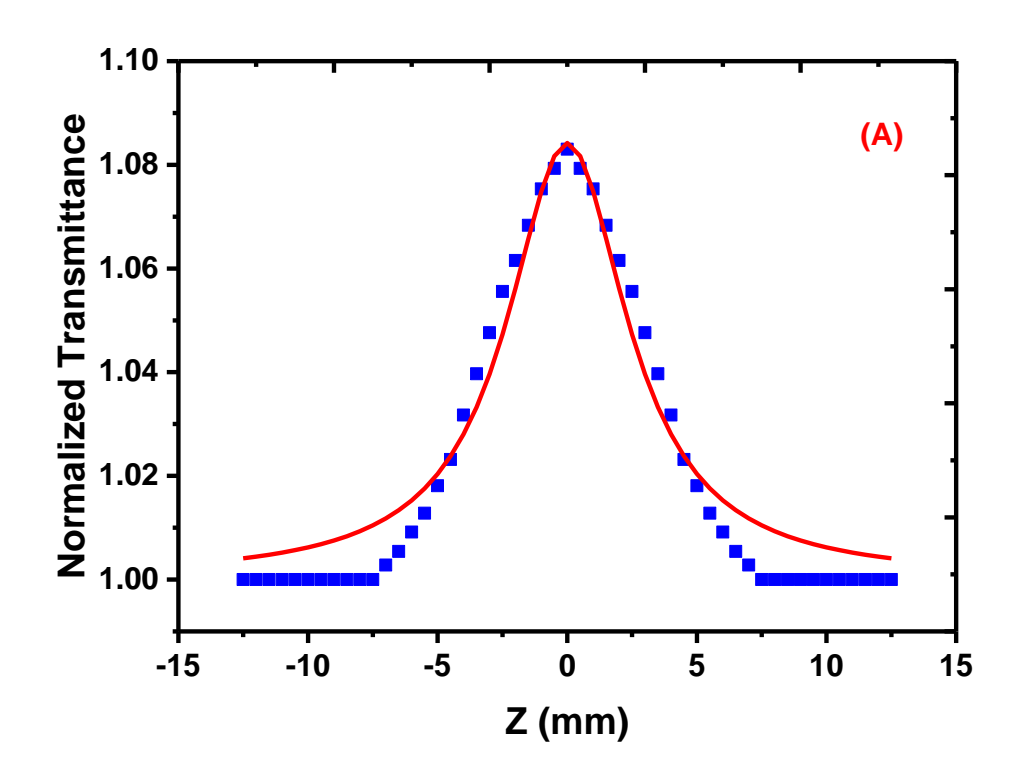


Figure 4.6 (A) OA and (B) CA Z-scan pattern of 2A5NPFB



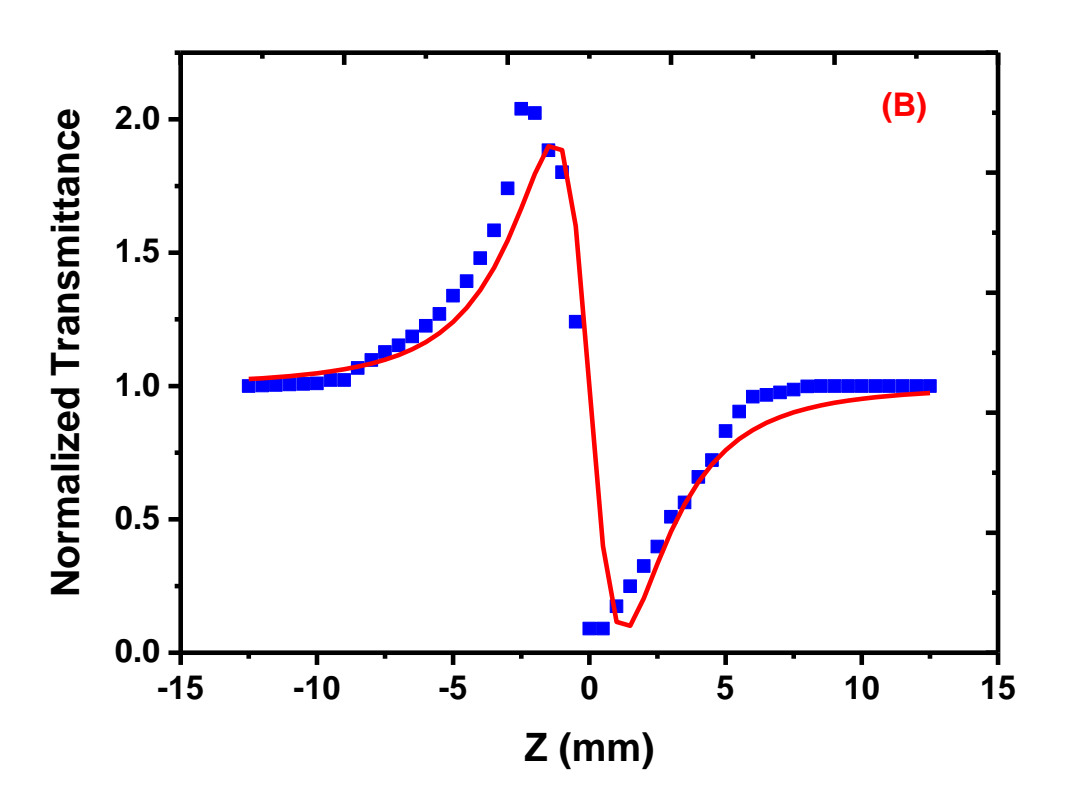
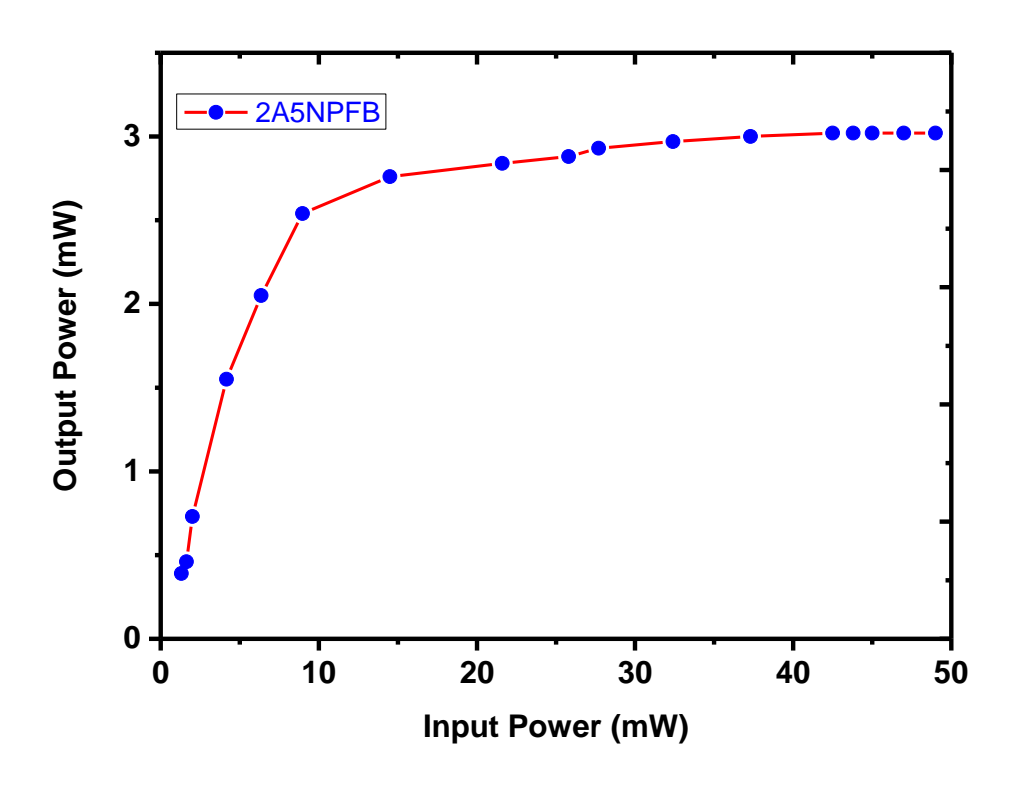


Figure 4.7 (A) OA and (B) CA Z-scan pattern of GO: 2A5NPFB



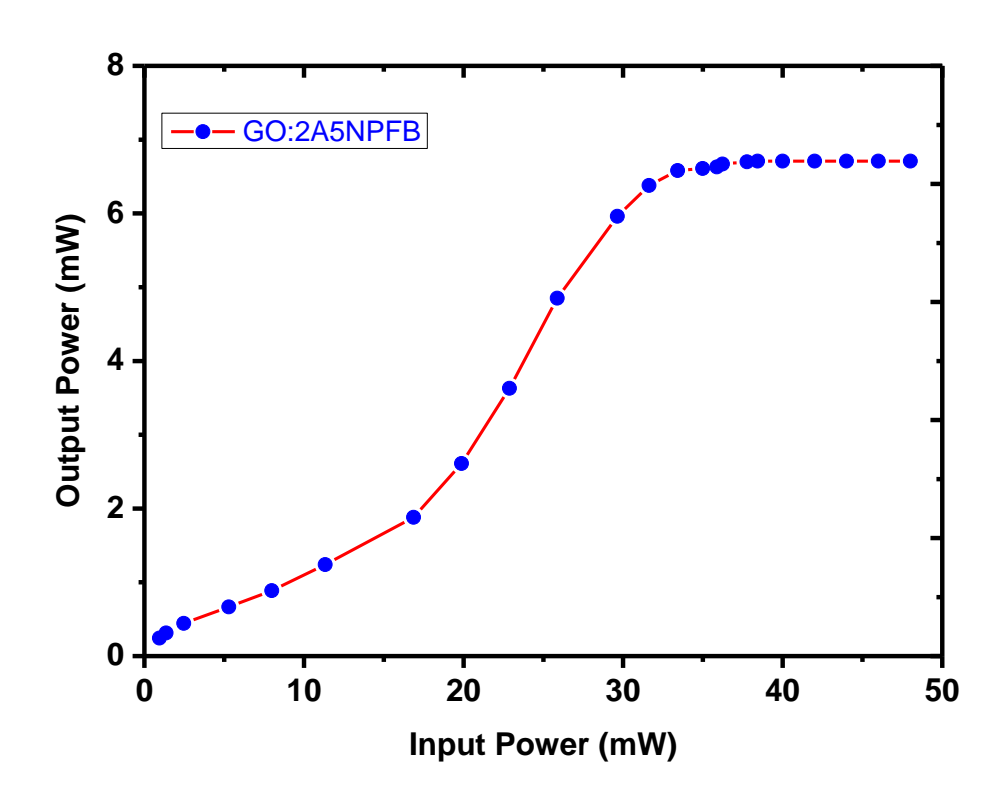


Figure 4.8 OL Curve of GO and GO: 2A5NPFB

Table 4.3 Third-order NLO properties of 2A5NPFB and GO: 2A5NPFB

NLO Parameters	2A5NPFB	GO: 2A5NPFB
Nonlinear refractive index	3.93	6.06
$(n_2) \times 10^{-8} \text{ cm}^2/\text{W}$		
Nonlinear absorption coefficient	7.64	13.95
$(\beta) \times 10^{-3} \text{ cm/W}$		
Real part of NLO susceptibility	1.95	3.06
[Re [x ⁽³⁾]] x 10 ⁻⁷ esu		
Imaginary part of NLO susceptibility	1.61	2.98
[Im [x ⁽³⁾]] x 10 ⁻⁶ esu		
NLO susceptibility	2.53	4.27
$(x^{(3)}) \times 10^{-6} \text{ esu}$		
Optical limiting threshold (mW)	36.23	37.73
Clamping amplitude (mW)	6.7	3.02

Table 4.3 summarizes the third-order NLO values of 2A5NPFB and GO: 2A5NPFB following the Sheik Bahae formalism as discussed in Chapter I (Eqn. 1.43 to Eqn. 1.47) [20]. As witnessed in Table 4.3, the saturable absorption coefficient and the nonlinear refractive index of GO: 2A5NPFB is much higher than pure 2A5NPFB. In both cases, Re $[x^{(3)}]$ is higher than Im $[x^{(3)}]$ which signifies that nonlinear refraction is the stronger mechanism involved. Almost a two-fold increase in NLO susceptibility is witnessed in GO: 2A5NPFB composite than 2A5NPFB which arises mainly due to the inclusion of graphene sheets.

Fig. 4.8 shows the optical limiting behavior of 2A5NPFB and GO: 2A5NPFB composite. For incident power less than 36 mW, 2A5NPFB and GO: 2A5NPFB obeys Beer's law and then its output saturates leading to nonlinear behavior. The onset limiting threshold value of 2A5NPFB and GO: 2A5NPFB composite is 36 mW and 37 mW respectively. The observed nonlinear optical limiting action arises from the nonlinear refraction (self-defocusing) behavior. Due to the change in NLO coefficients, limiting parameters were found to be different. Here GO: 2A5NPFB composite (3.02 mW) exhibits lower clamping amplitude than 2A5NPFB (6.7 mW). This confirms that 2A5NPFB and GO: 2A5NPFB can be used as optical limiting material, in which superiority belongs to the GO: 2A5NPFB composite [3, 19].

4.6 Conclusion

5-nitropyridinium 2-amino fluoroborate (2A5NPFB) was synthesized using 2A5NP and tetra fluoro boric acid in an aqueous medium. Using graphene oxide obtained through a modified Hummers method as host and 2A5NPFB as a decorative element, GO: 2A5NPFB composite was prepared. Optical quality defect-free crystal of 2A5NPFB of dimension 9 x 7 x 5 mm³ were grown by the solvent evaporation method. 2A5NPFB crystallizes in acentric space group Fdd2 having orthorhombic crystal system with lattice parameter a=22.474 (1) Å, b=30.127 (9) Å, c=4.9584 (1) Å and α=β=γ= 90°. The charge transfer interaction between tetrafluoroboric acid (donor) and 2-amino 5-nitropyridinium (acceptor) was ascertained by FTIR analysis. Prepared composites possess the characteristic peak of both GO and a slight shift in the peak positions are due to the interaction of graphene layers and 2A5NP molecules. The incorporation of inorganic species is confirmed by the presence of new peaks at 750 cm⁻¹ (BF4- anion) in 2A5NPFB. In SEM image, the formation of thin,

continuous, and twisted like graphene structures randomly oriented with additional bright spots depict the successful attachment of 2A5NPFB on the surface of GO. 2A5NPDP possesses strong absorption (λ_{max} =2199, 350 nm) in the ultraviolet region and has a broad transparency window (420-1100 nm). In the UV-Vis absorption pattern of composite, the characteristic peak of both GO and 2A5NP was observed. The absorption maximum, cut-off wavelength and optical transmittance window of composites are 219, 352 nm, 405 nm, and 405-1100 nm. The relative second harmonic generation efficiency of 2A5NPFB crystal was 35 times that of KDP. Z-Scan studies with CW excitation show that the material exhibits saturable absorption, self-defocusing, and optical limiting action. And here GO: 2A5NPFB exhibit higher NLO performance than pure GO and 2A5NPFB.

4.7 References

- 1. R. L. Sutherland, *Handbook of nonlinear optics*, Marcel Decker Inc, New York, 2003.
- 2. P.N. Prasad, D.J. Williams, *Introduction to nonlinear optical effects in organic molecules and polymers*, Wiley, New York, 1991.
- 3. T.C. Sabari Girisun, S Dhanuskodi, G Vinitha, *Mater. Chem. Phys.*, 129 (2011) 9.
- 4. A. Ibanez, J.P. Levy, C. Mouset, E. Prieur, *J. Soild State Chem.*, 129 (1997) 22.
- 5. J. Pecaut, Y. L. Fur, R. Masse, *Acta Crystallogra Sect.*, B49 (1993) 535.
- 6. J. Zaccaro, B. Capelle, A. Ibanez, *J. Cryst. Growth*, 180 (1997) 229.
- 7. M. Thangaraj, G. Ravi, T.C. Sabari Girisun, *Physica B: Cond. Matter*, 449 (2014) 209.

- 8. T.C. Sabari Girisun, S Dhanuskodi, D Mangalaraj, J Phillip, *Curr. Appl. Phys.*, 11 (2011) 838.
- 9. M.S. Wong, J.F. Nicoud, C. Runser, A. Fort, M. Barzoukas, *Nonlinear Optics*, 9 (1995) 181.
- 10. M. Ambrose Rajkumar, S. Stanly John Xavier, S. Anbarasu, Prem Anand Devarajan, *Opt. Mater.*, 55 (2016) 153.
- 11. G. Anandha Babu, R.P. Ramasamy, P. Ramasamy, V.Krishna Kumar, *Cryst. Growth & Design*, 9 (2009) 3333.
- 12. S. Manivannan, S. Dhanuskodi, K. Kirschbaum, and S. K. Tiwari, *Cryst. Growth & Design*, 5 (2005) 1463.
- 13. G. Varsanyi, Assignments for vibrational spectra of seven hundred benzene derivatives, Adam Hilger, London, 1974.
- 14. P.S. Kalsi, *Spectroscopy of organic compounds*, New Age International (P) Limited Publishers, New Delhi, 2002.
- 15. B. Milton Boaz, A. Leo Rajesh, S. Xavier Jesu Raja, S. Jerome Das, J. Mater. Sci. Technol., 20 (2004) 505.
- T.C. Sabari Girisun, S. Dhanuskodi, Cryst. Res. Technol., 44 (2009) 1297.
- 17. S.K. Kurtz, T.T. Perry, J. Appl. Phys., 36 (1968) 3798.
- 18. Mansoor Sheik- Bahae, Ali A. Said, Tai-Huei Wei, *IEEE J. Quantum. Electron*, 26 (1990) 760.
- 19. M. Thangaraj, G. Ravi, T.C.Sabari Girisun, G. Vinitha, A. Loganathan, *Spectrochim. Acta Part A: Mol. and Biomol. Spectro.*, 138 (2015) 158.
- 20. G. Muruganadi, M.B. Jessie Raj, Optik, 182 (2019) 755.

Chapter - V

2-amino 5-nitropyridinium Tetrafluoroborate Decorated Graphene Oxide

CHAPTER V

2-amino 5-nitropyridinium Dihydrogen Phosphate Reduced Graphene Oxide

2-amino 5-nitropyridinium Dihydrogen Phosphate (2A5NPDP) was obtained by dissolving 2A5NP in an acidic solution of orthophosphoric acid and grown as single crystals. It crystallizes in orthorhombic crystal system with Pna2₁ space group (Z= 4). By hydrothermal method, decoration of 2A5NPDP upon GO sheets to form GO: 2A5NPDP composite was made. The presence of hydrogen bonds (N-H...O) was identified by the shifting of the peaks of NH2 group in the 2A5NPDP from the characteristic vibrational frequencies of 2A5NP. Further, the peak at 986 cm⁻¹ corresponds to symmetric stretching of PO₄ anions which confirm the formation of the 2A5NPDP compound. Prepared GO: 2A5NPDP composite possess the characteristic peak of both GO and 2A5NP which ascertains the formation of hybrid materials. SEM image of GO: 2A5NPDP composite possesses dense bright shades of 2A5NPDP with uniform concentration upon the ultrathin sheets with the stacking of GO. In the UV-Vis absorption pattern of GO: 2A5NPDP composite, the characteristic peak of both GO (235 nm) and 2A5NPDP (340 nm) was observed with the change in the linear transmittance. 2A5NPDP possesses a relative SHG efficiency of 4.2 times KDP with phase matching property. The nonlinear optical response of thermo-optic origin exhibited by pure and decorated 2A5NPDP at 532 nm low power CW laser was studied using the Z-scan technique. Saturable absorption, self-defocusing, and optical limiting action were observed in all samples. Interaction of 2A5NPDP with GO sheets enhanced the third-order NLO properties and thus 2A5NPDP decorated GO exhibit superior OL action.

5.1 Introduction

Over recent years, a series of studies have been performed on organic optical materials with high nonlinearity for a variety of applications in a second harmonic generation (SHG) and optical limiting (OL) devices [1-4]. Organic molecules with remarkable NLO activities, in general, owe their origin to the structural feature of having a π -electron conjugated moiety substituted by an electron donor group at one end and an electron acceptor group at the other end forming a push-pull conjugated design [5]. In the organic functional group materials, the conjugated π -bond electrons increase the polarizability of the molecule and the donor-acceptor groups contribute their own "mesomeric moments", which enhance their optical nonlinearity over inorganic counterparts. The donor and acceptor groups provide basic charge asymmetry to the molecules, an essential requirement for the realization of the noncentrosymmetric structure, required for second-order nonlinearity. But these materials, despite their increased SHG efficiency, display loss of optical transparency in the lower wavelength region (100-400 nm). The tradeoff between optical transparency and SHG efficiency turned out to be an important issue while developing the devices using NLO materials [6, 7]. Also, there are some disadvantages in using organic molecular crystals for frequency conversion and optical limiting applications. Though organic molecular crystals have been easily grown from solution, yet the size, softness, low thermal conductivity and absorption loss are preventing them from effective usage of SHG and OL devices [8-10].

As a result, worldwide attempts have been made to explore suitable semiorganic ionic systems that overcome the inherent limitation on the maximum attainable nonlinearity in inorganic materials and the moderate success in growing device grade single crystals in organic materials. The systems under this category include organic-inorganic salts and metal-organic coordination compounds [11, 12]. 2-amino 5-nitropyridine [2A5NP] is one of the derivatives of nitroaniline, which also forms numerous salts by reacting with [13-15]. inorganic acids These hybrid materials possess the advantages of the organic phase (high NLO efficiency) and mineral crystals (good stability, wide transparency) and are built up by the anchorage of organic molecules onto mineral matrices through strong hydrogen bonds. The 2A5NP molecule exhibits some classical features such as (i) a blue shift of crystal transparency resulting from the less polarizable nature of the 2A5NP+ cations, ii) the SHG efficiency is probably due to the density of chromophores, iii) the molecular derivatives of 2A5NP display zigzag or herringbone pattern following the number of hydrogen donor groups able to form one or several hydrogen bonds, iv) the nitro group is introduced to produce a strong dipole moment and also to favor crystallization in noncentrosymmetric space group. In the present study, the inorganic acids selected for the synthesis of the semiorganic salts are orthophosphoric acid (H₃PO₄) to form 2-amino 5-nitropyridinium dihydrogen phosphate (2A5NPDP). They are strong acids and they get ionized in the solution to release a hydrogen ion (H⁺). Hence the strong hydrogen bonds are formed, which favors the thermal stability of the material. The second-order NLO process in crystals is influenced by the molecular structure and their arrangement [16]. In continuation of the earlier attempt, decoration of GO with 2A5NPDP to form a hybrid is attempted. Here graphene oxide will act as host to accommodate interesting 2A5NPDP with phosphate unit. The second and third-order NLO behavior of the composite are studied for frequency conversion and optical limiting applications and the results are discussed.

5.2 Material Preparation

2A5NPDP was obtained by dissolving 2A5NP in an acidic solution of orthophosphoric acid (H₃PO₄) with the molar ratio 1: 3: 10 for 2A5NP, H₃PO₄, and H₂O respectively. Heating the solution at 60 °C for 2 hours resulted in a yellow mixture with no precipitation of 2A5NP. By the addition of ethanol light yellow needles of 2A5NPDP precipitated and are subsequently washed with ethyl acetate. The mother solution was distilled to eliminate alcohol and water and serves as the solution for crystal growth. Finally, a light yellow powder of 2A5NPDP was separated and was used for single crystal growth. In the typical crystal growth employed based on the solvent evaporation dissolved in method, the compound was ethanol and the supersaturated solution was filtered and kept for crystallization at 32 °C. Single crystals of 2A5NPDP (6 x 2 x 1 mm³) were grown from ethanol following the slow evaporation technique (Fig. 5.1). After 10 days, single crystals were grown from their mother solution with a growth rate of 0.7 mm/day.

By hydrothermal method, decoration of 2A5NPDP upon GO sheets to form GO: 2A5NPDP composite was made. Initially GO prepared by modified Hummer's method (as described in Chapter II) was taken as host precursor. Imitating the similar experimental procedure adopted for GO: 2A5NPFB, 20 mg of GO dissolved in 100 ml water was mixed in the synthesis process of 2A5NPDP as an additive. The obtained solution was not transparent due to the dominance of GO which was stirred for 4 hours under the heating condition of 60 °C to obtain the GO: 2A5NPDP composite in powder form. The interesting difference between the parent molecule and composite is that the light yellow 2A5NPDP turns mild black in GO: 2A5NPDP composite.

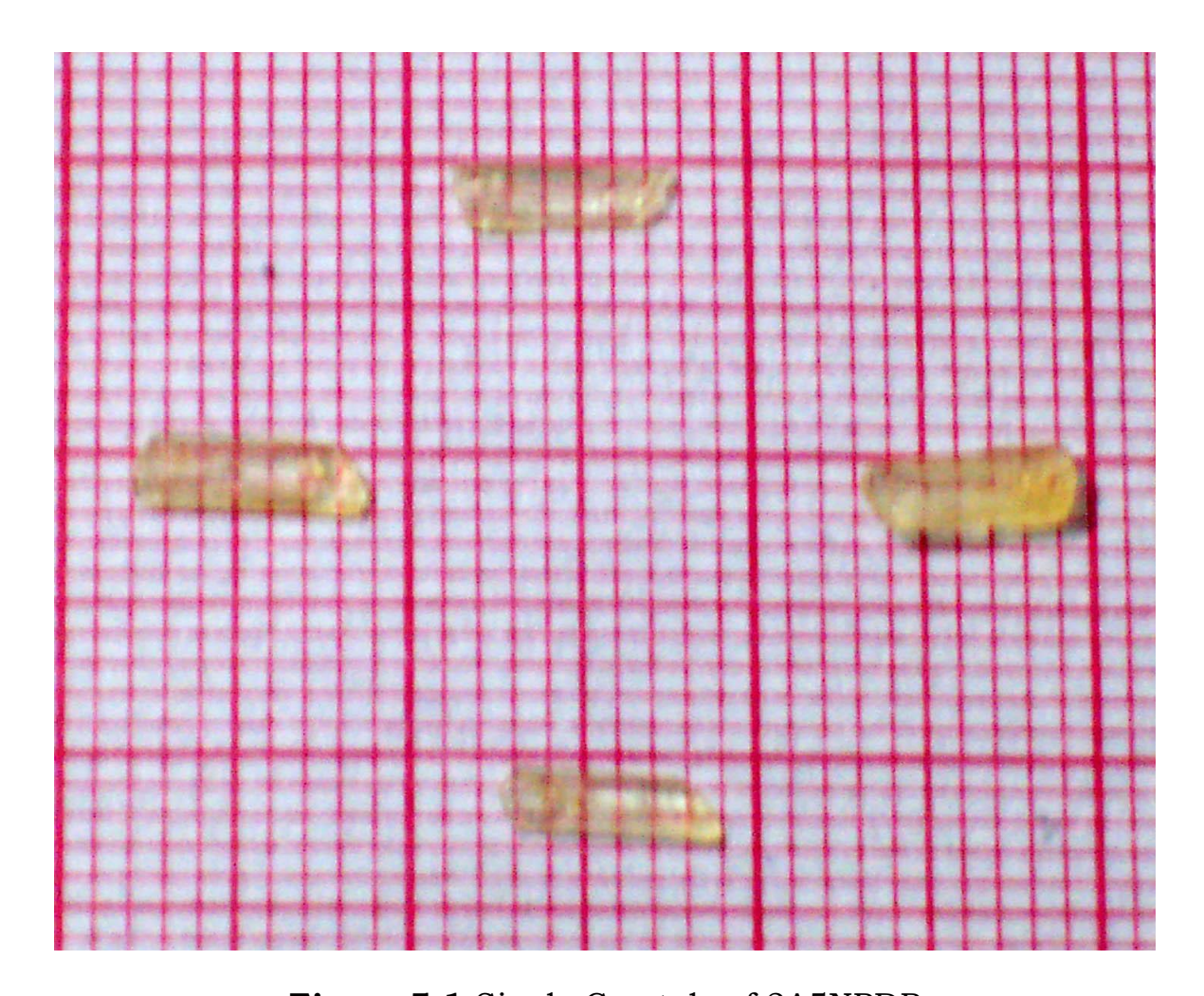


Figure 5.1 Single Crystals of 2A5NPDP

5.3 Structural Confirmation

The highly hyperpolarizable 2A5NPDP is arranged in a noncentrosymmetric fashion an arrangement, which is responsible for the quadratic nonlinear effect. It crystallizes in orthorhombic crystal system with Pna2₁ space group (Z= 4). The intermolecular H- bonding was observed between the cations and the anions, which is responsible for the tight packing of these molecules in the unit cell [14]. Table 5.1 shows the consistency of cell constants of 2A5NPDP between the present work and literature [17]. The crystal displays planar layers of phosphate ions parallel to (100) plane, which leads to an easy cleavage. The recorded powder XRD pattern of GO: 2A5NPDP is depicted in Fig. 5.2 and it shows amorphous nature. Here the

crystalline nature of 2A5NPDP was suppressed by the amorphous nature of GO and thus the XRD pattern turns amorphous.

Table 5.1 Cell Dimensions of 2A5NPDP

Cell parameters	2A5NPDP [17]	*2A5NPDP
a(Å)	25.645 (8)	24.133 (7)
b (Å)	6.228 (2)	6.503 (1)
c (Å)	5.675 (2)	5.108 (1)
V (Å ³)	906.394 (2)	801.633 (6)

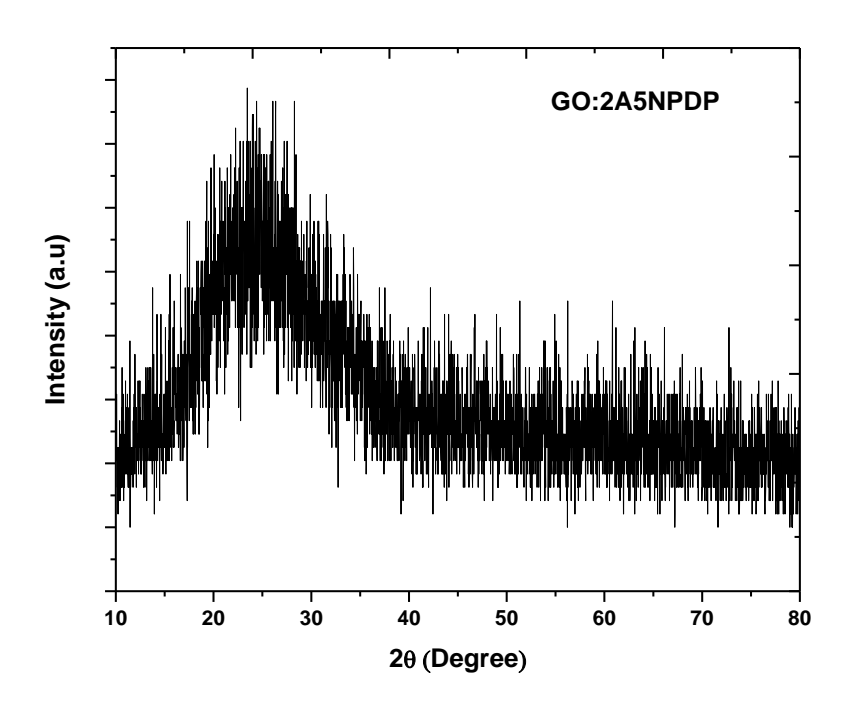
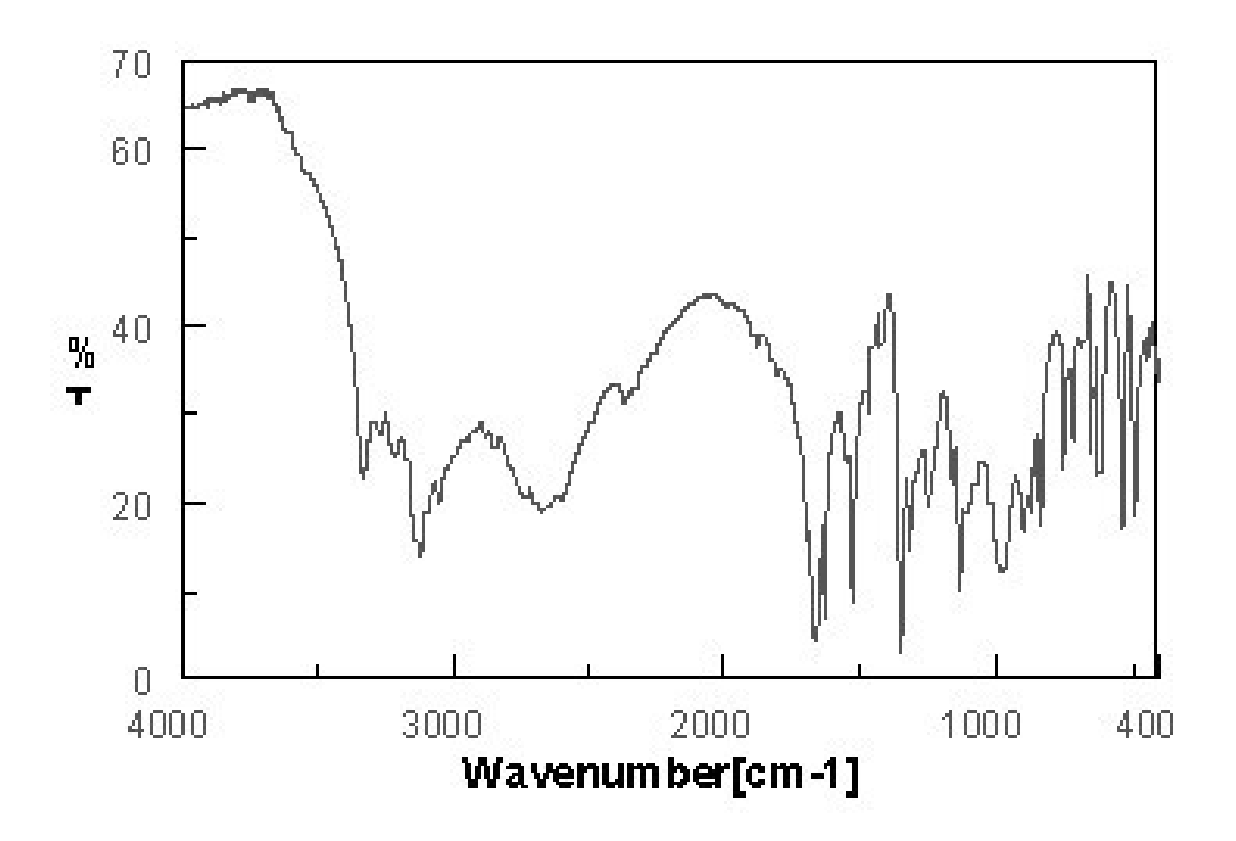


Figure 5.2 Powder XRD of GO: 2A5NPDP

The molecular structure of 2A5NPDP consists of one pyridinium ring and one phosphate tetrahedron connected through hydrogen bonds [14]. The FTIR spectrum of 2A5NPDP is shown in Fig. 5.3. The presence of hydrogen bonds (N-H...O) in the title compound was identified by the shifting of the peaks (3330 cm⁻¹, 3125 cm⁻¹) in the 2A5NPDP from the characteristic vibrational frequencies of the NH₂ group (3494 cm⁻¹, 3365 cm⁻¹) observed experimentally in the starting material 2A5NP. The hydrogen bond is also responsible for the broadening of the peak in this region, which is not observed in the parent material 2A5NP. The vibrational frequencies around 3000 cm⁻¹ were due to the C-H stretching of the aromatic ring. The 1321 cm⁻¹, 1250 cm⁻¹ are assigned to C-H vibrations of pyridine. The N-O stretching at 1524 cm⁻¹, 1355 cm⁻¹ confirm the presence of the nitro group. The C-N stretching band at 1662 cm⁻¹ originates from the pyridine ring. Similarly, 1130 cm⁻¹ is attributed to the P-O in-plane bending of the phosphate group. In particular, the peak at 986 cm⁻¹ corresponds to symmetric stretching of PO₄ anions thereby confirms the formation of the semiorganic 2A5NPDP compound.

Prepared GO: 2A5NPDP composite possess the characteristic peak of both GO and 2A5NP which ascertains the formation of hybrid materials. A slight shift in the peak positions is due to the interaction of graphene layers and 2A5NP molecules. It can be seen that the aromatic C=C stretching (1571 cm⁻¹), C-H stretching (2853 cm⁻¹), O-H stretching (3595 cm⁻¹) and C=O stretching (1676 cm⁻¹) of graphene oxide was shifted. Similarly, the presence of peaks at 3235, 1642, 1621, 1514, 1310, 1115, 980 cm⁻¹ represents the different vibrations of 2A5NPDP mostly shifted to the lower wavenumber. The observed FTIR peaks along with their assignments are given in Table 5.2 [18, 19] which clearly indicates the formation of GO: 2A5NPDP composite.



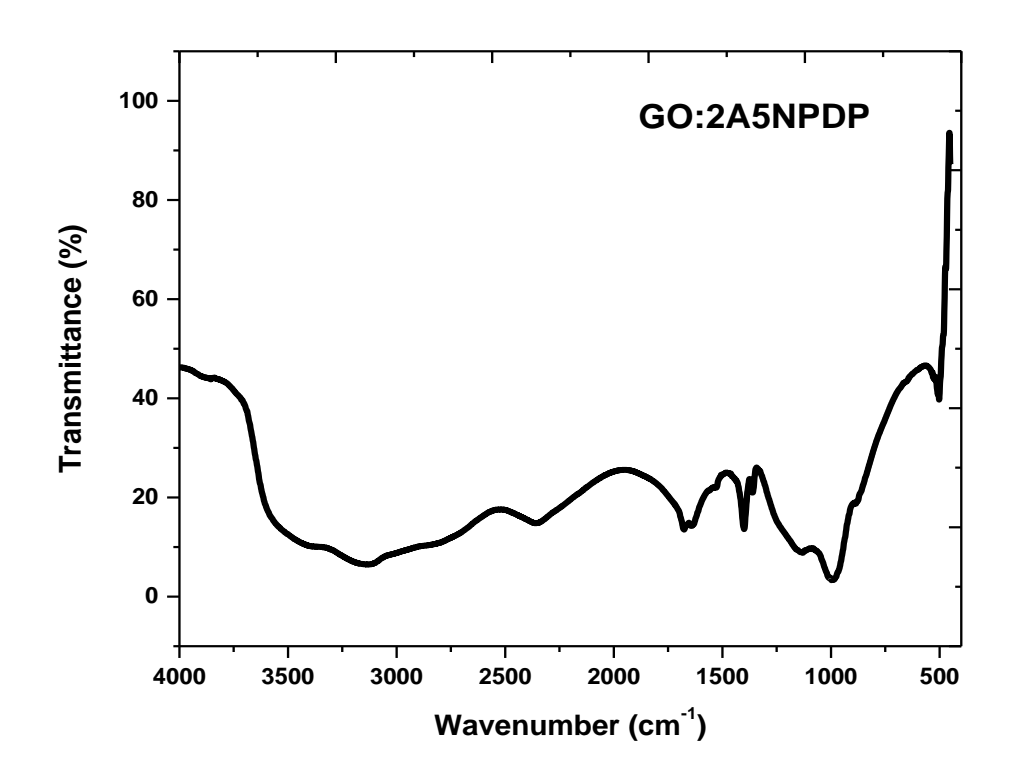


Figure 5.3 FTIR Pattern of Pure and GO composite of 2A5NPDP

Table 5.2 FTIR Peak Assignment of 2A5NPDPand GO: 2A5NPDP

Mode of vibration and	GO	2A5NPDP	O:2A5NPDP
type of bond			
C=C stretching	1572	-	1571
C-H stretching	2925	-	2853
O-H stretching of	3442	-	3595
hydroxyl groups			
C=O stretching of	2324	-	-
carboxy groups			
C=O stretching of	1738	-	1676
carbonyl groups			
C=O stretching of epoxy	1228	-	-
groups			
Symmetric stretching N-	-	3238, 3125	3235
НО			
C=N asymmetric	-	1662	1642
stretching			
N-H bending	-	1631	1621
N-O symmetric		1524, 1355	1514
stretching			
C-H in-plane bending	-	1321, 1250	1310
P-O in-plane bending	-	1130	1115
PO ₄ symmetric	-	986	980
stretching			



Figure 5.4 SEM Images of (a) GO and (b) GO: 2A5NPDP

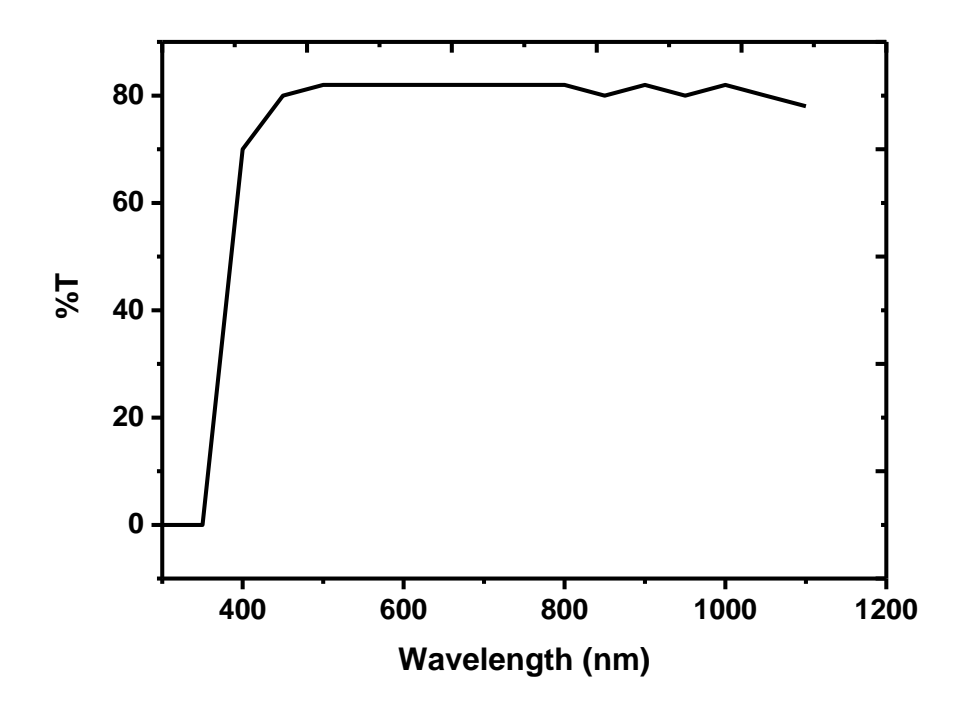
Textural arrangement of GO: 2A5NPDP composite was examined by SEM studies using Hitachi SEM 400 and is shown in Fig. 5.4. As expected the SEM image shows the presence of a thin-layered structure of graphene sheets. The twist and wrinkles in the graphene oxide were slightly reduced in the composite which was due to the reduction occurred during the decoration process. Earlier it is noted that wrinkled paper-like ultrathin sheets with stacking were observed for GO due to the harsh oxidation process during the composite synthesis. Unlike GO: 2A5NPFB composite where certain bright spots

additionally appeared depicting the attachment of 2A5NPFB on the surface of GO, GO:2A5NPDP composite possess dense bright shades with uniform concentration throughout the sheets. Here the possible growth mechanism mimics the GO:2A5NPFB composite wherein 2A5NP+ cations interact with inorganic anions (PO⁴⁻) to form them as 2A5NPDP. This molecule nucleates themselves in the graphene sheet through oxygen-containing functional groups. As the reaction continues, nucleation grows as clusters and decoration occurred. Thus incorporation of 2A5NPDP upon GO sheets is confirmed from SEM analysis.

5.4 Linear Optical Properties

wide 2-amino 5-nitropyridinium compounds exhibit transmittance window in the whole visible region irrespective of the anionic substitution. The UV-Vis spectrum of 2A5NPDP (Fig. 5.5(a)) shows that it possesses a cut-off wavelength of 400 nm which makes it a promising harmonic generator candidate suitable for tunable visible-NIR (450 –1300 nm) laser like LAP [20]. The protonation of pyridine in the acid medium (H₃PO₄) changes the transparency of the original molecule (2A5NP) and consequently shifts the transparency limit towards the blue wavelength. This protonation of the pyridine function introduces a hypsochromic shift in the 2A5NPDP i.e., it shifts the low lying π - π * transition of the aromatic 2A5NP towards higher energies [21, 22]. In the UV-Vis absorption pattern of GO:2A5NPDP composite (Fig. 5.5(b)), the characteristic peak of both GO (235 nm) and 2A5NPDP (340 nm) were observed. Compared to 2A5NPDP, the absorbance pattern of composite depicts stronger absorption in the UV and visible regions. Similar to GO:2A5NFB, the combination of absorbing GO with transparent 2A5NP has resulted in the alterations of electronic states associated with graphene and 2A5NP. As expected

the linear transmittance of the composite is higher than GO, which is an essential criterion for the optical limiting applications.



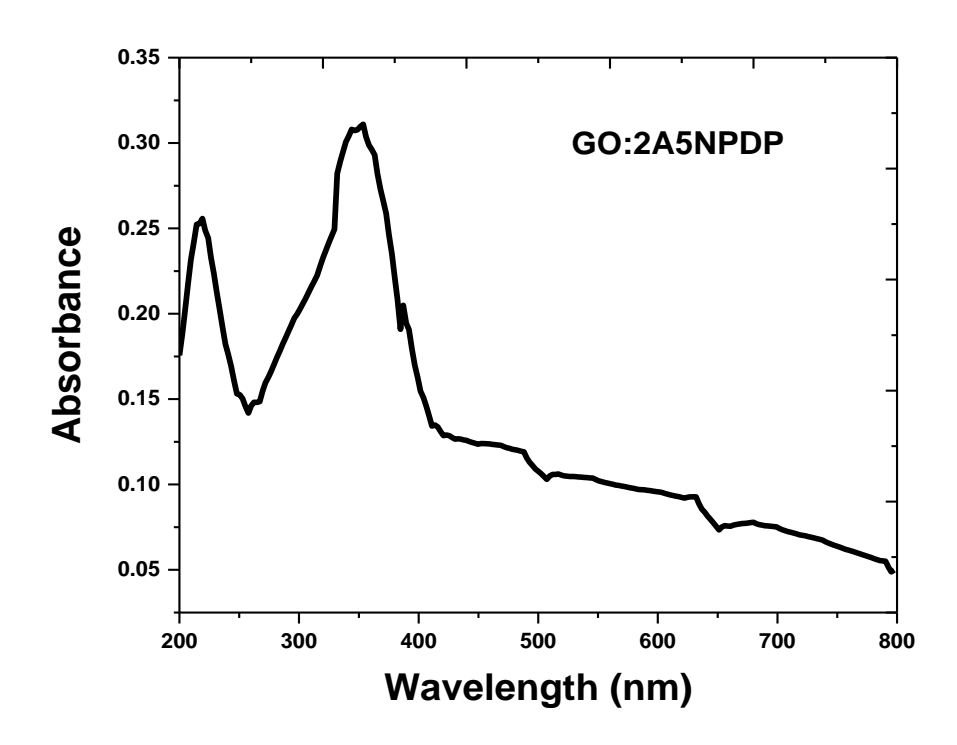


Figure 5.5 Absorbance Spectrum of 2A5NPFB and GO: 2A5NPDP

5.5 Second and Third-Order NLO Properties

5.5.1 Second Harmonic Generation Test

Ouantitative measurements of relative SHG efficiency 2A5NPDP single crystals concerning the well-known SHG material KDP were made by the Kurtz and Perry technique [23, 24]. Finely of powdered crystals 2A5NPDP were densely packed in microcapillary tube having a uniform bore. A laser beam from an Nd: YAG laser of fundamental wavelength 1064 nm, 8 ns pulse width with a 10 Hz pulse rate was made to fall normally on the sample cell. The transmitted fundamental wave was passed over a monochromator, which separates 532 nm (second harmonic signal) from 1064 nm and absorbed by CuSO₄ solution, which removes 1064 nm light and passed through a filter to remove the residual 1064 nm light.

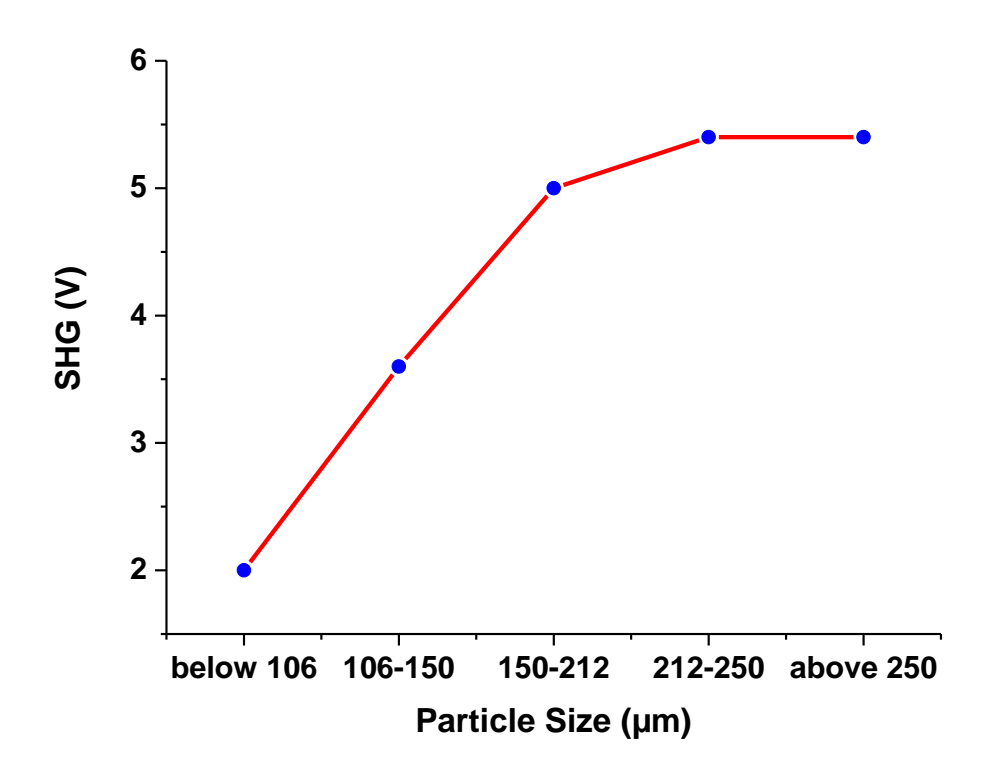


Figure 5.6 Phase Matching curve of 2A5NPDP

The green light was detected by a photomultiplier tube. KDP crystal powdered to the identical size was used as reference material in the SHG measurements. The relative SHG efficiency of the powder sample of 2A5NPDP was measured to be 4.2 times KDP. The intensity of the SHG output of 2A5NPDP as a function of particle size was measured and plotted in Fig. 5.6. The SHG output increases in proportion with increasing the particle size, confirm the phasematching behavior of the 2A5NPDP. As particle size becomes larger than the average coherence length, the SHG output remains constant, thus indicating the phase matchable character of the 2A5NPDP.

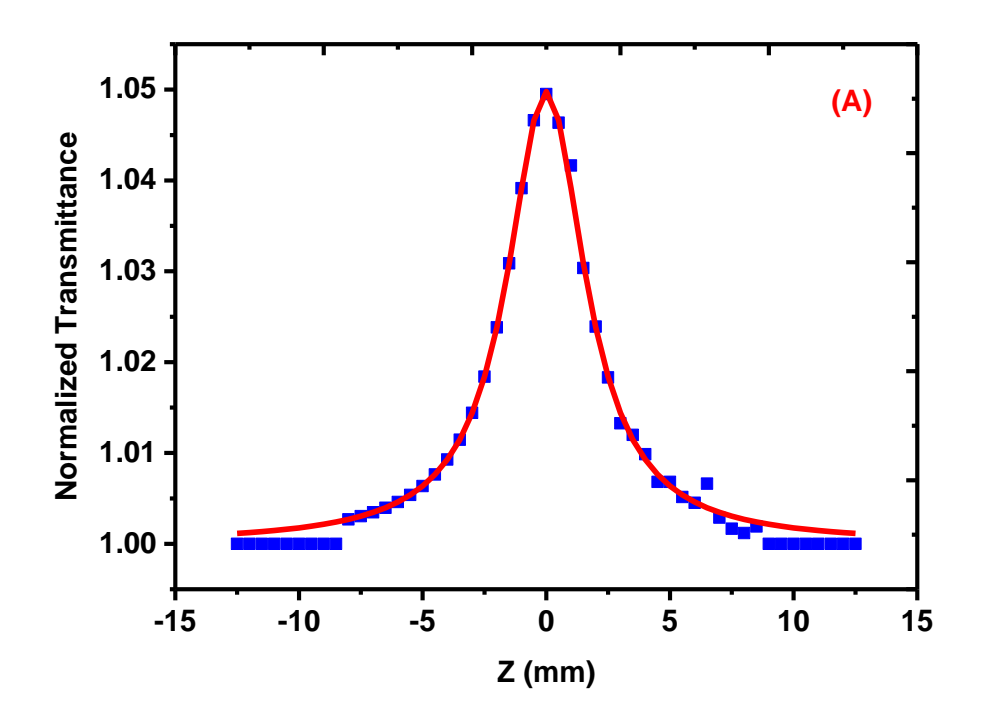
5.5.2 Z-Scan Studies

In the present study, a diode-pumped Nd: YAG laser of wavelength 532 nm was used as the excitation source for the Z-scan The nonlinear parameters of the technique. 2A5NPDP GO:2A5NPDP sample under CW laser illumination was determined by the well-known open and closed Z-scan set up formulated by Sheik-Bahae et al. [25, 26]. In the Z-scan technique, the translation was done to vary the incident beam intensity. According to Sheik Bahae formalism, as one moves away from the focus (Z=0), the normalized transmission should approach unity. Fig. 5.7(A) and Fig. 5.8(A) shows the typical Z-scan data for the open-aperture (S = 1) setup for the dispersed solution of 2A5NPDP and GO: 2A5NPDP in diethylene glycol at a concentration of 1 mM respectively. The enhanced transmission near the focus is indicative of the saturation of absorption at high intensity.

Fig. 5.7(B) and Fig. 5.8(B) shows the closed aperture Z-scan of 2A5NPDP and GO: 2A5NPDP at incident intensity 4.38 kW/cm². The peak followed by a valley normalized transmittance obtained from the

closed-aperture Z-scan data. It indicates that the sign of refraction nonlinearity is negative i.e. self-defocusing. Self- defocusing effect is due to the local variation of refractive index with temperature. The defocusing effect is attributed to a thermal nonlinearity resulting from the absorption of radiation at 532 nm. Localized absorption of a tightly focused beam propagating through an absorbing complex medium produces a spatial distribution of temperature in the 2A5NPDP and GO:2A5NPDP solution and consequently, a spatial variation of the refractive index, that acts as a thermal lens resulting in phase distortion of the propagating beam. Absorption saturation in the sample enhances the peak and decreases the valley in the closed-aperture Z-scan thus distorting the symmetry of the Z-scan curve about Z=0. Distortion of symmetry is an indication of existence of thermal nonlinearity.

Generally, the measurements of normalized transmittance versus sample position, for the cases of closed and open aperture, allow determination of nonlinear refractive index, n2, and the saturation absorption coefficient, β. Here, since the closed-aperture transmittance is affected by the nonlinear refraction and absorption, the determination of n2 is less straightforward from the closedaperture scans. It is necessary to separate the effect of nonlinear refraction from that of the nonlinear absorption. A method [27-29] to obtain purely effective n_2 is to divide the closed-aperture transmittance by the corresponding open-aperture scans. The data obtained in this way reflects purely the effects of nonlinear refraction. The nonlinear absorption coefficient β can be estimated from the openaperture Z -scan data. Table 4.3 summarizes the third-order NLO values of 2A5NPDP and GO: 2A5NPDP following the Sheik Bahae formalism.



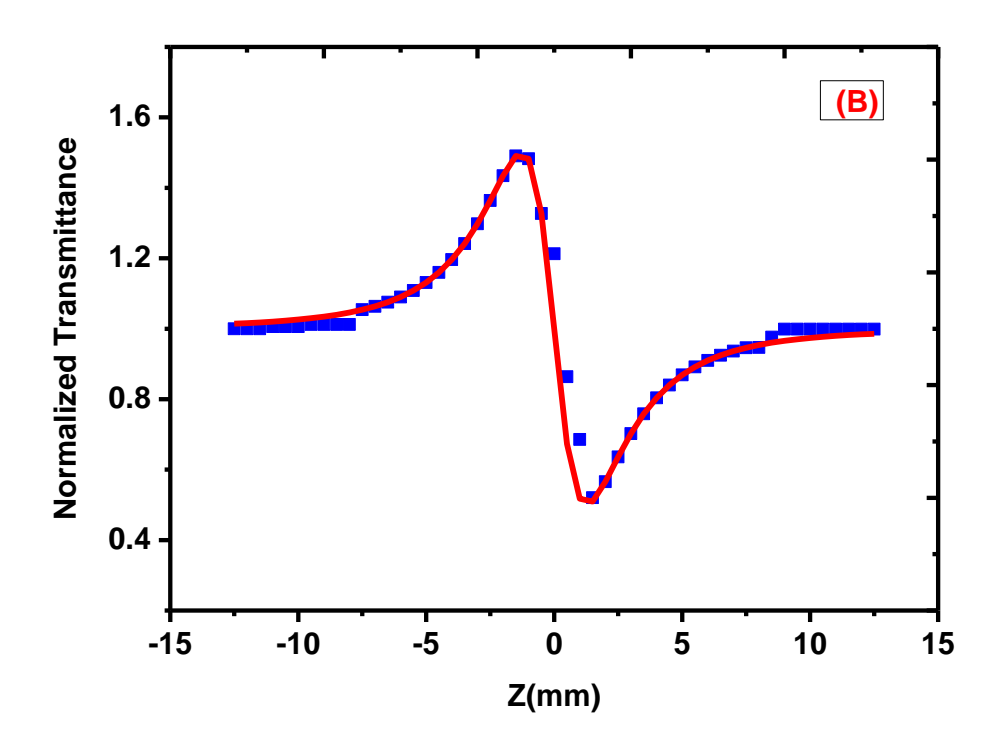
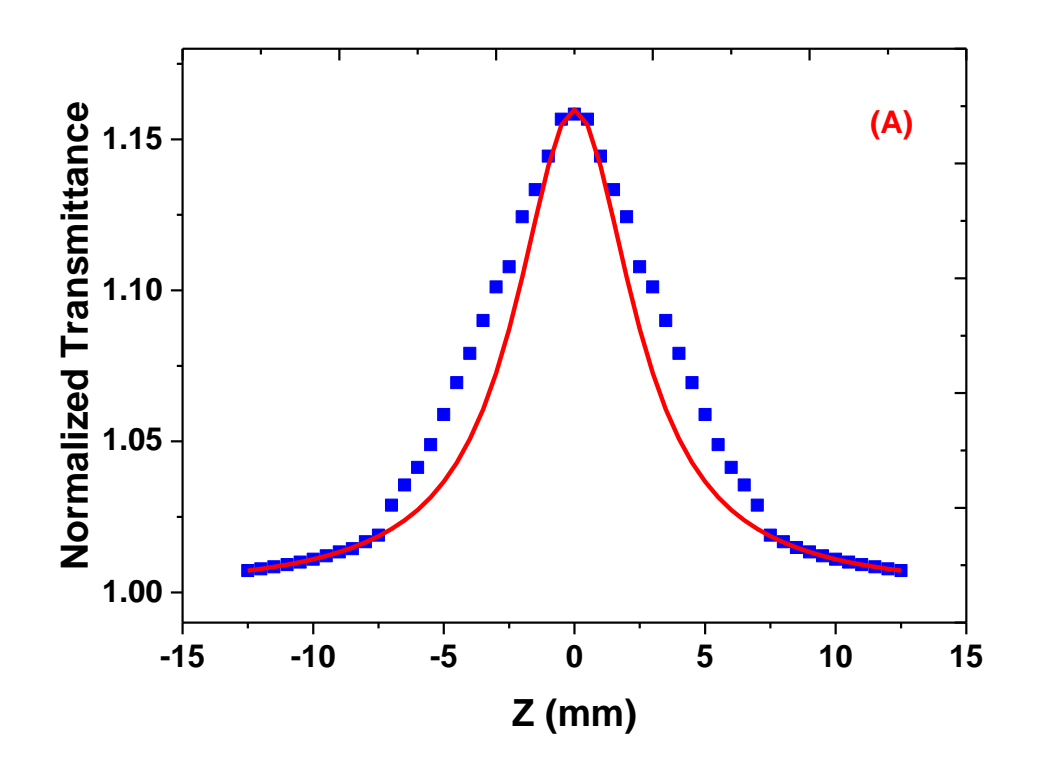


Figure 5.7 Z-scan Pattern of 2A5NPDP



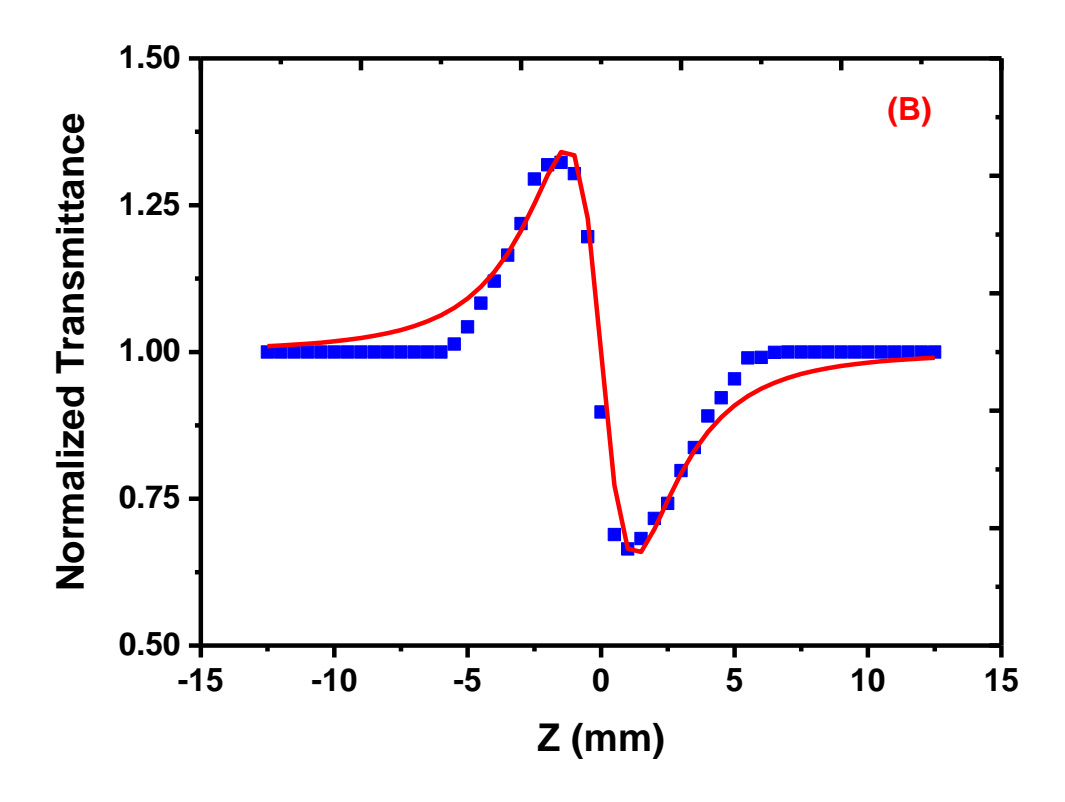
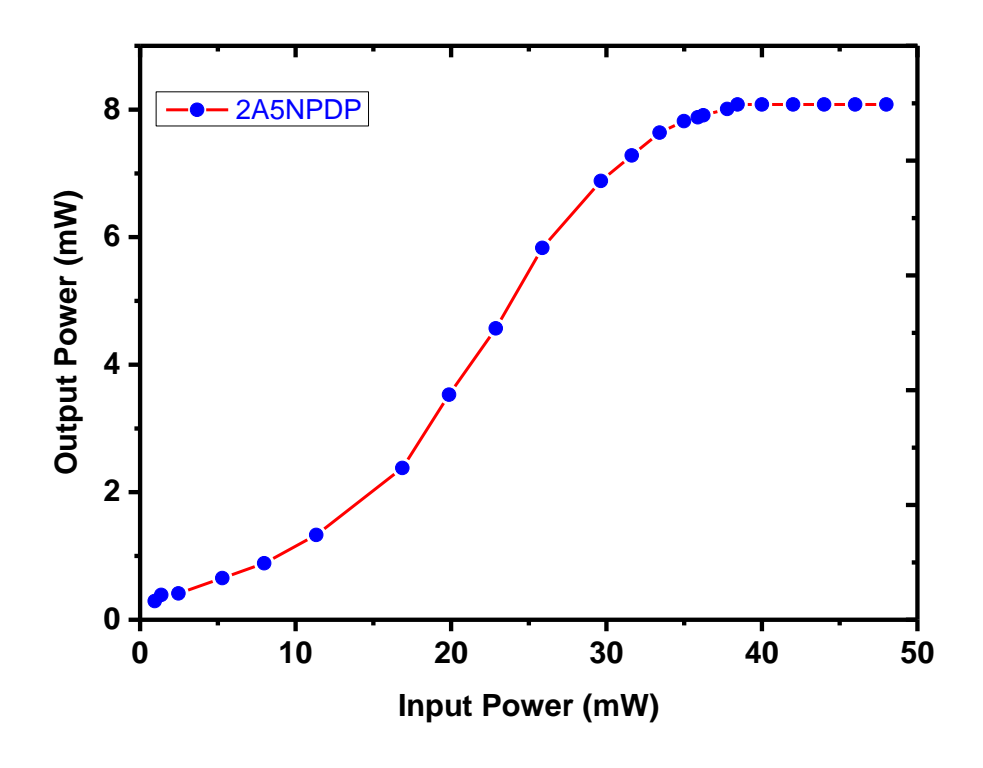


Figure 5.8 Z-scan Pattern of GO: 2A5NPDP



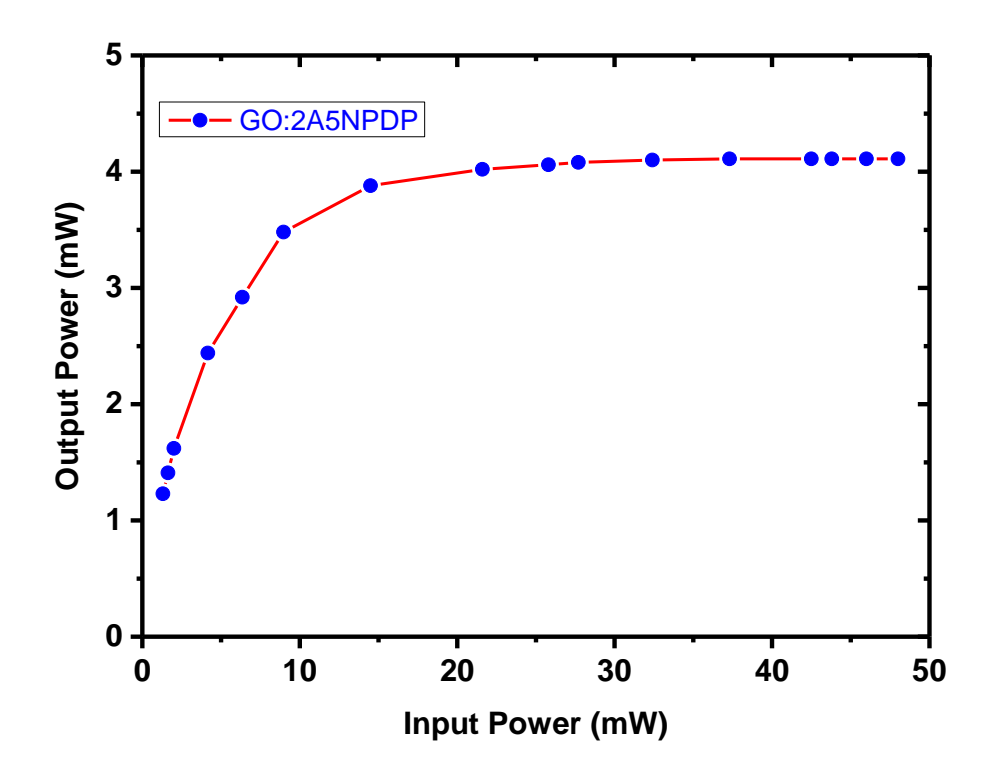


Figure 5.9 OL Pattern of GO and GO: 2A5NPDP Composite

Table 5.3 Third-order NLO Coefficients of 2A5NPDP and GO:2A5NPDP

NLO Parameters	2A5NPDP	GO:2A5NPDP
Nonlinear refractive index	5.89	6.51
$(n_2) \times 10^{-8} \text{ cm}^2/\text{W}$		
Nonlinear absorption coefficient	6.86	4.45
$(\beta) \times 10^{-3} \text{ cm/W}$		
Real part of NLO susceptibility	3.45	3.86
[Re [x ⁽³⁾]] x 10 ⁻⁷ esu		
Imaginary part of NLO susceptibility	1.71	1.12
[Im [x ⁽³⁾]] x 10 ⁻⁶ esu		
NLO susceptibility	3.85	4.02
$(x^{(3)}) \times 10^{-6} \text{ esu}$		
Optical limiting threshold (mW)	38.43	32.4
Clamping amplitude (mW)	8.08	4.1

It is well-known that the best position for a sample, when used for optical limiting based on self-defocusing, is at the valley of the Z-scan curve of the medium. Hence the optical limiting experiment of the samples was carried out by placing the sample beyond the focal point and the obtained characteristic curves are shown in Fig. 5.9. The transmitted output intensity was found to vary linearly with very low input intensities but it starts to deviate at high incident intensities. With a further increment of the input power, the transmitted intensity reaches a plateau and was saturated at a point defined as the limiting

amplitude: i.e. the maximum output intensity, showing an obvious limiting property. Fig. 5.9 shows the characteristic optical limiting curves as a function of incident power varying from 0.2 mW to 50 mW. The deviation from linearity began at 38.3 mW and the output clamping occurs at 8.08 mW for 2A5NPDP. At the same time, the limiting started occurring at 32.4 mW with output clamped at 4.1 mW for GO: 2A5NPDP composite. Thus at low incident powers, the output varies according to Beer's law and beyond limiting threshold, it becomes nonlinear [30, 31]. Hence 2A5NPDP and GO: 2A5NPDP composite acts as an efficient optical limiter in 532 nm regime of CW laser.

5.6 Conclusion

simple acid-base reaction, 2-amino 5-nitropyridinium dihydrogen phosphate (2A5NPDP) was synthesized. Single crystals of 2A5NPDP (6 x 2 x 1 mm 3) were grown from ethanol by slow evaporation technique. 2A5NPDP belongs to the orthorhombic crystal system with Pna2₁ space group with lattice parameter a=24.133 (7) Å, b=6.503 (1) Å, c=45.108 (1) Å. In the FTIR spectrum of GO: 2A5NPDP composite, the aromatic C=C stretching (1571 cm⁻¹), C-H stretching (2853 cm⁻¹), O-H stretching (3595 cm⁻¹) and C=O stretching (1676 cm⁻¹ 1) of graphene oxide was shifted. Similarly the presence of peaks at 3235 cm⁻¹ (N-H...O), 1642 cm⁻¹ (C=N), 1621 cm⁻¹ (N-H), 1514 cm⁻¹ (N-O), 1310 cm⁻¹ (C-H), 1115 cm⁻¹ (P-O), 980 cm⁻¹ (PO₄) represents the different vibrations of 2A5NPDP mostly shifted to the lower Thus wavenumber. the charge transfer interaction between orthophosphoric acid (donor) and 2-amino 5-nitropyridinium (acceptor) to form 2A5NPDP and its composite was ascertained by FTIR analysis. SEM image of GO: 2A5NPDP composite possesses dense bright shades of 2A5NPDP with uniform concentration

throughout the ultrathin wrinkled GO sheets. Here 2A5NPDP not only acts as a decorative element but also serves as a reducing agent which was confirmed by the reduction in the stacking of layers. In the UV-Vis absorption pattern of GO: 2A5NPDP composite, the characteristic peak of both GO (235 nm) and 2A5NPDP (340 nm) was observed. Compared to 2A5NPDP, the absorbance pattern of composite depicts stronger absorption in the UV and visible regions. Similar to GO: 2A5NFB, the combination of absorbing GO with transparent 2A5NP has resulted in the alterations of electronic states associated with graphene and 2A5NP. The SHG efficiency of the powder sample of 2A5NPDP was measured to be 4.2 times KDP and the saturation of SHG output at higher particle size confirms the phase-matching property. Z-Scan studies with CW excitation show that 2A5NPDP and GO:2A5NPDP composite exhibit saturable absorption, self-defocusing, and optical exhibit And here GO:2A5NPDP limiting action. higher NLO performance than pure GO and 2A5NPDP.

5.7 References

- J.D. Bierlin, L.K. Cheng, Y. Wang, W. Tam, Appl. Phys. Lett., 56 (1990) 423.
- 2. S.C. Sabarwal, Sangeeta, J. Cryst. Growth, 187 (1998) 253.
- 3. R.N. Rai, P. Ramasamy, C.W. Lan, *J. Cryst. Growth*, 253 (2002) 499.
- 4. A.M. Petrosyan, H.A. Karapetyan, A.A. Bush, R.P. Sukiasyan, *Mater. Chem. Phys.*, 84 (2004) 79.
- 5. P.N.Prasad, D.J.Williams, *Introduction to nonlinear optical effects in organic molecules and polymers*, Wiley, New York, 1991.
- 6. J. Zyss, J.F. Nicoud, M. Coquillay, *J. Chem. Phys.*, 81 (1984) 4160.
- 7. N.J. Long, Angew. Chem. Int. Ed., 34 (1995) 21

- 8. S. Ducharame, W.P. Risk, W.E. Moerner, V.Y. Lee, R.J. Twieg, G.C. Bjarkuland, *Appl. Phys. Lett.*, 57 (1990) 537.
- 9. N. Vijayan, R. Ramesh Babu, R. Gopala Krishnan, P. Ramasamy, W.T.A. Harrison, *J. Cryst. Growth*, 262 (2004) 490.
- 10. H. Minemoto, Y. Ozaki, N. Sonoda, *Appl. Phys. Lett.*, 63 (1993) 3565.
- 11. J. Milton Boaz, A. Leo Rajesh, S. Xavier Jesu Raja, S. Jerome Das, J. Cryst. Growth, 262 (2004) 531.
- 12. B.F. Levine, C.G. Bethra, C.D. Thurmond, R.T. Lynels, J.L. Bernstein, J. Appl. Phys., 50 (1979) 2523.
- 13. A. Ibanez, J.P. Levy, C. Mouset, E. Prieur, *J. Soild State Chem.*, 129 (1997) 22.
- 14. J. Pecaut, Y. L. Fur, R. Masse, *Acta Crystallogra Sect.*, B49 (1993) 535.
- 15. J. Zaccaro, B. Capelle, A. Ibanez, *J. Cryst. Growth*, 180 (1997) 229.
- 16. Y. Paula, *Organic chemistry*, Pearson Education (Singapore) Pvt. Ltd., India, 2002.
- 17. Z. Kotler, R. Hierle, D. Josse, J. Zyss, J. Opt. Soc. Am. B 914 (1992) 532.
- 18. G. Varsanyi, Assignments for vibrational spectra of seven hundred benzene derivatives, Adam Hilger, London, 1974.
- 19. P.S. Kalsi, *Spectroscopy of organic compounds*, New Age International (P) Limited Publishers, New Delhi, 2002.
- 20. D. Eimerl, S. Velsko, L. Davis, F. Wang, G. Loiacono, G. Kennedy, *IEEE. J. Quant. Electron.*, 25 (1989) 179.
- 21. R. Masse, J. Zyss, Mol. Eng., 1 (1991) 141.
- 22. J.L. Oudar, R. Hierle, J. Appl. Phys., 48 (1977) 2699.
- 23. S.K. Kurtz, T.T. Perry, J. Appl. Phys., 36 (1968) 3798.

- 24. K. Vasantha, S. Dhanuskodi, J. Cryst. Growth, 269 (2004) 333.
- 25. M. Sheik-Bahae, A.A. Said, T.H. Wei, D.J. Hagan, E.W. Van Stryland, *IEEE J. Quant. Electron*, 26 (1990) 760.
- 26. M. Sheik-Bahae, A.A. Said, E.W. Van Stryland, *Opt. Lett.*, 14 (1989) 955.
- 27. Seetharam Shettigar, G.Umesh, K.Chandrasekaran, Balakrishna Kalluraya, *Synt. Metals*, 157 (2007) 142
- 28. Yun Shan Zhou, En Bo Wang, Jung Peng, *Polyhedran*, 18 (1999) 1419
- 29. M.T. Zhao, B.P. Singh, P.N. Prasad, *J. Chem. Phys.*, 89 (1998) 5535.
- 30. R.A. Ganeev, I.A. Kulagin, A.I. Ryasnyansky, *Opt. Commun.*, 229 (2004) 403.
- 31. Guohui Zhang, Duxia Cao, Zhiqiang Liu, Guozhaong Li, *Acta Chim. Slov.*, 55 (2008) 315.

Chapter - VI

4-Dimethyl Aminopyridinium Dihydrogen Phosphate Decorated Graphene Oxide

CHAPTER VI

4-Dimethyl Aminopyridinium Dihydrogen Phosphate Decorated Graphene Oxide

Third-order optical nonlinearity of 4-dimethyl aminopyridinium dihydrogen phosphate (DMAPDP) and its graphene composite (GO: DMAPDP) was studied using diode-pumped Nd: YAG laser (532 nm, 50 mW). Both samples exhibit nonlinear refraction (self-defocusing) and nonlinear absorption (saturable absorption). Initially, DMAPDP crystal was grown by the solvent evaporation method and GO: DMAPDP was synthesized by hydrothermal technique. With a rise in pH, the growth was restricted towards one direction resulting in elongated rod-like morphology at higher pH. XRD analysis shows that DMAPDP crystallizes in triclinic crystal system with centric space group P1 . From powder XRD formation of GO: DMAPDP composite was confirmed by the presence of characteristic peak (001) plane of GO and (004) plane of DMAPDP. Formation of DMAPDP and GO: DMAPDP was confirmed by FTIR and FT-Raman studies. SEM image portrays the formation of spherical DMAPDP nanostructures upon the wrinkled layers of graphene sheets. In the UV-Vis absorption pattern of GO: DMAPDP composite, the absorption maxima were observed at 220 nm (GO) and 350 nm (DMAPDP). The observed optical limiting action under CW green laser excitation was ascribed due to the selfdefocusing effect. Third-order NLO coefficients of GO: DMAPDP composite was found to be higher than bare DMAPDP which makes them superior for optical limiting applications.

6.1 Introduction

In recent years, a lot of efforts have been paid off to prepare nonlinear optical (NLO) transmission materials which support the fabrication of nano-scale photonic and photoelectronic devices, with low thresholds, which can be used for the protection of eyes and sensitive optical devices from laser-induced damage [1]. For the optical device applications such as optical limiters, understanding the thirdorder NLO phenomenon is the most fundamental. Many optical limiting materials could serve as candidates for practical optical limiters. They have been found to show strong nonlinear extinction (NLE) (i.e. strongly attenuate high intense laser beams while transmitting low-intensity ambient light). Strong optical-limiting properties have been observed in various materials such as carbonbased suspensions, metallophthalocyanines and porphyrins [2-4]. Also, the rapid technological advancement of nanotechnology in the past few decades opens new opportunities to identify a large number of optical limiting materials with remarkable NLO properties. To design an optimal NLO material, the origin of the nonlinear response to the optical field must be understood.

The key modules in the "molecular engineering" of NLO complexes include the collaboration of skills in crystal growth and synthesis, optics and X-ray crystallography [5-8]. The carbon atom has the great ability to form a stable hybridized bonds like (a two-electron covalent bond σ $C_{\rm sp^3}$ - $C_{\rm sp^3}$ and a four-electron bond σ + π $C_{\rm sp^2}$ - $C_{\rm sp^2}$) provides diverse properties of organic compounds. The π -electrons in an organic molecule differentiate organic NLO materials from inorganic systems. The electron distribution can be perturbed by the interaction with a radiation field such as the intense optical electromagnetic field produced by a laser and if the perturbation is

asymmetric, a quadratic nonlinearity results. The search for a chromophore is likely to be assisted by the other physical methods satisfying the other requirements to realize the actual NLO device.

The ultimate practical organic NLO material must fulfill a plethora of requirements, such as a favorable balance of optimum nonlinearity and high transparency properties. However, this is not to underestimate a variety of equally important issues such as synthetic accessibility, cost, crystal growth capability, toxicity, environmental stability, optical damage properties, etc. [9-11]. The subsequent discussion involves not an arbitrary, but a mandatory separation of microscopic molecular properties and macroscopic crystal properties. The difficult challenges in simultaneously reconciling these molecular and crystal properties are considered and finally, a variety of specific examples of NLO molecules are synthesized. Their single crystals are grown and described in detail. Having made these observations, one should search for a model system, which contains the chromophore and therefore gives the expected properties [12, 13].

In continuation of the present investigation on the substituted pyridine based molecules like 2-amino-5-nitropyridine (2A5NP), here 4-dimethyl aminopyridine (DMAP) are considered as parent molecules. In this present work, a polarizable organic molecule 4-dimethyl aminopyridine (DMAP), was selected as a guest and anchored onto inorganic host orthophosphoric acid. The hydrogen bond networks formed will provide new crystalline semiorganic materials with improved stabilities. The third-order NLO behavior of 4-dimethyl aminopyridinium dihydrogen phosphate and its GO composite were explored in the regime of low laser power by the Z-scan technique. The possibility of utilizing the material for frequency doubling and optical limiting is explored.

6.2 Material Preparation

The involved acid-base reaction scheme for the formation of DMAPDP is indicated in Fig. 6.1. Here the weak Bronsted base (DMAP) gains a proton in acidic (H₃PO₄ at pH < 5) aqueous solution to form DMAPDP powder. In typical procedure 1 mole of 4-DMAP was dissolved in 1 mole of orthophosphoric acid taken in 20 mole of water solution at 65 °C to obtain DMAPDP salt. Due to higher solubility, the solution was cooled below room temperature, to extract white microcrystalline powder of DMAPPD. By repeated recrystallization process the material was purified. As DMAPDP salt exhibits a positive solubility temperature gradient in aqueous solution, the solvent evaporation method was adopted. Thus single crystals of DMAPDP were grown from saturated aqueous solution at 30 °C and by maintaining pH between 3.5 to 5. From spontaneously nucleated seed, good quality crystals of dimensions $7 \times 6 \times 4 \text{ mm}^3$ (pH = 3.5), $10 \times 5 \times 10^{-3}$ 2 mm^3 (pH = 4.45) and $11 \times 2 \times 1 \text{ mm}^3$ (pH = 5) was obtained after a typical growth period of 60 days (Fig. 6.2). With a rise in pH, the growth was restricted towards one direction resulting in elongated rodlike morphology at higher pH.

$$H_3C$$
 CH_3
 H_3C
 CH_3
 H_3C
 CH_3
 H_3C
 CH_3
 H_3C
 CH_3
 CH_3

Figure 6.1 Reaction Scheme of DMAPDP [14]

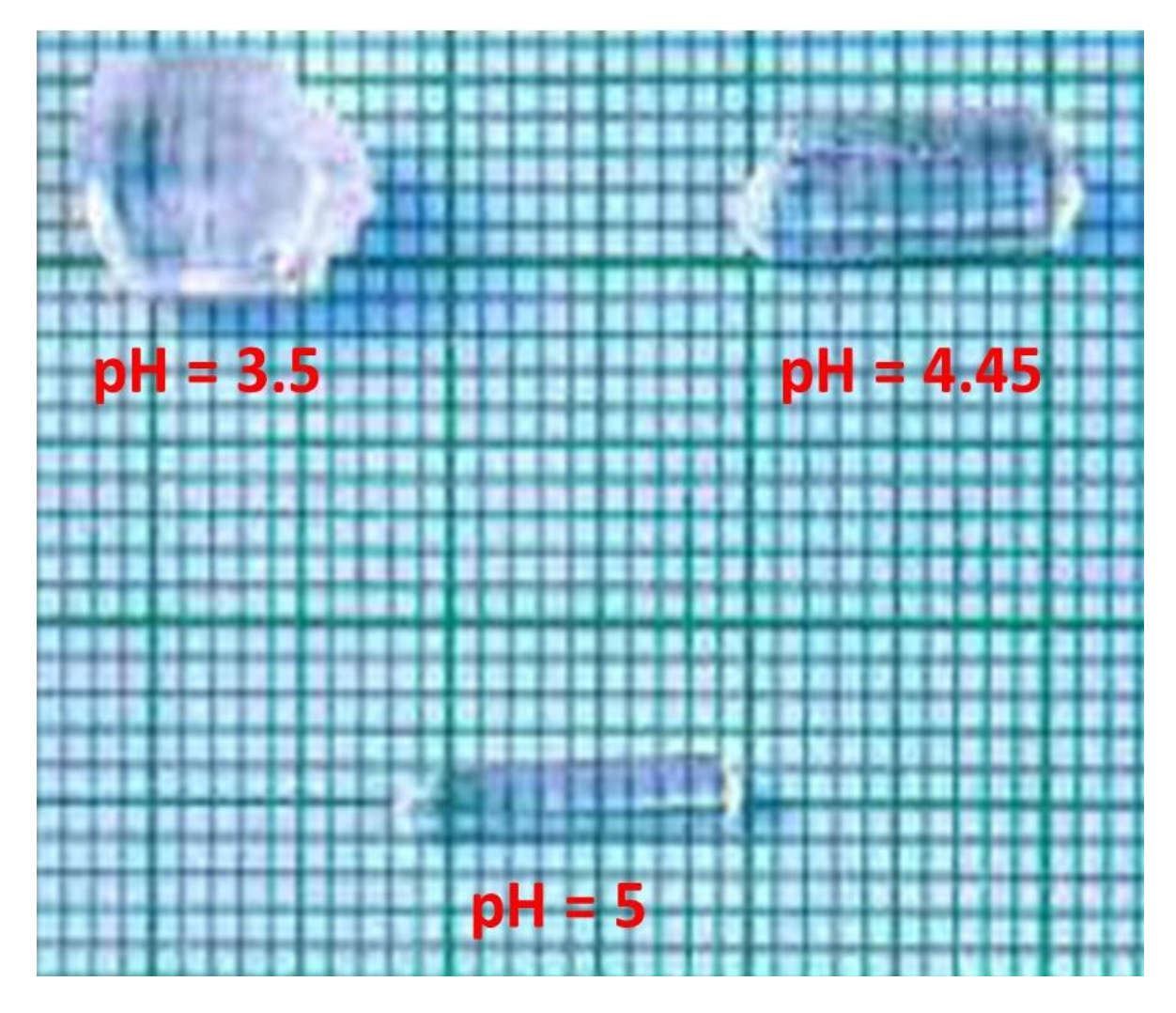


Figure 6.2 Single Crystals of DMAPDP Grown at Different pH

DMAPDP derivative-based GO composite was prepared by a simple hydrothermal method adopting the same procedure followed in GO: 2A5NP derivative composite [15, 16]. In the employed procedure, 20 mg of GO obtained from the modified Hummers method was dissolved in 100 ml water. The GO suspension was added as an additive in the reaction mechanism of DMAPDP (Fig. 6.1). The obtained solution was maintained at a pH of 4.45 and stirred for 6 hours at 30 °C. The precipitate deposited at the bottom of the beaker was collected through filtration and dried after subsequent washing to obtain the GO: DMAPDP composite in powder form.

6.3 Structural Confirmation

Preliminary identification of the semiorganic pyridine derivative was made through single-crystal XRD upon the grown crystals. DMAPDP crystallizes in the centrosymmetric space group P1 with two formula units of $[C_7H_{11}N_2][H_2PO_4]$ in the unit cell. The material crystallizes in triclinic crystal system with lattice parameters as a=7.792(8) Å, b=8.058(1) (9) Å, c=8.376(1) Å and $\alpha=98.378(1)$ °, β = 105.895(8)°, v= 98.642(1)°. The estimated values are found to be consistent with the already reported values of DMAPDP [14]. The recorded powder XRD pattern of GO: DMAPDP composite shown in Fig. 6.3 confirms the presence of GO along with DMAPDP. The peak at $2\theta = 12.4^{\circ}$ corresponds to the (001) plane of GO. Other diffraction peaks were identified and indexed using AUTOX software. Peaks at $2\theta = 18.5^{\circ}, 20.2^{\circ}, 21.16^{\circ}, 23.0^{\circ}, 28.54^{\circ}, 30.87^{\circ}$ corresponds to (111), (-112), (020), (103), (004), (213) plane of DMAPDP. Thus the formation of GO: DMAPDP composite was confirmed.

Table 6.1 Structural Parameters of DMAPDP Crystal

Lattice parameters	Experimental SXRD	Reported Value [14]
a (Å)	7.792(8)	7.793(2)
b (Å)	8.058(1)	8.058(2)
c (Å)	8.376(1)	8.375(2)
a (°)	98.378(1)	98.375(4)
β (°)	105.895(8)	105.896(4)
γ (°)	98.642(1)	98.643(4)

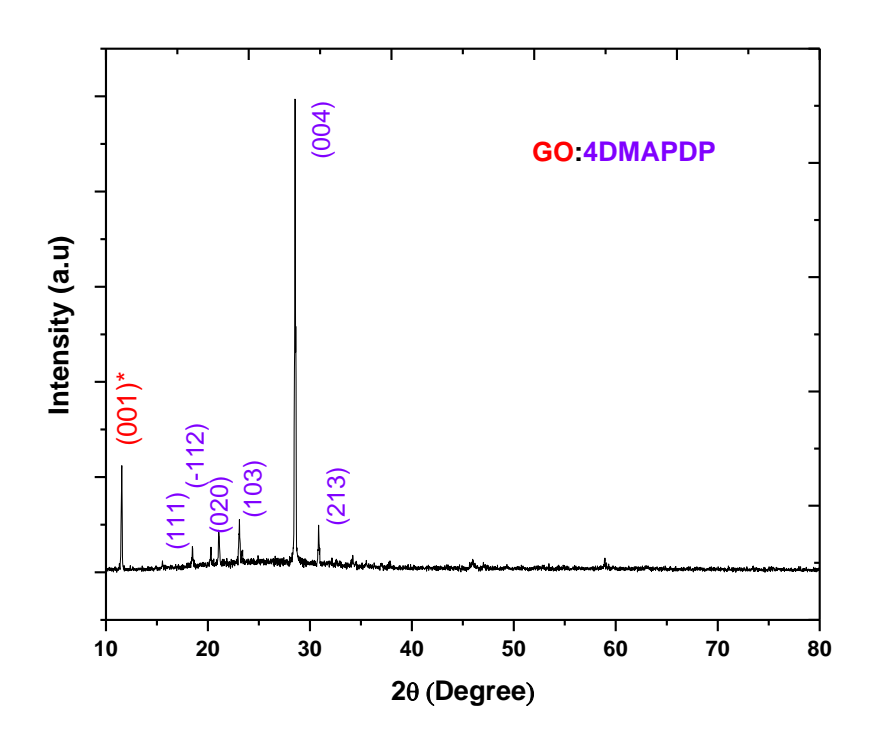


Figure 6.3 Powder XRD of GO: DMAPDP

From the FTIR spectrum (Fig. 6.4) the characteristic vibrational frequencies of the functional groups present in DMADP were assigned compared (Table 6.2) with the FT-Raman spectrum GO: DMAPDP. In the FTIR spectrum of DMAPDP, a broad vibration at 3386 cm⁻¹ and 2837 cm⁻¹ confirms the symmetric stretching N-H and N-CH₃ vibrations of the pyridine ring. Presence of stretching C-H vibrations (3067 cm⁻¹ and 2943 cm⁻¹), in-plane bending C-H vibrations (1217 cm⁻¹) and out-of-plane bending C-H vibrations (817 cm⁻¹ and 745 cm⁻¹) was confirmed. The strong absorption of out-of-plane ring bending frequently appears in the spectra of similarly substituted pyridines. The absorption peak at 1565 cm⁻¹ can be attributed to the symmetric stretching C=Cvibrations of the benzene ring. Delocalization of the π -electron and incorporation of inorganic elements causes absorption at lower wavenumbers. Here the H₂PO₄ stretching and P-OH deformation modes have an intense band at The broad envelope between 997 cm⁻¹ and 539 cm⁻¹ respectively.

2500-3600 cm⁻¹ is attributed to the hydrogen bonding interaction of H₂PO₄ and N⁺H with the adjacent molecules. The peaks at 938 and 1086 cm⁻¹ attest to the presence of P-OH stretching while the peak at 1299 cm⁻¹ represents the P=O stretching vibrations [17]. Thus the successful incorporation of phosphate ion in pyridine structure and formation of DMAPDP is confirmed.

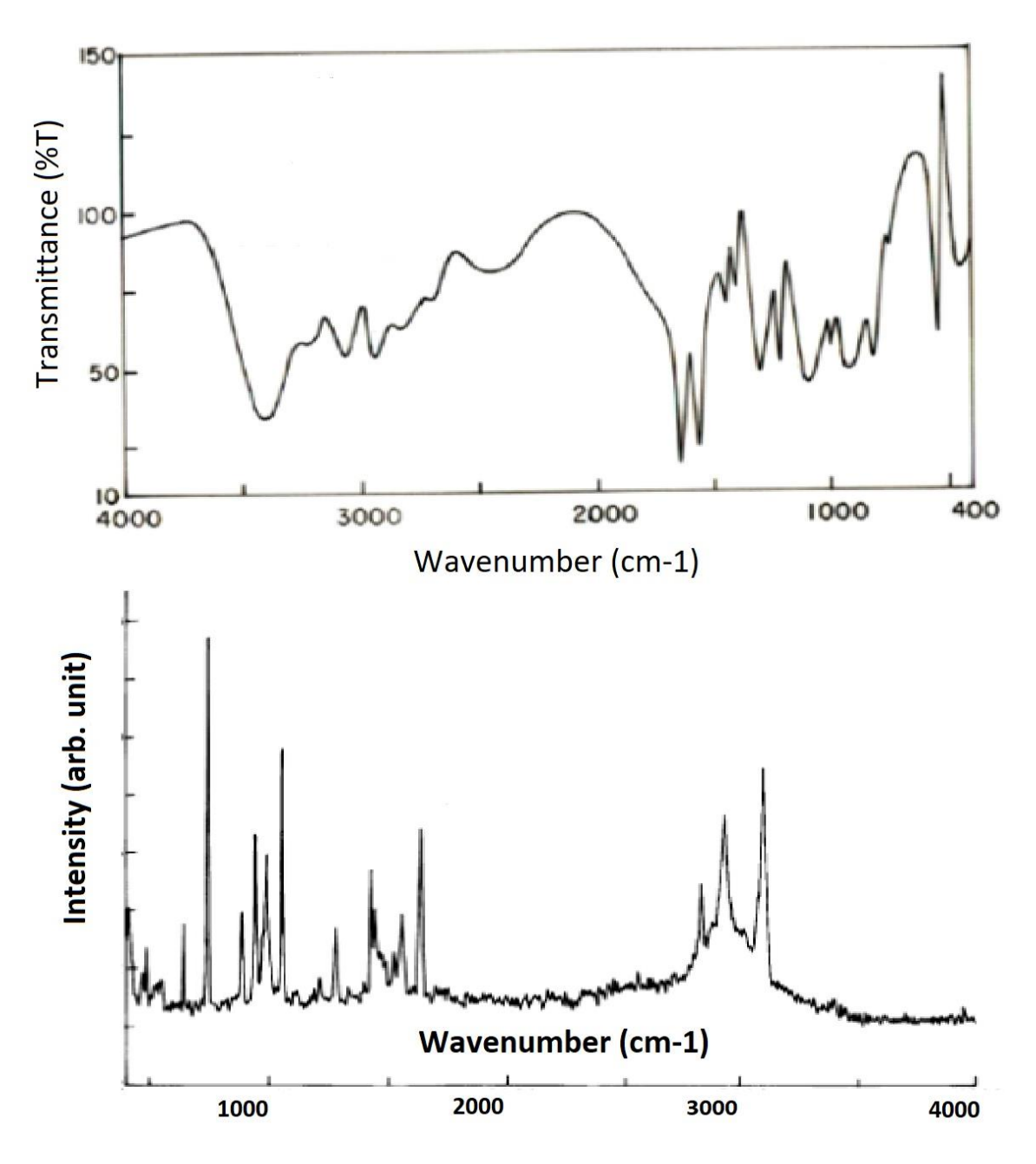


Figure 6.4 FTIR and FT Raman Pattern of DMAPDP and GO: DMAPDP Composite

Table 6.2 FTIR and FT Raman Peak Assignment of DMAPDP and GO: DMAPDP

Assignments	FTIR peaks of DMAPDP	FT-Raman peaks of GO: DMAPDP
ν (N-H) H - bonding	3386	
ν (C-H) or ν (O-H) H - bonding		3101
ν (C-H)	3067	
v (C-H)	2943	2935
v (N-CH ₃) or (C-H)	2837	2834
δ (N-H)	1646	
ν (C=C)	1565	1557
ν (C=N) or (C=C)		1527
ν (P=O)	1299	
δ (C-H)	1217	1218
v_3 (PO ₄) or δ (C-H)	1086	
ν (P-OH)		1058
v (P-OH)	997	
ν ₁ (PO ₄) or δ (P-OH)	938	947
π (C-H)	817	
π (C-H)	745	743
δ (C-H) or π (C-H)		649
v4 (PO4)	539	
v ₂ (PO ₄)	448	413
G-Band of GO		1639
D-Band of GO		1282

Further to confirm the formation of GO: DMAPDP composite, FT-Raman was recorded and the assignments are summarized in Table 6.2. The recorded Raman spectrum exposes the dominance of DMAPDP over the graphene oxide. Here the presence of graphene layers was confirmed from the observed G band at 1639 cm⁻¹ due to the E_{2g} phonon of sp² carbon atoms and the D band at 1282 cm⁻¹ which is a breathing mode of k-point phonons of A_{1g} symmetry, arising from the disordered carbon structures, edges and other defects. Peaks at 3101 cm⁻¹, 2935 cm⁻¹, and 1218 cm⁻¹, 743 cm⁻¹, 649 cm⁻¹ were due to the presence of stretching and bending C-H vibrations respectively. While the peaks at 2834, 1557 and 1527 cm⁻¹ correspond to the symmetric stretching N-CH₃, C=N and C=C vibrations of the pyridine ring. The other low-frequency phonon modes were due to metal ions involved in phosphate groups. The Raman modes at 1058 cm⁻¹ (P-OH), 947 and 413 cm⁻¹ (PO₄) belongs to the phosphate group of DMAPDP [18]. Thus the Raman spectrum of GO: DMAPDP composite illustrate the characteristics of both GO and DMAPDP were observed.

The thermal stability was obtained by thermogravimetric and differential thermal analysis. The thermal decomposition curve (40-720 °C) is illustrated in Fig. 6.5. The material is stable and free of moisture up to 192 °C. The DTA replicates the same changes shown by the TG and before the decomposition, there is no phase transition [14]. The material is proved to be stable in this region since there are no endothermic or exothermic transitions below 200 °C. From the DTA curve, it is observed that at about 192 °C the material undergoes an irreversible endothermic transition where the decomposition starts. The TGA clearly shows the decomposition initiates around 190 °C and loses its weight by almost 85 % due to the removal of the molecular fragments.

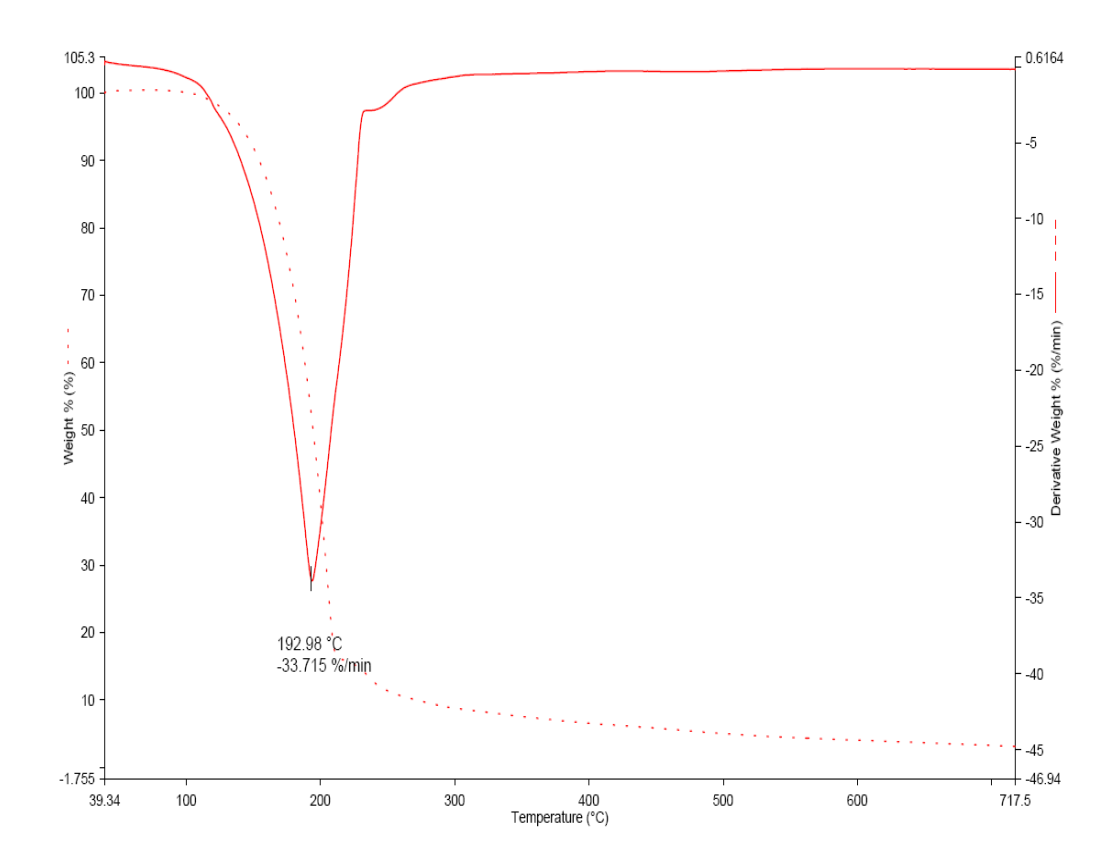


Figure 6.5 TG/DTA Curve of DMAPDP

Based on the thermal analysis, the obtained salts were sintered at 180 °C in an autoclave for 48 hours using a muffle furnace to form possible nanostructures [16]. The textural arrangement of composites was examined by SEM studies using Hitachi SEM 400. SEM image of DMAPDP (Fig. 6.6(a)) portrays the formation of nanoparticles with grain size in the range of 45 -170 nm. As the reaction was carried out in ambient pressure, the particles get sufficient time to form the most stable spherical like structure. However, the grains formed were not so uniform in shape. The recorded SEM image of GO: DMAPDP composite is as shown in Fig. 6.6(b). Here graphene appears as ultrathin sheets with a stacked layered structure. The presence of wrinkles and twists arises due to rapid oxidation happened during modified Hummer's experiment. Upon the thin layers, DMAPDP forms themselves as nanospheres with an average diameter of 160 nm. Compared to pure DMAPDP, agglomeration is well reduced and DMAPDP attaches

themselves randomly upon the graphene sheets. Here the possible growth mechanism imitates the growth of 2A5NP derivatives and here DMAP+ cations interact with inorganic anions (PO₄-) to form them as DMAPDP. This molecule nucleates upon the graphene layers and grow as nanospheres. Thus decoration of DMAPDP upon GO sheets is confirmed from SEM analysis.

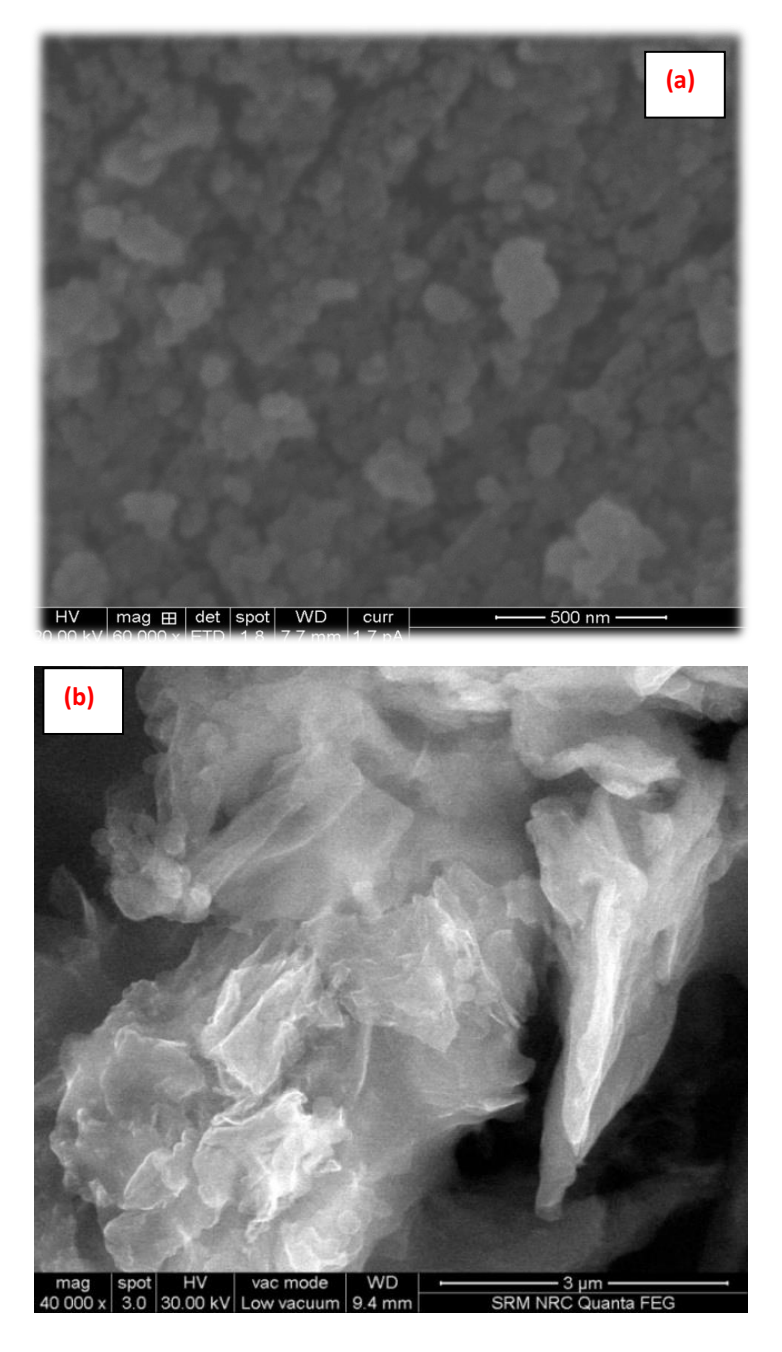


Figure 6.6 SEM Image of (a) DMAPDP and (b) GO: DMAPDP

6.4 Linear Optical Properties

Employing a JASCO UV-Vis spectrophotometer at 30 °C linear optical property of the samples was recorded. For optical device fabrications, the crystal should be highly transparent in the UV-Visible region. It can be seen that DMAPDP (Fig. 6.7(a)) possesses good transmission in the entire visible region which makes them suitable for photonic applications like optical limiting. Also, the transmission begins to increase abruptly around 310 nm, indicating an optical absorption edge in the UV region, which is an essential criterion for NLO applications [19, 20]. This makes the material suitable for short-wavelength optoelectronic devices, especially for UV LEDs and laser diodes. The transparency of DMAPDP is comparatively lower than 2A5NP derivatives and this decrease in transmittance arises due to trade-off with the larger nonlinearity of DMAPDP.

In the UV-Vis absorption pattern of GO: DMAPDP composite (Fig. 6.7(b)), the absorption maxima were observed at 220 nm and 350 nm. This corresponds to the characteristic peak of both GO and DMAPDP which confirms the formation of GO: DMAPDP composite. It can be seen that the characteristic peak of DMAPDP was red-shifted by 40 nm due to the interaction between DMAPDP and GO moiety. Further, the absorbance of DMAPDP was greatly increased due to the influence of absorbing GO. The absorption maximum, cut-off wavelength and optical transmittance window of composites are 220 nm, 350 nm, 415 nm, and 415-1100 nm. The pattern of GO: DMAPDP composite mimics the absorbance of GO: 2A5NPDP and this exposes the identical interaction of GO with complex organic species. Change in band structure can influence the NLO behavior of the sample and thus suitability of the material for laser application was tested further.

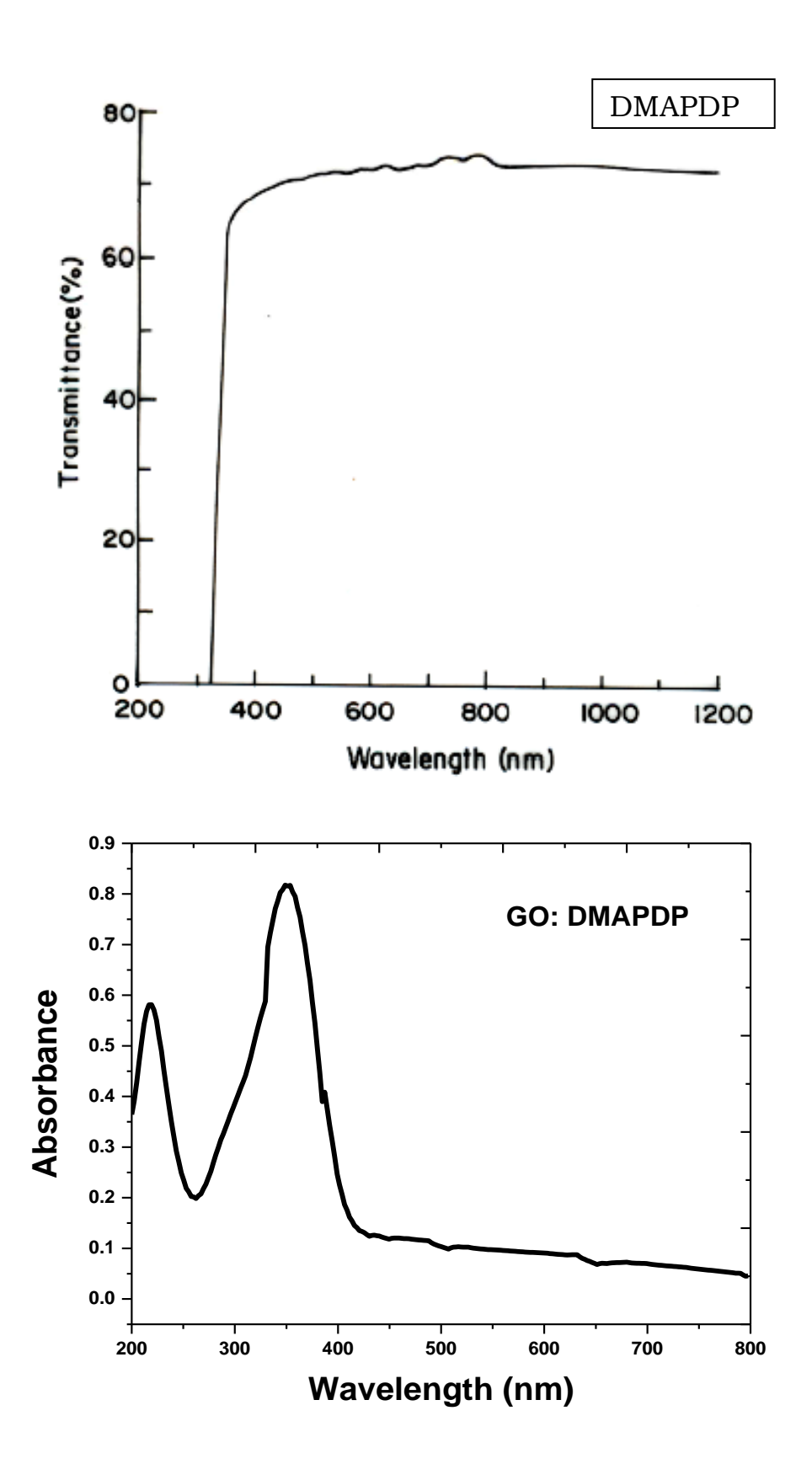
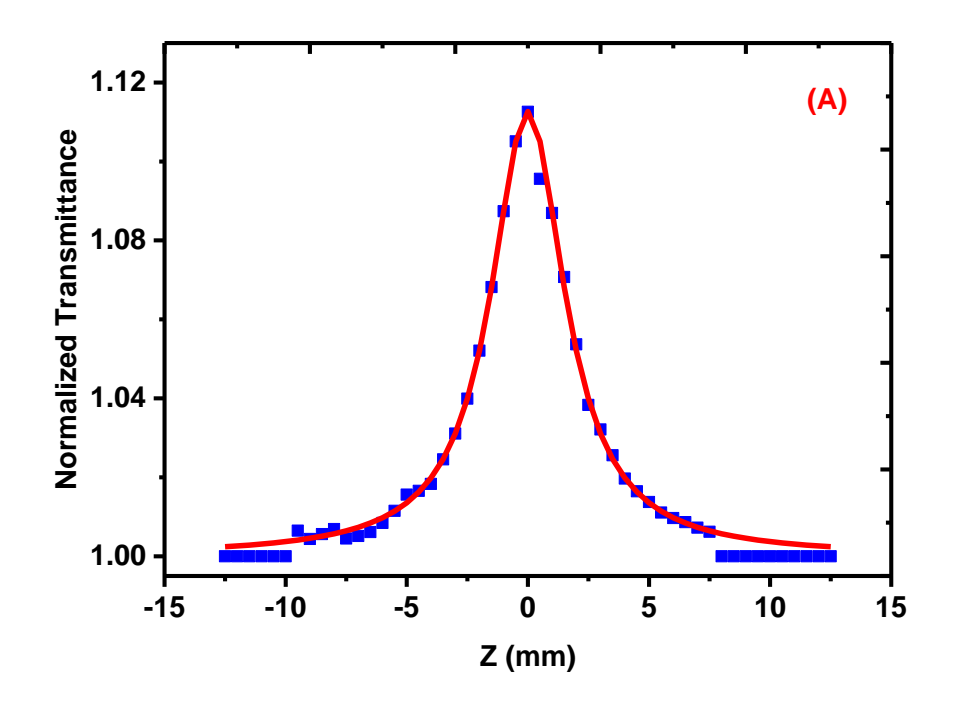


Figure 6.7 Optical Transmittance of DMAPDP Crystal and Absorbance Spectrum of GO: DMAPDP

6.5 Third-Order NLO Properties: Z-Scan Studies

As DMAPDP belongs to the inversion symmetry space group, it does not exhibit SHG in the Kurtz powder test. Thus the third-order NLO properties of DMAPDP and its composite were studied by the Z-scan experiment. The Z-scan technique is a powerful technique to characterize the NLO properties as it could measure the sign and magnitude of the real and imaginary parts of $x^{(3)}$. The principle of working is the measurement of aperture transmittance as a function of sample position, which depends on the magnitude and sign of n_2 . Also, it is known that the nonlinear index of refraction n2 is proportional to the real part of $x^{(3)}$ and the nonlinear absorption coefficient is proportional to its imaginary part of $x^{(3)}$. A diode-pumped Nd: YAG laser of 532 nm and 50 mW was used as the excitation source. The laser beam having beam waist ω_0 of 15.35 µm was focused by the lens of focal length 3.5 cm on a 1 mm cuvette containing the sample solution. As it satisfies Rayleigh condition, $z_0 = \pi \omega_0^2 / \lambda > L$, the sample can be considered as a thin medium, where L is the thickness of the sample and λ is the free space wavelength of the laser beam. The transmission of the beam through an aperture placed in the far-field was measured using a digital power meter. In the open aperture Z-scan technique, a lens was used to collect the entire laser beam transmitted through the sample. In materials that have both refractive and absorptive nonlinearities, closed aperture measurements have contributions from both. So the closed aperture Z-scan data of the samples are divided with the open aperture data to eliminate the effect of nonlinear absorption. The demonstration of optical limiting was made using the same Z-scan geometry. The input power of the laser beam was varied systematically

with beam splitter arrangement and the corresponding output power was measured by a power meter [21, 22].



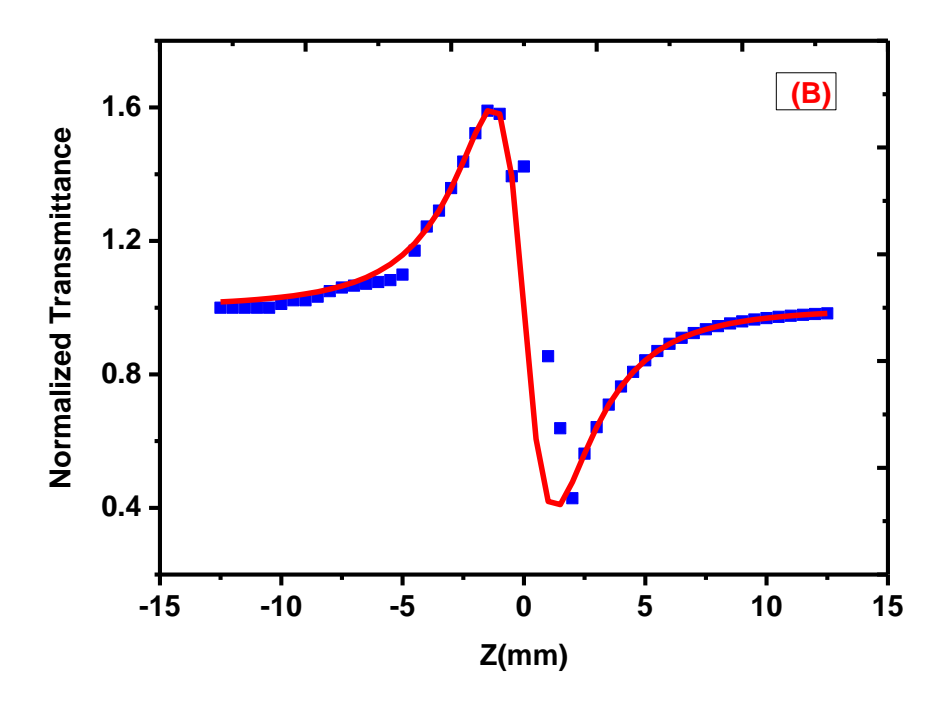
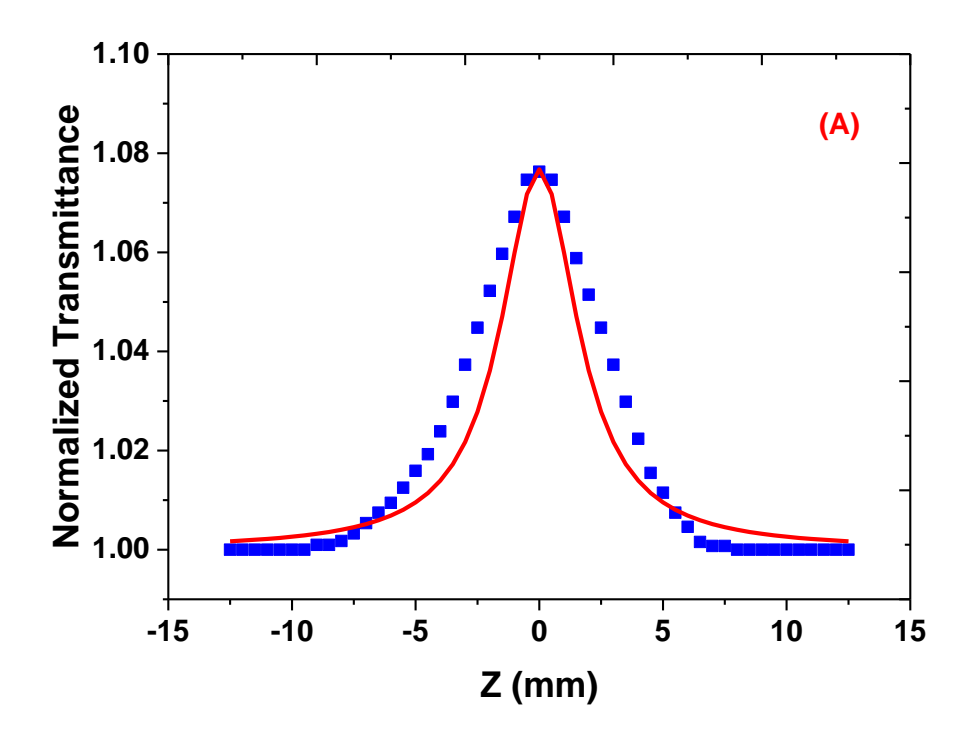


Figure 6.8 Z-scan (A) OA and (B) CA pattern of DMAPDP

The nonlinear absorption characteristics are evident from the symmetrical valley shape, shown by the open-aperture curves. The open aperture patterns (Fig. 6.8(A) and Fig. 6.9(A)) of both DMAPDP and GO: DMAPDP show the saturable absorption nature. Estimated saturable absorption coefficient (β) of DMAPDP and GO: DMAPDP composite was calculated to be 9.65 and 8.14 x 10-3 cm/W respectively. Surprisingly pristine DMAPDP exhibits stronger nonlinear absorption than GO: DMAPDP composite. In the closed aperture Z-scan experiment, the scan exhibits an asymmetric pre-focal peak followed by a post-focal valley indicating the nonlinearity of the sample to be negative and the lensing effect to be defocusing (Fig. 6.8(B) and Fig. 6.9(B)). A negative lens that focuses the beam on the aperture results in the increase of transmittance and beyond the focus (Z=0), the inverse effect occurs. The observed asymmetric nature of the Zscan measurements, along with the fact that the laser light is CW, shows the strong influence of thermal phenomena in the nonlinear optical behavior of samples. The nonlinear refractive index (n2) of DMAPDP and GO: DMAPDP composite was estimated to be 6.22 and 7.68 x 10⁻⁸ cm²/W respectively. Here the composite exhibit stronger nonlinear refraction due to the contribution from GO sheets.

Also the order of third-order NLO susceptibility of DMAPDP and GO: DMAPDP was found to be 3.98 and 4.56 x 10⁻⁶ esu respectively. Estimated NLO coefficients are summarized in Table 6.3. Fig. 6.9 shows the optical limiting behavior under the excitation of the second harmonic of diode-pumped Nd: YAG laser (532 nm, 50 mW), in the power range of 0-48 mW. In Fig. 6.10, the transmitted output intensity was found to vary linearly at very low input powers and turns nonlinear for high incident powers. Thus at low incident powers, the output varies according to Beers law and beyond 37.77 and 32.4 mW,

it becomes nonlinear for DMAPDP and GO: DMAPDP. Here GO: DMAPDP composite exhibits stronger optical limiting action than GO.



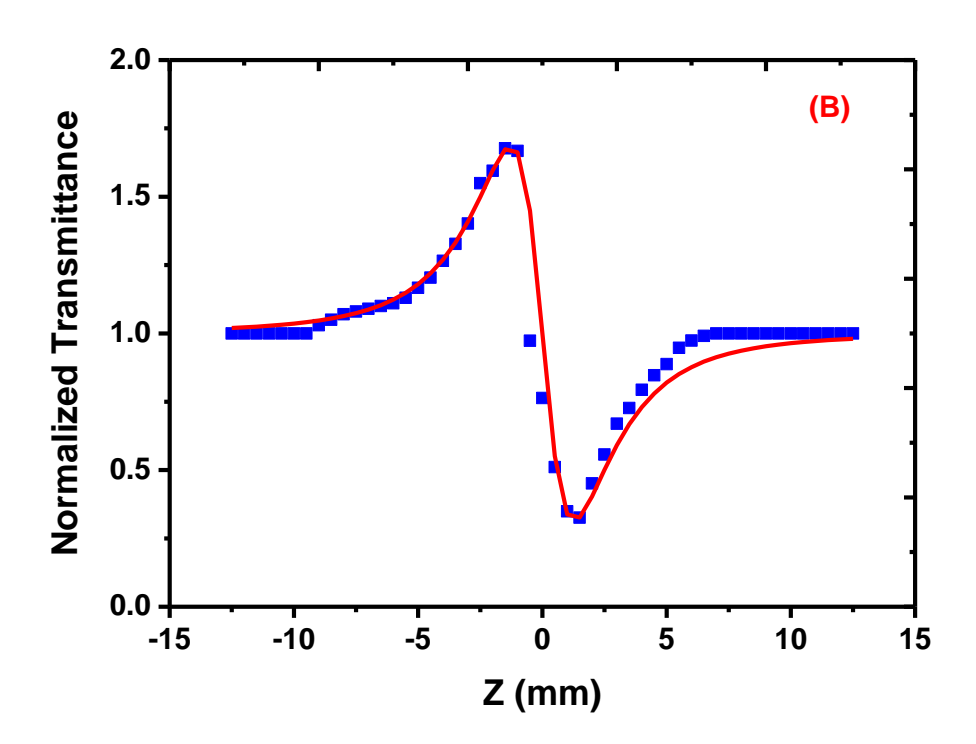
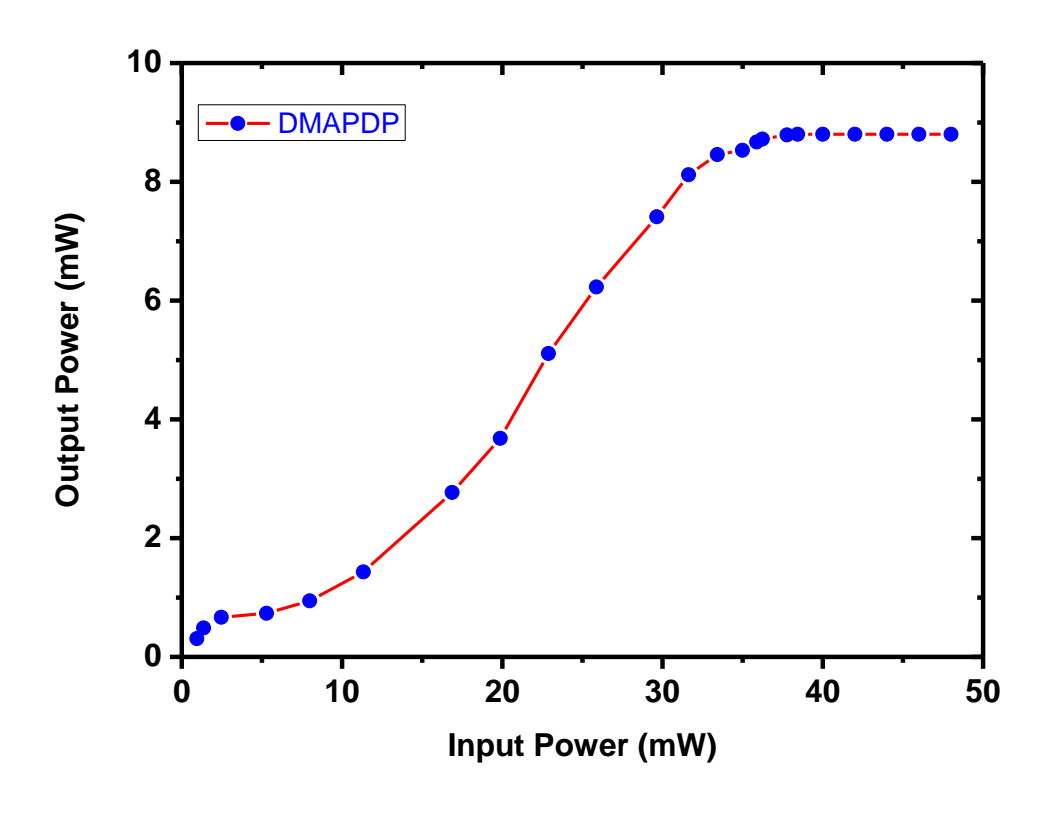


Figure 6.9 Z-scan (A) OA and (B) CA Pattern of GO: DMAPDP



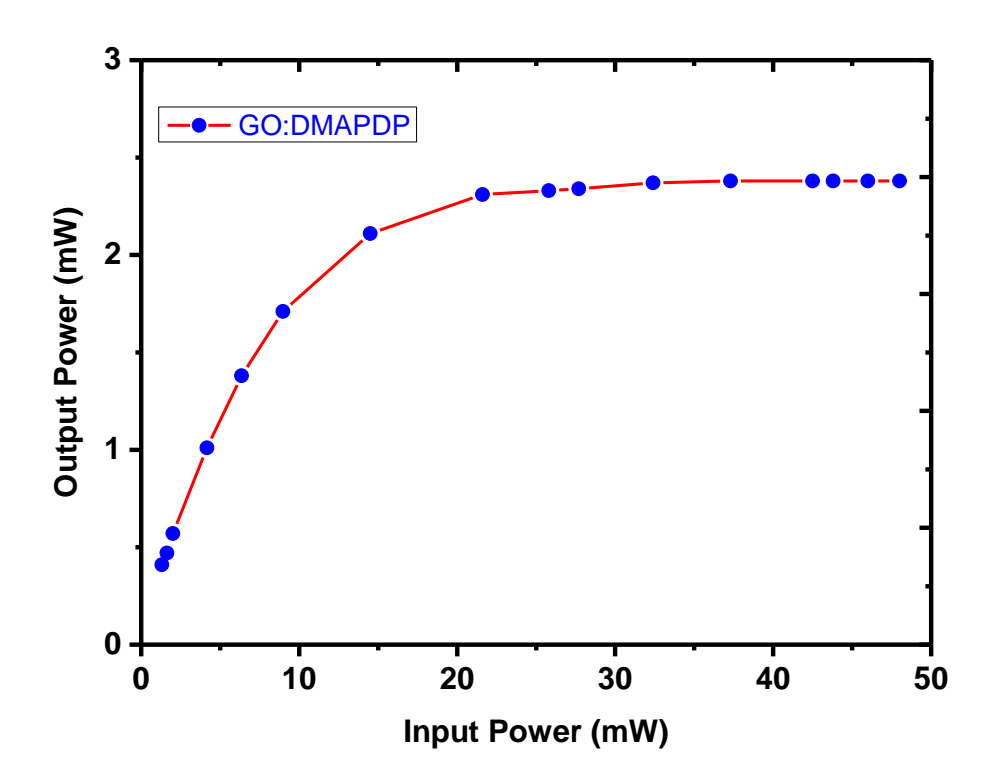


Figure 6.10 OL Pattern of DMAPDP and GO: DMAPDP

Chapter VI: DMAPDP@ GO

Table 6.3 Third-order NLO Coefficients of DMAPDP and GO: DMAPDP

NLO Parameters	DMAPDP	GO: DMAPDP
Nonlinear refractive index $(n_2) \times 10^{-8} \text{ cm}^2/\text{W}$	6.22	7.68
Nonlinear absorption coefficient (β) x 10 ⁻³ cm/W	9.65	8.14
Real part of NLO susceptibility [Re $[x^{(3)}]$] x 10 ⁻⁷ esu	3.21	4.16
Imaginary part of NLO susceptibility [Im [x ⁽³⁾]] x 10 ⁻⁶ esu	2.18	1.87
Third-order NLO susceptibility $(x^{(3)}) \times 10^{-6} \text{ esu}$	3.98	4.56
Optical limiting threshold (mW)	37.77	32.4
Clamping amplitude (mW)	8.8	2.38

6.6 Conclusion

By protonation transfer reaction, DMAPDP salt was obtained by dissolving DMAP in orthophosphoric acid solution at 65 °C. Employing solvent evaporation method, good quality crystals of dimensions $7 \times 6 \times 4 \text{ mm}^3$ (pH = 3.5), $10 \times 5 \times 2 \text{ mm}^3$ (pH = 4.45) and $11 \times 2 \times 1 \text{ mm}^3$ (pH = 5) was obtained after a typical growth period of 60 days. With a rise in pH (=3.5 to 5), the growth was restricted towards one direction

resulting in elongated rod-like morphology at pH=5. Nanostructures of DMAPDP and GO: DMAPDP composite was prepared by a simple hydrothermal method. DMAPDP crystallizes in the triclinic crystal system with centrosymmetric space group PI. In powder XRD of GO: DMAPDP, the peak at $2\theta = 12.4^{\circ}$ corresponds to the (001) plane of graphene oxide and other diffraction peaks at $2\theta = 18.5^{\circ}$, 20.2° , 21.16°, 23.0°, 28.54°, 30.87° corresponds to (111), (-112), (020), (103), (004), (213) plane of DMAPDP. The vibrational bands at 3067 and 2943 cm⁻¹ (C-H vibrations), 1565 cm⁻¹ (C=C vibrations), 997 and 539 cm⁻¹ (P-OH deformation) confirms the formation of DMAPDP and additional peaks at 1639 cm⁻¹ and 1282 cm⁻¹ (G and D-bands of GO) ascertains the formation of GO: DMAPDP composite. TG-DTA studies show, DMAPDP was stable up to 192 °C, beyond which decomposition starts. SEM image shows that DMAPDP nanostructures possess spherical morphology in the range of 45 -170 nm. Here graphene appears as wrinkled ultrathin sheets with staked layered structure with DMAPDP nanospheres form themselves as with an average diameter of 160 nm. The absorption maximum, cut-off wavelength and optical transmittance window of composites are 220 nm, 350 nm, 415 nm and 415-1100 nm which was red-shifted due to the interaction between moieties. The nonlinear optical response of thermo-optic origin exhibited by DMAPDP and GO DMAPDP composite at 532 nm low power CW laser was studied using the Z-scan technique. The optical limiting action of DMAPDP was demonstrated by the observed defocusing effect. The saturable absorption coefficient, nonlinear refractive index and third-order NLO susceptibility of GO: DMAPDP composite was found to be higher than bare DMAPDP. Thus GO: DMAPDP is expected to be a superior candidate for sensor protection in the CW low power regime.

6.7 References

- 1. T.C. Sabari Girisun, S. Dhanuskodi, D. Mangalaraj, J. Phillip, *Curr. App. Phy.*, 31 (2011) 838.
- 2. D. Vincent, App. Opt., 20 (2001) 6646.
- 3. Z. Hongbing, C. Wenzhe, W. Minquan, *J. Mater. Sci. Lett.*, 1 (2003) 283.
- 4. ZB. Liu, JG. Tian, Z. Guo, DM. Ren, F. Du, JY. Zheng, YS. Chen, *Adv. Mater.*, 4 (2008) 511.
- T.V. Timofeeva, V.N. Nesterov, F.M. Dolgushin, Y.V. Zubavichus,
 J.T. Goldshtein, D.M. Sammeth, R.D. Clark, B. Penn,
 M.Y. Antipin, Cryst. Eng., 3 (2000) 263.
- 6. J.F. Nicoud, C. Serbutoviez, Y. Barrans, D. Chasseau, I.G. Luneau, I. Ledoux, J. Zyss, *Nonlinear Optics* 9 (1995) 127.
- 7. M.S. Wong, J.F. Nicoud, C. Runser, A. Fort, M. Barzoukas, *Nonlinear Optics* 9 (1995) 181.
- 8. N. Bloembergen. *IEEE J. Selected Topics in Quantum Electronics* 6 (2000) 876.
- 9. C. Chen, N. Ye, J. Lin, J. Jiang, W. Zeng, B. Wu, *Adv. Mater.*, 11 13 (1999) 1071.
- 10. F. Wurthner, R. Wortmann, K. Meerholz, *Chem. Physchem.*, 3 (2002) 17.
- 11. P. Becker, Adv. Mater., 10 (1998) 979.
- 12. S. George, A. Nangia, C.K.Lam, T.C.W. Mak, J.F. Nicoud, *Chem. Commun.*, (2004) 1202.
- 13. K. Clays, B.J. Coe, Chem. Mater., 15 (2003) 642.
- 14. S. Manivannan, S. Dhanuskodi, Cryst. Growth & Design, 4 (2004) 845.

- 15. G. Muruganandi, M. Saravanan, G. Vinitha, M.B. Jessie Raj, T.C. Sabari Girisun, *Chem. Phy.*, 488 (2017) 55.
- 16. G. Muruganandi, M.B. Jessie Raj, T.C. Sabari Girisun, *Int. J. Nanosci.*, 4 (2017) 1760036.
- 17. P.S. Kalsi, *Spectroscopy of organic compounds*, New Age International (P) Limited Publishers, New Delhi, 2002.
- 18. G. Varsanyi, Assignments for vibrational spectra of seven hundred benzene derivatives, Adam Hilger, London, 1974.
- 19. B. Milton Boaz, A. Leo Rajesh, S. Xavier Jesu Raja, S. Jerome Das, *J. Mater. Sci. Technol.*, 20 (2004) 505.
- 20. T.C. Sabari Girisun, S. Dhanuskodi, *Cryst. Res. Technol.*, 44 (2009) 1297.
- 21. Mansoor Sheik- Bahae, Ali A. Said, Tai-Huei Wei, 1990, *IEEE J. Quantum. Electron*, 26 (1990) 760.
- 22. M. Thangaraj, G. Ravi, T.C. Sabari Girisun, G. Vinitha, A. Loganathan, *Spectrochim. Acta Part A: Mol. and Biomol. Spectro.*, 138 (2015) 158.

Chapter - VII

Summary and Future Directions

CHAPTER VII

Summary and Future Directions

Layer structured carbonaceous materials like graphene oxide (GO) stand high in NLO applications due to their stronger nonlinear optical response. This thesis focuses on the NLO investigation of Graphene oxide (GO) and Reduced Graphene Oxide (rGO), BBO nanorods decorated rGO, 2A5NPFB decorated GO, 2A5NPDP decorated GO and DMAPDP decorated GO. The prepared materials were subjected to systematic studies like XRD, FTIR (preliminary confirmation), SEM (morphology), absorption (linear optical properties) and Kurtz-powder, Z-scan (nonlinear optical properties) studies. SHG capability of the non-centric complexes was studied by the Kurtz powder technique. The nonlinear optical response of thermo-optic origin exhibited by pure and decorated complexes at 532 nm low power CW laser was studied using the Z-scan technique. Saturable absorption, self-defocusing, and optical limiting action were observed in all samples. BBO: rGO and GO: DMAPDP are identified as superior self-defocusing assisted optical limiters for the most widely used CW green low power laser.

Nonlinear Optical (NLO) phenomena are potentially useful in the context that they can alter the frequency of light and amplify one source of light with another, switch it or alter its transmission characteristics through a medium, depending on its intensity. The common thread running through the laser-based applications is the need for a powerful, compact, rugged, inexpensive source of laser light in the blue-green region of the electromagnetic spectrum. The generation of coherent blue-green light through second harmonic generation (SHG) from near infra-red (NIR) laser is an important technological problem that has attracted much attention. Potential applications of this technology include high-density optical data storage, high-resolution printing, spectroscopy inspection, biomedicine, and others. From the birth of NLO through the Franken experiment in 1961, intense research is being made to develop an efficient frequency doubler as an alternate for commercially available potassium dihydrogen phosphate, KDP.

At the same time, with the advent of optical detectors and sensors which are used for scientific and industrial purposes, there is a need for using optical limiting devices that protect the photosensitive components from intense optical radiation. Such NLO materials are passive devices and are referred to as intelligent or smart materials owing to actuating functions that are inherent in them. In this context, extensive research works have been carried out for identifying such materials as they can be used for protecting the human eye from the enfeebling laser effects as the maximum permissible exposure for human eyes even with a laser pointer is ~2.5 mW/cm² in the visible spectral region. And over recent years, a series of studies have been performed on different optical materials with high nonlinearity for a variety of applications in a second harmonic generation (SHG) and optical limiting (OL) devices.

Based on these facts, the main interest of this work is focused on the identification of novel materials for NLO applications. The ideal NLO material should possess a high laser damage threshold, fast optical response, flexible for molecular design, optical transparency, mechanical stability, thermal stability and ease of fabrication. Recent growing efforts in molecular engineering suggest that organic NLO materials possess comparably better NLO properties than inorganic materials. However, single organic material that meets all the characteristics are currently unavailable in the pre-realm of graphene. This is because graphene is an interesting layered carbonaceous material that has two-dimensional one-atom-thick sp²-bonded carbon networks. Oxygen-containing groups, such as hydroxyl, epoxy, carbonyl, and carboxylic on graphene oxide (GO) sheets can be used to decorate the graphene sheets. Thus layer structured carbonaceous materials like GO stand high in this domain due to their stronger nonlinear optical response. However, the basic requirement of high linear transmittance limits the possible usage as a harmonic generator and optical limiter.

Improvement of linear transmittance along with enhanced NLO action can be achieved through nanocomposite formation that possesses GO as host-matrix and known NLO material as a decorative element. In the process of nanocomposite formation, the optimization of GO that resembles the behavior of graphene is very important. The reduction of graphene was mainly aimed at eliminating epoxy and hydroxyl groups on the plane, while others, e.g. carboxyl, carbonyl, and ester groups are present at the edges or defective areas of rGO sheet. These functional groups will act as nucleation centers that allow decoration of many organic/inorganic NLO materials and thus optimization of desired content of these oxygen-containing functional

groups is very important. In the choice of inorganic materials, barium borate (BBO) nanostructures will be an interesting candidate, as it possesses large second harmonic generation (SHG) and has unique characteristics like wide transparency, large birefringence, high optical threshold, and excellent mechanical properties. Thus decorating BBO nanorods upon rGO can yield rGO:BBO nanocomposite.

Compared to inorganic NLO materials, the inclusion semiorganic NLO materials in rGO can yield high NLO coefficient nanocomposites. Among the available chromophore, a polarizable organic molecule 4-dimethyl aminopyridine (DMAP), can be selected as a guest and anchored onto inorganic host orthophosphoric acid. The hydrogen bond networks formed can provide crystalline semiorganic material, 4-dimethyl aminopyridinium dihydrogen phosphate (DMAPDP) with improved stabilities. Also, 2-amino 5-nitropyridine (2A5NP) can induce a high NLO character with a strong donor (NH₂) and acceptor (NO₂) group through a push-pull mechanism. In particular, the derivatives 2A5NP dihydrogen phosphate (2A5NPDP) and 2A5NP fluoroborate (2A5NPFB), are efficient NLO materials as it can attach inorganic elements to its herringbone pattern. Inclusion of these semiorganic NLO materials like 2A5NPFB, 2A5NPDP, and DMAPDP as decorative elements in GO can yield interesting nanocomposites that possess stronger nonlinear refraction, which is beneficial for power limiting applications. Thus this thesis aims to investigate, i) Graphene oxide and Reduced Graphene Oxide (rGO), ii) BBO nanorods decorated rGO, iii) 2A5NPFB decorated GO, iv) 2A5NPDP decorated GO and v) DMAPDP decorated GO. The prepared materials were subjected to systematic studies like XRD, FTIR (preliminary confirmation), SEM (morphology), UV-Vis absorption (linear optical properties) and Kurtzpowder, Z-scan (nonlinear optical properties) studies.

Initially, Graphene oxide was successfully prepared by a modified Hummers method. And reduced graphene oxide (rGO) was prepared by reduction method using hydrazine, sodium borohydride and ascorbic acid as reductant and its structure, morphology, emission, absorption and nonlinear optical properties were investigated. The preliminary identification of the sample was carried out by the powder XRD pattern. The reduced GO material consists of randomly aggregated, thin crumpled sheets closely associated with each other and forming disordered sheets. The emission peak in the near UV region at 365 nm corresponds to the band emission of rGO. The third-order NLO properties of dispersed graphene oxide (GO) was measured using an Nd: YAG laser (532 nm, 50 mW) by employing the Z-scan technique. Results show that the materials possess negative nonlinearity and selfdefocusing nature which is responsible for the optical limiting behavior in the regime of interest. The nonlinear optical response of thermo-optic origin exhibited by the sample at low CW laser powers (532 nm, 50 mW) was analyzed. The defocusing nature and large nonlinear saturable absorption coefficient make the sample to behave as a good optical limiter in the low power regime. All the materials exhibit optical limiting and rGO reduced by hydrazine monohydrate (rGO-H) has a better optical limiting action. Hydrazine reduced rGO is found to possess improved thermal and photostability, and excellent durability, which signifies the scope of utilizing them as smart materials for optical limiting applications.

By the simple hydrothermal method, nanorods of barium borate were successfully loaded on reduced graphene oxide sheets. Powder XRD confirms the incorporation of barium borate ($2\theta = 29^{\circ}$, (202)) along with the transition of graphene oxide ($2\theta = 12^{\circ}$, (001)) into reduced graphene oxide ($2\theta = 25^{\circ}$, (002)). In the FTIR spectra, the presence of

characteristic absorption peaks of rGO (1572 and 2928 cm⁻¹) and barium borate (510, 760 and 856 cm⁻¹) further evidences the formation of BBO:rGO nanocomposite. FESEM images portray the existence of graphene sheets as thin layers and growth of barium borate as nanorods on the sheets of reduced graphene oxide. Ground-state absorption studies reveal the hypsochromic shift in the absorption maxima of the graphene layers due to the reduction of graphene oxide and hypochromic shift in the absorbance intensity due to the inclusion of highly transparent barium borate. The photoluminescence of BBO:rGO shows maximum emission in the UV region which is due to direct transitions involving the valence band and conduction band in the bandgap region. Optical nonlinearity of BBO:rGO nanocomposite was studied by the Z-scan technique using CW diode-pumped Nd: YAG laser (532nm, 50 mW). Both nanocomposite and individual counterparts possess saturable absorption and self-defocusing behavior. Third-order nonlinear optical coefficients of BBO:rGO nanocomposite is found to be higher than bare graphene oxide. In particular, the nonlinear refractive index of nanocomposite is almost four times higher than GO which resulted in superior optical power limiting action. Strong nonlinear refraction (self-defocusing) and lower onset limiting threshold make the BBO:rGO nanocomposite preferable candidate for laser safety devices than rGO and BBO.

2-amino 5-nitropyridinium fluoroborate (2A5NPFB) was synthesized using 2A5NP and tetra fluoro boric acid. Using graphene oxide obtained through a modified Hummers method as host and 2A5NPFB as a decorative element, GO: 2A5NPFB composite was prepared. Single crystals of 2A5NPFB of dimension 9 x 7 x 5 mm³ were grown by the solvent evaporation method. 2A5NPFB crystallizes in acentric space group Fdd2 having an orthorhombic crystal system with

lattice parameter a=22.474 (1) Å, b=30.127 (9) Å, c=4.9584 (1) Å. Prepared composites possess the characteristic peak of both GO and a slight shift in the FTIR peak positions are due to the interaction of graphene layers and 2A5NP molecules. The incorporation of inorganic species is confirmed by the presence of new peaks at 750 cm⁻¹ (BF₄anion) in 2A5NPFB. In SEM image, the formation of thin, continuous, and twisted like graphene structures randomly oriented with additional bright spots which depict the successful attachment of 2A5NPFB on the surface of GO. 2A5NPDP possess strong absorption (λ_{max} =2199 nm, 350 nm) in the UV region with broad transparency window (420-1100 nm). In the UV-Vis absorption pattern of composite, the characteristic peak of both GO and 2A5NP was observed. The absorption maximum, cut-off wavelength and optical transmittance window of GO: 2A5NPFB are 219 nm, 352 nm, 405 nm, and 405-1100 nm. The relative SHG efficiency of 2A5NPFB crystal was 35 times that of KDP. Z-Scan studies with CW excitation show that the material exhibits saturable absorption, self-defocusing, and optical limiting action. And here GO:2A5NPFB exhibit higher NLO performance than pure GO and 2A5NPFB.

By simple acid-base reaction, 2-amino 5-nitropyridinium dihydrogen phosphate (2A5NPDP) was synthesized. Single crystals of 2A5NPDP (6 x 2 x 1 mm³) were grown from ethanol by slow evaporation technique. 2A5NPDP belongs to the orthorhombic crystal system with a Pna2₁ space group with lattice parameter a=24.133 (7) Å, b=6.503 (1) Å, c=45.108 (1) Å. In the FTIR spectrum of GO: 2A5NPDP composite, the aromatic C=C stretching (1571 cm⁻¹), C-H stretching (2853 cm⁻¹), O-H stretching (3595 cm⁻¹) and C=O stretching (1676 cm⁻¹) of graphene oxide was shifted. Similarly the presence of peaks at 3235 cm⁻¹ (N-H...O), 1642 cm⁻¹ (C=N), 1621 cm⁻¹ (N-H), 1514 cm⁻¹ (N-O), 1310 cm⁻¹ (C-H),

1115 cm⁻¹ (P-O), 980 cm⁻¹ (PO₄) represents the different vibrations of 2A5NPDP mostly shifted to the lower wavenumber. The SEM image of GO: 2A5NPDP composite possesses dense bright shades of 2A5NPDP with uniform concentration throughout the ultrathin wrinkled GO sheets. Here 2A5NPDP not only acts as a decorative element but also acts as a reducing agent which was confirmed by the reduction in the stacking of layers. In the UV-Vis absorption pattern of GO: 2A5NPDP composite, the characteristic peak of both GO (235 nm) and 2A5NPDP (340 nm) was observed. Compared to 2A5NPDP, the absorbance pattern of composite depicts stronger absorption in the UV and visible region. The SHG efficiency of the powder sample of 2A5NPDP was measured to be 4.2 times KDP and the saturation of SHG output at higher particle size confirms the phase-matching property. Z-Scan studies with CW excitation show that 2A5NPDP and GO: 2A5NPDP composite exhibit saturable absorption, self-defocusing, and optical limiting action. And here GO: 2A5NPDP exhibit higher NLO performance than pure GO and 2A5NPDP.

By protonation transfer reaction, DMAPDP salt was obtained by dissolving DMAP in orthophosphoric acid solution at 65 °C. Employing solvent evaporation method, good quality crystals of dimensions 7 x 6 x 4 mm³ (pH = 3.5), 10 x 5 x 2 mm³ (pH = 4.45) and 11 x 2 x 1 mm³ (pH = 5) was obtained after a typical growth period of 60 days. With rise in pH (=3.5 to 5), the growth was restricted towards one direction resulting in elongated rod-like morphology at pH=5. Nanostructures of DMAPDP and GO: DMAPDP composite was prepared by a simple hydrothermal method. DMAPDP crystallizes in the triclinic crystal system with centrosymmetric space group PT . The vibrational bands at 3067 cm⁻¹ and 2943 cm⁻¹ (C-H vibrations), 1565 cm⁻¹ (C=C vibrations), 997 cm⁻¹ and 539 cm⁻¹ (P-OH deformation) confirms the formation of DMAPDP

and additional peaks at 1639 cm⁻¹ and 1282 cm⁻¹ (G and D-bands of GO) ascertains the formation of GO: DMAPDP composite. TG-DTA studies show, DMAPDP was stable up to 192 °C, beyond which decomposition starts. SEM image shows that DMAPDP nanostructures possess spherical morphology with diameter in the range of 45 -170 nm. Here graphene appears as wrinkled ultrathin sheets with staked layered structure with DMAPDP nanospheres form themselves as with an average diameter of 160 nm. The absorption maximum, cut-off wavelength and optical transmittance window of GO: DMAPDP are 220 nm, 350 nm, 415 nm and 415-1100 nm which was red-shifted due to the interaction between moieties. The NLO response of thermo-optic origin exhibited by DMAPDP and GO: DMAPDP composite at 532 nm low power CW laser was studied using the Z-scan technique. The optical limiting action of DMAPDP was demonstrated by the observed defocusing effect. The saturable absorption coefficient, nonlinear refractive index and third-order NLO susceptibility of GO: DMAPDP composite was found to be higher than bare DMAPDP. Thus GO: DMAPDP is expected to be a suitable candidate for sensor protection in the CW low power regime.

Estimated NLO coefficients obtained for different graphene oxide complexes along with its individual molecule are summarized in Table 7.1. All the functionalized GO systems exhibit higher NLO coefficients than pristine GO. It is interesting to note that obtained reduced graphene oxide with different reducing agents show tunable NLO coefficients which may arise due to change in the functional group's concentration and layers of graphene sheets. As it is known that, hydrazine is the strongest reducing agent that has effectively reduced graphene oxide (rGO-H) and it shows higher NLO coefficients among the prepared reduced graphene oxide.

Table 7.1 Comparison of NLO Coefficients of Pure and Decorated GO Complexes Excited under Nd: YAG (532 nm, 50 mW) Laser

Compounds	eta_{SA} $ imes$ 10 $^{-3}$ cm/W	n_2 $\times 10^{-8} cm^2/W$	$\chi^{(3)}$ × 10 ⁻⁶ esu	OL_T , OL_C mW
GO	5.86	1.58	1.68	32.5, 1.9
rGO-H	7.73	4.18	3.03	32.5, 3
rGO-N	5.90	4.39	2.88	32.5, 3.6
rGO-A	5.88	2.60	2.05	32.5, 3.1
BBO	8.8	8.3	4.34	32.6, 0.85
BBO:rGO	6.05	6.26	4.84	9.5, 6.2
2A5NPFB	7.64	3.93	2.53	36.2, 6.7
2A5NPDP	6.86	5.89	3.85	38.43, 8.1
DMAPDP	9.65	6.22	3.98	37.8, 8.8
GO:2A5NPFB	13.95	6.06	4.27	37.7, 3.0
GO:2A5NPDP	4.45	6.51	4.02	32.4, 4.1
GO:DMAPDP	8.14	7.68	4.56	32.4, 2.4

Among the nitropyridine derivatives substituted GO complexes, GO: 2A5NPFB shows stronger nonlinear absorption with the highest saturable absorption coefficient of 13.95×10^{-3} cm/W and GO: DMAPDP

exhibit stronger nonlinear refraction with the maximum nonlinear refractive index of 7.68 x 10-8 cm²/W. Higher third-order NLO susceptibility was witnessed with BBO: rGO (4.84 x 10-6 esu) followed by GO: DMAPDP (4.56 x 10-6 esu). In the functionalized graphene oxide complexes, BBO: rGO shows the lowest optical limiting threshold arising due to the dominance of BBO. Under Nd: YAG CW green laser excitation observed optical limiting action is driven by self-defocusing nature and all samples are identified to be energy-spreading optical limiters. As the clamping amplitude and onset optical limiting threshold is varying randomly, the direct suggestion of superior OL material is not possible. However, based on third-order NLO susceptibility, BBO: rGO and GO: DMAPDP can be considered as superior self-defocusing assisted optical limiter for most widely used CW green low power laser.

The concept of understanding can be more authentic when complexes based on the left out other complexes of nitropyridine are taken into account. In such consideration, the model that has been framed will be complete for other aromatic based systems. Also, the work can be further extended to other known NLO aromatic complexes. In succeeding, the concept can be still challenging when other known NLO aromatic complexes are taken for consideration. As all the materials show significant NLO response, the limiting behavior based on pulsed lasers will yield more interesting results for high-speed optoelectronic applications. Research attempts on limiting behavior as a function of wavelength will yield more interesting results. Hence all such research attempts are left as pathways for future work.

Annexure

Reprints

DOI: 10.1142/S0219581X17600365



Nonlinear Optical Behavior of Nanostructured 4-Dimethyl-Aminopyridinium Dihydrogen Phosphate

G. Muruganandi* and M. B. Jessie Raj

Department of Physics

Bishop Heber College

Tiruchirappalli - 620 017, India

*qmuruqanandi@qmail.com

T. C. Sabari Girisun
School of Physics
Bharathidasan University
Tiruchirappalli - 620 024, India

Received 31 May 2015 Accepted 21 June 2017 Published 28 September 2017

Optical nonlinearity of 4-dimethyl aminopyridinium dihydrogen phosphate (DMAPDP) was studied using continuous wave of diode pumped Nd:YAG laser (532 nm, 50 mW). The nonlinear refractive index, nonlinear absorption coefficient and nonlinear optical (NLO) susceptibility of the sample were found to be in the order of 10^{-8} cm²/W, 10^{-3} cm/W and 10^{-6} esu respectively. The observed self defocusing effect was used to demonstrate the optical limiting action at 532 nm. Initially, XRD analysis showed that DMAPDP crystallizes in triclinic crystal system with centrosymmetric space group $P\overline{1}$. Thermal studies explored that the material undergoes an irreversible endothermic transition at 192°C which correspond to the decomposition of material. SEM image portrays the formation of nanoparticles with grain size in the range of 45–170 nm. Hence 4-dimethyl aminopyridinium dihydrogen phosphate nanoparticles can be used as potential candidate for optical limiting applications.

Keywords: Semi-organic; nanoparticles; Z-scan; nonlinear optical coefficient.

1. Introduction

In recent years, a lot of efforts have been made to prepare nonlinear optical (NLO) materials which support the fabrication of nanoscale photonic and photoelectronic devices, with low thresholds, which can be used for the protection of eyes and sensitive optical devices from laser-induced damage. For the optical device applications such as optical limiters,

understanding the third-order NLO phenomenon is the most fundamental. Many optical limiting materials could serve as candidates for practical optical limiters. They have been found to show high nonlinear extinction (NLE) (i.e., strongly attenuate intense and potentially dangerous laser beams while readily transmitting low-intensity ambient light). Strong optical-limiting properties have been observed in various materials such as

^{*}Corresponding author.

carbon-based suspensions, porphyrin complexes and metallophthalocyanines.^{2–4} Also with rapid advancement of nanoscience and nanotechnology, a large number of optical limiting materials have been shown to possess remarkable NLO properties, which motivates the design of practical optical limiters. In order to design an optimal NLO material, the origin of the nonlinear response to the optical field must be understood. The carbon atom has the great ability to form stable hybridized bonds (a two-electron covalent bond σ $C_{sp}^3-C_{sp}^3$ and a four-electron bond $\sigma + \pi$ $C_{sp}^2-C_{sp}^2$) which provide diverse properties of organic compounds. The availability of π -electrons in an organic molecule differentiates organic NLO materials from inorganic systems. These electron distributions can be perturbed by the interaction with a radiation field such as the intense optical electromagnetic field produced by a laser and if the perturbation is asymmetric, a quadratic nonlinearity results. The search for a chromophore is likely to be assisted by the various physical methods satisfying the other requirements to realize the actual NLO device. In this present work, a polarizable organic molecule 4-dimethylaminopyridine (DMAP) was selected as a guest and anchored onto inorganic host orthophosphoric acid. The hydrogen bond networks formed in this semiorganic structure can provide crystalline materials with improved stabilities. The third-order NLO behavior of nanostructured 4-dimethyl-aminopyridinium dihydrogen phosphate (DMAPDP) were explored by Z-scan technique using a low laser power continuous wave (CW) diode pumped Nd:YAG laser (532 nm, 50 mW).

2. Experimental

The reaction scheme for the formation of DMAPDP on chemical reaction with involved acids is indicated in Fig. 1. DMAP is a weak Bronsted base that

$$H_3C$$
 CH_3
 H_3C
 CH_3
 CH_3

Fig. 1. Reaction scheme of DMAPDP.

gains a proton in acidic solution and forms the salt of the respective acid. The DMAPDP salt was obtained by dissolving DMAP in orthophosphoric acid solution at 65°C in the molar ratio 1:1:20 for DMAP, H₃PO₄ and triple distilled water, respectively. On cooling below room temperature, the salt crystallized as a white microcrystalline powder. By repeated recrystallization process, the material was further purified. DMAPDP exhibits positive solubility temperature gradient in aqueous solution. Hence by slow evaporation technique, single crystals of DMAPDP were grown from saturated agueous solution (pH = 4.45) maintained at 30° C. Good quality crystals of dimension $10 \times 5 \times 2 \,\mathrm{mm}^3$ were obtained after a typical growth period of 60 days.

3. Structural and Morphological Characterization

 1 H and 13 C NMR spectrum (Fig. 2) of the DMAPDP was recorded to elucidate its molecular structure. In the 1 H NMR, the presence of dimethyl group was confirmed by the singlet at $\delta = 3.5$ ppm. The influence of the adjacent proton of CH was ascertained by the presence of doublet centered at $\delta = 6.9$ ppm. Due to the low electron density, another doublet was observed in the downfield at $\delta = 8.1$ ppm which confirms the protonation of

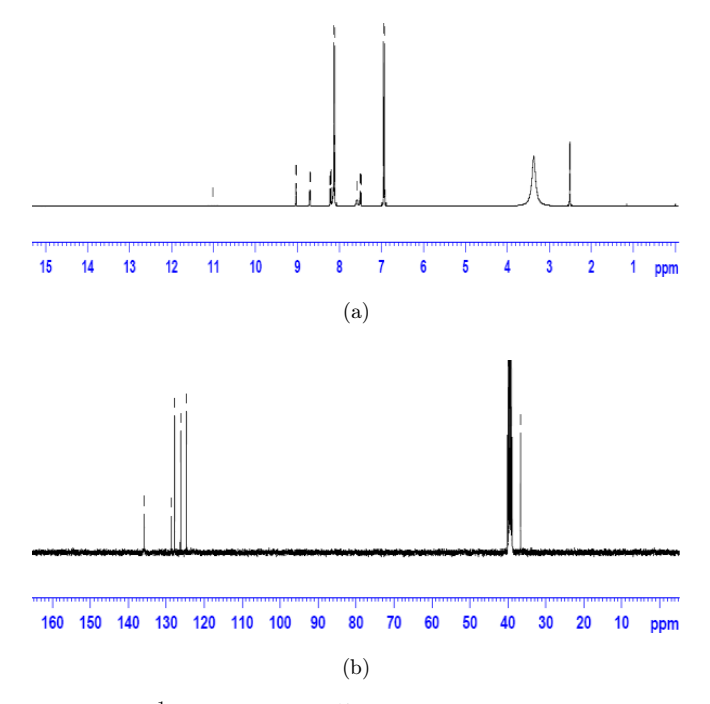


Fig. 2. (a) ¹H NMR and (b) ¹³C NMR spectrum of DMAPDP.

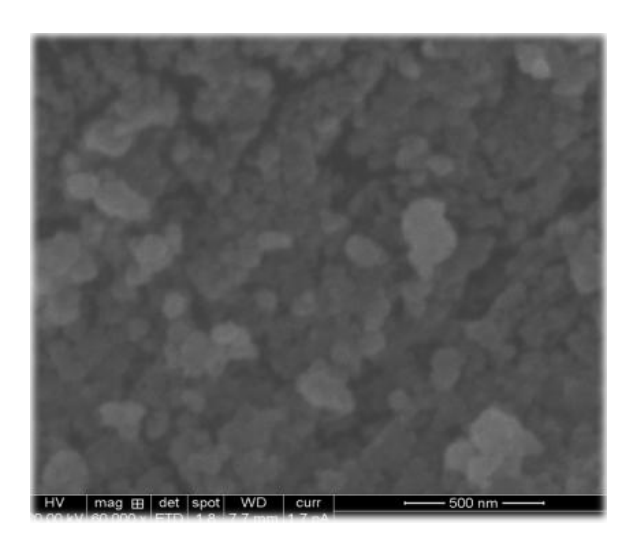


Fig. 3. SEM image of DMAPDP.

nitrogen (N⁺) in the pyridine ring. The three prominent signals in ¹³C NMR also confirm the predicted molecular structure of DMAPDP. Based on the thermal analysis made, the obtained salts were sintered at 180°C in an autoclave for 48 h using muffle furnace to form possible nanostructures. SEM image portrays the formation of nanoparticles with grain size in the range of 45–170 nm. As the reaction was carried out in ambient pressure, the particles get sufficient time to form the most stable sphere-like structure. However in the present case, the grains formed were not so uniform in shape.

4. Thermal Studies

The thermal stability of DMAPDP was assessed by thermogravimetric and differential thermal analysis. The recorded thermal decomposition curve (40–720°C) is illustrated in Fig. 4. The material was found to be stable and free of moisture till 192°C. The TGA clearly shows that the decomposition initiates around 190°C and loses its weight by almost 85% due to the removal of the molecular fragments. The DTA reveals exactly the same changes shown by the TGA.⁵ Before the decomposition, material does not suffer any phase transition, since no endothermic or exothermic transitions were observed below 200°C. From the DTA curve, it can be further confirmed that the material undergoes an irreversible endothermic transition at about 192°C where DMAP decomposes as NO₂, CO₂, CO, NH₃ gases.

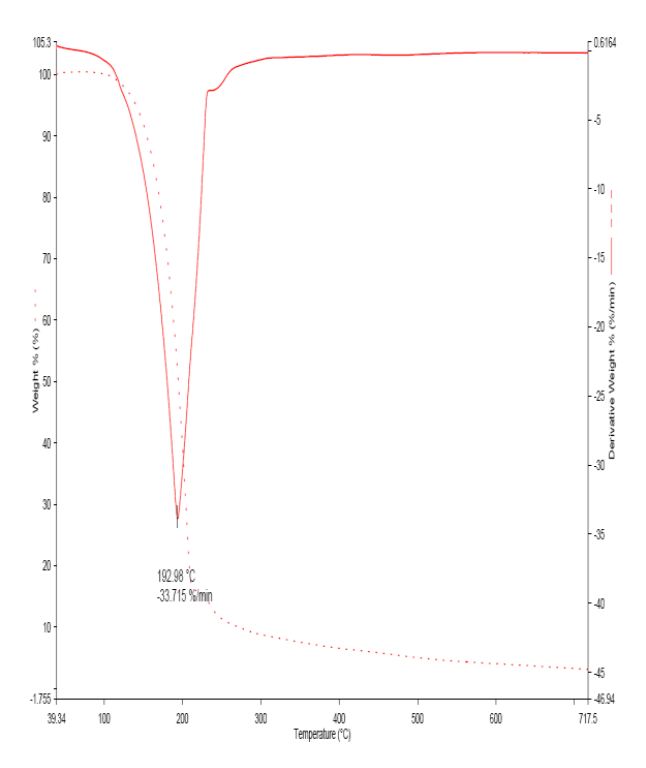


Fig. 4. TG/DTA curves of DMAPDP.

5. Linear Optical Studies

Employing a JASCO UV-Vis spectrophotometer at 30°C linear optical property of DMAPDP was recorded. For optical fabrications, the crystal should be highly transparent in UV-Visible region. In the recorded transmission pattern (Fig. 4), transmission begins to increase abruptly around 310 nm, indicating an optical absorption edge in the UV region, which is an essential criterion for NLO

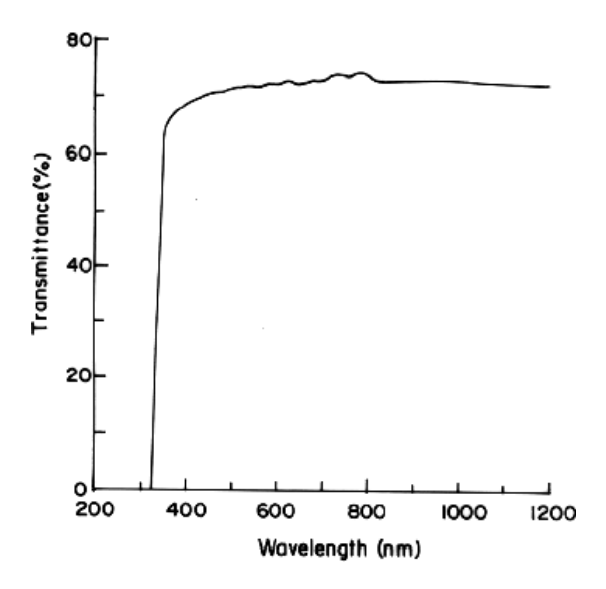


Fig. 5. Optical transmittance window of DMAPDP crystal.

applications.⁶ Also the material possesses good transmission in the entire visible region which makes them suitable for short wavelength optoelectronic devices such as UV LEDs and laser diodes.

6. Nonlinear Optical Properties

The Z-scan technique is a powerful tool to characterize the NLO properties as it can measure the sign and magnitude of nonlinear index of refraction (n_2) and nonlinear absorption coefficient (β). Knowing the values of nonlinear refractive index and nonlinear absorption coefficient, third-order NLO susceptibility can also be obtained. In typical experimental procedure, a diode-pumped Nd: YAG laser (Neodymium vttrium-aluminum-garnet) of $532\,\mathrm{nm}$ and $50\,\mathrm{mW}$ was used as the excitation source. The laser beam was focused by lens of focal length 3.5 cm on a 1 mm cuvette containing the sample solution to produce a beam waist ω_0 of $15.35 \,\mu\mathrm{m}$. Here, the sample was considered as thin film as it satisfies Rayleigh condition, $z_o =$ $\pi\omega_0^2/\lambda > L$, where L is the thickness of the sample and λ is the free space wavelength of the laser beam. The transmission of the beam through the sample as a function of position in the far field was measured using a digital power meter with (closed) and without (open) aperture. In the open aperture Z-scan technique, a lens was used to collect the entire laser beam transmitted through the sample. The demonstration of optical limiting was made using the same Z-scan geometry. The input power of the laser beam was varied systematically using a variable beam splitter and the corresponding output power through the aperture was detected by a power meter. The nonlinear parameters of the samples under continuous wave laser illumination was determined by the closed Z-scan set up formulated by Sheik-Bahae et al.^{7,8}

In the closed aperture Z-scan experiment, the observed nonlinearity was due to self-focusing or defocusing effect of the beam. A negative or positive self-lens tends to collimate or diverge the beam on the aperture so that the measured transmittance increases or decreases, respectively. After the focal plane, the inverse effect occurs. Results of closed aperture Z-scan experiments are presented in Fig. 6. The scan exhibits an asymmetric pre-focal peak followed by a post-focal valley indicating the nonlinearity of the sample to be negative and the lensing effect to be defocusing. The observed

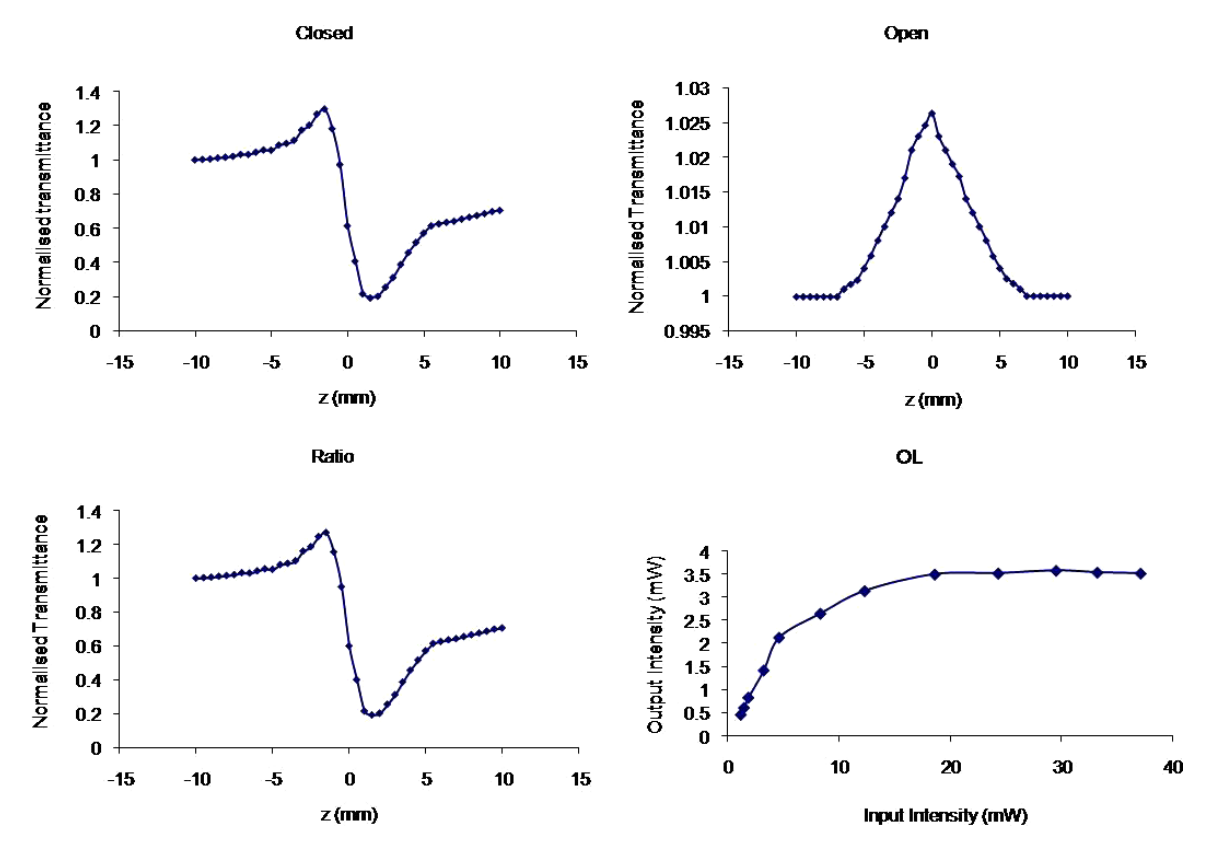


Fig. 6. Z-scan pattern of DMAPDP.

asymmetric nature of the Z-scan measurements, along with the fact that the laser light is CW, confirmed the strong influence of thermal component in the NLO behavior of the sample. The non-linear refractive index of DMAPDP was estimated to be in the order of $10^{-8} \, \mathrm{cm}^2/\mathrm{W}$.

The nonlinear absorption characteristics are evident from the symmetrical valley shape, shown by the open-aperture curves. The open aperture pattern (Fig. 6) of the sample showed the saturable absorption due to the self-defocusing nature. In materials which have both refractive and absorptive nonlinearities, closed aperture measurements have contributions from both. So the closed aperture Z-scan data of the sample was divided with the open aperture data in order to eliminate the effect of nonlinear absorption. From the open aperture Z-scan data, the nonlinear absorption coefficient¹⁰ was calculated to be 10^{-3} cm/W. Also the thirdorder NLO susceptibility of DMAPDP was found to be 10^{-6} esu. Figure 6 represents the optical limiting behavior at 532 nm using the second harmonic of diode pumped Nd: YAG laser (1064 nm, 50 mW), in the power range of 0.45–47.1 mW. The transmitted output intensity was found to vary linearly at very low input powers and turn nonlinear for high incident powers. 11 Thus at low incident powers, the output varies according to Beers law and beyond 13 mW, it becomes nonlinear. The limiting threshold value was found to be 13 mW with corresponding output value clamped at 3.5 mW.

7. Conclusion

DMAPDP salt was obtained by dissolving DMAP in orthophosphoric acid solution at 65° C. DMAPDP crystallizes in triclinic crystal system with centric space group $P\overline{1}$. Formation of nanoparticles with grain size in the range of $45-170\,\mathrm{nm}$ was observed. The molecular structure was

confirmed by NMR analysis. The material was stable upto 192°C, beyond which decomposition starts. The NLO response of thermo-optic origin exhibited by DMAPDP at 532 nm low power CW laser was studied using Z-scan technique. The optical limiting action of DMAPDP was demonstrated by the observed self-defocusing effect. Nonlinear absorption based limiters have been used for high power pulsed laser sources, but thermo-optic origin limiter can be used as an efficient power limiter in the low power CW regime. Hence DMAPDP nanoparticles are expected to be a suitable candidate for the protection of photosensitive components.

References

- 1. T. C. Sabari Girisun, S. Dhanuskodi, D. Mangalaraj and J. Phillip, *Curr. App. Phys.* **31**, 838 (2011).
- 2. D. Vincent, App. Optics. 20, 6646 (2001).
- Z. Hongbing, C. Wenzhe and W. Minquan, J. Mater. Sci. Lett. 1, 283 (2003).
- Z. B. Liu, J. G. Tian, Z. Guo, D. M. Ren, F. Du, J. Y. Zheng and Y. S. Chen, Adv. Mater. 4, 511 (2008).
- 5. S. Manivannan and S. Dhanuskodi, *Cryst. Growth Des.* **7**, 845 (2004).
- S. Sudhahar, M. Krishna Kumar, A. Silambarasan, R. Muralidharan and R. Mohan Kumar, J. Mater. 28, 539312 (2013).
- M. Sheik-Bahae, A. A. Said, Tai-hue Wei, David J. Hagan and E. W. Van Stryland, *IEEE J. Quantum Electron.* 26, 760 (1990).
- 8. M. Maryam and D. Dorranian, *Optik Int. J. Light Electron. Opt.* **125**, 5612 (2014).
- R. L. Sutherland, Handbook of Nonlinear Optics, 2nd edn. (Marcel Dekker, New York, 2003).
- Z. Dehghani, E. S. Iranizad and M. Nadafan, Opt. Commun. 1, 16 (2015).
- M. Saravanan, T. C. Sabari Girisun and S. Vinitha, J. Mater. Sci. 1, 3289 (2016).



Contents lists available at ScienceDirect

Chemical Physics

journal homepage: www.elsevier.com/locate/chemphys



Effect of reducing agents in tuning the third-order optical nonlinearity and optical limiting behavior of reduced graphene oxide



G. Muruganandi ^a, M. Saravanan ^b, G. Vinitha ^c, M.B. Jessie Raj ^{a,*}, T.C. Sabari Girisun ^{b,*}

- ^a Department of Physics, Bishop Heber College, Tiruchirappalli 620 017, India
- ^b Nanophotonics Laboratory, School of Physics, Bharathidasan University, Tiruchirappalli 620 024, India
- ^c Division of Physics, School of Advanced Science, VIT Chennai, Chennai 600 127, Tamilnadu, India

ARTICLE INFO

Article history: Received 25 November 2016 In final form 15 March 2017 Available online 18 March 2017

ABSTRACT

Reduced graphene oxide (rGO) was prepared by reduction method using various reductants like hydrazine, sodium borohydride and ascorbic acid. XRD and Raman analysis confirmed the effective removal of functional groups in GO. SEM revealed that rGO consists of thin crumpled and disordered sheets closely associated with each other. Blue shift in UV-absorption maxima was due to weak interlayer coupling between the layers of rGO. Third order NLO properties of dispersed rGO were measured by Z-scan technique (532 nm, 50 mW). Both GO and rGO possess self defocusing, saturable absorption and optical limiting behavior. The nonlinear component of refractive index, absorption coefficient and optical susceptibility were found to be $10^{-8} \, \mathrm{cm}^2/\mathrm{W}$, $10^{-3} \, \mathrm{cm/W}$ and $10^{-6} \, \mathrm{esu}$ respectively. Tunability of NLO coefficients with altering functional groups upon rGO was achieved. rGO prepared using hydrazine with high NLO coefficient and excellent durability, signify the scope of utilizing them as optical limiters.

© 2017 Elsevier B.V. All rights reserved.

1. Introduction

With the extensive use of continuous wave (CW) lasers at power levels ranging from µW to kW in various applications, the need for protecting the human eye and sensors has become increasingly important. The optical-limiting (OL) effect is a phenomenon where in a medium exhibit high transmittance at lowintensity light and attenuate an intense optical beam, limiting the output fluence at a certain range [1]. Especially human eye has its spectral sensitivity maximum at green regime and with widespread usage of green CW lasers in human interactive sectors, optical limiters are most necessary thing to ascertain safety precautions. The well known materials found to exhibit a strong OL effect and explored as candidates for practical optical limiters. include inorganic, organics, organometallic complexes such as oligothienylenevinlenes, dimethylaminostyryl substituted BODIPY, ligand, ruthenium-acetylide organometallic complexes and bisdithiafulvenyl substituted tetrathifulvalene [2-11]. In this search, the versatile chemistry of carbon materials, functionalizing as a building block of many fascinating new stable and structurally improved carbon nano materials, has resulted in a huge interest on studying carbonaceous matter for optical limiting applications. Among them graphene (G) with two dimensional one-atom-thick sp²-bonded carbon networks, has attracted great attention due to its promising properties like high flexibility, linear transmittance and thermal stability [12]. Literature clearly shows that graphene possess strong nonlinear refraction due to large sp² hybridized carbon conjugated structure under pulsed excitations [13–14].

Although graphene is identified to be a superior OL materials, the major barrier in the device realization, is its cost to attain high purity. Hence as an alternate, reduced graphene oxide (rGO) which resembles the properties of graphene and that can be delivered from inexpensive graphene oxide (GO) are under attraction. The most attractive property of GO is that it can be (partly) reduced to graphene-like sheets (rGO) by removing the oxygen-containing groups such as hydroxyl, epoxy, carbonyl and carboxylic with the recovery of a conjugated structure by reduction process [15]. Some of known reducing agents used for preparation of rGO includes hydrazine [16], sodium borohydride (NaBH₄) [17], ascorbic acid [18], hydroquinone [19], pyrogallol [20], hot strong alkaline solutions (KOH, NaOH) [21] and hydroxylamine [22]. It is worthy to be noted that, the optical properties of rGO is greatly influenced by the presence of various functional groups available after the reduction process. Therefore tunability of nonlinear optical properties can be achieved by properly monitoring the functional groups upon the graphene sheets, which in turn can be achieved by varying the reducing agents. Hence it is interesting to understand the role of reducing agents in achieving the desired NLO properties. Although investigation of rGO in pulsed regime is available in liter-

^{*} Corresponding authors.

E-mail address: sabarigirisun@bdu.a.cin (T.C. Sabari Girisun).

ature, study of nonlinear response in CW regime still remains unexplored. The main motivation of the present work is to make a systematic investigation of the nonlinear optical properties and their correlation with the structure of some finely dispersed GO and rGO sheets. Hence this article presents the nonlinear optical response of rGO samples studied by Z-scan experiments using continuous wave Nd: YAG laser (532 nm, 50 mW).

2. Experimental

2.1. Materials preparation

Firstly graphene oxide (GO) was prepared by a modified method originally proposed by Hummers. GO was synthesized from as purchased AR grade graphite flakes by oxidation process using powerful oxidants like NaNO₃, H₂SO₄ and KMnO₄. The details of the synthesis procedure involved were described elsewhere [23]. To obtain rGO, reduction of graphene oxide was employed using various reducing agents like hydrazine monohydrate (H), sodium borohydride (N) and ascorbic Acid (A). Here hydrazine acts as a strong reducing agent and hence can remove most of the functional groups upon the surface of GO effectively. While sodium borohydride is most effective in reducing C=O species but has low efficiency in the reduction of epoxy and carboxyl groups [24]. Ascorbic acid acts as mild reducing agent and has great advantage of its non-toxicity in contrast to hydrazine and a higher chemical stability with water than NaBH₄. Furthermore, the reduction in colloid state does not result in the aggregation of rGO sheets as produced by hydrazine, which is beneficial for further applications. The procedure involved can be described as follows.

2.1.1. Hydrazine monohydrate (rGO-H)

Initially, GO (100 mg) was sonicated in 100 ml of distilled water for three hours. After that, 1 ml of hydrazine monohydrate (N_2H_2 - H_2O) which acts as a reducing agent was added into the suspension and it was placed in an oil bath at 80 °C for 30 min. Later the oil bath was removed and solution was placed in a condenser for 24 h, yielding a black precipitate. After cooling the solution to room temperature (30 °C), the solution was centrifuged and the obtained powder was dried at 30 °C.

2.1.2. Sodium borohydride (rGO-N)

GO (50 mg), was mixed with 50 ml of methanol and they were allowed to disperse for 1 h. Sodium borohydride (NaBH₄) of 0.5 mg which acts as a reducing agent was added into the solution and placed in a condenser along with stirring process at 70 °C for 2 h. The resulting solution was washed with methanol and double distilled water till the pH becomes neutral. The particles were allowed to settle down at the bottom. The solution was centrifuged and the powder was dried at 30 °C.

2.1.3. Ascorbic acid (rGO-A)

GO (0.1 g), was mixed with ascorbic acid (0.1 g) in 100 mL of double distilled water. The solution was allowed to disperse for 30 min at 60 °C. 30% of $\rm H_2O_2$ was added to the solution and once again they were allowed to disperse for 30 min at 60 °C. The resulting solution was washed with double distilled water. Followed by centrifugation, the obtained sample was dried at 120 °C.

2.2. Physical measurements

The preliminary identification of the prepared samples were employed by powder X-ray diffraction using CuK α radiation at the scanning rate of $0.02~\text{s}^{-1}$ in the angle of 10 to 80 degree. Vibrational studies were carried out by JASCO FTIR 460 PLUS spectrom-

eter from 400 cm⁻¹ to 4000 cm⁻¹ to identify various functional groups available in GO and rGO surfaces. Raman spectrum was recorded to study the disorder defects in GO and rGO with 758 nm laser as excitation source. Morphologies of these samples were investigated by Scanning Electron Microscope (SEM) using Hitachi SEM 400. The optical absorption spectrum was collected for dispersed GO and rGO using UV-Vis-NIR Perkin Elmer Spectrophotometer in range 200-1100 nm. The room temperature (30 °C) emission studies were carried out using a Perkin Elmer LS 55 luminescence spectrometer. The third-order nonlinear optical properties of the GO and rGO dispersed in ethylene glycol by ultrasonication (concentration of 5 mg) were studied by Z-scan technique in both closed and open aperture mode. Here the laser used for excitation is a continuous wave Nd:YAG laser with 532 nm wavelength having power of 50 mW. The sample cell was moved using a translation system along the propagation direction (Z-axis) of a focused Gaussian beam through its focal plane. By moving the sample through the focus, the intensity dependent nonlinear refraction and nonlinear absorption was measured from the changes of the transmittance through the sample. Under similar Z-scan geometry, the optical limiting behavior of the samples was also investigated.

3. Results and discussion

3.1. Preliminary confirmation: XRD

The X-ray diffraction pattern for GO prepared by modified Hummers method showed a strong amorphous nature with sharp peak at 12° which corresponds to (001) plane of GO with an interlayer spacing of 0.72 nm. This major characteristic peak arises due to sp² hybridization of GO. In the XRD pattern of rGO obtained with various reducing agents (Fig. 1), the major peak of GO disappeared completely, giving preliminary confirmation of reduction process.

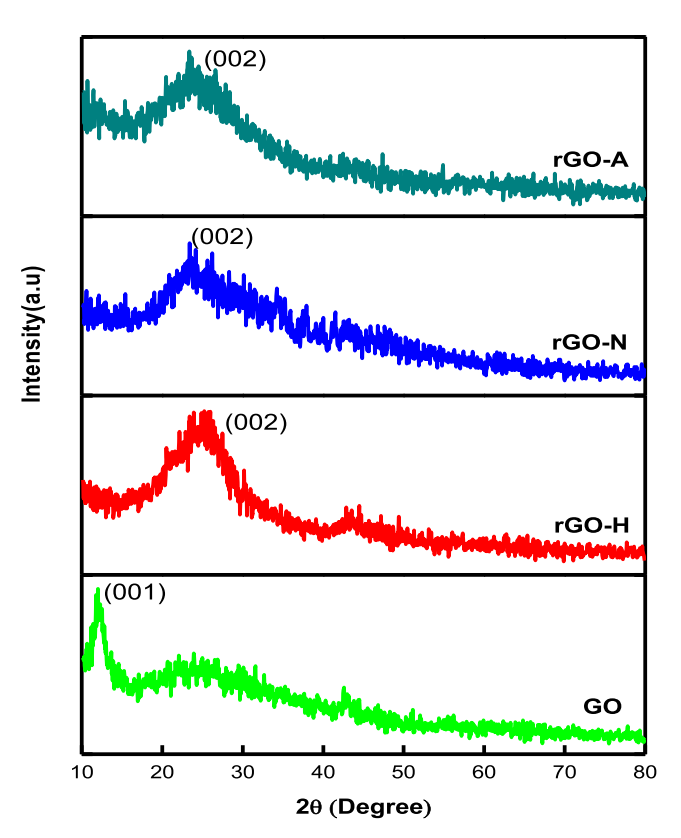


Fig. 1. XRD Pattern of GO and rGO.

The broad peak located around 26° (signature of rGO) confirmed the formation of rGO which was indexed to be (002) plane. The interlaying distance which corresponds to spacing between the carbon layers was found to be 0.34 nm, 0.38 nm and 0.75 nm for rGO-H, rGO-N and rGO-A respectively. The interlayer distance value of rGO-H and rGO-N was found to be much smaller than that of GO (0.72 nm). This reduction was due to effective removal of the functional groups and the layers were brought quite closer to each other. However the interlayer value of rGO-A (d = 0.75 nm) was almost equal to the value of GO which indicate that the functional groups were not completely removed upon ascorbic treatment. Based on the interlayer distance it can be confirmed that hydrazine monohydrate is a best reducing agent to attain rGO when compared to sodium borohydride and ascorbic acid which points out that the functional groups were not completely removed.

3.2. Functional group identification: FTIR

Fig. 2 shows the comparative FTIR spectra of GO and rGO. In GO, the aromatic ring of graphitic structure was confirmed by the presence of peaks at 1572 cm⁻¹ (C=C stretching) and 2925 cm⁻¹ (C-H stretching). The presence of different types of functionality upon graphene oxide sheets were confirmed by the peaks at 3442 cm⁻¹ (O—H stretching vibration of hydroxyl groups), 2324 cm⁻¹ (C=O stretching vibration of carboxyl groups), 1738 cm⁻¹ (C=O stretching vibration of carbonyl groups), 1228 cm⁻¹ (C=O stretching of epoxy group) and 1031 cm⁻¹ (C--O stretching of alkoxy groups). The presence of characteristic peaks of graphitic structure was observed for all the samples after reduction process. It is interesting to be noted that, ascorbic acid leaves all the functional groups untreated, other than carbonyl group and hence resembles the pattern of GO. While sodium borohydride is effective in removing C=O vibrations of carboxyl and carbonyl groups. And hydrazine is more effective in eliminating

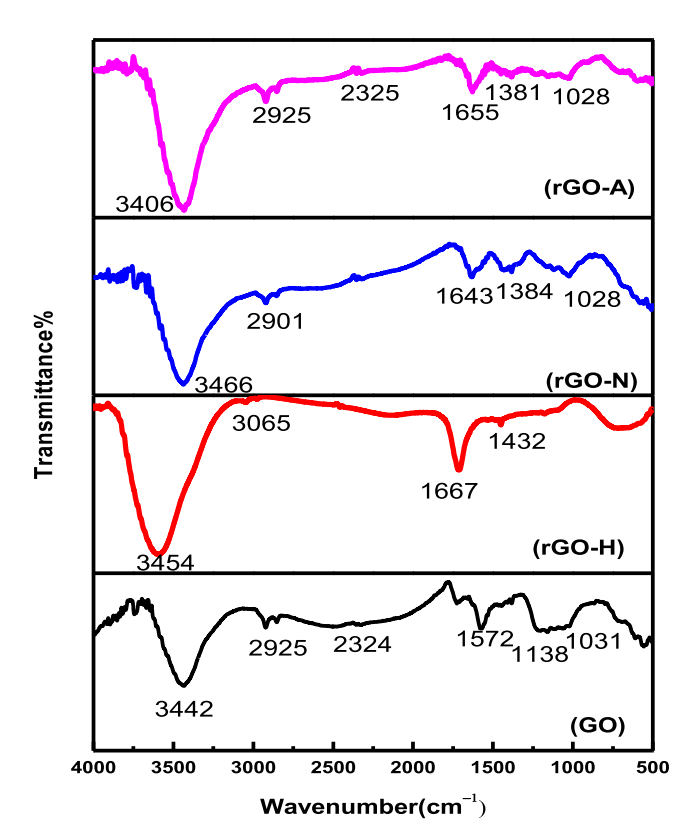


Fig. 2. FTIR Pattern of GO and rGO.

most of oxygen functional groups like carboxyl, carbonyl, epoxy and alkoxy groups, resulting in the formation of reduced graphene oxide which resembles graphene structure. The detailed peak assignments and identification of functional groups is summarized in Table 1. Thus FTIR analysis clearly indicates, different reducing agents have resulted in the formation of reduced graphene oxide with various functional groups on the surface.

3.3. Disorder and defect estimation: Raman and SEM

Raman spectroscopy is widely used to characterize disorder and defects in carbonaceous materials like graphene. Fig. 3. represents the recorded Raman spectra of GO and rGO. All the Raman curves have two obvious vibration peaks consisting of D peak which corresponds to the disordered structure (sp³) and G peak to the ordered structure (sp²) of material. Thus the intensity ratio of D peak and G peak (I_D/I_G) can be used to evaluate the sp² domain size and degree of disorder of the graphene-based materials. The I_D/I_G of GO, rGO-A, rGO-N and rGO-H were 1.07, 1.37, 1.46 and 1.48 respectively. The increase in I_D/I_G is usually the result of (a) the increase of the amount of amorphous carbon (b) the decrease of the crystalline size and (c) higher defect density. In the present case, the increase in I_D/I_C ratio of reduced samples further confirms the formation of rGO and hydrazine to be an effective reducing agent. From the relative intensity ratio, the perfect graphene domain (La) was estimated using the well-known formula [25]

$$L_a(nm) = \frac{560}{E_{\lambda}^4} \left(\frac{I_D}{I_G}\right)^{-1}$$

where E_{λ} is the excitation energy (eV). Thus, GO has perfect graphene domain (L_a) of \sim 74 nm, which upon functionalization reduces to 53, 54 and 57 nm for rGO-H, rGO-N, rGO-A respectively. This small change further confirms a decrease in the lower size and a higher defect density of in-plane graphitic crystallite sp² domains due to reduction of GO. Considering the relationship of I_D/I_G with the extent of π -conjugation of defects on rGO, the present route thus allows the modification of optical properties of rGO readily. Fig. 4 shows that GO have layered structure and ultra thin inhomogeneous graphene sheets. However in the recorded picture of rGO, it is possible to distinguish the edges of the individual sheets. SEM images revealed that the reduced GO material consists of randomly aggregated, thin crumpled sheets closely associated with each other and forming disordered sheets.

3.4. Linear optical properties: absorption and emission

As shown in the UV–Vis spectrum (Fig. 5), GO exhibits a π – π * absorption band at 234 nm. While reduced graphene oxide (rGO–H, rGO–N and rGO–A), suffers a blue shift in absorption peak to 210, 215 and 208 nm. Interestingly, shifting in the absorption peak occurs due to the decrease in functional groups and weak interlayer coupling between the layers, causing electrons to be easily excited at lower energy level. From the blue shifted peaks, it can be confirmed that the electronic conjugation within the sheets were restored after reduction process. Among UV patterns of the reduced GO, rGO-H shows less absorption and high linear transmittance due to the efficient reduction of all the functional groups.

Under the exposure of 325 nm light, GO exhibits an intensive blue luminescence at 360 nm (Fig. 6) and is related to isolated sp² domains generated by oxidation process. However, the epoxide groups on basal plane and carboxylic groups at GO edge often induce non-radiative recombination of localized electron-hole pairs, leading to a very weak emission. Hence upon reduction of functional groups, rGO showed a bright blue emission at 360 nm.

Table 1 FTIR peak assignment and identification of functional groups.

Peak Position (cm ⁻¹)			Peak assignments	
GO	rGO-H	rGO-N	rGO-A	
1572	1667	1690	1655	C=C stretching (skeletal vibrations of aromatic domain)
2925	3065	2901	2925	C—H stretching (aromatic hydrocarbons)
3442	3454	3466	3406	O—H stretching (hydroxyl groups)
2324	_	_	2325	C=O stretching (carboxyl groups)
1738	_	_	_	C=O stretching (carbonyl groups)
1228	_	1384	1381	C—O stretching (epoxy groups)
1031	_	1028	1028	C—O stretching (alkoxy groups)

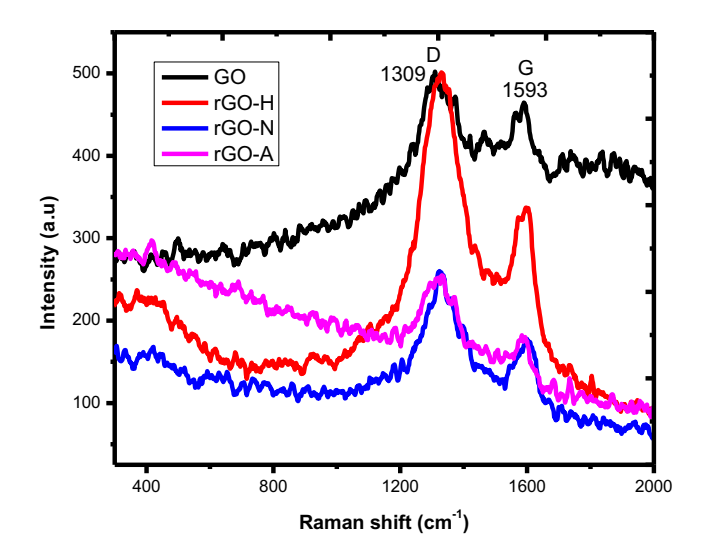


Fig. 3. Raman spectra of GO and rGO.

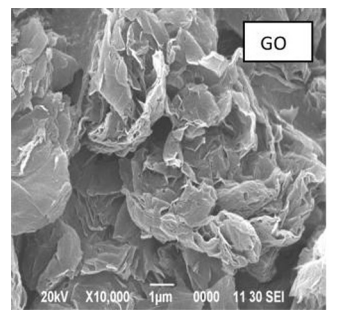
Also the emission peaks at 493 nm and 521 nm were ascribed to the surface defects formed during the reduction process.

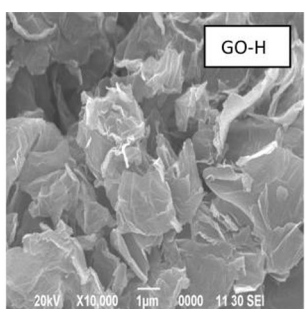
3.5. Nonlinear optical properties and limiting action: Z scan

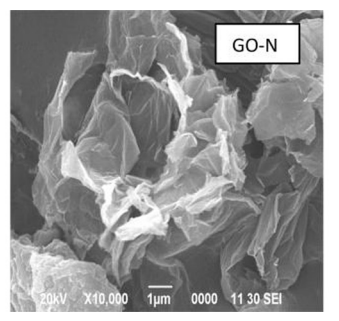
The open aperture Z-scan data (Fig. 7) shows a maxima for normalized transmittance at the principal focus (Z=0) for both GO and rGO. Hence the observed nonlinear absorption is due to saturable absorption (SA) nature of the material. Absorption saturation in the sample enhances the peak and decreases the valley in the closed aperture Z-scan and results in distortions in the symmetry of the Z-scan about Z=0. The recorded normalized closed aperture Z-scan (Fig. 8) curve exhibits a pre-focal transmittance maximum (peak) followed by a post-focal transmittance minimum (valley) for all the samples. This peak-valley signature indicates the self-defocusing property and it is represented by negative nonlinear refractive index (n_2). Thus under CW laser excitation, the non-

linear refraction behavior of the sample is equivalent to the formation of induced negative lens resulting in self-defocusing behavior [26]. It is interesting to note that mechanism responsible for nonlinear refraction in graphene strongly depends upon the nature of sample (graphene/graphene oxide layers in solution dispersions and graphene sheets on a substrate) and laser (CW or Pulsed) considered for excitation. As thermal diffusion co-efficient of graphene is very higher, cumulative thermal effects can be neglected in graphene layers on a substrate and only π electron contributes. In liquid media (dispersed in solution), π electron along with reorientation, alignment of the graphene sheets contributes to nonlinear refraction under continuous wave or long pulse laser. However for GO sheets in dispersions, electron of sp² and sp³ domain, free carriers and π electron can contribute to the NLR. Also reorientation and thermal effects are considered according to the duration of pulse. Since the samples were excited with CW laser excitation in the present case, the observed nonlinear refraction mechanism is predominantly thermal in origin [14].

When the medium was irradiated by cw laser, a small portion of its energy was absorbed by the medium which turns the system thermally agitated. Hence this local heating of the absorbed medium resulted in temperature varied nonlinear refraction index in sample. Thus, the observed nonlinearity is thermal in origin and they are of third-order optical nonlinearity. The curve of measured output power as a function of input power of laser is as shown in Fig. 9. The transmitted output intensity was found to be nonlinear at high incident powers and hence confirming optical limiting behavior for all samples. At higher input powers, the output reaches a plateau and is saturated at a point defined as the limiting amplitude: i.e. the maximum output intensity, showing obvious limiting property. In all cases the optical limiting threshold of rGO was found to be 14.46 mW and there is a slight change in its clamping value (1.43-3.35 mW) based on reducing agent chosen for synthesis of GO. Here in optical limiting, initially the deviation from Beer's law takes place and when the molecules available are sufficiently high, clamping takes place. In the present case, as rGO was prepared with different reducing agents, the functional groups available on the graphene layers are different and hence clamping has occurred at different values. Also it is known that higher the







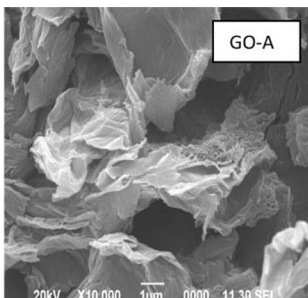


Fig. 4. SEM images of GO and rGO.

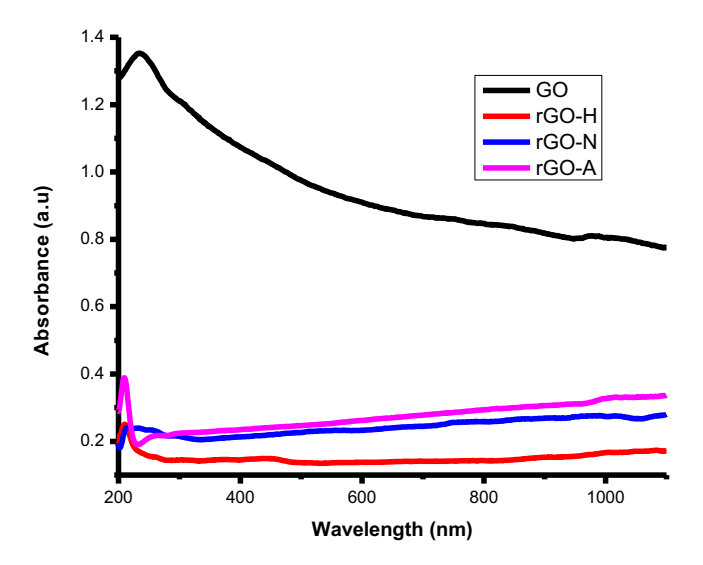


Fig. 5. UV-Vis-NIR absorption spectra of GO and rGO.

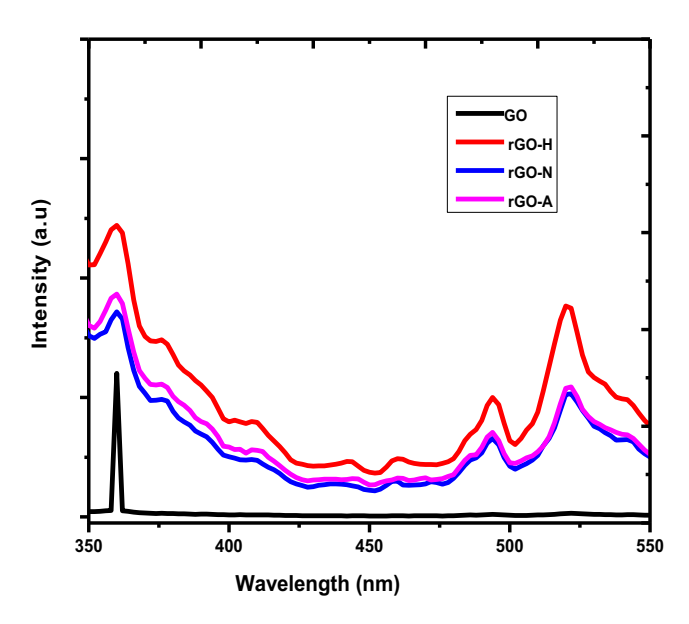


Fig. 6. Emission spectra of GO and rGO.

nonlinear absorption coefficient lower will be its limiting threshold (limiting amplitude). As rGO-H has higher nonlinear absorption coefficient it possess better limiting behavior.

Since closed aperture data obtained from Z-scan contain both nonlinear refraction and nonlinear absorption components, it is necessary to separate the nonlinear absorption components from the nonlinear refraction so as to extract pure nonlinear refraction and hence the ratios of both data were made to estimate the NLO coefficients [27]. The third order NLO parameters such as nonlinear refractive index, real part of nonlinear optical susceptibility, imaginary part of nonlinear optical susceptibility and third order nonlinear optical susceptibility were calculated using the following relations

$$\Delta T_{p-\nu} = 0.406(1-S)^{0.25} |\Delta \phi|$$

where S is the aperture linear transmittance and is calculated using the relation

$$S = 1 - exp(-2r_a^2/\omega_a^2)$$

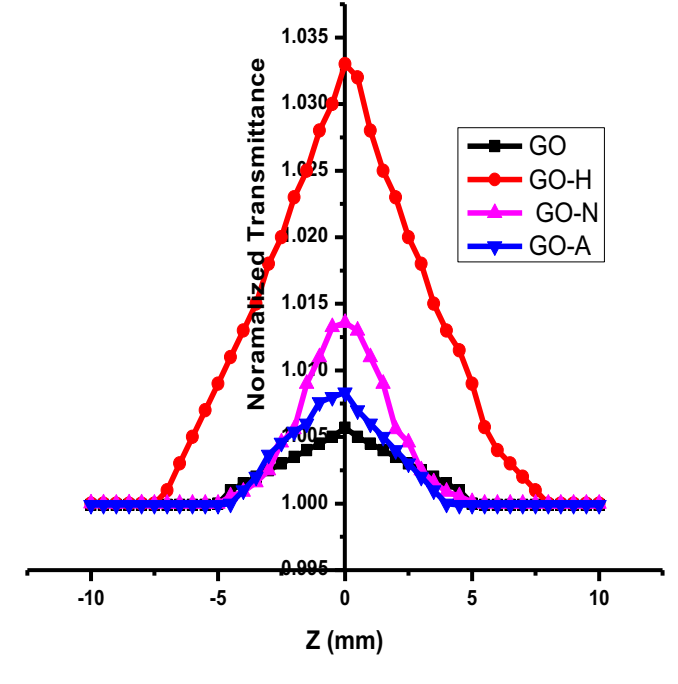


Fig. 7. Z-scan open-aperture pattern of GO and rGO.

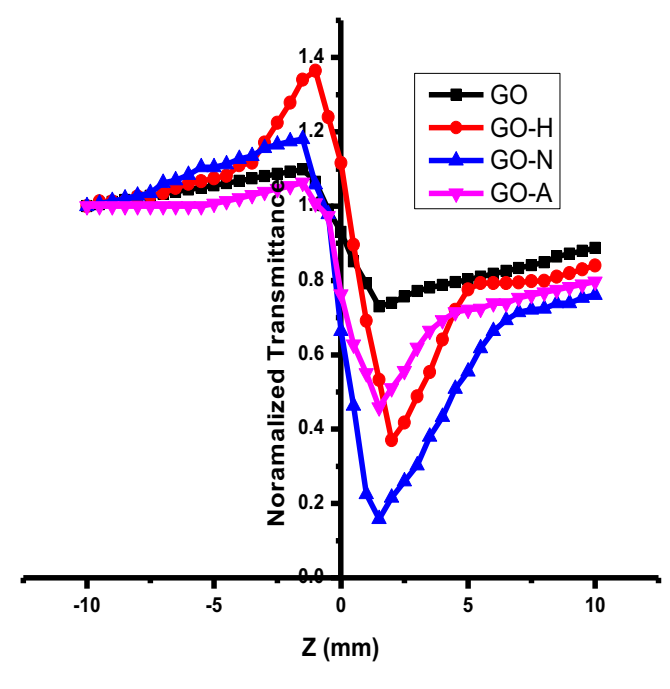


Fig. 8. Z-scan closed-aperture pattern of GO and rGO.

where r_{a} is the aperture and ω is the beam radius at the aperture. The non-linear refractive index is given by

$$n_2 = \frac{\Delta \phi}{K I_0 L_{eff}}$$

where, $K = 2\pi/\lambda$ (λ is the laser wavelength), I_0 is the intensity of the laser beam at the focus (Z = 0) and $L_{eff} = (1 - exp(-\alpha L)/\alpha)$ is the effective length of the sample.

The nonlinear absorption (β) coefficient was also estimated from the original valley value (ΔT) at the experimental open aperture Z-scan curve as

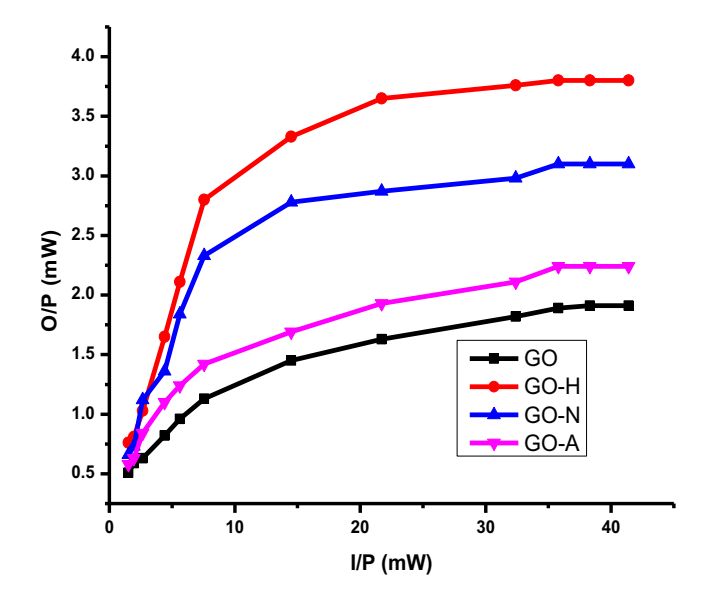


Fig. 9. Optical limiting pattern of GO and rGO.

$$\beta = \frac{2\sqrt{2}\Delta T}{IL_{eff}}$$

The saturation intensity ($I_s = \alpha_o/\beta$) is defined as the ratio between linear absorption co-efficient and nonlinear absorption co-efficient [28]. The estimated I_s for all the samples was found to be 3.7 kW/cm². The real and imaginary parts of the third order nonlinear optical susceptibility $\chi^{(3)}$ are defined as [29,30]

$$Re\chi^{(3)} = \frac{10^{-4}(\epsilon_0 C^2 n_0^2 n_2)}{\pi} (cm^2/W)$$

$$Im \chi^{(3)} = \frac{10^{-2} (\epsilon_0 C^2 n_0^2 \lambda \beta)}{4 \pi^2} (cm/W)$$

where ε_0 is the permittivity of vacuum, n_0 is the linear refractive index of the sample and c is the velocity of light in vacuum. The third order nonlinear optical susceptibility is thus

$$\chi^{(3)} = \sqrt{\left(Re(\chi^{(3)})\right)^2 + \left(Im(\chi^{(3)})\right)^2}$$

The estimated NLO coefficients are given in Table 2 and it can be clearly seen that rGO possess stronger NLO behavior than GO. In both cases, the nonlinear absorption was found to be more dominant than nonlinear refraction process and thus $\text{Im}(\chi^3)$ was found to be higher than $\text{Re}(\chi^3)$ of nonlinear optical susceptibility. Also it can be seen that the NLO coefficient was found to be varying for rGO with respect to the reducing agent use. Tunability of NLO coefficient was confirmed and the order of preference for higher nonlinearity is rGO-H > rGO-N > rGO-A > GO. The variation in thermal nonlinearity mainly arises due to the variation in extent of conjugation which depends upon the functional groups on the graphene

surface. Also it can be related to the variation in I_D/I_G ratio, La and interplannar distance of the samples. In the present case, ascorbic acid being a mild reducing agent provides rGO with most of the functional groups as present in GO. So the estimated NLO coefficients of rGO-A posses almost equivalent values as that of GO. As sodium borohydride has removed few functional groups, the extent of conjugation was better than GO and rGO-A and hence possess slightly higher values. In particular rGO-H was found to possess higher nonlinear refractive index (2.7 times) and third order NLO susceptibility (1.7 times) than GO. It is to be noted that, hydrazine is a strong reducing agent and hence removes most of functional groups available in GO. Thus the obtained structure of rGO almost resembles the layered structure of graphene. Hence the rGO-H has higher delocalization and thermal phonon transfer than other rGO's prepared and thus it has comparably higher value than other systems. This is because hydrazine has effectively reduced most of the functional groups and the obtained rGO was almost similar to graphene structure, having the maximum extent of conjugation. This planar layered structure provides the enhanced thermal transport which resulted in the increase of NLO coefficient. Also as discussed in the Raman analysis, rGO-H has the dominant sp² domain which resulted in higher delocalization of π -conjugation. The detailed mechanism needs further investigation, but the current work demonstrates that the optical transmittance and limiting properties are a sensitive function of the oxygen functional groups and structural defects in graphene. Here it should be noted that the estimated nonlinear absorption coefficient of rGO is found to higher than other known systems [11] as thermal (Kerr) component contributes under CW excitation. Since Z-scan experiment is very sensitive to excitation parameters, direct comparison with known materials is not viable in the present case. The nonlinear absorption coefficient of the reduced GO materials under CW excitation (532 nm, 50 mW) was found to be very higher than other graphene composite like GO $(5.4 \times 10^{-4} \text{ cm/W})$, and tetra amino porphyrin with GO $(13.1 \times 10^{-4} \text{ cm/W})$ [31]. The rGO-H show higher nonlinear absorption coefficient, nonlinear refractive index and third order nonlinear optical susceptibility than other samples suggesting the good optical limiting applications. Thus it can be concluded that rGO prepared using hydrazine with linear transmittance and nonlinear optical coefficients can be a potential candidate for optical limiting applications against continuous wave lasers.

4. Conclusion

By simple reduction process, reduced graphene oxide was prepared using different reducing agents like hydrazine, sodium borohydride and ascorbic acid. In the XRD pattern of rGO, the major peak (12°, (001)) of GO disappeared completely, giving preliminary confirmation of reduction process. FTIR showed that different reducing agents have resulted in the elimination of various functional groups (ascorbic: carbonyl, sodium borohydride: carboxyl and carbonyl and hydrazine: carboxyl, carbonyl, epoxy, alkoxy) and thus forming rGOs with different functional groups on the sur-

Table 2Third Order NLO Parameters of the samples.

Parameters	GO	rGO-H	rGO-N	rGO-A
Nonlinear refractive index $(n_2) \times 10^{-8} \text{ cm}^2/\text{W}$	1.61	4.47	4.37	2.67
Nonlinear absorption coefficient($\beta \times 10^{-3}$) cm/W	5.86	6.02	5.90	5.88
Real part of the third-order susceptibility $[Re(\chi^3)] \times 10^{-6}$ esu	1.08	3.01	2.95	1.80
Imaginary part of the third-order susceptibility $[Im(\chi^3)] \times 10^{-6}$ esu	1.68	1.69	1.72	1.68
Third-order nonlinear optical susceptibility $(\chi^3) \times 10^{-6}$ esu	2.00	3.45	3.41	2.46
Optical limiting threshold	14.46	14.46	14.46	14.46
[Limiting amplitude] mW	(1.43)	(3.35)	(2.77)	(1.70)

face of graphene. A decrease in the lower size and a higher defect density of in-plane graphitic crystallite sp² domains due to reduction of GO was confirmed through Raman analysis. The reduced GO material consists of randomly aggregated, thin crumpled sheets closely associated with each other and forming disordered sheets. GO exhibits a π - π * absorption band at 234 nm and reduced graphene oxide (rGO-H, rGO-N and rGO-A), suffers a blue shift in absorption peak due to the decrease in functional groups and weak interlayer coupling between the layers. Z-scan experiment showed that both GO and rGO possess negative nonlinear refraction (self defocusing) and negative nonlinear (saturable) absorption. The observed nonlinearity was found to be thermo-optic in origin. Tunability of NLO coefficient was confirmed and the order of preference for higher nonlinearity is rGO-H > rGO-N > rGO-A > GO. The variation in thermal nonlinearity mainly arises due to the variation in extent of conjugation which depends upon the functional groups on the graphene surface. Also it can be related to the variation in I_D/I_C ratio, La and interplannar distance of the samples. The limiting threshold of all samples was found to be 14.46 mW, with appreciable change in the limiting amplitude (1.43-3.35 mW). Thus it can be concluded that rGO prepared using hydrazine with higher linear transmittance, nonlinear absorption coefficient, nonlinear refractive index and third order nonlinear optical susceptibility can be a potential candidate for optical limiting applications against continuous wave lasers.

References

- Kaladevi Sendhil, C. Vijayan, M.P. Kothiyal, Opt. Laser Technol. 38 (2006) 512– 515.
- [2] B. Kulyk, S. Taboukhat, H. Akdas-Kilig, J.L. Fillaut, Y. Boughaleb, B. Sahraoui, RSC Adv. 6 (2016) 84854–84859.
- [3] I. Fuks-Janczarek, J.M. Nunzi, B. Sahraoui, I.V. Kityk, J. Berdowski, A.M. Caminade, J. Roncali, Opt. Commun. 209 (2002) 461–466.
- [4] B. Sahraoui, J. Luc, A. Meghea, R. Czaplicki, J.L. Fillaut, A.J. Migalska-Zalas, Optics A: Pure Appl. Optics 11 (2009) 024005.
- [5] B. Sahraoui, G. Rivoire, N. Terkia-Derdra, M. Salle, J. Zaremba, JOSA B 15 (1998) 923–928.
- [6] L.W. Tutt, A. Kost, Nature 356 (1992) 225-226.

- [7] Chunying He, Wubiao Duan, Guang Shi, Yiqun Wu, Qiuyun Ouyang, Yinglin Song, Appl. Sur. Sci. 255 (2009) 4696–4701.
- [8] Y.P. Sun, J.E. Riggs, H.W. Rollins, R. Guduru, J. Phys. Chem. B 103 (1999) 77–82.
- [9] L.W. Tutt, T.F. Boggess, Prog. Quan. Elect. 17 (1993) 299–338.
- [10] Q.D. Zheng, S.K. Gupta, G.S. He, L.S. Tan, P.N. Prasad, Adv. Funct. Mater. 18 (2008) 2770–2779.
- [11] Konstantinos Iliopoulos, Abdelkrim El-Ghayoury, Hasnaa El Ouazzani, Mindaugas Pranaitis, Esmah Belhadj, Emilie Ripaud, Miloud Mazari, Marc Sallé, Denis Gindre, Bouchta Sahraoui, Opt. Express 20 (2012) 25311–25316.
- [12] Haijun Zeng, Junhe Han, Dongjin Qian, Gu Yuzong, Optik 125 (2014) 6558-6561.
- [13] Panit Chantharasupawong, Reji Philip, Narayanan T. Narayanan, Parambath M. Sudeep, Akshay Mathkar, Pulickel M. Ajayan, Jayan Thomas 116 (2012) 25955– 25961
- [14] Xiao-Liang Zhang, Zhi-Bo Liu, Xiao-Chun Li, Qiang Ma, Xu-Dong Chen, Jian-Guo Tian, Xu Yan-Fei, Yong-Sheng Chen, Opt. Express 21 (2013) 7511–7520.
- [15] L. Shahriary, A.A. Athawale, IJREEE 2 (2014) 58–63.
- [16] Hongtao Liu, Lei Zhang, Yunlong Guo, Cheng Cheng, Lianjiang Yang, Lang Jiang, Yu Gui, Hu Wenping, Yunqi Liu, Daoben Zhu, J. Mater. Chem. C 1 (2013) 3104.
- [17] Yanwu. Zhu, Weiwei. Cai, Richard D. Piner, Aruna. Velamakanni, Rodney S. Ruoff, Appl. Phys. Lett. 95 (2009) 103104.
- [18] H.-J. Shin, K.K. Kim, A. Benayad, S.-M. Yoon, H.K. Park, I.-S. Jung, Adv. Funct. Mater. 19 (2009) 1987–1992.
- [19] Xu. Zhu, Qin Liu, Xiaohua Zhu, Chunlan Li, Xu Maotian, Yong Liang, Int. J. Electrochem. Sci. 7 (2012) 5172–5184.
- [20] G. Wang, J. Yang, J. Park, X. Gou, B. Wang, H. Liu, et al., J. Phys. Chem. C 112 (2008) 8192–8195.
- [21] M.J. Fernández-Merino, L. Guardia, J.I. Paredes, S. Villar-Rodil, P. Solís-Fernández, A. Martínez-Alonso, J.M.D.J. Tascón, Phy. Chem. C 114 (2010) 6426–6422
- [22] X. Fan, W. Peng, Y. Li, X. Li, S. Wang, G. Zhang, et al., Adv. Mater. 20 (2008)
- [23] X. Zhou, J. Zhang, H. Wu, H. Yang, J. Zhang, S. Guo, J. Phys. Chem. C 115 (2011) 11957–11961.
- [24] W.S. Hummers Jr, R.E.J. Offeman, Am. Chem. Soc. 80 (1958), 1339-1339.
- [25] A. Wang, W. Yu, Y. Fang, Y. Song, D. Jia, L. Long, C. Zhang, Carbon 89 (2015) 130–141.
- [26] M. Saravanan, T.C. Sabari Girisun, G. Vinitha, J. Mater. Sci. 51 (2016) 3289–3296.
- [27] T.C. Sabari Girisun, S. Dhanuskodi, Chem. Phys. Lett. 491 (2010) 248-253.
- [28] R.A. Ganeev, A.I. Ryasnyansky, A.L. Stepanov, T. Usmanov, Opt. Quantum. Electron. 36 (2004) 949–960.
- [29] R.L. Sutherland, Handbook of Nonlinear Optics, 2nd ed., Marcel Dekker, NewYork, 2003.
- [30] S. Valligatla, K.K. Haldar, A. Patra, N.R. Desai, Optics Laser Technol. 84 (2016) 87–93.
- [31] R. Yamuna, S. Ramakrishnan, K. Dhara, R. Devi, N.K. Kothurkar, E. Kirubha, P.K. Palanisamy, J. Nanopart. Res. 15 (2013) 1–9.



Contents lists available at ScienceDirect

Optical Materials

journal homepage: www.elsevier.com/locate/optmat



Barium borate nanorod decorated reduced graphene oxide for optical power limiting applications



G. Muruganandi ^a, M. Saravanan ^b, G. Vinitha ^c, M.B. Jessie Raj ^a, T.C. Sabari Girisun ^{b,*}

- ^a Department of Physics, Bishop Heber College (Autonomous), Tiruchirappalli 620 017, India
- ^b Nanophotonics Laboratory, School of Physics, Bharathidasan University, Tiruchirappalli 620 024, India
- ^c Division of Physics, School of Advanced Sciences, VIT Chennai, Chennai 600 127, Tamilnadu, India

ARTICLE INFO

Article history: Received 8 October 2017 Received in revised form 7 November 2017 Accepted 10 November 2017

Keywords:
Decorated rGO
Third-order nonlinearity
Z-scan
Self-defocusing

ABSTRACT

By simple hydrothermal method, nanorods of barium boate were successfully loaded on reduced graphene oxide sheets. Powder XRD confirms the incorporation of barium borate ($2\theta = 29^{\circ}$, (202)) along with the transition of graphene oxide ($2\theta=12^{\circ}$, (001)) into reduced graphene oxide ($2\theta=25^{\circ}$, (002)). In the FTIR spectra, presence of characteristic absorption peaks of rGO (1572 and 2928 $\,\mathrm{cm}^{-1}$) and barium borate (510, 760 and 856 cm⁻¹) further evidences the formation of BBO:rGO nanocomposite. FESEM images potray the existence of graphene sheets as thin layers and growth of barium borate as nanorods on the sheets of reduced graphene oxide. Ground state absorption studies reveal the hypsochromic shift in the absorption maxima of the graphene layers due to reduction of graphene oxide and hypochromic shift in the absorbance intensity due to the inclusion of highly transparent barium bortae. The photoluminescence of BBO:rGO shows maximum emission in the UV region arising from the direct transitions involving the valence band and conduction band in the band gap region. Z-scan technique using CW diode pumped Nd:YAG laser (532 nm, 50 mW) exposes that both nanocomposite and individual counterpart possess saturable absorption and self-defocusing behavior. Third-order nonlinear optical coefficients of BBO:rGO nanocomposite is found to be higher than bare graphene oxide. In particular the nonlinear refractive index of nanocomposite is almost four times higher than GO which resulted in superior optical power limiting action. Strong nonlinear refraction (self-defocusing) and lower onset limiting thershold makes the BBO:rGO nanocomposite preferable candidate for laser safety devices.

© 2017 Elsevier B.V. All rights reserved.

1. Introduction

The major concerns of the electro-optical sensors that are widely used in laser applications are its susceptible to overexposure leading to permanent optical damage. Since the invention of laser in 1960, the protection of human eyes and sensors against intended or unintended damage by laser radiation has been an ongoing research field. Laser protection measures are typically realized using conventional optical filters based on linear absorption or interference effects. Unfortunately, these filters work only for predefined wavelength, but not beyond [1]. So a laser beam of high intensity can easily damage the retina and hence significant research effort has been invested on optical power limiting (OL) materials to achieve some measure of protection from such high

intense laser beams. An efficient optical limiting material exhibits high transmittance for low intensity ambient light, while strongly attenuating intense and potentially dangerous laser beams [2]. Layer structured carbonaceous materials like graphene oxide (GO) stand high in this domain due to their stronger nonlinear optical response. However the basic requirement of high linear transmittance limits the possible usage as power limiter. Improvement of linear transmittance along with enhanced nonlinear action can be achieved through nanocomposite formation. The availability of several types of oxygen-containing functional groups on the basal plane (epoxide groups) and the sheet edge (ketone groups) allows GO to interact with a wide range of inorganic materials so that functional hybrids and composites with unusual properties can be readily synthesized. In the choice of inorganic materials, barium borate (BBO) nanostructures can be an interesting candidate as it possesses have unique characteristics like wide transparency, large birefringence, high laser damage threshold and excellent mechanical properties. In the wide variety of morphologies, 1D

^{*} Corresponding author.

E-mail address: sabarigirisun@bdu.ac.in (T.C. Sabari Girisun).

nanostructures provides an opportunity to understand both functional behavior in ultra low dimension and to develop high performance next generation devices. Efficient transport of optical excitations due to two dimensional confinements arising from intrinsic anisotropic nature also makes fabrication of 1D nanostructures promising route [3.4]. The origin of large nonlinear optical susceptibility in BBO arises from the anionic structural units and as boron atoms has two kind of co-ordination, a boron atom coordinate with three oxygen atom to form triangle [BO₃] unit and with four oxygen atom to form tetrahedral [BO₄] unit. The network of interconnected [BO₃] and [BO₄] forms infinite chains of [B₃O₆], [B₃O₃] anionic groups whose negative charge is compensated by the Ba²⁺ cations and hence resulting in diversity of structures. Hence most of research is focused on β-BBO nanostructures and reports show that nanorods, nanoplatelets and network like structures of β-BBO exhibits higher SHG performance than bulk form. Also γ-BBO (rich in BO₃ unit) nanostructure exhibited higher third order nonlinearities in the continuous wave (CW) regime demonstrating maximum thermal stability against intense laser radiations among the known NLO materials and hence rendering them ideal for optical limiting applications [5]. Based on these facts, this article reports the optical limiting performance of γ -BBO nanorod decorated rGO with CW laser pulses at a wavelength of 532 nm. It is found that BBO: rGO nanocomposite possesses stronger nonlinear refraction which are beneficial for power limiting applications.

2. Material preparation

Hydrothermal method is an elegant technique to prepare and incorporate barium borate upon graphene sheets. Preparation of barium borate: reduced graphene oxide nanocomposite involves a three step process. In the first step, graphene oxide (GO) was prepared from graphene flakes by Modified Hummer's method [6]. In the second step, the obtained GO was reduced to reduced graphene oxide (rGO) by using ascorbic acid as reducing agent [7]. In the third step of employed experimental procedure, 10 mmol of BaCl₂·2H₂O, 15 mmol of H₃BO₃ and 20 mmol of NaOH were dissolved in 60 ml distilled water and used as starting precursor to obtain barium boate [5]. To the above mentioned solution, 20 mg of rGO was added and continuously stirred for 8 h to attain homogenous mixing. The solution was then transformed to 100 ml autoclave setup and placed in an oven at 120 °C for 24 h. The obtained slurry was washed with water and ethanol for several times to remove the suspended impurities and other byproducts. Finally the obtained powder was dried at 60 °C for 12 h resulting in the formation of ash colored powder. In each step, the obtained powders were taken out and indexed as GO, rGO and BBO: rGO for further characterization.

3. Structural confirmation

The prepared samples were subjected to powder X-ray diffraction using CuK α radiation (1.54 Å) in the angle of $10^\circ-80^\circ$. Fig. 1 shows the recorded XRD patterns of GO, rGO and BBO: rGO. The characteristic peak (001) observed at $2\theta=12^\circ$ confirms the formation of graphene oxide in the modified Hummer's method. After reduction process no diffraction peaks of GO is observed and the presence of diffraction peak at $2\theta=12^\circ$ signatures the formation of rGO. Recorded XRD pattern of BBO: rGO forecast the diffraction peaks of both rGO with BBO and thus confirms the formation of nanocomposite. All the additional peaks were indexed and are found to be consistent with the values in the standard card of γ -BBO [JCPDS: 01-071-2501]. The peak at $2\theta=24^\circ$, 26° , 29° , 32° , 34° , 40° , 42° , 47° , 53° , 61° and 68° represents planes (1 1 2), (0 2 1), (2 1 1), (1 0 4), (0 2 3), (0 1 5), (3 1 2), (3 1 3), (3 2 3), (2 17) and (4 2 4) of

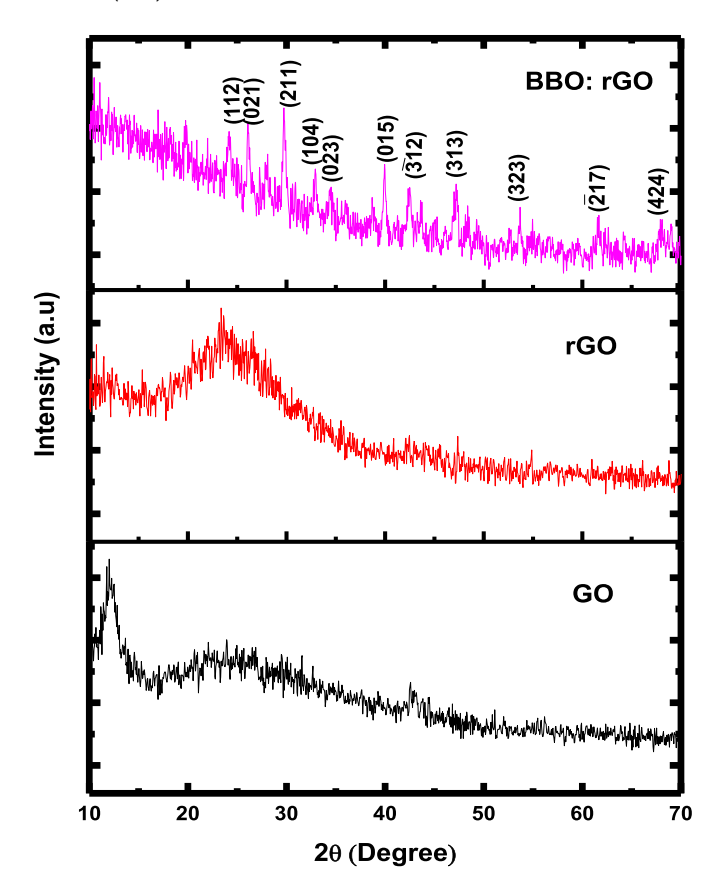


Fig. 1. XRD pattern of GO, rGO and BBO: rGO.

barium borate and thus formation of BBO:rGO nanocomposite is confirmed. As the samples were prepared at low temperature (120 °C), γ -BBO was obtained and thus expected to attain higher third-order NLO co-efficient [5]. The widths of the reflection peaks are considerably broadened, indicating the crystalline particles fall in the nanoscale range [8]. The average grain size of BBO:rGO composite is deliberated to be 17 nm from the Debye–Scherrer equation. No characteristic peaks that correspond to the possible byproducts and other impurities are identified.

IR spectra were recorded with JASCO 460 PLUS FTIR spectrometer in the range of 400-4000 cm⁻¹ with spectral resolution of 1 cm⁻¹ to identify various functional groups and the available molecular vibration of the samples. The recorded FTIR spectra of the samples (Fig. 2) show strong absorption peaks which corresponds to the various vibrational modes of GO and BBO (Table 1). It is interesting to note that the in the modified Hummer's method, graphene sheets were successfully incorporated with various oxygen containing functional groups such as aromatic hydrocarbons (2825 cm⁻¹), hydroxyl (3442 cm⁻¹), carboxyl (2324 cm⁻¹), carbonyl (1738 cm⁻¹), epoxyl (1243 cm⁻¹) and alkoxy (1207 cm⁻¹) groups. Ascorbic acid being a mild reducing agent removes carboxyl groups during reduction and leaves most of the functional groups in the graphene sheets. It is interesting to note that, during incorporation of BBO upon graphene layers, some of the functional groups (namely carboxyl and epoxy) were effectively removed. Also in the FTIR spectrum of BBO: rGO, the additional absorption peaks at 510 and 760 cm⁻¹ corresponds to the bending vibrations of B-O-B bond [9] and peak at 856 cm⁻¹ is due to stretching vibration of B–O bond in BO₃ unit [5] of barium borate (γ -BBO), by which the formation of BBO: rGO composite is confirmed.

Morphologies of the samples were investigated by Field

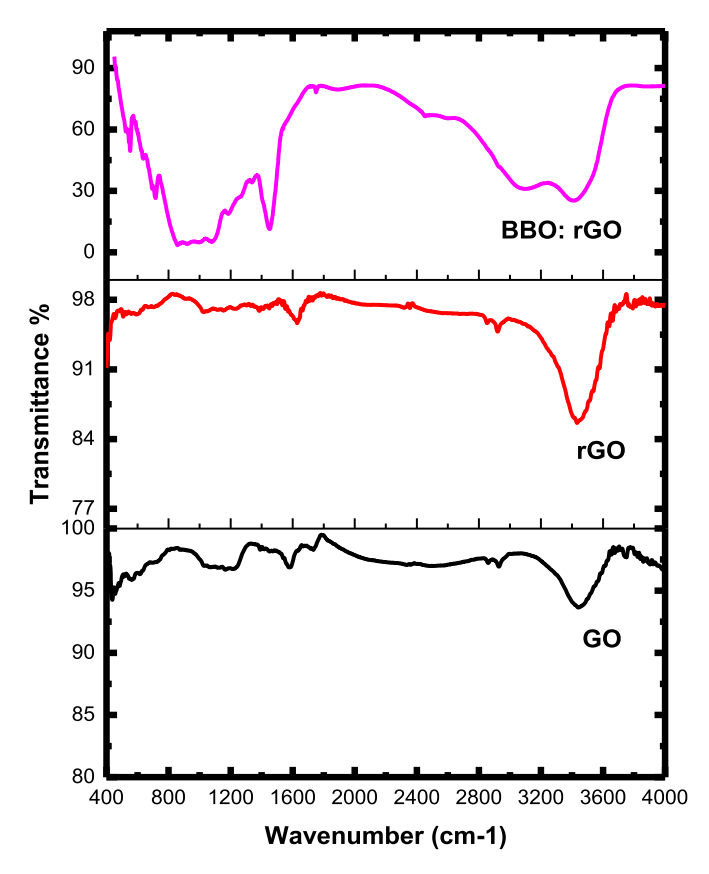


Fig. 2. FTIR pattern of GO, rGO and BBO: rGO.

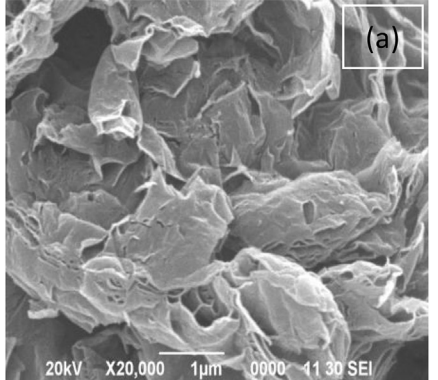
Emission Scanning Electron Microscope (FEI-QUANTA-FEG 250). FESEM images (Fig. 3) show the panoramic morphology of the products. Fig. 3 (a) shows the presence of graphene layers as thin crumpled sheets and here the observed folding are due to the harsh oxidation taken place during the employed Hummer's process. Compared to the GO image, rGO (Fig. 3b) shows less agglomeration and individual sheets are easily identifiable. This clearly demonstrates the reduction of graphene oxide upon ascorbic acid interaction. From the FESEM image of BBO: rGO composite (Fig. 3c), BBO nanorods are grown randomly on the surface of rGO sheets. These nanorods have a good uniform diameter of 22 nm and 3.0 µm length. The possible growth mechanism can be explained as follows: During the third step of hydrothermal process, Ba²⁺ sticks on the surface of graphene layers and forms as barium borate. These BBO acts as nucleation sites and grow as elongated nanorod upon the graphene layers. Similar formation of pure γ -BBO nanorods due to prolonged heating (120 °C, 24 h), was already reported [5,10]. Compared to the earlier report, length of BBO nanorod is well increased (1.2 μ m-3 μ m) along with considerable reduction in diameter (354 nm-22 nm). This might be due to the availability of graphene surface which promotes aggregation of nanoclusters (alignment of same type of crystal planes to minimize the interface stain energy) along a particular direction to form rod like structure. As hydrothermal technique cannot control the content of loading, barium borate nanorods appears to be clusters. Thus the morphological analysis clearly pictures that barium borate nanorods are randomly arranged on the layers of reduced graphene oxide.

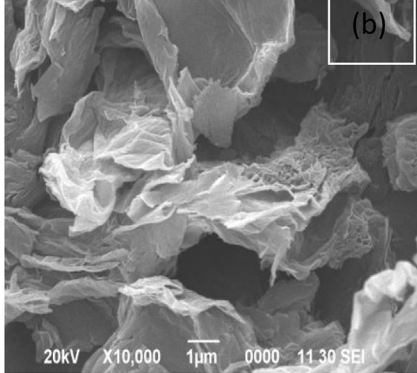
4. Linear absorption and emission properties

Linear optical properties of the samples were investigated by

Table 1Vibrational assignments of GO, rGO and BBO: rGO.

Peak assignments	Peak Positions (cm ⁻¹)		
	GO	rGO	BBO:rGO
C=C stretching (sp ² hybridized)	1572	1655	1572
C-H stretching (aromatic hydrocarbons and C-OH stretching)	2925	2925	2928
O–H stretching (hydroxyl groups)	3442	3406	3438
C=O stretching (carboxyl groups)	2324	2325	_
C=O stretching (carbonyl groups)	1738	_	_
C—O stretching (epoxyl groups)	1243	1381	_
C—O stretching (alkoxy groups)	1207	1028	1207
B-O-B bond	_	_	760 and 510
B–O bond in BO ₃ unit	_	_	856





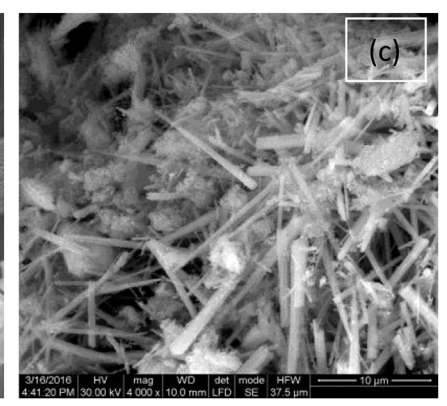


Fig. 3. FESEM images of (a) GO, (b) rGO and (c) BBO: rGO.

UV-Vis-NIR (JASCO Corp., V-570) spectroscopy in the range 190-1100 nm with spectral resolution of 1 nm. The maximum absorption peak of GO, rGO and BBO: rGO are observed at 236 nm, 210 nm and 207 nm respectively. The maximum absorption peak corresponds to the π - π * transition of aromatic C=C bond [11]. Interestingly, shifting in the absorption peak of GO and rGO (263 nm-210 nm) occurs due to the decrease in functional groups and weak interlayer coupling between the layers causes electrons to easily excite at lower energy. Similar blue shift in the absorption maxima (207 nm) of BBO: rGO arises from the restored electronic conjugation within the sheets due to reduction and inclusion of barium borate. It is also to be noted that the contribution of anharmonic phonons has to be considered for two-dimensional thin crystals with honey comb lattice structure like graphene at high temperature. Under high density (laser) photo-excitation, the local heating raises the temperature of the material and anharmonic phonon contributes to optical properties and thermal transport properties of the materials [12,13]. Among the inorganic NLO material, barium borate possess low cutoff in the UV region (below 200 nm) and hence the observed maxima is the characteristic peak of graphene sheets. In Fig. 4, the absorbance of BBO: rGO composite is found to be very lower throughout the visible region when compared with pure GO and rGO. This hypochromic shift in the absorbance intensity of BBO: rGO clearly shows that the high linear transmittance (transparent properties) of composite arises from the contribution of highly transparent barium borate [5,14]. For laser safety applications like protection of optical sensors from laser induced damage it is desirable for an optical limiter to have high linear transmittance at low intensity (obeying Beer's law) and should turn opaque at high intensity (which can harm the photosensitive components). Thus the composite fulfills the essential requirement for optical limiter i.e., high linear transmittance.

Emission studies were carried out by Fluoromax 4 spectrophotometer under the excitation of 325 nm wavelength scanned over the domain 350–650 nm with spectral resolution of 1 nm. Under the exposure of 325 nm light, GO exhibits a blue luminescence at

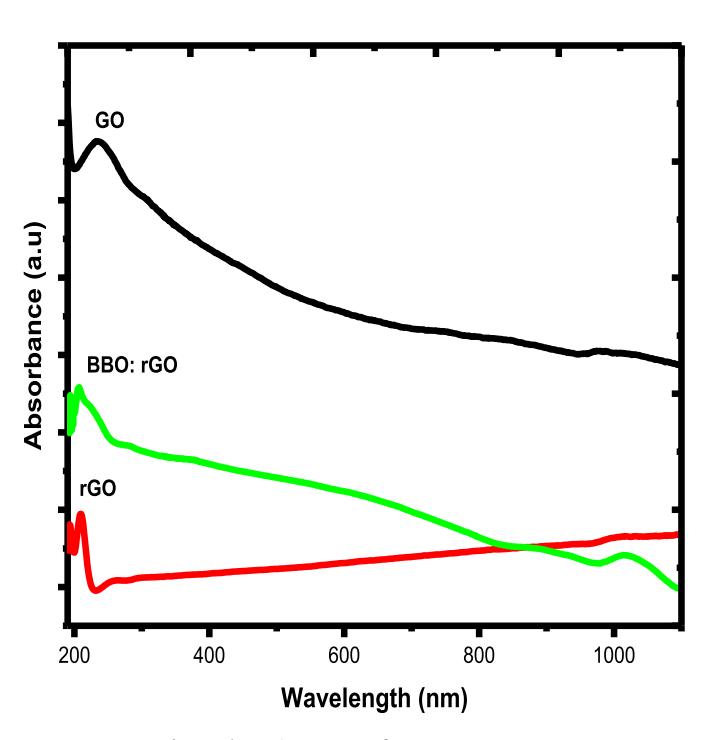


Fig. 4. Absorption spectra of GO, rGO, BBO: rGO.

360 nm (Fig. 5) due to isolated sp² domains generated by oxidation process. Here the epoxide groups on basal plane and carboxylic groups at GO edge often induce non-radiative recombination of localized electron-hole pairs, leading to very weak emission. Hence upon reduction of functional groups, rGO showed a bright blue emission at 360 nm. Also because of deoxygenation, there is a considerable decrease in disorder induced states within π - π^* gap. The electron hole recombination among the sp² clusters which lie within the σ - σ * states of sp³ matrix acts as localized luminescence states exhibit blue emission (493 nm) [15,16]. In the PL spectrum of BBO:rGO, the characteristic peak of graphene is slightly red shifted to 370 nm (sp² domains of rGO) due to incorporation of barium borate. Additional peak at 350 nm arises due to the radiative annihilation of self trapped exciton localized in the crystal defects of barium borate [5]. Thus incorporation of barium borate in rGO sheets and alteration in the electronic states due to these interactions is confirmed from the emission studies.

5. Third order nonlinear optical refraction and absorption

Z-scan technique is a single beam method for measuring the sign and magnitude of nonlinear absorption and refraction coefficients simultaneously. This technique uses single laser beam in tight focus geometry. The transmittance of a nonlinear medium through a finite aperture is measured in the far field as a function of the sample position 'Z' referenced with respect to the focal plane. Nonlinear absorption and nonlinear refraction can be measured all together when an aperture is placed in front of the detector (closed aperture). Nonlinear absorption is detected when the aperture is absent (open aperture). The third-order nonlinear optical

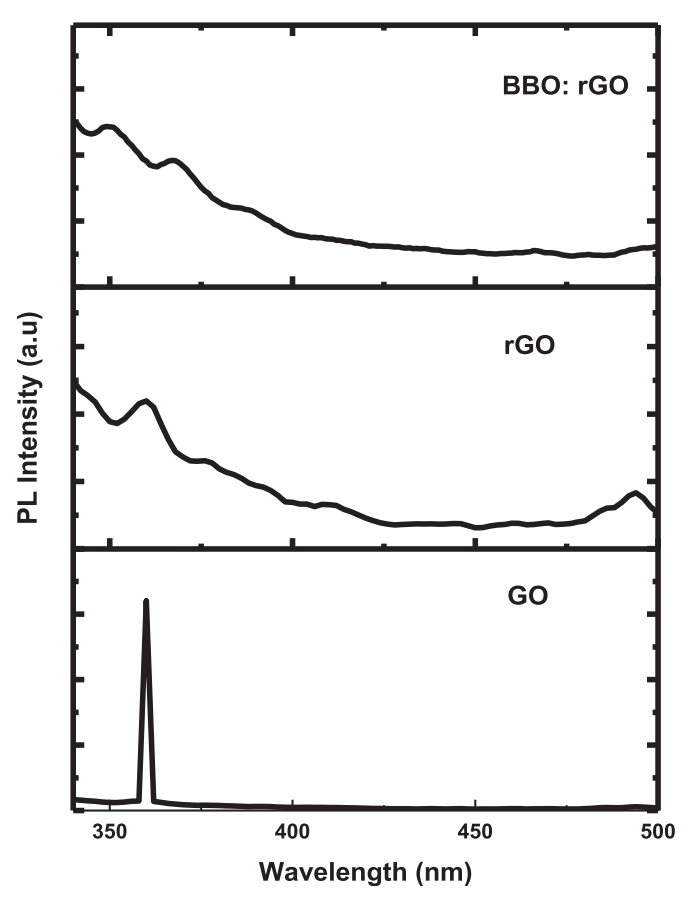


Fig. 5. Emission spectra of GO, rGO, BBO: rGO.

properties of the samples, dispersed in ethylene glycol by ultrasonication were studied by closed and open Z-scan technique. The sample cell was moved using a translation system along the propagation direction (Z-axis) of a focused Gaussian beam through its focal plane. By moving the sample through the focus, the intensity-dependent nonlinear refraction and absorption can be measured from the changes of the transmittance through the sample. Under similar Z-scan geometry, the optical limiting behavior of the samples was also investigated [17].

Fig. 5 shows the closed aperture pattern of GO, rGO and BBO: rGO composite. In the obtained closed aperture curves, the peak precedes the valley indicating a negative variation of the nonlinear index (n_2) arising due to self-defocusing mechanism. The observed nonlinearity is of thermal in origin, as the materials were excited with continuous wave laser. Here the laser heating induced thermal nonlinearity which arises from the absorption of a tightly focused beam. This produces a spatial distribution of temperature and refractive index creating a thermal lens resulting in severe phase distortion of the propagating beam. Although all the samples exhibit self-defocusing behavior, the peak-valley difference and width of the pattern is not uniform. BBO:rGO possess broader peakvalley pattern with maximum peak-valley difference confirming the enhanced nonlinear refraction. Fig. 6 shows the open aperture pattern of GO, rGO, BBO: rGO composite. In the pattern the maximum lies near the focus (Z = 0) and hence exhibit nonlinear absorption. The peak pattern clearly reveals the presence of saturable absorption property, where the absorption of light decreases with increasing light intensity. At sufficiently high incident light intensity, atoms in the ground state get excited to higher state at such a rate that there is insufficient time to decay back to the ground state before the ground state becomes depleted and hence absorption gets subsequently saturated. As in the case of nonlinear refraction, the strength of nonlinear absorption (peak position, ΔT) varies with sample and BBO: rGO possess stronger nonlinear absorption.

Earlier the obtained experimental data is fitted with the theoretical normalized equation as proposed by Sheik Bahae [18,19].

$$TN = 1 + \Delta \phi \frac{4x}{(1+x^2)(9+x^2)} \tag{1}$$

$$T[Z, S = 1] = \sum_{m=0}^{\infty} \left[\frac{(-q_0(z, 0))^m}{(m+1)^{\frac{3}{2}}} \right]$$
 (2)

In Figs. 5 and 6, the solid line represents the theoretical fit and dotted symbols represent the experimental data. As seen the fit matches well with experimental data ensuring the reliability of

measured normalized transmittance. From the peak-valley difference (ΔT_{p-v}) of closed aperture and peak value (ΔT_p) of open aperture, the nonlinear refractive index and nonlinear absorption coefficient of the material is estimated using the relations [20,21].

$$n_2 = \frac{|\Delta \varphi|}{KI_0L_{eff}} \tag{3}$$

$$\beta = \frac{2\sqrt{2}\Delta T}{I_0 L_{eff}} \tag{4}$$

where $k=2\pi/\lambda$ (λ is the wavelength of laser), I_0 is the intensity of the laser beam at the focus (z=0), $L_{eff}=\frac{[1-exp(-\alpha L)]}{\alpha}$ is the effective thickness of the sample, α is the linear absorption and L is the thickness of the sample, ΔT is the one valley value at the open aperture Z-scan curve and I_0 is calculated to be 4.38 kW/cm².

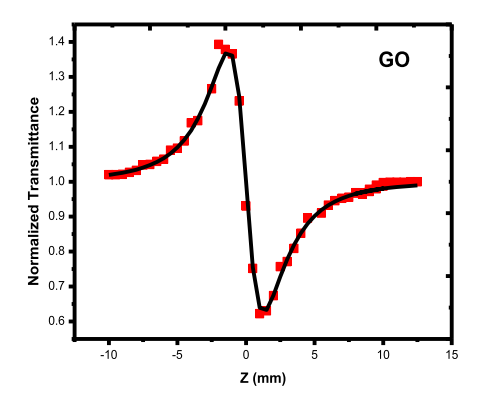
From the estimated nonlinear absorption coefficient and nonlinear refractive, third-order NLO susceptibility is calculated as [22].

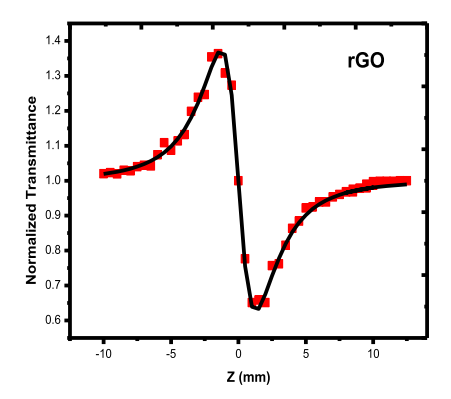
Re
$$\chi^{(3)} = \frac{10^{-4} C^2 n_0^2 n_2 \varepsilon_0}{\pi}$$
 (esu) (5)

Im
$$\chi^{(3)} = \frac{10^{-2}C^2 n_0^2 \beta \lambda \varepsilon_0}{4\pi^2}$$
 (esu) (6)

$$\chi^3 = \sqrt{\left[\text{Re }\chi^3\right]^2 + \left[\text{Im }\chi^3\right]^2} \tag{7}$$

The estimated third-order NLO co-efficient of the samples are summarized in Table 2. As photoexcitation is made under CW mode, thermal nonlinearity is found to be more dominant and the contribution due to electronic effects is negligibly small. It is interesting to observe that, all samples exhibit strong nonlinear refraction than nonlinear absorption. This is evident from the fact that imaginary part of third-order NLO susceptibility is greater than real part of third-order NLO susceptibility. As Kerr component contributes much to the observed nonlinearity, molecular and textural arrangements play a dominant role in deciding the strength of nonlinearity. Here the removal of functional groups upon reduction, incorporation of barium borate and morphology of inorganic species contributes to the enhanced Kerr nonlinearity of the composite. Especially nonlinear refraction drastically varies, as the nonlinear refractive index of created thermal lens strongly relies on the potential to create the spatial variation in temperature and density. As expected the combination of BBO and rGO has yielded composite system that possesses the advantage of both elements leading to enhanced third-order nonlinearity. It is to be





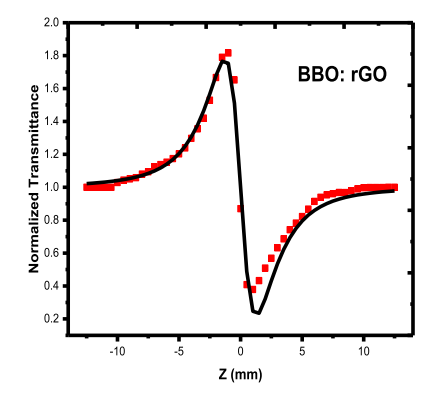
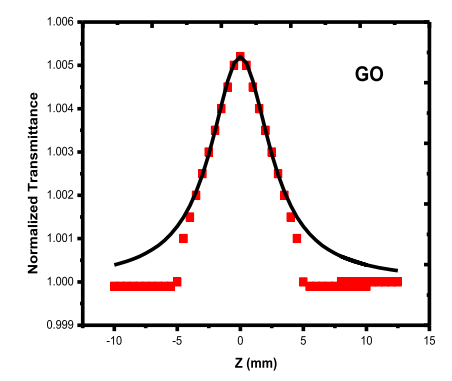
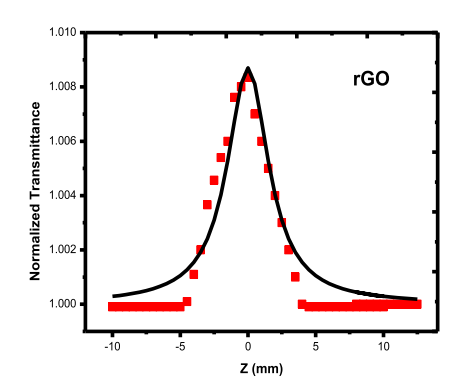


Fig. 6. Closed aperture pattern of GO, rGO, BBO: rGO.

Table 2Third-order NLO coefficients of bare and composite of BBO: rGO.

Parameters	GO	rGO	γ-BBO [5]	BBO:rGO
Nonlinear refractive index (n ₂) 10 ⁻⁸ cm ² W ⁻¹	1.59	2.62	$8.3 \times 10^{-12} \text{ m}^2\text{W}^{-1}$	6.26
Nonlinear absorption coefficient (β) 10^{-3} cmW ⁻¹	5.86	5.88	$8.8 \times 10^{-5} \ mW^{-1}$	6.05
Real part of $\chi^{(3)}$ (10 ⁻⁶ esu)	0.76	1.32	_	4.48
Imaginary part of $\chi^{(3)}$ (10 ⁻⁶ esu)	1.20	1.25	_	1.83
Third order nonlinear susceptibility $\chi^{(3)}$ (10 ⁻⁶ esu)	1.42	1.82	$4.34 \times 10^{-6} \text{ esu}$	4.84
Limiting threshold (mW)	14.59	14.59	32.6	9.51
Clamping value (mW)	1.91	2.23	850 μW	6.23





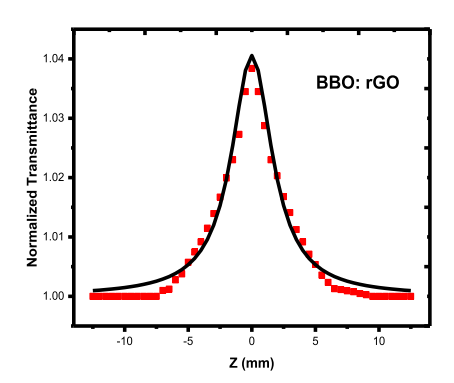


Fig. 7. Open aperture patterns of GO, rGO, BBO: rGO.

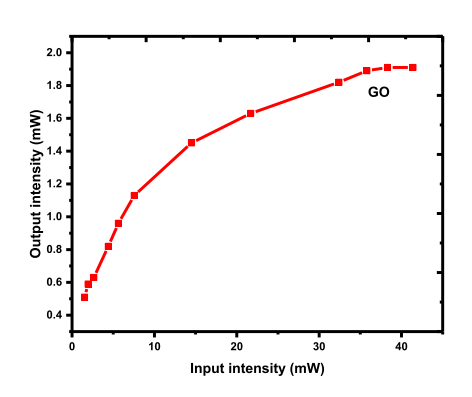
noted that the composite is highly dispersive since it contains nanorods with a length large enough to scatter the incoming light. This resulted in the enhanced third-order NLO properties of BBO:rGO composite compared to bare rGO which further confirms the sensitivity of the composite to nanorod size dispersion.

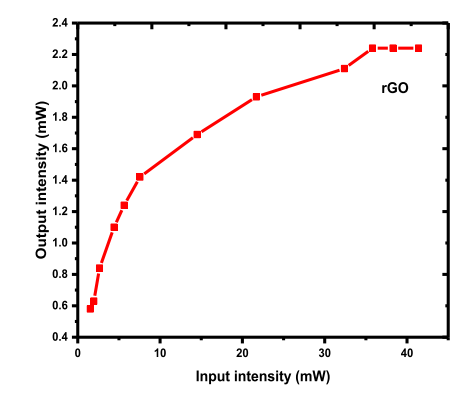
6. Optical limiting and third-order NLO coefficients

The optical limiting behavior of GO, rGO and BBO: rGO is shown in the Fig. 7. The optical limiting behavior is investigated by plotting the output power versus the input power. The transmitted output intensity obeys Beer's law and is found to vary linearly with the input intensities at very low input intensities. Beyond a critical value, the output starts deviating to become nonlinear and the transmitted intensity reaches a plateau and gets saturated. From the critical point, the input power at which the nonlinearity saturate is termed as onset limiting thershold and its corresponding output power is called as limiting amplitude. All the samples exhibit strong limiting action and is found to be varying with respect to their strength of nonlinearity. Here the observed nonlinearity mainly originates due to the self-defocusing nature of

the samples. BBO:rGO with strong nonlinear refraction possess strong optical limiting action with lowest onset limiting thershold (see Fig. 8).

The estimated third-order NLO coefficient (Table 2) clearly exposes the dominance of BBO: rGO composite over individual counterpart. Upon reduction the nonlinear absorption coefficient and nonlinear refractive index of rGO is found to be increased. Appreciable changes in the third-order NLO coefficients of rGO shows the influence of functional groups and textural arrangements of graphene layers. Interestingly BBO:rGO composite possess enhanced nonlinear refraction with almost four fold increase in nonlinear refractive index than pure GO. The reason for such enhanced nonlinear refraction is due to the contribution of graphene sheets and barium borate, which possess high thermal conducting properties. Upon CW laser radiation, both rGO and BBO involve themselves in the photoexcitation resulting in enhanced thermal nonlinearity. Also the 1D morphology of BBO contributes to channelized optical excitation. Similarly nonlinear absorption is also slightly increased which arises due to change in the electronic band structure of composite. The nonlinear absorption coefficient of BBO: rGO composite is higher than GO and rGO, which is due to





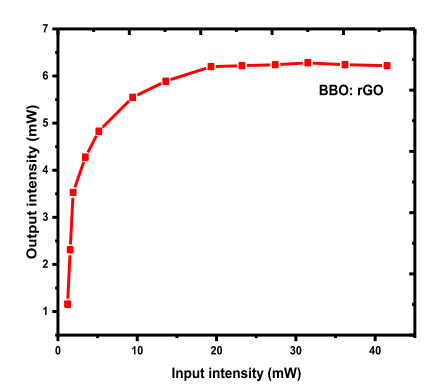


Fig. 8. Optical limiting patterns of GO, rGO, BBO: rGO.

the additional involvement of BBO. This enhancement has resulted in the higher third-order NLO susceptibility of BBO: rGO composite and thus suggesting the superiority of composite over its individual counterparts. As the excitation being CW and the samples possess saturable absorption, the observed nonlinear limiting behavior mainly originates from the self-defocusing nature. As BBO: rGO composite possess enhanced nonlinear refraction, it has low onset-limiting threshold (19.4 mW) arising from the strong thermal lens behavior. Thus the BBO nanorods decorated rGO is identified to be superior in its third-order NLO behavior and can be considered as preferable candidate for optical limiting applications than pure graphene systems.

7. Conclusion

Barium borate – Reduced graphene oxide nanocomposite is successfully prepared by hydrothermal method. XRD and FTIR analysis confirms the incorporation of barium borate upon reduced graphene oxide. FESEM shows the formation of nanorods of barium borate on the graphene layers. From absorption spectra, the blue shift in absorption maxima is identified to be arising from the restored electronic structure due to reduction and inclusion of barium borate. Also the linear transmittance of BBO:rGO is higher than pure GO, which is much essential for optical limiting applications. Tunning of electronic spectra due to composite formation is clearly witnessed from the emission spectra. Strong emission in the UV region arises due to the direct transition in the bandgap region and additional peak arises from the radiative annihilation of selftrapped exciton of BBO. Z-scan experiment performed with CW Nd:YAG laser clearly shows GO, rGO and BBO:rGO exhibits saturable absorption (peak pattern in OA mode) and self-defocusing (peak-valley pattern in CA mode) nature. Order of nonlinearity is found to be BBO: rGO > rGO > GO. Reduction of functional groups and incorporation of BBO nanorod contributes to changes in the magnitude of third-order nonlinearity. BBO:rGO composite with strong self-defocusing behavior and optical limiting action can be potential eternant for power limiting applications in the laser safety devices.

Acknowledgments

T.C. Sabari Girisun acknowledges the financial support from CSIR, India [03(1375)/16/EMR-II].

References

- [1] Ritt Gunnar, Bernd Eberle, Automatic laser glare suppression in electro-optical sensors. Sensors 15 (2015) 792–802.
- [2] Jinhui Zhu, Yongxi Li, Yu Chen, Jun Wang, Bin Zhang, Jinjuan Zhang, Werner

- J. Blau, Graphene oxide covalently functionalized with zing phthalocyanine for broadband optical limiting, Carbon 49 (2011) 1900–1905.
- [3] Qingrui Zhao, Xi Zhu, Xue Bai, Haihua Fan, Yi Xie, Synthesis and optical properties of β -BaB $_2O_4$ network-like nanostructures, Eur. J. Inorg. Chem. (2007) 1829–1834.
- [4] Zhengshan Tian, Chunxiang Xu, Jitao Li, Gangyi Zhu, Jing Wu, Zengliang Shi, Yueyue Wang, A facile preparation route for highly conductive borate crosslinked reduced graphene oxide, New. J. Chem. 39 (2015) 6907.
- [5] C. Babeela, T.C. Sabari Girisun, Low temperature phase barium borate: a new optical limiter in continuous wave and nano pulsed regime, Opt. Mater. 49 (2015) 190–195.
- [6] Leila Shahriary, Anjali A. Athawale, Graphene oxide synthesized by using modified hummers approach, Inter. J. Ren. Energy Envi. Eng. 02 (2014) 58–63.
- [7] G. Muruganandi, M. Saravanan, G. Vinitha, M.B. Jessie Raj, T.C. Sabari Girisun, Effect of reducing agents in tuning the third-order optical nonlinearity and optical limiting behavior of reduced graphene oxide, Chem. Phys. 488 (2017) 55–61
- [8] You-Fu Zhou, Mao-Chun Hong, Yan-Qing Xu, Bai-Quan Chen, Chang-Zhang Chen, Yuan-Sheng Wang, Preparation and characterization of β -BaB₂O₄ nanoparticles via coprecipitation, J.Cryst. Grow. 276 (2005) 478–484.
- [9] P. Muralimanohar, R. Parasuraman, J. Rajeev Gandhi, M. Rathnakumari, P. Sureshkumar, Photoluminescence in cerium doped barium aluminium borate difluoride-BaAlBO₃F₂ glass ceramics, Optik 127 (2016) 8956–8962.
- [10] T.C. Sabari Girisun, R. Madhura Somayaji, N. Priyadarshani, S. Venugopal Rao, Femtosecond third order optical nonlinearity and optical limiting studies of (γ and β)—barium borate nanostructures, Mater. Res. Bull. 87 (2017) 102–108.
- [11] Vahib Babaahmadi, Majid Montazer, Reduced graphene oxide/SnO₂ nanocomposite on PET surface: synthesis, characterization and application as an electro-conductive and ultraviolet blocking textile, Coll. Surf. A Physiochem. Eng. Asp. 506 (2016) 507–513.
- [12] K.H. Michel, S. Costamagna, F.M. Peeters, Theory of anharmonic phonons in two-dimensional crystals, Phys. Rev. B 91 (2015), 134302.
- [13] Muneaki Hase, Masahiro Kitajima, Shinichi Nakashima, Kohji Mizoguchi, Dynamics of coherent anharmonic phonons in bismuth using high density photoexcitation, Phys. Rev. Lett. 88 (6) (2002), 0674011.
- [14] C. Babeela, T.C. Sabari Girisun, G. Vinitha, Optical limiting behavior of β -BaB₂O₄ nanoparticles in pulsed and continuous wave regime, J. Phys. D. Appl. Phys. 48 (2015), 065102.
- [15] Chih-Tao Chien, Shao-Sian Li, Wei-Jung Lai, Yun-Chieh Yeh, Hsin-An Chen, I-Shen Chen, LiChyong Chen, Kuei-Hsien Chen, Takashi Nemoto, Seiji Isoda, Mingwei Chen, Takeshi Fujita, Goki Eda, Hisato Yamaguchi, Manish Chhowalla, Chun-Wei Chen, Tunable photoluminescence from graphene oxide, Angew. Chem. Int. Ed. 51 (2012) 6662—6666.
- [16] Goki Eda, Yun-Yue Lin, Cecilia Mattevi, Hiasto Yamaguchi, Hsin-An Chen, I-Shen Chen, Chun-Wei Chen, Manish Chhowalla, Blue photoluminescence from chemcially derived graphene oxide, Adv. Mater. 22 (2010) 505–509.
- [17] M. Saravanan, T.C. Sabari Girisun, G. Vinitha, Third-order nonlinear optical properties and power limiting behavior of magnesium ferrite under CW laser (532 nm, 50 mW) excitation, J. Mater. Sci. 51 (2016) 3289–3296.
- [18] F.L.S. Cuppo, A.M. Figueiredo Neto, S.L. Go'mez, P. Palffy-Muhoray, Thermallens model compared with the Sheik-Bahae formalism in interpreting Z-Scan experiments on lyotropic liquid crystals, J. Opt. Soc. Am. B 19 (2002) 1342.
- [19] T.C. Sabari Girisun, S. Dhanuskodi, Nonlinear optical susceptibilities of diglycinyl thiourea for frequency conversion and optical limiting applications, Chem. Phys. Lett. 491 (2010) 248–253.
- [20] M. Sheik-Bahae, A.A. Said, T. Wei, D.J. Hagan, E.W. Van Stryland, Sensitive measurement of optical nonlinearities using a single beam, IEEE J. Quant. Electron. 26 (1990) 760–769.
- [21] RL, Sutherland Handbook of Nonlinear Optics, second ed., Marcel Dekker, NewYork. 2003.
- [22] T.C. Sabari Girisun, S. Dhanuskodi, G. Vinitha, $\chi^{(3)}$ measurement and optical limiting properties of metal complexes of thiourea using Z-scan, Mater. Chem. Phys. 129 (2011) 9–14.



Contents lists available at ScienceDirect

Optik

journal homepage: www.elsevier.com/locate/ijleo



Second and third-order NLO response of 2-amino-5-nitropyridinium tetrafluoroborate



G. Muruganandi, M.B. Jessie Raj*

Department of Physics, Bishop Heber College, Tiruchirappalli, 620 017, India

ARTICLE INFO

Keywords: Semiorganic Borate SHG Z-scan

ABSTRACT

Based on host-guest chemistry, a semiorganic NLO material 2-amino-5-nitropyridinium tetra-fluoroborate [2A5NPFB] was synthesized and grown as single crystals. SXRD of 2A5NPFB reveals its crystal structural details as orthorhombic crystal system, Fdd2 space group, a = 22.474 (1) Å, b = 30.127 (9) Å, c = 4.9584 (1) Å and $\alpha = \beta = \gamma = 90^\circ$. Protonation site, charge transfer interaction and molecular structure were studied by FTIR analysis. Thermal studies predicts the melting point of 2A5NPFB as 145 °C. 2A5NPFB possess strong absorption ($\lambda_{max} = 350$ nm) in ultraviolet region and has a broad transparency window (420–1100 nm). Kurtz and Z-scan technique explores the second and third-order NLO response of 2A5NPFB single crystal. Compared to KDP crystal, 2A5NPFB single crystal possesses 35 times higher Second Harmonic Generation efficiency. 2A5NPFB crystal exhibit saturable absorption, self defocusing and optical limiting action under continuous wave Nd:YAG green laser.

1. Introduction

Considering the factors of sudden hike in the utilization of high intense short-wavelength (green) lasers and eye of human has maximum sensitivity (88%) to green color, the need for second harmonic generation (SHG) and optical limiting (OL) material have increased tremendously [1]. Thus frequency doublers made of second-order nonlinear optical (SONLO) materials capable of converting longer wavelength (IR) to visible (green) wavelength radiation are of considerable interest. Also optical limiters made of third-order nonlinear optical (TONLO) materials that can protect the optical components from intense laser radiation are also under limelight [2,3]. Thus investigation on materials has reached a point of balance between second and third-order nonlinearity, which ultimately require a material with high NLO coefficients. In this line of search, 2-amino 5-nitropyridine (2A5NP) can induce high NLO character with strong donor (NH₂) and acceptor (NO₂) group through push-pull mechanism [4-6]. In particular the derivatives of 2amino-5-nitropyridine are efficient NLO materials as it can attach inorganic elements to its herringbone pattern [7–9]. Some of the important compounds belonging to this class includes: 2A5NP dihydrogenphosphate, 2A5NP dihydrogenarsenate, 2A5NP acetophosphate, 2A5NP fluoroborate, 2A5NP chloride, 2A5NP bromide and 2A5NP L-monohydrogentartrate [9-11]. These materials exhibit improved chemical, thermal, and mechanical stabilities due to the availability of hydrogen-bonded networks [11]. In particular, 2-amino-5-nitropyridinium fluoroborate [2A5NPFB] was identified to be an excellent SONLO material with high powder SHG efficiency of 40 times KDP [12]. Although these compounds were already investigated and their powder SHG efficiency was available in literature, their bulk second and third-order NLO response still remains unexplored. Based on these facts, this article aims to investigate the second and third-order NLO response of 2A5NPFB single crystal grown by slow evaporation method. The SHG

^{*} Corresponding author at: Department of Physics, Bishop Heber College (Autonomous), Tiruchirappalli, 620 017, India. E-mail address: drjessiebhc@gmail.com (M.B. Jessie Raj).



Fig. 1. Single Crystals of 2A5NPFB.

capability (Kurtz technique) and optical limiting (Z-scan technique) behavior of 2A5NPFB single crystals were presented in detail.

2. Material preparation

By acid-base reaction, a semiorganic NLO material 2-amino 5-nitropyridinium fluoroborate [2A5NPFB] was synthesized [12]. Here the reaction involves a proton transfer between the nitrogen atom (basic acceptor) of 2-amino 5-nitropyridinium molecule and the hydrogen atom (acidic donor) of tetrafluoroboric acid. This induces the formation of semiorganic material, 2A5NPFB through the hydrogen bond formed by the electrostatic interaction between the $2A5NP^+$ cation and BF_4^- anion. In a typical experimental procedure, 1 mol of 2A5NP was treated with 2 mol of HBF4 acid in aqueous medium (20 mol of H₂O). The solution was thoroughly mixed with a magnetic stirrer and maintained at 60 °C using a water bath. As 2A5NPFB possess positive solubility temperature gradient in water, controlled solvent evaporation method was employed to grow single crystals at ambient temperature. Single crystals with average dimension of $9 \times 7 \times 5$ mm³ (Fig. 1) were grown in a period of 25 days.

The obtained crystals were subjected to single crystal XRD (SXRD) to confirm the formation of hybrid material through the estimation of lattice parameter and space group. SXRD shows that 2A5NPFB possess orthorhombic crystal system with acentric space-group Fdd2 having lattice parameter a=22.474 (1) Å, b=30.127 (9) Å, c=4.9584 (1) Å and $\alpha=\beta=\gamma=90^\circ$. As the estimated lattice constants was found to be different from the cell constants of parent molecule (2A5NP, HBF₄) and consistent with the already reported values of 2A5NPFB [12], the formation of semiorganic system was confirmed. In the recorded XRD pattern of 2A5NPFB powder depicted in Fig. 2, the prominent peaks confirm the perfect crystalline nature of the material. All the reflections were indexed for orthorhombic system and the corresponding lattice parameters were estimated using AUTOX program. As shown in Table 1, the lattice parameters of 2A5NPFB agree very well in both the modes of XRD. As 2A5NPFB belongs to noncentrosymmetric space group, it can be used for the generation of short-wavelength lasers through frequency doubling phenomenon [7].

3. Molecular structure

The molecular arrangement of 2A5NPFB was analyzed and its protonation site was identified by FTIR analysis [13]. The recorded FTIR spectrum is shown in Fig. 3. The charge transfer interaction between tetrafluoroboric acid (donor) and 2-amino 5-nitropyridinium (acceptor) was ascertained through the peaks in the range of 3100–3500 cm⁻¹ [14].

The presence of peaks at 3329, 3129 cm⁻¹ corresponds to the N–H···F hydrogen bond which confirms the presence of intramolecular hydrogen bonding between the nitrogen of 2A5NP⁺ cation and the flourine atom of the BF₄- anion. The asymmetric stretching vibration of aromatic C—N has shifted to 1662 cm⁻¹ than its parental 2A5NP⁺ at 1648 cm⁻¹. Also due to protonation, the peak which corresponds to N–H bending (1633 cm⁻¹) of 2A5NPFB was deviated from the parental arrangement and this has resulted in the increased hyperpolarizability of the molecule. The presence of peaks at 1474, 1418, 1345 cm⁻¹ represents the symmetric stretching vibrations of N–O. The vibrations in the lower wavenumber domain 500–800 cm⁻¹ confirm the presence of inorganic elements. In particular the peaks at 751, 711, 680, 536 cm⁻¹ corresponds to symmetric stretching and asymmetric bending of BF₄-

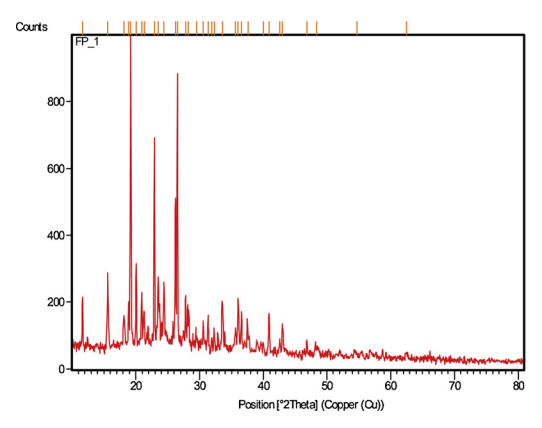


Fig. 2. Powder XRD of 2A5NPFB.

Table 1
Structural parameters of 2A5NPFB crystal.

Lattice parameters	Experimental		Reported
	SXRD	PXRD	Value [12]
a (Å) b (Å) c (Å)	22.474 (1)	22.47	22.474 (4)
b (Å)	30.127 (9)	30.12	30.128 (5)
c (Å)	4.9584 (1)	4.95	4.9583 (8)
α (°)	90	90	90
β (°)	90	90	90
γ (°)	90	90	90
System	Orthorhombic	Orthorhombic	Orthorhombio

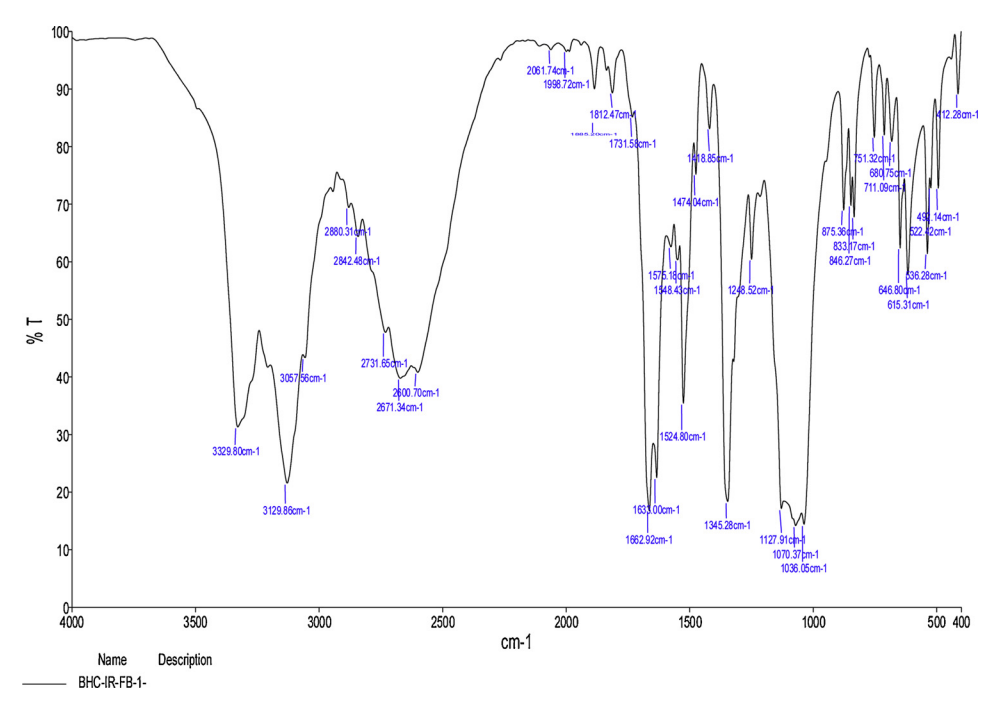


Fig. 3. FTIR Pattern of 2A5NPFB.

anions respectively [12]. The observed FTIR peaks were confirmed with the parent molecule 2A5NP and the assignments are given in Table 2.

4. Thermal studies

Thermal stability of 2A5NPFB was assessed from the TG/DTA curve (Fig. 4). In the DTA curve, the first endothermic peak represents the melting point of 2A5NPFB which occurs at the vicinity of 145 °C. This was followed by two endothermic peaks at

Table 2 FTIR peak assignment of 2A5NPFB crystal.

Wave number (cm ⁻¹)			Assignmen
2A5NP *	2A5NPFB [12]	2A5NPFB *	
_	3329	3329	ν (N–H…F)
_	3127	3129	ν (N=H···F)
1648	1668	1662	ν (C=N)
1632	1630	1633	δ (N-H)
1332	1472, 1416, 1353	1474, 1418, 1345	ν (N-O)
_	750, 710, 680	751, 711, 680	$\nu (BF_4)^-$
	535	536	δ (BF ₄) ⁻

 $[\]nu$ - stretching vibrations and δ - bending vibrations.

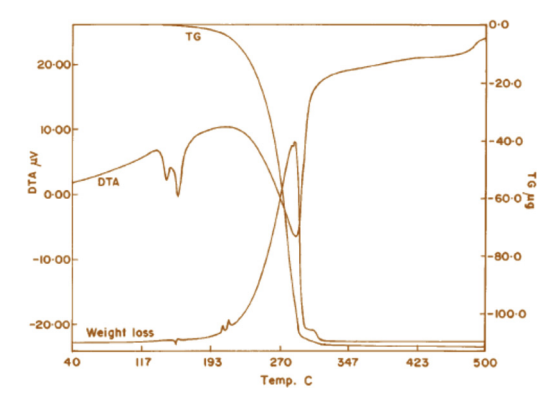


Fig. 4. TG-DTA pattern of 2A5NPFB.

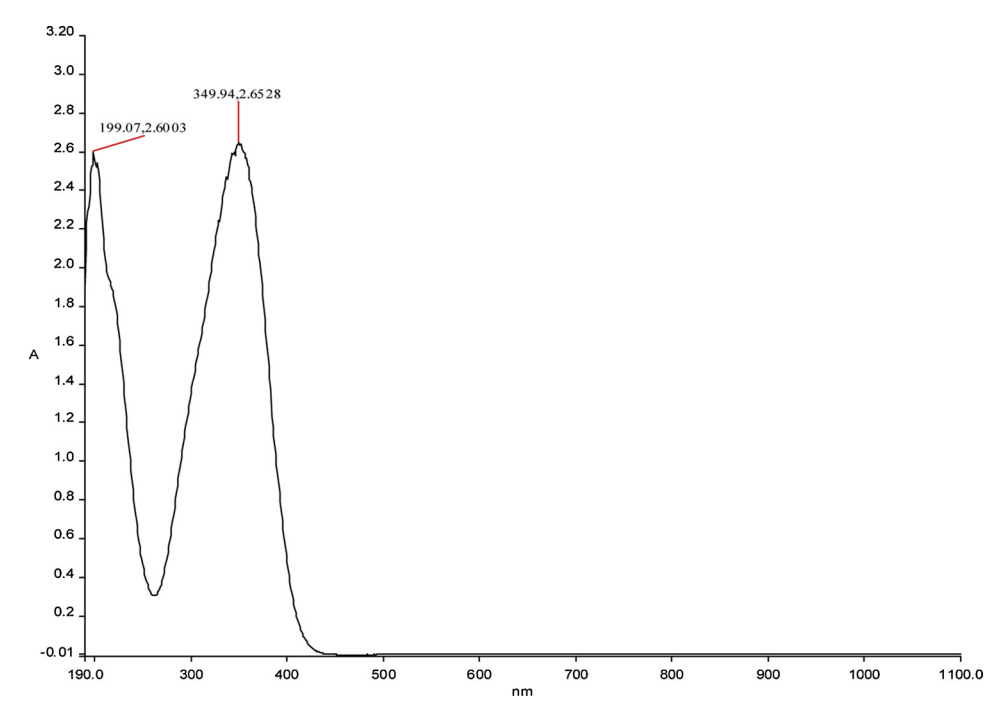


Fig. 5. UV-vis absorption spectrum of 2A5NPFB.

177 °C and 287 °C which was accompanied by weight loss in TG pattern and thus corresponds to the decomposition of the material. 2A5NPFB loses almost 95% of its total mass at 288 °C, which indicates the complete decomposition of the material through the dissociation of volatile substances as various gaseous fragments (NH₂, NO₂ or Br). As 2A5NPFB does not decompose before melting, it makes them suitable for device fabrication for second and third order NLO materials. The enhancement in the thermal stability of 2A5NPFB arises due to the strong forces acting between the $2A5NP^+$ cation and $BF4^-$ anion as a result of the proton transfer and due to inclusion of inorganic species (BF_4^-) in the molecular structure [12].

5. UV visible studies

UV–VIS absorption pattern of 2A5NPFB (Fig. 5) clearly exposes the significant absorption in the ultraviolet region with absorption maxima at $\lambda_{max} = 199$ nm, 350 nm. Hence the cutoff wavelength of 2A5NPFB was estimated to be 350 nm. Also the material has wide optical window of 420–1100 nm, with almost negligible absorption in the visible and NIR region. Here it is to be noted that alteration in intramolecular charge transfer takes place due to the formation of 2-amino 5-nitropyridine cation which lengthens C–NO₂ and shortens C–NH₂, C=C, C=N bond lengths [12]. This complex formation red shifts the transparency of parental 2-amino 5-nitropyridine by 40 nm [11]. Thus lower cutoff along with wide range of transparency in UV and visible region enables good transmission which make 2A5NPFB to be an entrant material for NLO applications in both second-order (second-harmonic generation) and third-order (optical limiting) NLO applications [15,16].

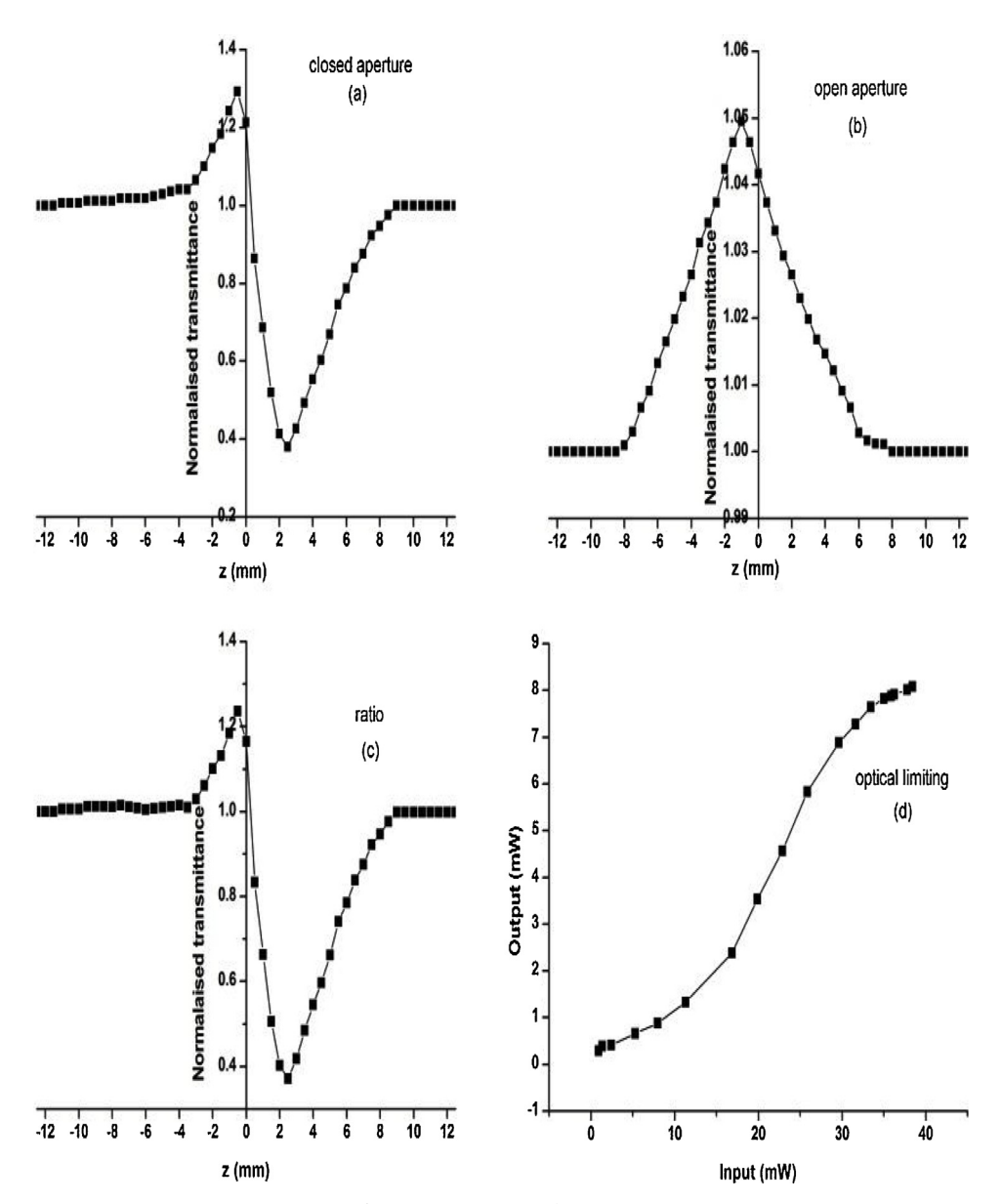


Fig. 6. Z-scan pattern of 2A5NPFB.

Table 3Third order NLO properties of 2A5NPFB.

NLO Parameters	Estimated Values
Refractive index (n_2)	$4.01 \times 10^{-9} \text{ cm}^2/\text{W}$
Absorption coefficient (β)	$5.91 \times 10^{-3} \text{ cm/W}$
Real part of susceptibility $[Re(\chi 3)]$	$2.13 \times 10^{-7} \text{ esu}$
Imaginary part of susceptibility $[Im(\chi 3)]$	$1.33 \times 10^{-6} \text{ esu}$
Optical susceptibility $(\chi 3)$	$1.35 \times 10^{-6} \text{ esu}$

6. Second harmonic generation test

The second harmonic generation test on bulk crystal of 2A5NPFB was made by Kurtz method [17]. A defect free 2A5NPFB crystal of dimension $7 \times 5 \times 3 \text{ mm}^3$ was cut and polished from the grown crystals for SHG test. Here the crystal was illuminated using a Nd:YAG laser (1064 nm, 10 Hz, 5 ns, 20 mJ). The input laser with spot radius of 1 mm was directed on the crystal. The transmitted light was filtered through IR filter and was measured by means of a photo detector. When a laser of 1064 nm was radiated directly on

the crystal, a green light beam of double frequency 532 nm was observed which indicate that 2A5NPFB possesses SHG behavior. The second harmonic generation efficiency of the 2A5NPFB sample was estimated by taking the KDP crystal ($3 \times 3 \times 3$ mm³) as reference system. The test show a green signal output of 2722 mV and 80 mV for 2A5NPFB and KDP respectively. Thus frequency doubling efficiency of 2A5NPFB single crystal was found almost 35 times higher than KDP crystal. The observed higher second harmonic generation efficiency arises mainly from the highest density of the chromophores. Although 2A5NPFB possess very high second-order NLO coefficient than other materials, its major concern is the non-phase matchable property of the material [12]. Thus the crystal was further subjected to its third-order NLO studies.

7. Z-scan studies

The third-order NLO properties of 2A5NPFB were studied by Z-scan experiment. The nonlinear refractive index and the nonlinear absorption coefficient of 2A5NPFB were determined by the Sheik-Bahae formalism [3,18] where a Gaussian beam from a Nd:YAG laser (532 nm, 50 mW) was used as the excitation source. Fig. 6 gives the nonlinear pattern of 2A5NPFB. The closed aperture Z-scan curve in Fig. 6(a) has peak-valley pattern which indicates the presence of self-defocusing behavior with negative nonlinear refraction. Although 2A5NPFB shows a small linear absorption (0.2) at excitation domain, it has strong nonlinear which is seen from the peak pattern (Fig. 6(b)) in open aperture Z-scan mode [8]. Thus 2A5NPFB possess saturable absorption. The ratio of closed-aperture to open-aperture transmittance is shown in Fig. 6(c) which represents the pure nonlinear refraction behavior of the sample.

Table 3 summarizes the third-order NLO values of 2A5NPFB following the Sheik Bahae formalism. Fig. 6(d) shows the optical limiting behavior of 2A5NPFB. For incident power less than 36 mW, 2A5NPFB obeys Beer's law and then its output saturates leading to nonlinear behavior. The onset limiting threshold value is 36 mW with clamping amplitude of 7.91 mW. This confirms that 2A5NPFB can be used as optical limiting material [3,19].

8. Conclusion

2-amino 5-nitropyridinium fluoroboate (2A5NPFB) was synthesized using 2A5NP and tetraflouoro boric acid in an aqueous medium. Optical quality defect free crystal of 2A5NPFB of dimension $9 \times 7 \times 5$ mm³ was grown by solvent evaporation method. 2A5NPFB crystallizes in acentric space group Fdd2 having orthorhombic crystal system with lattice parameter parameter a=22.474 (1) Å, b=30.127 (9) Å, c=4.9584 (1) Å and $\alpha=\beta=\gamma=90^\circ$. The charge transfer interaction between tetrafluoroboric acid (donor) and 2-amino 5-nitropyridinium (acceptor) was ascertained by FIR analysis. Thermal studies show that 2A5NPFB was stable upto 145 °C and there is no phase transition before decomposition. 2A5NPDP possess strong absorption ($\lambda_{max}=2199,350$ nm) in the ultraviolet region and has a broad transparency window (420–1100 nm). The relative second harmonic generation efficiency of 2A5NPFB crystal was 35 times that of KDP. Z-Scan studies with CW excitation shows that the material exhibit saturable absorption, self-defocusing and optical limiting action.

References

- [1] R.L. Sutherland, Handbook of Nonlinear Optics, Marcel Decker Inc, New York, 2003.
- [2] P.N. Prasad, D.J. Williams, Introduction to Nonlinear Optical Effects in Organic Molecules and Polymers, Wiley, New York, 1991.
- [3] T.C. Sabari Girisun, S. Dhanuskodi, G. Vinitha, Mater. Chem. Phys. 129 (2011) 9.
- [4] A. Ibanez, J.P. Levy, C. Mouset, E. Prieur, J. Soild State Chem. 129 (1997) 22.
- [5] J. Pecaut, Y.L. Fur, R. Masse, Acta Crystallogr. Sect. B49 (1993) 535.
- [6] J. Zaccaro, B. Capelle, A. Ibanez, J. Cryst. Growth 180 (1997) 229.
- [7] M. Thangaraj, G. Ravi, T.C. Sabari Girisun, Phys. B: Cond. Matter 449 (2014) 209.
- [8] T.C. Sabari Girisun, S. Dhanuskodi, D. Mangalaraj, J. Phillip, Curr. Appl. Phys. 11 (2011) 838.
- [9] M.S. Wong, J.F. Nicoud, C. Runser, A. Fort, M. Barzoukas, Nonlinear Opt. 9 (1995) 181.
- [10] M. Ambrose Rajkumar, S. Stanly John Xavier, S. Anbarasu, Prem Anand Devarajan, Opt. Mater. 55 (2016) 153.
- [11] G. Anandha Babu, R.P. Ramasamy, P. Ramasamy, V. Krishna Kumar, Cryst. Growth Des. 9 (2009) 3333.
- [12] S. Manivannan, S. Dhanuskodi, K. Kirschbaum, S.K. Tiwari, Cryst. Growth Des. 5 (2005) 1463.
- [13] G. Varsanyi, Assignments for Vibrational Spectra of Seven Hundred Benzene Derivatives, Adam Hilger, London, 1974.
- [14] P.S. Kalsi, Spectroscopy of Organic Compounds, New Age International (P) Limited Publishers, New Delhi, 2002.
- [15] B. Milton Boaz, A. Levo Rajesh, S. Xavier Jesu Raja, S. Jerome Das, J. Mater. Sci. Technol. 20 (2004) 505.
- [16] T.C. Sabari Girisun, S. Dhanuskodi, Cryst. Res. Technol. 44 (2009) 1297.
- [17] S.K. Kurtz, T.T. Perry, J. Appl. Phys. 36 (1968) 3798.
- [18] Mansoor Sheik-Bahae, Ali A. Said, Tai-Huei Wei, IEEE J. Quantum Electron. 26 (1990) 760 1990.
- [19] M. Thangaraj, G. Ravi, T.C. Sabari Girisun, G. Vinitha, A. Loganathan, Spectrochim. Acta Part A: Mol. Biomol. Spectrosc. 138 (2015) 158.